

TALLINN UNIVERSITY OF TECHNOLOGY
DOCTORAL THESIS
3/2018

Uni- and Bidirectional Stratified Flows in Submerged Openings of Built Environment

MONIKA KOLLO

TALLINN UNIVERSITY OF TECHNOLOGY

School of Engineering

Department of Civil Engineering and Architecture

This dissertation was accepted for the defence of the degree 15/11/2017

Supervisor:

Associate Professor Janek Laanearu
Department of Civil Engineering and Architecture
School of Engineering
Tallinn University of Technology
Tallinn, Estonia

Opponents:

Professor Paul Linden
Department of Applied Mathematics and Theoretical
Physics
University of Cambridge
Cambridge, United Kingdom

Associate Professor Claudia Adduce
Department of Engineering
University Roma Tre
Rome, Italy

Defence of the thesis: 16/01/2018, Tallinn

Declaration:

Hereby I declare that this doctoral thesis, my original investigation and achievement, submitted for the doctoral degree at Tallinn University of Technology has not been submitted for doctoral or equivalent academic degree.

Monika Kollo

signature



Copyright: Monika Kollo, 2018

ISSN 2585-6898 (publication)

ISBN 978-9949-83-195-1 (publication)

ISSN 2585-6901 (PDF)

ISBN 978-9949-83-196-8 (PDF)

TALLINNA TEHNIKAÜLIKOO
DOKTORITÖÖ
3/2018

**Ühe- ja kahe-suunaline stratifitseeritud
voolamine konstruktsioonipiirde uputatud
avades**

MONIKA KOLLO

Contents

List of Publications	7
Author's Contribution to the Publications	8
Introduction	9
Theoretical background	9
Stratified flows	11
Natural environment.....	13
Built environment	13
Internal-flow head.....	15
State of the art	17
Motivation and objectives	18
Limitations.....	19
Abbreviations	21
Symbols	22
1 Theory of internal-flow hydraulics	24
1.1 Theoretical framework.....	24
1.2 Unidirectional flow.....	25
1.3 Bidirectional flow	27
1.3.1 Rectangular opening	28
1.3.2 Circular opening	33
1.4 Hydraulic-modelling solutions.....	38
1.5 Discharge coefficients	39
1.6 Shape factors.....	40
2 Pilot studies.....	41
2.1 Oil spill.....	41
2.2 Water exchange	47
2.3 Ventilation.....	49
3 Optimisation method	54
3.1 Search techniques	54
3.2 Genetic Algorithm	56
3.3 Process optimisation	60
3.3.1 Physical modelling.....	60
3.3.2 Hydraulic-flow problem	60
3.3.3 Setup and run of process optimisation	61
3.3.4 Results of process optimisation	64
3.4 System optimisation.....	64
3.4.1 Engineering modelling	65
3.4.2 Integrated-system model problem	66
3.4.3 Setup and run of system optimisation	67
3.4.4 Results of system optimisation	69
4 Practical challenges.....	72
4.1 Risk assessment	72
4.2 Renewables	73
4.3 Energy efficiency	75
Summary of findings	78

List of Figures	81
List of Tables	83
References	84
Lühikokkuvõte	91
Abstract	94
Appendix 1	97
Appendix 2	107
Appendix 3	123
Appendix 4	133
Appendix 5	145
Curriculum vitae	159
Elulookirjeldus	161

List of Publications

The list of author's publications, on the basis of which the thesis has been prepared:

- I Sergejeva, M., Laanearu, J., Tabri, K. (2013). Hydraulic modelling of submerged oil spill including tanker hydrostatic overpressure. – Proceedings of 4th International Conference on Marine Structures, MARSTRUCT 2013, 25–27 March 2013, Espoo, Finland. Taylor & Francis, 209–217.
- II Kollo, M., Laanearu, J., Tabri, K. (2017). Hydraulic modelling of oil spill through submerged orifices in damaged ship hulls. – Ocean Engineering, 130, 385–397. doi: 10.1016/j.oceaneng.2016.11.032
- III Sergejeva, M., Laanearu, J., Tabri, K. (2017). On parameterization of emulsification and heat exchange in the hydraulic modelling of oil spill from a damaged tanker in winter conditions. – Proceedings of 6th International Conference on Marine Structures, MARSTRUCT 2017, 8 – 10 May 2017, Lisbon, Portugal.
- IV Sergejeva, M., Laanearu, J. (2013). Optimal utilization of rain-water heat in domestic water system of public building. – Proceedings of 11th REHVA World Congress and the 8th International Conference on Indoor Air Quality, Ventilation and Energy Conservation in Buildings, CLIMA 2013, 16 – 19 June 2013, Prague, Czech Republic. Elsevier, 1-10.
- V Kollo, M., Laanearu, J. (2017). An optimal solution of thermal energy usage in the integrated system of stormwater collection and domestic-water heating. – Urban Water Journal, 14 (2), 212–222. doi: 10.1080/1573062X.2015.1086006

Author's Contribution to the Publications

Contribution to the papers in this thesis are:

- I The author proposed the hydraulic theory solutions in the case of oil outflow through the submerged rectangular hole in the tank. The hydraulic formulae were applied in the case of unbalanced and balanced hydrostatic-pressure situations at the level of the hole. The hydraulic modelling solutions were used to determine the oil-spill duration and outflow volume from the side and bottom holes of single- and double-hull tankers. The effect of a shape factor in the analytical formula for volumetric flow rate of bidirectional stratified flow through the side hole of the tank was discussed.
- II The author derived the analytical formula for volumetric flow rate using the internal-flow hydraulic theory in the case of oil outflow through the submerged circular hole in the tank. The uni- and bidirectional stratified flows were analysed for different oil-spill scenarios of tanker accidents. Four oil-spill model versions were proposed to determine the oil-leak quantities in six test cases. Five test cases were used to determine the discharge coefficients according to the experimental results by Tavakoli et al. (2011). One test case for bidirectional stratified flow through a side hole in a double-hulled tank was presented as a demonstration of the modelling approach developed. GA was implemented to find the process parameters, such as discharge coefficients and emulsion density.
- III The author extended the internal-flow hydraulic model to account for the effects of emulsification and heat exchange. The emulsification was associated with an interfacial mixing between the counter-flowing layers. The effect of heat-exchange was considered in both cases i.e. uni- and bidirectional stratified flows. Two key parameters: i) the seawater inflow-rate reduction parameter and ii) the thermal expansion coefficient, were introduced in hydraulic-theory solutions to modify the formulae for the volumetric flow rate of uni- and bidirectional stratified flows developed in Publication II. The extended hydraulic model was tested to consider the outside temperature variations between summer and winter conditions.
- IV The author proposed the model of integrated system of stormwater collection and domestic-water heating. It was considered that the heat extraction from stormwater results in the stratified flow through the storage tank. Six months of rain in the north-eastern Baltic Sea region was examined to analyse a possibility of low-temperature water usage for domestic hot-water production. GA was employed for searching the dimensions of the integrated-system design parameters (rainwater storage amount and catchment area size) of public building.
- V The author applied a modified model of an integrated system of stormwater collection and domestic-water heating for different types of buildings (residential, public, and commercial). GA was employed to find the integrated system parameters, such as the number of storage tank fillings and the stormwater volume in storage tank. In the developed model the stratified flow due to heat extraction regulates the number of storage tank fillings. The system's cumulative expenses related to the stormwater storage and the rainwater harvesting expenses were discussed.

Introduction

Theoretical background

Density tends to vary from point to point in real fluids. The consequence of this is that the pressure variation with depth is "non-linear" also in a fluid in a static situation. In dynamic situations, the density can vary vertically between moving layers separated by interfaces, and horizontally between columns separated by fronts, as seen in the ocean and atmosphere. Air and water, largely immiscible fluids with a very large density contrast, is one example of stratified flow in which coupling between moving layers can be considered as "weak". An example of stratified flow with "strong" coupling between layers is flow with small density differences, such as buoyancy-driven flow in a river estuary, with water outflow having a negligible surface slope.

The buoyancy force allows the fresh water in a river estuary to flow above the saline water, and cold air to flow along a mountain slope. For a fluid column to be in equilibrium, the buoyancy force (i.e. upward force) must exactly be equal to the force due to weight. Therefore, the buoyancy is usually defined as the negative weight per unit volume for a fluid parcel (cf. Gill, 1977). However, in the case of a droplet of oil at rest in water, which can also be considered to be a submerged fluid parcel, the pressure-gradient force due to gravity is different from the weight of the droplet due to density differences. The pressure variation over the fluid parcel interface is the cause of the buoyancy force. The buoyancy force F_B (N) on a fluid parcel can be determined as the pressure integrated over the closed interface area. Applying the Gauss theorem, the equation for buoyancy force is as follows:

$$\vec{F}_B = -\oint_S p(z)\vec{n}dS = -\int_V \nabla p(z)dV, \quad (1)$$

where $p(z)$ is the pressure (Pa) at height z (m), S and V are the interface area (m^2) and the volume (m^3) of the fluid parcel, respectively. The buoyancy in the heterogeneous fluid is the product of gravity and varying density, i.e. the submerged fluid parcel that is denser than the surrounding fluid will sink; in contrast, a lighter parcel will rise inside the denser fluid. The reduced gravity g' of a submerged fluid parcel is the negative of relative buoyancy b ($m\ s^{-2}$):

$$g' = g \frac{\rho_{parcel} - \rho_{fluid}}{\rho_{fluid}} = -b, \quad (2)$$

where ρ_{parcel} and ρ_{fluid} are the density ($kg\ m^{-3}$) of the fluid parcel and ambient fluid, respectively (Wirth, 2017). Therefore, the buoyancy force is modified in the heterogeneous fluid due to the varying density. It follows that the submerged fluid parcel in a stratified fluid will settle at the equilibrium depth, where the relative buoyancy vanishes. It also follows that the resultant force on the submerged fluid parcel due to gravity and density differences is $F_R = b\rho_{fluid}V$.

The buoyancy-driven flow is by far a common flow in nature, and it exists obviously in the built environment, where usually fluid density changes result from temperature variations due to heating. The dynamics of two-layer flows with a small density jump

($\rho_{parcel} - \rho_{fluid} \ll \rho_{fluid}$), can be modelled as homogeneous layers of inviscid fluid (Zhu and Lawrence, 2000). In the case that the density jump is negligibly small; the Boussinesq approximation can be applied. This approximation ignores the density difference by assuming that its variation has no effect on the flow field, except where it gives rise to a buoyancy force, i.e. appears in terms multiplied by g . The flows with hydrostatic pressure distribution are illustrated for i) single-layer and ii) two-layer cases in Figure i-1. The main assumption is that the fluids are incompressible, which is a reasonable assumption for most of the flows of liquids, and also for gases at low Mach numbers ($M < 0.3$). For inviscid, steady, and incompressible flow, the density remains constant within the layer and the sum of pressure, elevation, and velocity heads is constant inside the homogeneous fluid layer. In the case of irrotational flow the principles of potential flow apply.

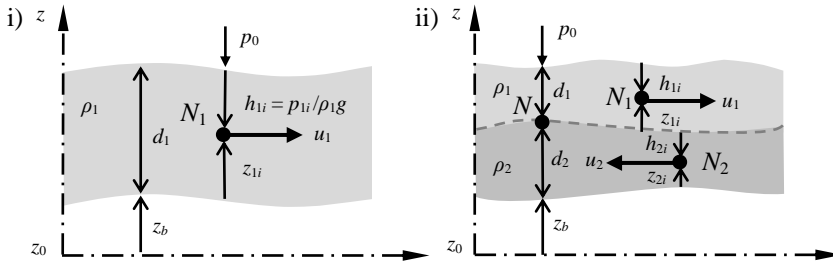


Figure i-1. Notations: i) single-layer flow and ii) two-layer flow.

In the case of single-layer flow, the Bernoulli function E_1 (Pa), i.e. Bernoulli head $B_1 = E_1 / \rho_1 g$ (m), yields the Bernoulli constant for any point N_1 within the homogeneous fluid layer ($0 \leq h_{1i} \leq d_1$ and $z_{1i} = d_1 - h_{1i}$):

$$E_1 = \frac{\rho_1 u_1^2}{2} + p_0 + \rho_1 g (h_{1i} + z_{1i} + z_b), \quad (3)$$

where u_1 is the horizontal flow velocity (m s^{-1}), p_0 is the pressure on top of the layer (Pa), ρ_1 is the fluid density (kg m^{-3}), and h_{1i} and z_{1i} are the fluid thicknesses (m) above and below the point N_1 in the fluid layer. The Bernoulli head also represents a reduced form of the energy conservation.

In the case of a heterogeneous fluid, the stratified flow can be approximated by two homogeneous fluid layers (1 and 2 representing the upper and lower layers) of different densities (Figure i-1ii). The Bernoulli function of both layers relate similarly the flow velocity, pressure, and elevation heads as in the single-layer case. The Bernoulli function of a particular layer yields the constant for any point N_1 within the upper homogeneous fluid layer ($0 \leq h_{1i} \leq d_1$ and $z_{1i} = d_1 - h_{1i}$), and for any point N_2 within the lower homogeneous fluid layer ($0 \leq h_{2i} \leq d_2$ and $z_{2i} = d_2 - h_{2i}$). Therefore, per the definition above, at the interfacial point N , the Bernoulli functions' difference ($E_2 - E_1$) of the layers of different density can be determined. In the study of coupled two-layer flows the internal-flow energy function is defined as:

$$\frac{E_2 - E_1}{\rho_2} = \left(\frac{u_2^2}{2} - \frac{\rho_1}{\rho_2} \frac{u_1^2}{2} \right) + g'(d_2 + z_b), \quad (4)$$

where E_1 (Pa) and E_2 (Pa) are the Bernoulli functions in the upper and lower layer, respectively, d_2 is the lower-layer thickness (m), and z_b is the bottom elevation (m). Henceforth, Equation (4) is simplified according to the assumption of a small density difference. If shear stresses (i.e. interfacial and boundary stresses) in the two-layer flow are considered, then the internal-flow head is not conserved along the channel.

Stratified flows

Stratified flows are of practical and scientific importance in fluid mechanics (Kundu et al., 2011). The variations in fluid density in stratified flows arise through temperature differences, salinity contrasts, the presence of different fluids of different densities, and combinations of these situations. The buoyancy-driven flow can be related to the coupling between fluid layers of different density. The stratified flows can be classified in a number of ways. Herein, the stratified flows are classified separately as flows of liquids and gases, both of which share the ability to follow the ideal flow conditions. When two fluids with similar properties flow, for instance liquid adjacent to liquid or gas adjacent to gas, the coupling between layers in buoyancy-driven flow can be considered as "strong", e.g. Kelvin-Helmholtz type instability at the interface between two horizontal parallel streams of different velocities and densities (Kundu et al., 2011). Thus, the dynamics of an interface that separates layers is strongly dependent on both fluids' behaviours. However, when fluids' properties vary on a larger scale, for instance in simultaneous flows of gas and liquid, the dynamics of the interface (surface) are essentially related to the denser fluid (liquid) layer's behaviour, and therefore, coupling can be considered to be "weak", e.g. wave breaking in the sloping bottom (Oldekop and Liiv, 2013). It should be noted that the strength of coupling is also associated with the stratified fluid layers' thicknesses. This is apparent in the dense fluid shallow flow, which is submerged in the deep fluid body with small density difference. In this case, the lower layer buoyancy-driven flow has no significant effect on superimposed fluid layer behaviour, i.e. coupling between the layers with small density differences can be considered to be "conditionally weak".

The stratified flows consider the miscibility criterion, according to which two different situations should be distinguished: miscible and immiscible fluid flow. When two fluids are miscible, when mixed together in any proportion at given conditions they form a single homogeneous layer that shares the properties of both fluids. By contrast, fluids are immiscible if a significant proportion does not form a homogeneous layer. This results in the formation of emulsion, e.g. one fluid disperses in another as droplets.

In order to simplify the classification of buoyancy-driven flows, the interactions between fluids are mapped into four categories in Table i-1, where the coupling "strength" and the miscibility criteria are considered. It should be noted that the active and passive layers of a buoyancy-driven flow are important for interfacial dynamics in the case of small density difference. The active layer represents the fluid layer that has significantly different flow behaviour compared to the passive layer, due to the different thicknesses of the layers. Therefore, the gravity currents in the ocean and atmosphere can be considered to be buoyancy-driven flows with the layers that are "conditionally weakly" coupled. Furthermore, in the case of the interaction of immiscible fluids, such as air and water, the coupling of fluid layers in the gravity-driven

flow can be considered as "weak", e.g. surface currents in rivers and channels without wind effects. If the surface flow is driven by wind, herein it is considered as shear-driven flow, and is not of interest to this study.

Table i-1. Interaction of fluids in buoyancy-driven flows.

	Strongly coupled	Weakly coupled
Miscible	<ul style="list-style-type: none"> ▪ Liquid-liquid interaction with two active layer flow (e.g. bi-directional stratified flow in river estuary). ▪ Gas-gas interaction with two active layer flows (e.g. bidirectional stratified flow through the opening of a building). 	Conditionally weakly coupled <ul style="list-style-type: none"> ▪ Liquid-liquid interaction with one active layer flow (e.g. uni-directional submerged gravity current in the ocean). ▪ Gas-gas interaction with one active layer flow (e.g. uni-directional submerged gravity current in the atmosphere).
Immiscible	<ul style="list-style-type: none"> ▪ Liquid-liquid interaction with two active layer flows (e.g. bidirectional oil-spill through the opening of a ship). 	<ul style="list-style-type: none"> ▪ Gas-liquid interaction with one active layer flow (e.g. open channel gravity-driven flow without the wind effect).

The aim of this study is to investigate stratified flows, specifically, in which the density jump between layers is small. Some examples of such uni- and bidirectional stratified flows in the natural environment (NE) and built environment (BE) are described in Table i-2.

Table i-2. Uni- and bidirectional stratified flows of miscible and immiscible fluids in the natural environment (NE) and built environment (BE) for small-density-difference cases.

	Unidirectional stratified flow	Bidirectional stratified flow
Miscible	<ul style="list-style-type: none"> ▪ Stratified flow of water in an estuary with a dynamically blocked upper or lower layer (NE). ▪ Pressure-driven air flow through the opening of a building envelope (BE). 	<ul style="list-style-type: none"> ▪ Exchange flow of water in a strait (NE). ▪ Exchange flow of air in a valley (NE). ▪ Exchange flow of air through the opening of a building envelope (BE).
Immiscible	<ul style="list-style-type: none"> ▪ Pressure-driven oil flow through a hole in a damaged tanker (BE). 	<ul style="list-style-type: none"> ▪ Exchange flow of oil and water through a hole in a damaged tanker (BE).

The hydrostatic pressure difference between the connected fluids at a submerged opening in a built environment determines the surface-slope-driven (pressure-head-difference-driven) flow conditions. In the natural environment, for instance in a river estuary, the unidirectional stratified flow with the interface between saline and fresh water layers, can be driven by buoyancy. In the built environment, for instance in the submerged opening of an enclosure, the unidirectional stratified flow can be driven by the excess hydrostatic pressure. However, in both natural and built environment cases, the bidirectional stratified flow can be buoyancy driven.

Natural environment

Stratified flows of miscible fluids are common in the ocean and atmosphere. Flows with an abrupt horizontal density front occur, for instance, in estuaries, which are the connections between salt- and freshwater sources. Fresh riverine water inflow into the sea is a good example of gravity-driven unidirectional flow. However, when river water meets seawater in man-made deep river inlets, a bidirectional stratified flow can exist (Arita and Jirka, 1987). The near-bottom dense saline water intrudes into the estuary beneath the outflowing river water and thus flows against the direction of surface less-dense water. For instance, the archival field measurements of the Pärnu River estuary analysed by Laanearu et al. (2010) reveal the occurrence of such stratified bidirectional flows under variable sea-level situations and river-outflow conditions. In Figure i-2 the camera image of gravity currents of the saline water intruding beneath the fresh water across the submerged trapezoidal sill before flowing down the inclined slope into the “river” basin (see PIV image of velocity field of this gravity current in Carr et al., 2015).

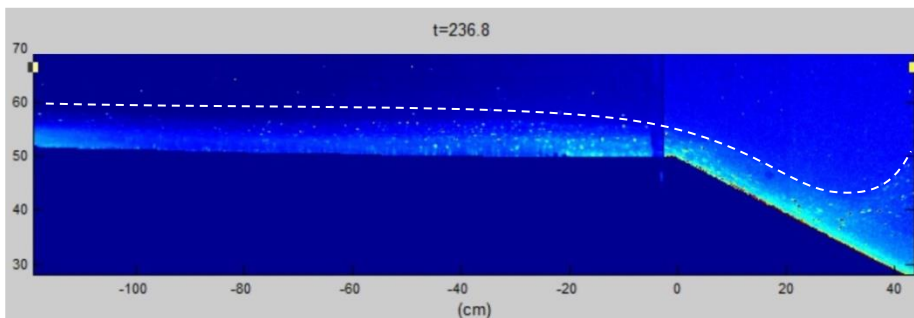


Figure i-2. Gravity current across the submerged sill (Carr et al., 2015). The data source: Experimental program, funded under the EU FP7 Hydralab IV Initiative, conducted in the largest rotating platform in the world; the LEGI Coriolis Platform II in Grenoble.

Similar phenomena occur in sea straits, which are naturally-formed narrow waterways connecting two larger water bodies. Observations and experiments of the two-layer water exchange through the Bosphorus Strait, first published in the 1681 book by Marsigli (Gill, 1977), show that the less-dense Black Sea water flows along the surface over the denser Mediterranean water inflow.

Air flow between mountain valleys is another stratified flow example in the natural environment, which represents miscible fluid flows. The density difference occurs due to the solar heating and cooling of mountain slopes, leading to upslope and downslope flows. In this situation, a layer of dense air adjacent to the ground is overlain by less-dense air, and usually the interface between layers is made visible by clouds.

Built environment

Stratified flows are common phenomena in built environment systems. Different from natural environment settings, i.e. straits and mountain valleys, the stratified flows in built environment systems are on a smaller scale and often originate in flows through submerged openings connecting two physically separated environments. The excess hydrostatic pressure situation is typical for built environment enclosures such as liquid storage tanks and rooms inside buildings.

The built environment comprises several liquid storage systems where stratified flows are possible. Oil spills from oil tankers are one example that attracts attention

(Figure i-3i), since tanker accidents such as collisions and groundings are one of the major types of accidents in maritime transportation leading to significant environmental and economic consequences (Ehlers, 2009). When the tanker hull is breached, the inner cargo oil is exposed to the outside and can cause pollution of the marine environment. The density difference is due to different fluids, here, oil and seawater, which represent the stratified flow of two immiscible liquids. The hydrostatic pressure difference at the opening relates to the liquid column depths on both sides of the hole. If the pressure is hydrostatically unbalanced at hole level, unidirectional stratified flow occurs, before the bidirectional stratified flow takes place. According to the basic principle of stratified flows where the density is greater in the bottom layer, the less-dense oil flows in the upper-layer against the direction of the denser seawater in the lower-layer. This process lasts until the system is stable, that is, until the oil in the vertically-fixed tank is replaced by the inflowing seawater to the upper lip of the hole.

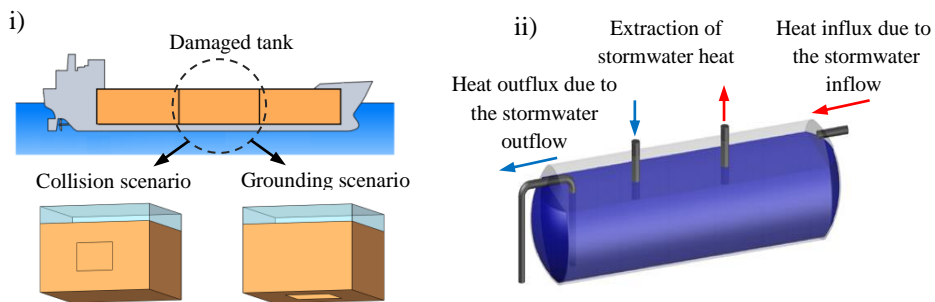


Figure i-3. Stratified flows of built environment storage systems. i) Oil spill from a damaged tanker. ii) Storage tank of a stormwater collection and domestic-water heating integrated system.

Storage tanks in stormwater and domestic-water heating integrated system is an example of stratified flows of miscible liquids, whose density difference arises from temperature differences (Figure i - 3ii). Maintaining stable stratification in a storage tank allows the maximising of the operation of the collected stormwater imposed for external domestic-water heating applications. A displacement flow takes place due to buoyancy forces since the warmer stormwater is usually supplied from the upper opening and the colder water is extracted near the bottom. The liquid flow through the tank may be thought of as generally horizontal due to unidirectional stratified inflow and outflow. Liquid and heat cross-flow is possible due to the formation of vertical stratification, horizontal flow arrangement, and location of the heat extraction connections in the tank. The greater the temperature difference and distance between inflow and outflow, the greater the increase in density with depth and the greater the vertical gradient.

Natural ventilation through open windows and doorways is one prevalent example of stratified flow of miscible fluids. If a window is opened between a sealed room and an open space, the buoyancy sets up an exchange flow through the opening (Figure i-4i). The density difference is mainly due to a temperature difference between indoor and outdoor environments, however, the exchange flow relates to humidity, pollutants, and pressure difference as well, which are important in a variety of ventilation contexts. Another example is mechanical ventilation in buildings, which can be described as a man-made buoyancy-driven exchange flow (Figure i-4ii). The interface

between fresh and contaminated air layers in a room is intentionally elevated by the excess fresh air supply. This results in the excess pressure condition between the indoor and outdoor environments, and causes unidirectional outflow of the indoor air through the open window. The bidirectional stratified flow follows when the unidirectional stratified flow spins down in the balanced situation, which is established at the level of the opening. Large temperature gradients and different substance concentrations in layers, for instance in hot smoke movement during a building fire, can influence the outflow volumes and the durations of uni- and bidirectional stratified flows.

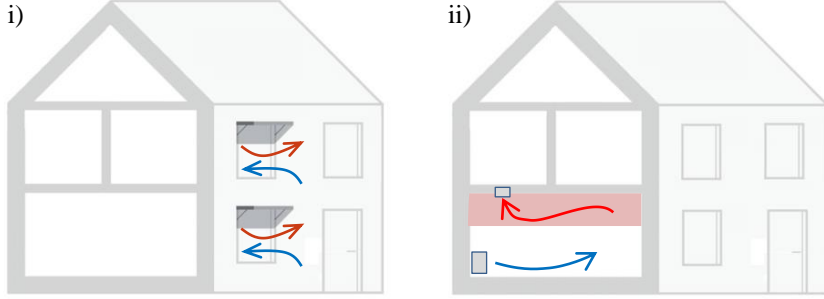


Figure i-4. Buoyancy-driven flows of miscible fluids. i) Bidirectional stratified flow through open windows. ii) Unidirectional stratified flow in a room with displacement ventilation.

Internal-flow head

The internal-flow energy function, Equation (4), has been considered as an inviscid flow case. In the study of coupled two-layer flow, the internal-flow energy head (E_{int}) at a section is defined as:

$$E_{int} = \frac{E_2 - E_1}{\rho_2 g'}. \quad (5)$$

In the case of frictional flow, the layers' energy difference ($E_2 - E_1$) is not conserved (Figure i-5). According to Cuthbertson et al. (2017), the internal-flow head loss due to the dissipative changes of E_1 and E_2 over a flow section between points 1 and 2 is given as:

$$\Delta E_{int} = \left(\frac{E_{21} - E_{11}}{\rho_2 g'} \right) - \left(\frac{E_{22} - E_{12}}{\rho_2 g'} \right) = \left(\frac{E_{21} - E_{22}}{\rho_2 g'} \right) + \left(\frac{E_{12} - E_{11}}{\rho_2 g'} \right). \quad (6)$$

The internal-flow energy head loss is considered to be positively defined i.e. $\Delta E_{int} > 0$, when the difference in the layers' energy is considered to occur along the flow i.e. $E_{21} - E_{22} > 0$ and $E_{12} - E_{11} > 0$.

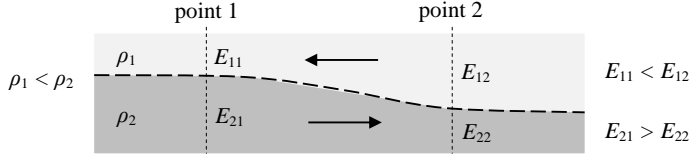


Figure i-5. Sketch of two-layer frictional flow with a density jump between layers. The internal-flow energy head loss ΔE_{int} is positive when the flow in the fluid layers is in opposite directions, as in the case of buoyancy-driven flow.

Sudden changes of topography in a natural environment can be viewed as a source of stratified flow disturbances and turbulent energy transfer into the flow domain, which causes a series hydrodynamic phenomena and exchange mixing between layers (Ravlic and Gjetvaj, 2003). However, in built environment systems, a fluid passing through a submerged opening, such as an open window, will experience a drop in pressure across the opening, thus for real flows it is important to account for the effects of shear stresses. For this purpose, in practical applications, where the continuous calculation of uni- and bidirectional flows is performed, the discharge coefficient depends on the Reynolds number for an opening. This is a useful parameter for determining the irrecoverable losses associated with the "flow resistance" due to boundary layers. The overall effect of shear stresses marginally reduces the flowrate through openings. The flow resistance in the stratified unidirectional flow is due to flow separation in the opening, i.e. boundary stress. However, in the stratified bidirectional flow, the flow resistance is due to both boundary stresses and interfacial stresses. Shear stresses in the bidirectional stratified flow can also be present due to mixing (miscible fluids case) and emulsification (immiscible fluids case) between the counter-flowing layers. The non-dimensional bulk Richardson number that characterises the stability of stratified flows can be useful in determining the amount of mixing in hydraulically controlled two-layer exchange flows. The bidirectional stratified flow can be considered stable when the depths and velocities of both layers satisfy the condition (Armi, 1986):

$$\frac{(u_{upper} - u_{lower})^2}{g'(d_{upper} + d_{lower})} < 1. \quad (7)$$

Generally, the discharge coefficients are found from experiments through the ratio of actual discharge to the theoretical discharge, and the values range between 0 (blocked flow case) and 1 (inviscid flow case).

In addition to losses associated with the flow separation at hole edges and the dynamic interaction of superimposed layers (e.g. mixing), fluids' physical properties, such as density and viscosity, vary when fluids originating from different environments at different temperatures meet. It is important to consider the heat-exchange modified shear-induced mixing processes in stratified flows. One particular goal of the hydraulic modelling presented in this thesis is to investigate the sensitivity of uni- and bidirectional stratified flows with different temperature gradients. The effect of heat-exchange affects both flow cases i.e. uni- and bidirectional stratified flows, and can be parametrized by the introduction of the thermal expansion coefficient α (see

Publication III). The effect of interfacial mixing between counter-flowing layers, however, relates to bidirectional flow only and can be parametrized by the fluid flow-rate reduction parameter f (see Publication III). Furthermore, in the presence of bottom heat sources in the enclosure and due to the heat losses through boundaries, the thermal stratification in the enclosure may be unstable. Unstable stratification with decreasing density with depth causes intense vertical exchange and mixing inside the enclosure.

State of the art

The internal-flow theory was initially established for constricted stratified flows with interface in natural settings such as straits (Whitehead et al., 1974), which can be considered to be "conditionally weakly" coupled flow. The internal-flow energy function was introduced by Armi (1986), Armi and Farmer (1986), and Farmer and Armi (1986), who presented analytical treatments for "strongly" coupled two-layer flow by introducing the composite Froude number and exchange flow solutions. Even though the theory was proposed for incompressible fluid layers with constant density and negligible vertical velocities, it has been demonstrated that it accurately and qualitatively describes the behaviour of stratified fluids in motion (Dalziel, 1988; Dalziel and Lane-Serff, 1991; Cuthbertson et al., 2006).

Dalziel (1988) presented the first attempt to apply the two-layer hydraulic model of flow through a rectangular cross-section to the buoyancy-driven exchange flow through an opening. He reported that a doorway that opens up into a wide and high room can be treated as a rectangular channel with an inverted sill and symmetrical contraction in width. This was confirmed in the later paper of Dalziel and Lane-Serff (1991) who demonstrated that the main features of doorway exchange flow can be described in terms of the two-layer hydraulic theory. This has inspired the employment of internal-flow hydraulic theory for submerged openings in this thesis. An exchange flow through a rectangular doorway or window can be regarded, according to Dalziel (1990), as a two-layer flow in a channel with a sharp contraction in height and width, representing a "strongly" coupled flow of miscible fluids through a submerged opening. This complies also with Armi and Farmer (1986), who pointed out that variations in the channel width are felt equally by both layers, whereas variations in the depth (unless such variations are symmetric in both top and bottom boundaries, e.g. a window) are felt directly by only one of the two layers (e.g. a doorway).

Dalziel (1991) offered an alternative formulation of the two-layer hydraulic problem based on the functional formalism of Gill (1977). He derived a simple relationship between the composite Froude number and the hydraulic functional, and applied it to the flow through a contraction in width and to flow over a simple sill (Dalziel 1991, 1992). He outlined that the derivation, features, and solution process may also be applied to channels of non-rectangular cross-sections, which supports the derivation of hydraulic-theory solutions for circular openings herein. A more generalised approach to two-layer exchange flow was proposed by Laaneau and Davies (2007) who extended the treatment of a rectangular channel to consider the effects of channel geometry. According to their analysis, the effects of channel cross-sectional geometry can be quantified satisfactorily in terms of a shape parameter ξ , which represents the ratio of the cross-sectional area of the channel in terms of the equivalent rectangular channel having the same values of width and depth. Making use of their hydraulics model for

exchange flow for the quadratic constrictions makes it possible to determine the volumetric flow rates for different non-rectangular openings.

There exist quite a few hydraulic models for immiscible stratified flows in submerged openings. Published models for oil outflow calculations from leaking tanks (e.g. Simecek-Beatty et al., 2005; Tavakoli et al., 2008, 2010, 2011) are scarce and mostly limited to calculating the final outflow volume, with little or no consideration of variations in the outflow dynamics with time. Stratified flows are usually modelled as a homogeneous layer with inviscid liquids subjected to a hydrostatic pressure distribution. For incompressible, inviscid, and steady flow, the Bernoulli approach is widely used. For instance, in the work of Tavakoli et al. (2008, 2010) the Bernoulli principle was used in the development of simplified analytic models, which rely on basic assumptions introduced by Fannelop (1994). However, in the Bernoulli approach, coupling between superimposed layers can be considered "weak", and thus a simplified treatment of the internal-flow energy complicates the modelling for two-layer stratified flow (Armi, 1986). Researchers have addressed this issue by using numerical modelling (e.g. CFD), which is one possible method. The numerical simulation was implemented in further work of Tavakoli et al. (2010, 2012) for the verification of proposed simple models. The performance of experiments on the current topic is the second method that is required in order to validate the hydraulic models. The oil and water experiments conducted by Tavakoli et al. (2011) have provided valuable insights into the dynamics of immiscible fluid stratified flows. However, the main limitation of verifying the performance of their proposed models can be related to the unfortunate circumstances due to differences in opening shape. While the experimental results were published for circular opening (Tavakoli et al., 2011), the model was developed for rectangular and triangular openings (Tavakoli et al., 2012). Thus, an application of the internal-flow hydraulic theory, that is somewhat different in approach, is employed in the case of stratified flow through submerged circular opening, which can be verified according to the published experimental results.

Several researchers have used theoretical analysis based on the plume theory, presented by Morton et al. (1956), that is found to be practical in the field of modelling the buoyancy-driven airflows in building ventilation (Linden et al., 1990; Hunt and Linden, 1999, 2001; Lin and Linden, 2002). Their approach is useful for investigating the evolution of the flow field in the ventilated enclosures driven by a buoyant plume due to localised sources of heating or cooling in an enclosure. In this specific field, the attention is mostly drawn to investigating the internal conditions, and not so much on the dynamics of stratified flows in submerged openings. Small-scale salt-water experiments are commonly used among researchers to model the buoyancy-driven exchange flows of miscible fluids (e.g. Thomas et al., 2008; Dalziel and Lane-Serff, 1991; Linden et al., 1990), and Computational Fluid Dynamics is used for airflow simulations and visualisation in buildings (e.g. Fang et al., 2012).

Motivation and objectives

One purpose of this thesis is to propose hydraulic-theory solutions for uni- and bidirectional stratified flows with small density differences through submerged openings of built environment enclosures. It is a topic of interest in decision-making processes in a number of stratified flow problems in the built environment (Gualtieri and Mihailovic, 2012). This thesis comprises three pilot studies that are associated with four practical motivations.

Firstly, fast calculations of oil outflow volumes and spill durations are necessary for planning and preparing effective response strategies to minimise adverse environmental impacts of tanker accidents. Secondly, the growing demand for energy in cities, in combination with national renewable energy targets (Directive 2009/28/EC), have precipitated the search for solutions for the development of energy from on-site low-temperature water sources, the employment of which may increase the energy efficiency of buildings. Thirdly, increasing concerns about energy efficiency have led to renewed interest in the use of operable windows in buildings. To make significant progress toward the integration of operable windows, it is important to be able to understand the dynamics of temperature-stratified flows. Fourthly, built environment systems require practical solutions for engineering purposes due to the complexity of systems and lack of specific experimental investigations. Optimisation of process parameters allows the implementation of the theoretical models to deal with real fluid flows. Additionally, the optimisation of integrated system parameters makes it possible to find optimal dimensions for an efficient design.

The following objectives are proposed:

1. Develop a methodology for hydraulic formulae of uni- and bidirectional stratified flows through the submerged opening using the internal-flow hydraulic theory.
2. Develop hydraulic-theory solutions for stratified flows through the submerged rectangular opening using the internal-flow hydraulic theory. Consider shape factor in the analytical formula for the volumetric flow rate of bidirectional stratified flow through a non-rectangular opening.
3. Develop hydraulic-theory solutions for stratified flows through the submerged circular opening using the internal-flow hydraulic theory.
4. Implement GA for determining process parameters such as the discharge coefficients and emulsion density for unidirectional stratified flow through submerged openings. Develop a single-objective function with three design variables.
5. Determine the discharge coefficients for submerged circular openings from the experimental verification of the uni- and bidirectional volumetric flow rate solutions.
6. Modify the uni- and bidirectional volumetric flow rate solutions to account for the emulsification and heat-exchange for different temperature gradients.
7. Employ GA for the optimisation of system parameters, which are related to the engineering design. Develop a single-objective function with two design variables.

Limitations

This thesis is limited for the following conditions:

1. The proposed hydraulic models are derived for quasi-stationary conditions, since they provide satisfactory results, thus, can be adapted to the changing hydrostatic pressure.
2. The proposed approach is applicable for strongly-coupled stratified flows with small density difference, at low velocities, and under small pressure changes.
3. The hydraulic models are essentially limited for submerged openings.
4. The temperature changes due to the effect of heat exchange, which causes significant changes in the fluids density, may result in flow conditions (foaming, freezing) that are not applicable for hydraulically-driven flows.

5. For flow through an opening, the discharge coefficients are also dependent on the contraction and opening shape, and thus for specific cases experiments or numerical solitons should be used to determine the flowrate.

Abbreviations

ADSAM	Accidental Damage and Spill Assessment Model
BONUS	Strategic and Operational Risk Management for Wintertime
STORMWINDS	Maritime Transportation System
CFD	Computational Fluid Dynamics
GA	Genetic Algorithm
GRST	Guided Random Search Technique
HVAC	Heating, Ventilation and Air Conditioning
MIMIC	Minimizing Risks of Maritime Oil Transport by Holistic Safety Strategies
SWMM LID	Storm Water Management Model with Low Impact Development controls

Symbols

A	area of opening, m^2
A_{lower}	lower layer cross-sectional area (denser fluid), m^2
A_{upper}	upper layer cross-sectional area (less-dense fluid), m^2
B_{lower}	Bernoulli head of lower layer, m
B_{upper}	Bernoulli head of upper layer, m
C_d	discharge coefficient, 1
d_0	maximum depth of opening, m
d_{lower}	lower-layer depth (denser fluid), m
d_{upper}	upper-layer depth (less-dense fluid), m
E_{int}	internal-flow energy head, m
E_{lower}	Bernoulli function of lower layer, Pa
E_{upper}	Bernoulli function of upper layer, Pa
f	fluid flow-rate reduction parameter, 1
Fr_{lower}	lower-layer densimetric Froude number, 1
Fr_{upper}	upper-layer densimetric Froude number, 1
G	composite Froude number, 1
g	acceleration due to the gravity, m s^{-2}
g'	reduced gravity, m s^{-2}
h	height of opening lower lip, m
H_i	fluid total depth inside enclosure, m
H_o	fluid total depth outside enclosure, m
k	head-loss coefficient, 1
K	volume flux parameter, m^5
p_0	pressure at opening upper lip, Pa
p_{air}	air pressure at sea surface (atmospheric pressure), Pa
p_{gas}	gas pressure above fluid level inside enclosure, Pa
p_i	internal pressure at opening, Pa
p_o	external pressure at opening, Pa
q	ratio of upper- and lower-layer flow rates (flow-rates-ratio), 1
Q_0	unidirectional volumetric flow rate, $\text{m}^3 \text{s}^{-1}$
Q_{lower}	lower-layer volumetric flow rate (denser fluid), $\text{m}^3 \text{s}^{-1}$
Q_{upper}	upper-layer volumetric flow rate (less-dense fluid), $\text{m}^3 \text{s}^{-1}$
r	ratio of upper- and lower-layer densities ($r = \rho_{\text{upper}} / \rho_{\text{lower}}$), 1
S	fluid surface area in enclosure (inner fluid), m^2
T_{bi}	bidirectional outflow duration (inner fluid), s
T_{total}	total outflow duration (inner fluid), s
T_{uni}	unidirectional outflow duration (inner fluid), s
u_0	unidirectional velocity, m s^{-1}
V_{bi}	bidirectional outflow volume (inner fluid), m^3
V_{total}	total outflow volume (inner fluid), m^3

V_{uni}	unidirectional outflow volume (inner fluid), m^3
u_{lower}	lower-layer velocity (denser fluid), $m\ s^{-1}$
u_{upper}	upper-layer velocity (less-dense fluid), $m\ s^{-1}$
w_0	maximum width of opening, m
w	interfacial width, m
w_{lower}	lower layer width (denser fluid), m
w_{upper}	upper layer width (less-dense fluid), m

Greek symbols

α	thermal expansion coefficient, 1
ΔE_{int}	internal-flow head loss, m
Δl	fluid depth above opening upper lip inside enclosure (inner fluid), m
Δl_0	fluid depth above opening upper lip outside enclosure (outer fluid), m
ξ	shape factor of opening, 1
Π	sum on the local head-loss coefficients, 1
ρ_1	fluid density inside enclosure (less-dense fluid), $kg\ m^{-3}$
ρ_2	fluid density inside enclosure (denser fluid), $kg\ m^{-3}$
ρ_l	fluid density inside enclosure (inner fluid), $kg\ m^{-3}$
ρ_{lower}	lower-layer fluid density (denser fluid), $kg\ m^{-3}$
ρ_o	fluid density outside enclosure (outer fluid), $kg\ m^{-3}$
ρ_{upper}	upper-layer fluid density (less-dense), $kg\ m^{-3}$

1 Theory of internal-flow hydraulics

1.1 Theoretical framework

The internal-flow hydraulic theory has been applied to deal with stratified flows through submerged openings of built environment enclosures. In natural settings, the stratified flows characterised by the presence of a liquid-gas interface (free surface) are under atmospheric pressure. The pressure at a free surface can be considered as constant and, thus, this is what determines the hydrostatic pressure in open-channel flow (Çengel and Cimbala, 2010). There is no such restriction in flows through submerged openings since the free surface is absent, or is located above the upper lip of the submerged opening. Though the stratified flow of fluids completely fills a submerged opening, it is possible to substitute the free surface with the hydrostatic pressure difference at the level of the upper lip of an opening. The driving forces for free surface flows are the elevation difference and the density gradient. For flows through submerged openings, on the other hand, there may be an additional driving force due to excess hydrostatic pressure on either side of an opening. In such cases, a unidirectional stratified flow takes place until excess pressure reduces to equilibrium.

When two fluids of slightly different densities are connected at a submerged opening, buoyancy-driven flow can take place. Through the opening, two types of stratified flows, i.e. unidirectional and bidirectional, are possible, which can be related to two "key parameters": the difference between the pressures on both sides of the opening and the difference in fluid density. If the excess pressure is present inside of the enclosure (as in many practical applications), unidirectional fluid outflow takes place until equilibrium is established. If the enclosure has substantially lower pressure inside, outside fluid tends to enter the enclosure as long as the highest point of the opening is below the hydrostatic balance level. However, under balanced inside and outside hydrostatic pressure, the internal flow through a submerged side opening is bidirectional, with the upper-layer (less-dense) fluid flowing against the direction of the lower-layer (denser) fluid. It should be noted that in the case of excess hydrostatic pressure in the bottom opening of an enclosure, unidirectional stratified flow is mainly possible.

In the internal-flow hydraulic theory, two geometrical configurations of submerged openings are introduced: rectangular and circular. In rectangular openings, the flow has constant width and thickness, while in circular openings the flow width varies with depth. The internal-flow hydraulic theory applications to the two-layer exchange flow in a quadratic-type channel with maximum width at the surface was developed by Laanearu and Davies (2007).

An opening is considered either in the i) side wall or ii) bottom of built environment enclosure. It is expected that the opening is the sole area for fluid exchange between the inner and outer environments. The heat exchange between environments is neglected and the temperatures of the inner and outer environments are initially considered identical. Also, it is assumed that there is no heat transfer by conduction through the walls of an enclosure, implying that all the walls, bottom, and ceiling are insulated. Mixing of fluids (i.e. emulsification in case of immiscible fluids) between counter-flowing layers is also initially ignored, and densities in each layer are assumed to be that of the environments from which the fluid originates. The internal-flow

hydraulic model is extended to account for the effects of emulsification and heat exchange in the pilot study of oil spills in Chapter 2.1.

The Coriolis force is important in many geophysical applications of the internal-flow hydraulic theory (Laanearu et al., 2000). In this thesis, stratified flows through submerged openings of built environment enclosures are dealt with as flows without background rotation, therefore, the effects of the Coriolis force are ignored. A small aspect ratio corresponding to situations where the horizontal length scale of flow is much greater than the vertical length scale, allows usage of shallow-water approximation in fluid mechanics. This condition allows the application of the shallow-water equations, under which the pressure is assumed to be hydrostatic within each layer of bidirectional stratified flow in channels (Dalziel, 1991).

In simple fluid applications, the flow is assumed to be immiscible, steady, inviscid, incompressible, and hydrostatic. In a density-stratified fluid, gravity can play a significant role without the presence of a free surface (Kundu et al., 2012). In the internal-flow hydraulic theory, the stratified flows can be parametrized in terms of the densimetric Froude number (Fr) for each layer (Armi, 1986), thus for layer i it is expressed as:

$$Fr_i^2 = \frac{u_i^2}{g' d_i}, \quad (8)$$

where u_i is the flow velocity (m s^{-1}), and d_i is the layer thickness (m). For single-layer flows the flow is critical when the $Fr^2 = 1$. For two-layer flows the degree of exchange between environments containing fluids with different densities is regulated by the two fluid layers (Cuthbertson et al., 2006). According to Armi (1986), the appropriate non-dimensional number for parametrizing two-layer flows with a free surface is a composite Froude number that is defined as:

$$G^2 = Fr_{upper}^2 + Fr_{lower}^2 - (1-r)Fr_{upper}^2 Fr_{lower}^2. \quad (9)$$

An internal hydraulic control is known to form at a location for which the flow is critical, i.e. $G^2 = 1$ (Farmer and Armi, 1986). The critical condition distinguishes the super-critical flow from sub-critical flow in an exchange flow (Laanearu and Davies, 2007).

1.2 Unidirectional flow

In the case of excess hydrostatic pressure, corresponding to the inside and outside pressure-head differences at the submerged opening level, stratified flows through the submerged opening are unidirectional (Figure 1-1). Fluid outflow occurs when the internal pressure (p_i) exceeds the external pressure (p_o) at the opening level. Excess hydrostatic pressures in liquid-liquid systems can also result from a relatively high inner fluid level (Δl) and gas pressure (p_{gas}) in a non-vented enclosure, as compared to the fluid level (Δo) and gas pressure (p_{air}) outside. Here, the density of the inner fluid (ρ_i) is considered to be slightly lower than the outer fluid (ρ_o), i.e. $(\rho_o - \rho_i)/\rho_o \ll 1$.

It should be noted that, in the case of a bottom opening, the unidirectional stratified flow finishes when the hydrostatic balance is attained at the level of the bottom opening.

1.3 Bidirectional flow

In the case of a hydrostatically-balanced situation at the level of the opening, and small density difference between inner (ρ_I) and outer (ρ_O) fluids, the stratified flows through the submerged side opening are bidirectional. During the buoyancy-driven exchange flow, the upper-layer less-dense fluid (ρ_{upper}) flows against the direction of the lower-layer denser fluid (ρ_{lower}) through a submerged opening. The bidirectional stratified flow results in a changing interface that separates the less-dense (ρ_1) and denser (ρ_2) fluids in an enclosure. If an enclosure is initially filled with less-dense fluid ($\rho_I < \rho_O$), then the interface ascends towards the upper lip of the opening due to lower-layer denser fluid inflow (Figure 1-2). In the contrary case ($\rho_I > \rho_O$), the interface descends towards the lower lip of the opening due to upper-layer less-dense fluid inflow. The bidirectional stratified flow lasts until the system is stable, that is, the fluid in the enclosure is replaced by the inflowing outer fluid to the corresponding interface level.

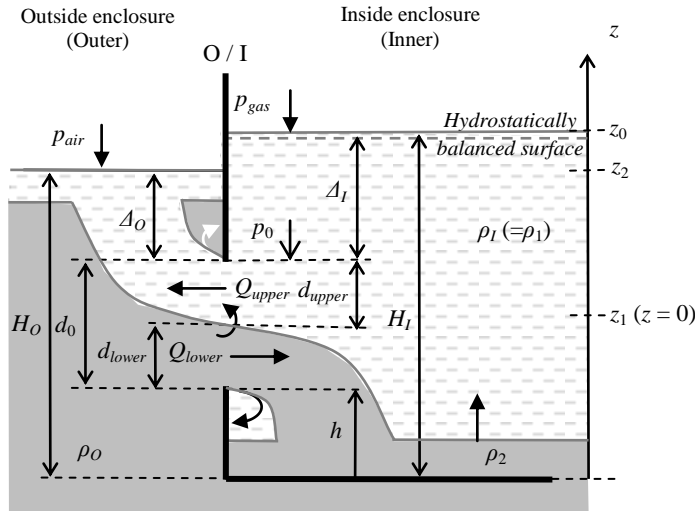


Figure 1-2. Sketch of bidirectional stratified flow through the submerged side opening with less-dense fluid inside the enclosure, and notations.

A barotropic net exchange flow is possible during a transitional stage between the unidirectional and following bidirectional stratified flows. However, this transitional stage can be essentially ignored in a vertically-fixed enclosure, which is apparent from the experimental results by Tavakoli et al. (2011). Apparently, the barotropic-flow component will compensate the fluid mass inside the enclosure to maintain the difference between inner and outer liquid surfaces that is required for a hydrostatic balance at the level of a vertically-moving side opening. That, however, may be considered as a topic of a future study, where CFD modelling could be useful for solving

the fluid engineering problems of stratified flows through an opening of a vertically-moving enclosure.

1.3.1 Rectangular opening

In Figure 1-3 a flow configuration scheme is presented for buoyancy-driven exchange flow through a submerged side opening of rectangular shape, connecting fluids with small density difference.

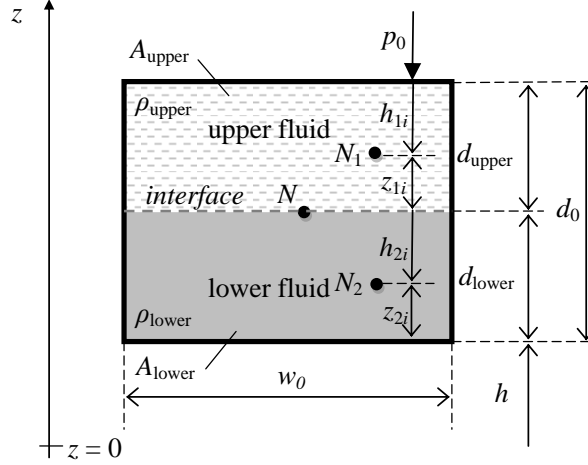


Figure 1-3. Sketch of a bidirectional stratified flow through the side opening of rectangular shape with less-dense fluid inside the enclosure, and notations.

Herein, the flow in the upper and lower layers represent the less-dense ($\rho_l = \rho_{upper}$) and denser ($\rho_o = \rho_{lower}$) fluids, respectively. These layers have corresponding exchange flow rates (see Figure 1-2):

$$Q_{upper} = u_{upper} A_{upper} , \quad (13)$$

$$Q_{lower} = u_{lower} A_{lower} . \quad (14)$$

The rectangular opening area ($A = w_0 d_0$) is related to the areas of the layered flows as:

$$A = A_{upper} + A_{lower} . \quad (15)$$

The total thickness (d_0) for two-layer flow through an opening with changing layer thicknesses, d_{upper} and d_{lower} , is:

$$d_0 = d_{upper} + d_{lower} . \quad (16)$$

The degree of exchange is regulated by the total thickness of the two fluids (Cuthbertson et al., 2006). For changing layers' thicknesses, the maximum width of opening, interfacial width, and upper- and lower-layer widths of the two-layer flow are constant in a rectangular opening ($w_0 = w = w_{upper} = w_{lower} = \text{const.}$).

In the case of the two-layer exchange flows the Bernoulli heads (B_{upper} and B_{lower}) for both layers at the level of the interface (point N in Figure 1-3), are expressed as:

$$B_{upper} = \frac{u_{upper}^2}{2g} + \frac{p_0 + \rho_{upper} g d_{upper}}{\rho_{upper} g} + d_{lower} + h, \quad (17)$$

$$B_{lower} = \frac{u_{lower}^2}{2g} + \frac{p_0 + \rho_{upper} g d_{upper}}{\rho_{lower} g} + d_{lower} + h. \quad (18)$$

The Bernoulli head of particular layer yields the constant for any point N_1 within the upper homogeneous fluid layer ($0 \leq h_{1i} \leq d_{upper}$ and $z_{1i} = d_{upper} - h_{1i}$), and for any point N_2 within the lower homogeneous fluid layer ($0 \leq h_{2i} \leq d_{lower}$ and $z_{2i} = d_{lower} - h_{2i}$). The hydrostatic pressure of the two layers can be expressed in terms of the layers' thicknesses:

$$d_{upper} = z_{1i} + h_{1i} = z_{1i} + \frac{p_{1i}}{\rho_{upper} g}, \quad (19)$$

$$d_{lower} = z_{2i} + h_{2i} = z_{2i} + \frac{p_{2i}}{\rho_{lower} g}, \quad (20)$$

where z_{1i} and z_{2i} are the fluid thicknesses (m) below the points N_1 and N_2 in the corresponding fluid layers, respectively, and p_{1i} and p_{2i} are the respective hydrostatic pressures (Pa) at these points. The Bernoulli functions for the upper and lower layers, respectively, can be expressed as:

$$E_{upper} = \frac{1}{2} \rho_{upper} u_{upper}^2 + p_0 + \rho_{upper} g (d_{upper} + d_{lower} + h), \quad (21)$$

$$E_{lower} = \frac{1}{2} \rho_{lower} u_{lower}^2 + p_0 + \rho_{upper} g d_{upper} + \rho_{lower} g (d_{lower} + h). \quad (22)$$

In the study of strongly-coupled two-layer flows, corresponding to the small density difference i.e. $(1 - r) \ll 1$ between connected fluids, the internal-flow energy head (E_{int}) for a submerged opening is the Bernoulli sum for layers at the opening, and is defined as:

$$E_{int} = \frac{E_{lower} - E_{upper}}{\rho_{lower} g'} = \left(\frac{u_{lower}^2}{2g'} - \frac{\rho_{upper}}{\rho_{lower}} \frac{u_{upper}^2}{2g'} \right) + (d_{lower} + h), \quad (23)$$

where the reduced gravity g' in the two-layer exchange flow is defined as:

$$g' = g(1 - r) = g \left(1 - \frac{\rho_{upper}}{\rho_{lower}} \right). \quad (24)$$

Note that in the case of $(1 - r) \ll 1$, the internal-flow energy head (Equation 23) becomes:

$$E_{int} = \left(\frac{u_{lower}^2}{2g'} - \frac{u_{upper}^2}{2g'} \right) + d_{lower} + h, \quad (25)$$

The flow velocities of the upper and lower layers are defined as the flow rates per flow area of each of the layers:

$$u_{lower} = \frac{Q_{lower}}{d_{lower} w}, \quad (26)$$

$$u_{upper} = \frac{Q_{upper}}{d_{upper} w} = \frac{Q_{upper}}{(d_0 - d_{lower}) w}. \quad (27)$$

The volume flux parameter K is determined by the flow rate in the lower layer accordingly:

$$K = \frac{Q_{lower}^2}{2g'}, \quad (28)$$

and the dimensionless flow-rates-ratio parameter, i.e. the ratio between the upper- and lower-layers' discharges, can be expressed as:

$$q^2 = \frac{Q_{upper}^2}{Q_{lower}^2}. \quad (29)$$

By implementing Equations (26), (27), (28), and (29), the internal-flow energy head (Equation 25) becomes:

$$E_{int} = \frac{K}{w^2} \left(\frac{1}{d_{lower}^2} - \frac{q^2}{(d_0 - d_{lower})^2} \right) + d_{lower} + h. \quad (30)$$

The non-dimensional form of the internal-flow energy head for the two-layer exchange flow through the submerged opening is:

$$E_{int}^* = \frac{K^*}{w^{*2}} \left(\frac{1}{d_{lower}^{*2}} - \frac{q^2}{(1 - d_{lower}^*)^2} \right) + d_{lower}^* + h^*, \quad (31)$$

where the following quantities made non-dimensional by the total two-layer thickness (d_0) are used:

$$E_{int}^* = \frac{E_{int}}{d_0}; \quad K^* = \frac{Q_{lower}^2}{2g' d_0^5}; \quad w^* = \frac{w}{d_0}; \quad d_{lower}^* = \frac{d_{lower}}{d_0}; \quad h^* = \frac{h}{d_0}.$$

Functional approach

For the Bernoulli functions of the upper and lower layer, respectively, the function can be written by expressing the velocity in the layers by the flowrate:

$$J_1 = \frac{Q_{upper}^2}{2d_{upper}^2 w^2} + \frac{p_0}{\rho_{upper}} + d_{upper}g + (d_{lower} + h)g - E_{lower}g, \quad (32)$$

$$J_2 = \frac{Q_{lower}^2}{2d_{lower}^2 w^2} + \frac{p_0}{\rho_{lower}} + \frac{\rho_{upper}}{\rho_{lower}} d_{upper}g + (d_{lower} + h)g - E_{lower}g. \quad (33)$$

The Jacobian matrix of all first order partial derivatives of a vector-valued function is used. The critical conditions where the matrix is equal to zero make it possible to solve the following matrix:

$$\begin{vmatrix} \frac{\partial J_1}{\partial d_{upper}} & \frac{\partial J_1}{\partial d_{lower}} \\ \frac{\partial J_2}{\partial d_{upper}} & \frac{\partial J_2}{\partial d_{lower}} \end{vmatrix} = \frac{\partial J_1}{\partial d_{upper}} \frac{\partial J_2}{\partial d_{lower}} - \frac{\partial J_2}{\partial d_{upper}} \frac{\partial J_1}{\partial d_{lower}} = 0. \quad (34)$$

Partial derivatives are solved as:

$$\frac{\partial J_1}{\partial d_{upper}} = -\frac{2Q_{upper}^2}{2d_{upper}^3 w^2} + g = -\frac{u_{upper}^2}{d_{upper}} + g, \quad (35)$$

$$\frac{\partial J_1}{\partial d_{lower}} = g, \quad (36)$$

$$\frac{\partial J_2}{\partial d_{upper}} = \frac{\rho_{upper}}{\rho_{lower}} g, \quad (37)$$

$$\frac{\partial J_2}{\partial d_{lower}} = -\frac{2Q_{lower}^2}{2d_{lower}^3 w^2} + g = -\frac{u_{lower}^2}{d_{lower}} + g, \quad (38)$$

and the critical condition becomes:

$$\left(-\frac{u_{upper}^2}{d_{upper}} + g \right) \left(-\frac{u_{lower}^2}{d_{lower}} + g \right) - g \frac{\rho_{upper}}{\rho_{lower}} \cdot g = 0. \quad (39)$$

By further manipulation:

$$\frac{u_{upper}^2}{d_{upper}} g + \frac{u_{lower}^2}{d_{lower}} g - \frac{u_{upper}^2}{d_{upper}} \frac{u_{lower}^2}{d_{lower}} = g^2 \left(1 - \frac{\rho_{upper}}{\rho_{lower}} \right) = g \cdot g', \quad (40)$$

and by multiplying Equation (40) with $1/gg'$ and substituting the ratio of upper- and lower-layer densities with r , the equation becomes:

$$\frac{u_{upper}^2}{g'd_{upper}} + \frac{u_{lower}^2}{g'd_{lower}} - \frac{u_{upper}^2}{g'd_{upper}} \frac{u_{lower}^2}{g'd_{lower}} (1-r) = 1. \quad (41)$$

According to densimetric Froude' number definitions (cf Armi, 1986) for the upper and lower layer, respectively:

$$Fr_{upper}^2 = \frac{u_{upper}^2}{g'd_{upper}}, \quad (42)$$

$$Fr_{lower}^2 = \frac{u_{lower}^2}{g'd_{lower}}, \quad (43)$$

Equation (41) becomes:

$$Fr_{upper}^2 + Fr_{lower}^2 - Fr_{upper}^2 \cdot Fr_{lower}^2 (1-r) = 1. \quad (44)$$

In the case of $(1-r) \ll 1$, the critical condition for a submerged bidirectional stratified flow is:

$$\frac{u_{upper}^2}{g'd_{upper}} + \frac{u_{lower}^2}{g'd_{lower}} = 1. \quad (45)$$

Maximal flow rate

An essential consideration in the theoretical analyses of the two-layer internal-flow hydraulics is the existence of critical-flow sections. The fully-controlled flow is maximal in the sense that it yields the largest exchange flow rate of any possible flow (Dalziel, 1990). Several sub-maximal flow regimes are made possible by maximising the exchange flow through the opening. The critical-flow solutions corresponding to the sub-maximal flow can be determined by using the implicit-function differentiation theorem, as applied to Equation (31) with respect to the lower-layer depth variable

d_{lower}^* :

$$\begin{aligned} \frac{\partial E_{int}^*}{\partial d_{lower}^*} &= 0 \\ \frac{K^*}{w^{*2}} \left(-\frac{2}{d_{lower}^{*3}} + \frac{2q^2(-1)}{(1-d_{lower}^*)^3} \right) + 1 &= 0 \\ \frac{Q_{lower}^2}{w^{*2} 2g'd_0^5} \left(-\frac{2}{d_{lower}^{*3}} + \frac{2q^2}{(1-d_{lower}^*)^3} \right) &= 1 \end{aligned} \quad (46)$$

The analytical formula for the upper-layer fluid volumetric flow rate maximum of the bidirectional stratified flow through a rectangular opening is:

$$Q_{upper} = \left[g' w^2 d_0^3 q^2 \left(\frac{1}{d_{lower}^{*3}} + \frac{q^2}{(1 - d_{lower}^*)^3} \right)^{-1} \right]^{1/2}. \quad (47)$$

Here, the hydraulic-theory solutions are limited to cases of maximal exchange. An essential consideration in the analysis of two-layer flow hydraulics is the determination of the location of the two sections of the control (Laaneau and Davies, 2007). In inviscid internal-flow hydraulic theory, the primary control is denoted at the channel's narrowest section control, and the second control is considered to be virtual (Armi and Farmer, 1986). To verify the above-derived equation it is assumed that the position of the control section, where the flow is critical, is located in the opening. Critical conditions occur at such sections, which are known as hydraulic controls (Dalziel and Lane-Serff, 1991). The Equation (45) can be presented for upper and lower layer volume fluxes as:

$$\frac{Q_{upper}^2}{g' d_{upper}^3 w^2} + \frac{Q_{lower}^2}{g' d_{lower}^3 w^2} = 1. \quad (48)$$

By substituting the opening depth in the Equation (48), this equation can be modified as:

$$\begin{aligned} \frac{Q_{upper}^2}{g' (d_0 - d_{lower})^3 w^2} + \frac{Q_{lower}^2}{g' d_{lower}^3 w^2} &= 1, \\ \frac{Q_{lower}^2}{g' w^2} \left(\frac{Q_{upper}^2}{Q_{lower}^2} \frac{1}{(d_0 - d_{lower})^3} + \frac{1}{d_{lower}^3} \right) &= 1. \end{aligned} \quad (49)$$

The analytical formula for the lower-layer fluid volumetric flow rate maximum of the bidirectional stratified flow can be given by the formula:

$$Q_{lower} = \left[w^2 g' \left(\frac{1}{d_{lower}^3} + \frac{q^2}{(d_0 - d_{lower})^3} \right)^{-1} \right]^{1/2} = \left[g' w^2 d_0^3 \left(\frac{1}{d_{lower}^{*3}} + \frac{q^2}{(1 - d_{lower}^*)^3} \right)^{-1} \right]^{1/2} \quad (50)$$

1.3.2 Circular opening

In Figure 1-4 a flow configuration scheme is presented for two-layer exchange flow through a submerged side opening of circular shape connecting two fluids with a small density difference.

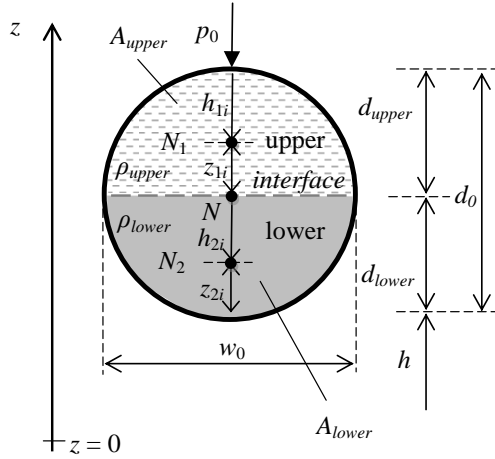


Figure 1-4. Sketch of a bidirectional stratified flow through the side opening of circular shape (orifice) with less-dense fluid inside the enclosure and notations.

The flows in the upper and lower layers are the less-dense ($\rho_i = \rho_{upper}$) and denser ($\rho_o = \rho_{lower}$) fluids, respectively. These layers have corresponding exchange flow rates Q_{upper} and Q_{lower} according to Equation (13) and (14), respectively. The circular opening area ($A = \pi d_0^2/4$), where the total thickness (d_0) for two-layer flow at the opening is the sum of the changing layer thicknesses (Equation 16), is related to the areas of the layered flows according to Equation (15). Due to the changing depths of the layers, the interfacial width (w) of the two-layer exchange flow is not constant at the circular opening. The maximum interface width occurs in the middle of the opening (i.e. $w_{max} = d_0$) and the degree of exchange is regulated by the total thickness (d_0) of the two fluids.

The Bernoulli heads (B_{upper} and B_{lower}) for both layers at the level of the interface (point N on Figure 1-4), respectively, can be expressed similarly to those of the rectangular opening (see Equations 17 and 18). It should be mentioned that the hydrostatic pressure of two layers can be expressed in terms of the layers' thicknesses, d_{upper} and d_{lower} , by Equations (19) and (20), respectively. The Bernoulli functions E_{upper} and E_{lower} can be determined for the upper layer (Equation 21) and lower layer (Equation 22), respectively, and in the case of $(1 - r) \ll 1$, the internal-flow energy head (E_{int}) for a submerged circular opening can be defined according to Equation (25).

The flow velocities of the upper and lower layers are defined as the flow rates per flow area of each of the layers:

$$u_{lower} = \frac{Q_{lower}}{A_{lower}}, \quad (51)$$

$$u_{upper} = \frac{Q_{upper}}{A_{upper}} = \frac{Q_{upper}}{(A - A_{lower})}. \quad (52)$$

By implementing the Equations (51) and (52) for the layers' flow velocities, Equation (28) for the volume flux parameter (K), and Equation (29) for flow-rates-ratio (q), the internal-flow energy head for circular openings becomes:

$$E_{int} = K \left(\frac{1}{A_{lower}^2} - \frac{q^2}{(A - A_{lower})^2} \right) + d_{lower} + h, \quad (53)$$

Particular attention is given to the circular opening, where its interfacial width (w) is a function of the layer depth. The cross-sectional area of a lower layer expressed by the dimensionless thickness of the lower layer ($d_{lower}^* = d_{lower} / d_0$), is given by the expression (cf. Hou et al., 2014):

$$A_{lower}(d_{lower}^*) = \frac{1}{8} \pi d_0^2 \left[1 + \frac{2}{\pi} \operatorname{asin}(2d_{lower}^* - 1) + \frac{4}{\pi} (2d_{lower}^* - 1) \sqrt{d_{lower}^* - d_{lower}^{*2}} \right]. \quad (54)$$

The dimensionless area of the lower layer is:

$$A_{lower}^* = \frac{A_{lower}}{A} = \frac{4A_{lower}}{\pi d_0^2}. \quad (55)$$

The interface width of a two-layer flow at the circular opening is:

$$w(d_{lower}^*) = 2d_0 \sqrt{d_{lower}^* - d_{lower}^{*2}}. \quad (56)$$

The interface width (w) of the two-layer exchange flow, per the definition, is the lower layer's upper width, which is equal to the lower width of the upper layer. The dimensionless lower-layer area is:

$$A_{lower}^* = \left[\frac{1}{2} + \frac{1}{\pi} \operatorname{asin}(2d_{lower}^* - 1) + \frac{2}{\pi} (2d_{lower}^* - 1) \sqrt{d_{lower}^* - d_{lower}^{*2}} \right]. \quad (57)$$

The non-dimensional form of the internal-flow energy head for the two-layer exchange flow through the circular submerged orifice is:

$$E_{int}^* = \frac{16}{\pi^2} K^* \left(\frac{1}{A_{lower}^{*2}} - \frac{q^2}{(1 - A_{lower}^*)^2} \right) + d_{lower}^* + h^*, \quad (58)$$

where the following quantities, made non-dimensional by the total two-layer thickness (d_0), are used:

$$E^* = \frac{E_{int}}{d_0}; \quad K^* = \frac{Q_{lower}^2}{2g'd_0^5}; \quad A_{lower}^* = \frac{A_{lower}}{A}; \quad d_{lower}^* = \frac{d_{lower}}{d_0}; \quad h^* = \frac{h}{d_0}.$$

Functional approach

For the Bernoulli functions of the upper and lower layer, respectively, the function can be written by expressing the velocity in the layers by the flowrate:

$$J_1 = \frac{Q_{upper}^2}{2A_{upper}^2} + \frac{p_0}{\rho_{upper}} + d_{upper}g + (d_{lower} + h)g - E_{lower}g , \quad (59)$$

$$J_2 = \frac{Q_{lower}^2}{2A_{lower}^2} + \frac{p_0}{\rho_{lower}} + \frac{\rho_{upper}}{\rho_{lower}}d_{upper}g + (d_{lower} + h)g - E_{lower}g . \quad (60)$$

The Jacobian matrix of all first order partial derivatives of a vector-valued function is used (Equation 34), with the critical conditions where the matrix is equal to zero. Partial derivatives are solved as:

$$\frac{\partial J_1}{\partial d_{upper}} = -\frac{Q_{upper}^2}{A_{upper}^3} \frac{\partial A_{upper}}{\partial d_{upper}} + g , \quad (61)$$

$$\frac{\partial J_1}{\partial d_{lower}} = g , \quad (62)$$

$$\frac{\partial J_2}{\partial d_{upper}} = \frac{\rho_{upper}}{\rho_{lower}} g , \quad (63)$$

$$\frac{\partial J_2}{\partial d_{lower}} = -\frac{Q_{lower}^2}{A_{lower}^3} \frac{\partial A_{lower}}{\partial d_{lower}} + g , \quad (64)$$

and the critical condition becomes:

$$\left(-\frac{Q_{upper}^2}{A_{upper}^3} \frac{\partial A_{upper}}{\partial d_{upper}} + g \right) \left(-\frac{Q_{lower}^2}{A_{lower}^3} \frac{\partial A_{lower}}{\partial d_{lower}} + g \right) - g \frac{\rho_{upper}}{\rho_{lower}} \cdot g = 0 . \quad (65)$$

By substituting the upper and lower layers flow rates with the flow velocities (Equations 51 and 52), respectively, the equation becomes:

$$\left(-\frac{u_{upper}^2}{A_{upper}} \frac{\partial A_{upper}}{\partial d_{upper}} + g \right) \left(-\frac{u_{lower}^2}{A_{lower}} \frac{\partial A_{lower}}{\partial d_{lower}} + g \right) - g \frac{\rho_{upper}}{\rho_{lower}} \cdot g = 0 . \quad (66)$$

By further manipulation:

$$\frac{u_{upper}^2}{A_{upper}} \frac{\partial A_{upper}}{\partial d_{upper}} g + \frac{u_{lower}^2}{A_{lower}} \frac{\partial A_{lower}}{\partial d_{lower}} g - \frac{u_{upper}^2}{A_{upper}} \frac{\partial A_{upper}}{\partial d_{upper}} \cdot \frac{u_{lower}^2}{A_{lower}} \frac{\partial A_{lower}}{\partial d_{lower}} = g^2 \left(1 - \frac{\rho_{upper}}{\rho_{lower}} \right) = g \cdot g' \quad (67)$$

and by multiplying Equation (67) with $1/gg'$ and substituting the ratio of upper- and lower-layer densities with r , the equation becomes:

$$\frac{u_{upper}^2}{g' A_{upper}} \frac{\partial A_{upper}}{\partial d_{upper}} + \frac{u_{lower}^2}{g' A_{lower}} \frac{\partial A_{lower}}{\partial d_{lower}} - \frac{u_{upper}^2}{g' A_{upper}} \frac{\partial A_{upper}}{\partial d_{upper}} \cdot \frac{u_{lower}^2}{g' A_{lower}} \frac{\partial A_{lower}}{\partial d_{lower}} (1 - r) = 1 \quad (68)$$

Generalised densimetric Froude' numbers for the upper and lower layers, respectively, are:

$$Fr_{upper}^2 = \frac{u_{upper}^2}{g' A_{upper}} \frac{\partial A_{upper}}{\partial d_{upper}}, \quad (69)$$

$$Fr_{lower}^2 = \frac{u_{lower}^2}{g' A_{lower}} \frac{\partial A_{lower}}{\partial d_{lower}}, \quad (70)$$

and in the case of $(1 - r) \ll 1$, the critical condition for a submerged bidirectional stratified flow is:

$$\frac{u_{upper}^2}{g' A_{upper}} \frac{\partial A_{upper}}{\partial d_{upper}} + \frac{u_{lower}^2}{g' A_{lower}} \frac{\partial A_{lower}}{\partial d_{lower}} = 1. \quad (71)$$

Maximal flow rate

The maximal flow rate can be derived from the dimensionless internal-flow energy head (Equation 58) by applying the implicit function differentiation theorem to the dimensionless lower-layer depth (d_{lower}^*):

$$\begin{aligned} \frac{\partial E_{int}^*}{\partial d_{lower}^*} &= 0 \\ \frac{\partial E_{int}^*}{\partial d_{lower}^*} &= \frac{16}{\pi^2} K^* \left(-\frac{2}{A_{lower}^{*3}} \frac{\partial A_{lower}^*}{\partial d_{lower}^*} - \frac{2q^2}{(1 - A_{lower}^*)^3} \frac{\partial A_{lower}^*}{\partial d_{lower}^*} \right) + 1 = 0 \end{aligned} \quad (72)$$

The analytical formula for the less-dense (upper-layer) fluid volumetric flow rate maximum of the bidirectional stratified flow through a circular opening is:

$$Q_{upper} = \left[\frac{g' \pi^2 d_0^5 q^2}{8} \left(\frac{2}{A_{lower}^{*3}} \frac{\partial A_{lower}^*}{\partial d_{lower}^*} + \frac{2q^2}{(1 - A_{lower}^*)^3} \frac{\partial A_{lower}^*}{\partial d_{lower}^*} \right)^{-1} \right]^{1/2}, \quad (73)$$

where the following function applies:

$$\frac{\partial A_{lower}^*}{\partial d_{lower}^*} = \frac{2}{\pi} \frac{1}{\sqrt{1 - (2d_{lower}^* - 1)^2}} + \frac{4}{\pi} \sqrt{d_{lower}^* - d_{lower}^{*2}} + \frac{1}{\pi} \frac{(2d_{lower}^* - 1)}{\sqrt{d_{lower}^* - d_{lower}^{*2}}} (1 - 2d_{lower}^*). \quad (74)$$

The denser (lower layer) fluid volumetric flow rate of bidirectional stratified flow through a circular opening can be determined by:

$$Q_{lower} = \frac{Q_{upper}}{q}. \quad (75)$$

Due to flow continuity, the flow rates in the lower and upper layer relate to the flow velocities and layer areas:

$$Q_{lower} = u_{lower} A_{lower}, \quad (76)$$

$$Q_{upper} = u_{upper} A_{upper} = u_{upper} (A - A_{lower}). \quad (77)$$

1.4 Hydraulic-modelling solutions

Analytical formulae of hydraulic-modelling solutions are proposed for fluid outflow volume and duration calculation from the submerged side and bottom openings of rectangular or circular shapes. The time-dependent unidirectional fluid outflow through the side opening results from the reduction of internal pressure due to a descending inner fluid surface in the enclosure as compared to the outer fluid level, which is fixed ($H_o = \text{const.}$). The fluid outflow volume (V_{uni}) of unidirectional stratified flow is fixed due to the difference in the hydrostatic pressure of the less-dense and denser fluid columns relative to the level of the opening. The fluid outflow duration (T_{uni}) of unidirectional stratified flow is dependent on the discharge coefficient, and the shortest duration is associated with the inviscid case (i.e. $C_d = 1$). In the case of unidirectional stratified flow through the submerged side opening, the fluid outflow volume and duration with changing internal pressure can be calculated by analytical formulae:

$$V_{uni} = \left(\left(A_I + \frac{d_0}{2} \right) - \frac{\rho_o}{\rho_l} \left(A_o + \frac{d_0}{2} \right) \right) S, \quad (78)$$

$$T_{uni} = \frac{2S}{A\sqrt{2g}} \frac{1}{C_d} \sqrt{\frac{V_{uni}}{S}}. \quad (79)$$

In the case of bidirectional stratified flow through the submerged side opening, the upper-layer fluid outflow volume and duration in a balanced internal and external pressure situation can be calculated by analytical formulae:

$$V_{bi} = (d_0 + h)S, \quad (80)$$

$$T_{bi} = \frac{Q_{upper}}{V_{bi}}, \quad (81)$$

where Q_{upper} can be calculated by the analytical formula for the less-dense (upper-layer) fluid volumetric flow rate maximum of the bidirectional stratified flow through a rectangular opening (Equation 47) or a circular opening (Equation 73). The total outflow volume (V_{total}) and duration (T_{total}) from submerged side opening is the sum of uni- and bidirectional outflow volumes and durations, respectively, i.e.:

$$V_{total} = V_{uni} + V_{bi}, \quad (82)$$

$$T_{total} = T_{uni} + T_{bi}. \quad (83)$$

In the case of a bottom opening, only unidirectional stratified flow is possible, resulting in a descending fluid surface in the enclosure due to a high inner hydrostatic

pressure-head (Δ_I), as compared to the outer hydrostatic pressure-head ($\rho_O / \rho_I \Delta_O$). The inner fluid unidirectional outflow volume $V_{uni} = V_{total}$ and duration $T_{uni} = T_{total}$ with changing internal pressure can be calculated using the analytical formulae:

$$V_{uni} = \left(\Delta_I - \frac{\rho_O}{\rho_I} \Delta_O \right) S, \quad (84)$$

$$T_{uni} = \frac{2S}{A\sqrt{2g}} \frac{1}{C_d} \sqrt{\frac{V_{uni}}{S}}. \quad (85)$$

1.5 Discharge coefficients

The flow resistance, i.e. the local head-loss coefficient (k), is expressed as a unit-less parameter, which is related to the discharge coefficient as:

$$C_d = \frac{1}{\sqrt{1 + \sum_i k_i}}. \quad (86)$$

Generally, the discharge coefficients are found from experiments, and the values are positive and less than 1. For the inviscid flow case the $C_d = 1$. By definition, the discharge coefficient is the ratio of actual discharge to the theoretical discharge and is calculated as:

$$C_d = \frac{Q_{actual}}{Q_{theoretical}}, \quad (87)$$

where Q_{actual} is the actual flow rate ($\text{m}^3 \text{s}^{-1}$) determined by an experiment, and $Q_{theoretical}$ is the calculated theoretical flowrate ($\text{m}^3 \text{s}^{-1}$) for inviscid fluid flow. For a given opening geometry, the discharge coefficient changes as a function of the flow rate passing through it. Customarily, this functionality for a circular opening is expressed in terms of the Reynolds number for an opening as:

$$\text{Re}_{opening} = \frac{Q D_h}{A \nu}, \quad (88)$$

where Q is the fluid flow rate ($\text{m}^3 \text{s}^{-1}$) through an opening, D_h is the opening hydraulic diameter (m), and ν is the kinematic viscosity ($\text{m}^2 \text{s}^{-1}$) of the fluid. For instance, in the case of stratified unidirectional outflow through submerged side and bottom openings of circular shape, the equations for calculating the Reynolds number are:

$$\text{Re}_{side} = \frac{\sqrt{2g((\Delta_I + d_0/2) - \rho_O / \rho_I (\Delta_O + d_0/2))} d_0}{\nu}, \quad (89)$$

$$\text{Re}_{bottom} = \frac{\sqrt{2g((\Delta_I - \rho_O / \rho_I \Delta_O))} d_0}{\nu}, \quad (90)$$

where $d_0 = D_h$ and ν is the inner fluid kinematic viscosity ($\text{m}^2 \text{s}^{-1}$). It should be noted that for submerged side and bottom openings of rectangular shape, the hydraulic diameter is:

$$D_h = \frac{2w_0d_0}{w_0 + d_0}. \quad (91)$$

1.6 Shape factors

The shape factor (ξ) is the cross-sectional shape parameter representing the inverse ratio of the cross-sectional flow area of the chosen opening geometry to the equivalent rectangular cross-sectional area having identical width and depth maxima (Laanearu and Davies, 2007). In general, ξ can take any value greater than unity. Here, the shape factor definition for an opening admits symmetrical cross-sections, such as rectangular, circular and triangular, with respect to the vertical axial plane passing through the depth maximum. According to Laanearu and Davies (2007), the bidirectional stratified flow analytical formula for determining the maximal upper-layer fluid volumetric flow rate through a quadratic-type opening is the following:

$$Q_{upper} = \left[\frac{g' w^2 d_0^3 q^2}{\xi^3} \left[\left(\frac{d_0}{d_{lower}} \right)^{2\xi+1} - \frac{q^2 (d_{lower}/d_0)^{(\xi-1)}}{(1 - (d_{lower}/d_0)^\xi)^3} \right]^{-1} \right]^{1/2}. \quad (92)$$

In determining the maximal flow rate through different-shaped cross-sections, the shape factor ξ should be specified. For instance, in the case of $\xi = 1$ the open channel flow corresponds to the rectangular cross-section, and in the case of $\xi = 3/2$ and $\xi = 2$, the flow corresponds to parabolic and triangular cross-sections, respectively. In Publication I Equation (92) is applied for a submerged opening where the opening maximum depth is set equal to the maximum width (i.e. $d_0 = w$). The circular hole is approximated by the shape factor $\xi = 4 / \pi$.

2 Pilot studies

If the exchange flow is present in an opening, then the volumetric flux of flow through this opening can be zero. However, the net mass flux of the flow is not zero for two-way exchange through the opening in the case of stratified flow. Therefore, the integral mass flux of an enclosure is not zero, which results in a density change inside the enclosure. For instance, this is possible in the case of bidirectional stratified flow, when the exchange of fluids through an opening takes place.

This chapter presents three pilot studies of internal-flow hydraulics for stratified flows through submerged openings in the built environment. Presence of stratified flows is shown in two different built environment enclosures: a fluid-storage tank and a room of a building. In the following pilot studies, the density difference is related to the presence of different liquids and the temperature variation.

Firstly, liquid-liquid interaction with two active layer flows is demonstrated by oil spills from a damaged tanker representing stratified flow of immiscible fluids through a hole of circular shape (orifice). The hydraulic-theory solutions are used for determining the discharge coefficients from the available experimental results for a single-hull tank side and bottom orifice. The dynamical effects due to mixing (emulsification) and heat exchange are parametrized for uni- and bidirectional stratified flows, which affect the flow rates, outflow volumes, and process durations.

Secondly, water exchange in a thermally-stratified storage tank, representing a miscible liquid-liquid stratified system, is described. The internal-flow hydraulic theory is used for dealing with the dynamics of stratified flow through submerged openings, which regulate the water exchange in the storage tank. The number of tank fillings is introduced, which is important in the design of a tank for integration with on-site end-users.

Thirdly, gas-gas interaction with two active layer flows is demonstrated by an illustration case of natural ventilation through an open window representing stratified flow of miscible fluids through a submerged opening of a building envelope. Indoor and outdoor air interaction in cold and hot season conditions is described.

2.1 Oil spill

Ship collisions and groundings due to navigation errors at sea are the main reasons for large oil spills. In order to assess the amount and duration of a potential oil spill, it is important when modelling the oil outflow to consider the tanker configuration, hydrostatic pressure situation, location, and extent of the damage. Holes in tanker side hulls usually result from ship collisions, whereas tanker grounding can result in bottom holes.

In Publication I, the internal-flow hydraulic theory is employed in the case of submerged oil outflow through the rectangular hole in the tank. The hydraulic-modelling solutions are used to determine the oil-spill duration and outflow volume from side and bottom holes with different non-dimensional hole areas in single- and double-hull tanks. The circular hole is approximated by the shape factor ($\xi = 4 / \pi$) in the analytical formula for the volumetric flow rate of bidirectional stratified flow (Equation 92) to determine the oil outflow rate for a side hole in a single-hull tank. In Publication II, the hydraulic-theory solutions for a circular opening are used to determine the discharge coefficients according to the experimental results of Tavakoli et al. (2011).

Herein, two example scenarios of single-hull tanker accidents are presented: (1) a grounding case, with a hole in the bottom hull and (2) a collision case, with a hole in the side hull. Table 2-1 presents the experimental results of chosen lab tests by Tavakoli et al. (2011). Note that the fluid density in the tank corresponds to the oil density ($\rho_l = \rho_{oil}$) and the fluid density in the environment to water density ($\rho_o = \rho_{water}$).

Table 2-1. Experimental results of lab tests by Tavakoli et al. (2011).

Test no	Scenario	Flow case	Orifice	H_l	H_o	T_{total}	V_{total}
			(m)	(m)	(m)	(s)	(l)
N4	Grounding	Unidirectional	0.022	0.80	0.47	460	138
N9	Collision	Unidirectional	0.022	0.80	0.40	385	145
N9*	Collision	Bidirectional	0.022	0.51	0.40	18600	50

The grounding scenario in Figure 2-1 corresponds to the submerged oil spill from the bottom orifice of the single-hull tank in lab test N4 (Table 2-1).

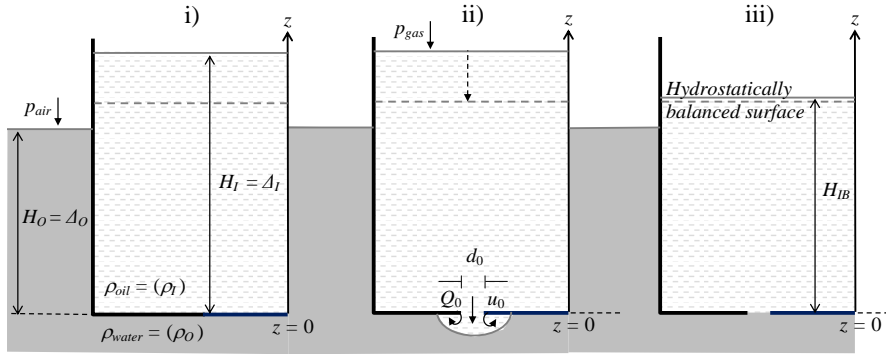


Figure 2-1. Sketch of single-hull oil tank with bottom orifice: (i) no damage, (ii) damage with excess hydrostatic pressure and oil spill, and (iii) damage without oil spill.

The unidirectional oil outflow occurs, resulting in a descending oil level ($H_l \rightarrow H_{IB}$) in the tank (Figure 2-1ii) due to a high inner hydrostatic pressure-head (Δ_l) as compared to the outer hydrostatic pressure-head ($\rho_{water} / \rho_{oil} \Delta_o$) at the orifice level. It should be mentioned that the fluid total depth (H_l) in the tank is a dynamical parameter, which depends directly on the parameter $\Delta_l(t)$ during the unidirectional-flow process, whereby Δ_o is constant due to the fixed lab tank and comparatively large water pool. When the hydrostatically-balanced surface level (H_{IB}) in the tank is reached (Figure 2-1iii) the unidirectional oil outflow ends.

The analytical formulae for the volumetric flow rate of unidirectional stratified flow through a submerged bottom opening (Equation 12) is implemented for oil outflow rate calculations through the bottom orifice of a single-hull tank. In Figure 2-2i, the unidirectional oil outflow rates are presented for viscous and inviscid stratified flows as well as experimental results by Tavakoli et al. (2011). A total of 138 litres of oil leaked into the pool over 460 sec. The determined discharge coefficients at different orifice Reynolds numbers are presented in Figure 2-2ii. The experimental data indicate that the C_d value changes (in the range $C_d = 0.55$ – 0.7) during the unidirectional oil outflow, as a function of the orifice Reynolds number (Equation 90). The mean discharge coefficient $C_d = 0.64$ and the mean minor head-loss coefficient $k_{1, bottom} = 4.94$.

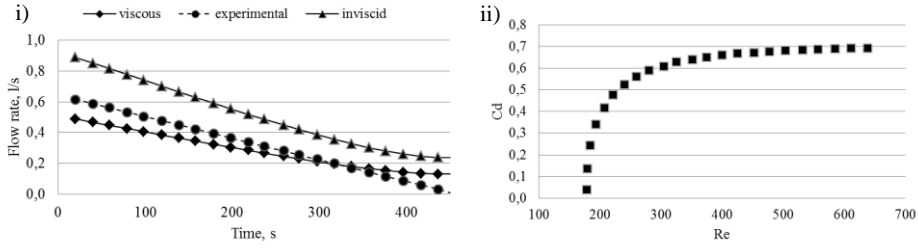


Figure 2-2. Charts of i) oil flow rates of unidirectional stratified flow through a bottom orifice in lab test N4, and ii) experimentally determined discharge coefficients at different orifice Reynolds numbers. The curve "experimental" is reproduced according to the results in Tavakoli et al. (2011). Curve "viscous" corresponds to the hydraulic solution with mean discharge coefficient.

The collision scenario in Figure 2-3 corresponds to the submerged oil spill from the side orifice of the single-hull tank in lab tests N9 and N9* (Table 2-1).

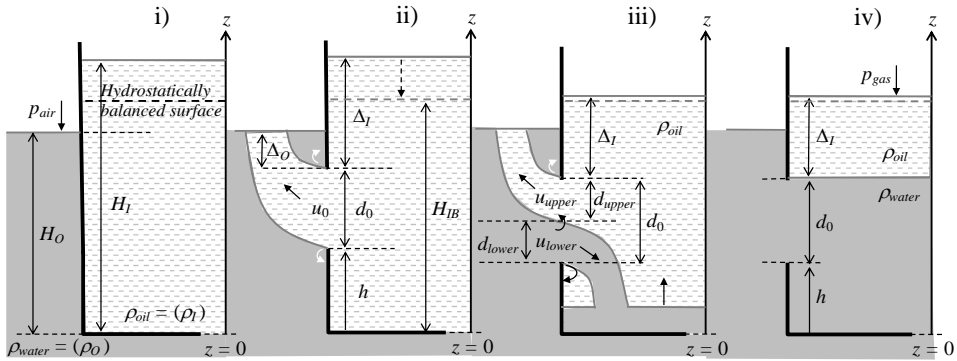


Figure 2-3. Sketch of single-hull oil tank with side orifice: (i) no damage, (ii) damage with excess hydrostatic pressure and oil spill, (iii) damage without excess hydrostatic pressure and oil spill, and (iv) damage without horizontal density difference and no oil spill.

The difference between the water level outside and the oil level inside of the tank, together with the difference between the liquid densities, determine the oil-leak dynamics after the accident. According to the pressure situation at the orifice level, the oil outflow can be divided into two stages: 1) unidirectional stratified flow, and 2) bidirectional stratified flow.

In the first stage, the unidirectional oil outflow through the side orifice of single-hull tank takes place due to the unbalanced internal and external hydrostatic pressure situation at the orifice level (Figure 2-3ii). The unidirectional oil outflow results in a descending oil level ($H_I \rightarrow H_{IB}$) in the tank due to the excess hydrostatic pressure in the tank, i.e. $(\Delta_I + d_0 / 2) > \rho_{water} (\Delta_O + d_0 / 2) / \rho_{oil}$. Similar to the case with the bottom orifice, the total fluid depth (H_I) in the tank with the side orifice is a dynamical parameter, which depends directly on the parameter $\Delta_I(t)$ during the unidirectional-flow process, whereby $\Delta_O = \text{const}$.

The analytical formula for the volumetric flow rate of unidirectional stratified flow through a submerged side opening (Equation 11) is implemented for oil outflow rate calculations through a side orifice in a single-hull tank. In Figure 2-4i the unidirectional oil outflow rates are presented for viscous and inviscid stratified flows as well as the experimental results by Tavakoli et al. (2011). The experimental data indicated that 145 litres of oil leaked into the pool over 385 sec. It was found that the C_d value changed

during the unidirectional oil outflow according to the orifice Reynolds number (Equation 89). The mean discharge coefficient $C_d = 0.50$ and the mean minor head-loss coefficient $k_{1, side} = 4.30$. The discharge coefficients determined experimentally at different orifice Reynolds numbers are presented in Figure 2-4ii.

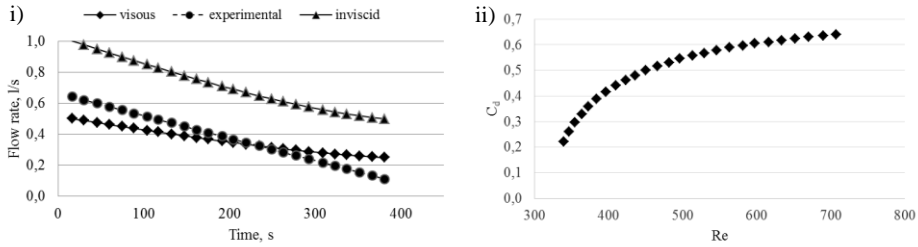


Figure 2-4. Charts of i) oil flow rates of unidirectional stratified flow through a side orifice in lab test N9 and ii) experimentally-determined discharge coefficients at different orifice Reynolds numbers. The curve "experimental" is reproduced according to the results in Tavakoli et al. (2011). Curve "viscous" corresponds to the hydraulic solution with mean discharge coefficient.

In the second stage, oil outflow through a side orifice of a single-hull tank continues under the balanced hydrostatic pressure situation $(\Delta_l + d_o / 2) = \rho_{water} / \rho_{oil} (\Delta_o + d_o / 2)$ due to the adjusted oil level inside the tank (Figure 2-3iii). The bidirectional stratified flow takes place with the ascending oil-water interface in the tank. The total oil outflow volume for the bidirectional flow is fixed by the oil-water interface at the orifice level. The oil outflow ends when the tank is filled with water up to the upper lip of the orifice (Figure 2-3iv).

The analytical formula for the volumetric flow rate of bidirectional stratified flow through a circular opening (Equation 73) is implemented for oil outflow rate calculations through a side orifice of a single-hull tank. In Figure 2-5, the bidirectional oil outflow rates are presented for viscous and inviscid stratified flows, as well as experimental results by Tavakoli et al. (2011).

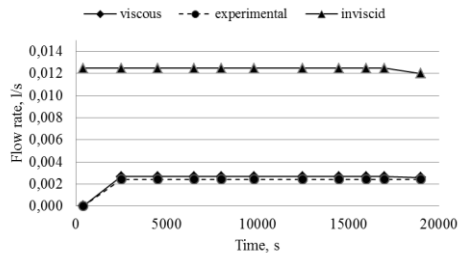


Figure 2-5. Chart of oil outflow rates of bidirectional stratified flow through a side orifice in lab test N9*. The curve "experimental" is reproduced according to the results in Tavakoli et al. (2011). Curve "viscous" corresponds to the hydraulic solution with mean discharge coefficient.

In the second stage, 50 litres of oil leaked into the pool over 18,600 sec. In the case of the bidirectional flow, the discharge coefficient cannot be determined in a straightforward manner. Only by assuming the maximal two-layer exchange flow conditions (i.e. the interfacial depth $d_{lower} = d_o / 2$) can the oil outflow rate be determined. Making use of the ascending oil-water interface during the bidirectional stratified flow, the discharge coefficient $C_d = 0.22$. It was found that the discharge

coefficient is considerably smaller than the C_d values for the first-stage oil outflow. The corresponding mean minor head-loss coefficients are $k_{1, side} = 4.30$ and $k_{2, side} = 16.27$.

In Publication III, the internal-flow hydraulic model is extended to account for the effects of emulsification and heat exchange, which is used for a parametric study on the influence of winter conditions on oil spill outflow quantities. When modelling oil outflow dynamics in winter conditions, when ship navigation is challenging due to the presence of ice, in addition to hydrostatic driving pressure and hull-damage characteristics, it is essential to include changes of liquids' physical properties (density and viscosity) due to temperature variations. It is important to consider the heat-exchange-modified shear-induced mixing processes in the hydraulic modelling. In the assessment of environmental impacts, oil emulsification plays a significant role in the modelling of an oil slick trajectory (see Alves et al., 2015), as emulsion with an 80% water content may have a volume that is five times the spilled volume of the parent oil (Xie et al., 2007). To assess the sensitivity of uni- and bidirectional stratified flows, the two key parameters can be parametrized: i) the seawater inflow-rate reduction parameter in the bidirectional stratified flow and ii) the thermal expansion coefficient of oil in the uni- and bidirectional stratified flows.

The analytical formula for the outflow volume of unidirectional stratified flow through a side opening (Equation 78) is modified to account for the effect of heat exchange. The unidirectional oil spill volume $V_{uni}(T_o)$ (m^3) due to the density difference between oil at the inner temperature (T_i) and water at the outer temperature (T_o), and the spilt oil cooling outside can be determined as:

$$V_{uni}(T_o) = \left(\left(\Delta_I + \frac{d_0}{2} \right) - \frac{\rho_o(T_o)}{\rho_I(T_i)} \left(\Delta_o + \frac{d_0}{2} \right) \right) S \frac{\rho_I(T_o)}{\rho_I(T_i)}, \quad (93)$$

where $\rho_o(T_o)$ is water density ($kg\ m^{-3}$) at the outside temperature, $\rho(T_o)$ is oil density ($kg\ m^{-3}$) at the outside temperature, and $\rho(T_i)$ is oil density ($kg\ m^{-3}$) at the inside temperature. The analytical formula for the outflow duration of unidirectional stratified flow through a side opening (Equation 79) is modified to account for the oil spill volume $V_{uni}(T_o)$ accordingly:

$$T_{uni}(T_o) = \frac{2S}{A \sqrt{2g}} \frac{1}{C_d} \sqrt{\frac{V_{oil}(T_o)}{S}}. \quad (94)$$

It is assumed that the flow separation occurs at the external orifice edges, and this process can be parametrized by the discharge coefficient. The flow separation of oil results in the formation of emulsions due to the mixing promoted by turbulence.

In Figure 2-6, heavy-fuel unidirectional oil spill volumes and durations are presented for summer and winter conditions. Oil at an inner temperature of 60°C is reduced in volume by 3% and outflow duration by 1% between summer (18°C) and winter (-1°C) conditions. It can be recognised that with small temperature gradients the oil outflow duration is longer, compared to the situation with large temperature gradients. In the presence of ice, the oil may be frozen and captured in growing ice or spread below an ice sheet. In addition, the effects due to the cooling of oil below the pour point temperature may be associated with the blockage of outflow in the winter.

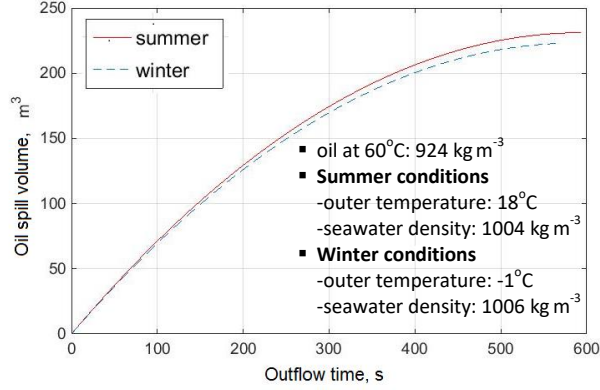


Figure 2-6. Unidirectional oil spill in summer and winter conditions with the effect of heat exchange.

For the bidirectional stratified oil outflow, the effects of emulsification and heat exchange can be considered by modifying the flow-rates-ratio parameter (q) in the hydraulic calculations. To consider the effect of emulsification, the non-dimensional parameter $f = 1 - \Delta Q / Q_{lower}$ is introduced, where ΔQ is the added volume ($\text{m}^3 \text{s}^{-1}$) due to mixing in the orifice. To consider the effect of heat exchange, the lost volume due to the cooling of oil during the outflow can be considered as a relative change of the upper layer volume:

$$\frac{\delta Q_{upper}}{Q_{lower}} \rightarrow \frac{\rho_l(T_l) - \rho_l(T_o)}{\rho_o(T_o)} = \frac{\alpha_{oil}}{\rho_o(T_o)}(T_l - T_o), \quad (95)$$

where δQ_{upper} is the lost volume ($\text{m}^3 \text{s}^{-1}$) due to the cooling of the oil, and α_{oil} is the thermal expansion coefficient (1) of oil. Thus, the flow-rates-ratio parameter in the analytical formula for the volumetric flow rate of bidirectional stratified flow through a circular opening (Equation 73) is modified as:

$$q_o = q + (1 - f) - \frac{\alpha_{oil}}{\rho_o(T_o)}(T_l - T_o), \quad (96)$$

where q is the standard flow-rates-ratio parameter determined by Equation (29).

According to the bidirectional stratified flow hydraulic analysis in Figure 2-7, the oil outflow volumes and durations increase for larger temperature gradients, i.e. in winter conditions. However, the oil spills in winter conditions can reveal different outflow characteristics compared to spill situations with smaller temperature gradients, corresponding to the summer conditions. It is still not known how the emulsification and heat exchange are related, however, it is evident that temperature affects them both. For this purpose, experimental investigation or CFD modelling may be useful, which is considered as a topic for a future study. The real values due to the cooling of oil may be considered to be located on the dotted lines in Figure 2-7 of the bidirectional oil spill. As the temperature of outflowing oil decreases, its physical properties change; the oil becomes denser and more viscous, thus the emulsification rate decreases.

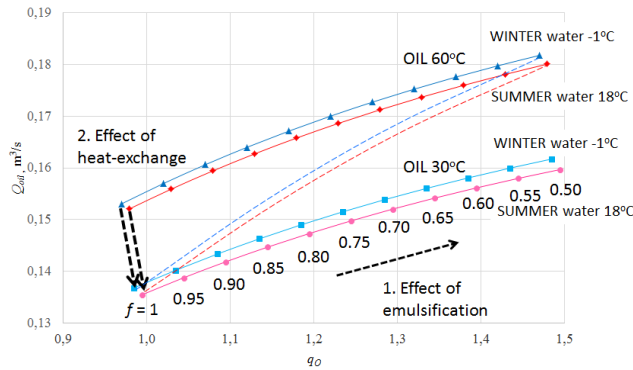


Figure 2-7. The oil outflow rate and flow-rates-ratio parameter variation of heavy crude oil (at inner temperature 60°C and 30°C) at different emulsification rates $f=1\ldots0.50$ for summer (18°C) and winter (-1°C) conditions.

2.2 Water exchange

Rainwater harvesting in urban catchments and stormwater storage in tanks have become essential components of water management systems within cities and other densely-populated urban areas. The rain falling over a watershed in the urban environment becomes almost entirely runoff. This occurs because urban areas are characterised by widespread impervious areas and man-made water courses. Precipitation is normally drained into the environment or into the city drainage system, which can sometimes cause widespread flooding during intense rain events in the city (Yan et al., 2011). Finding alternatives for urban flood risk management has become an important issue in dealing with urban runoff (Evers et al., 2012). Storage tanks offer several possibilities to exploit natural water in more diverse ways.

Publication IV presents the developed integrated-system model of stormwater collection and domestic-water heating that is used to analyse the possibility of low-temperature water usage for domestic hot-water production in a public building. In Publication V, the integrated-system modified model of stormwater collection and domestic-water heating is applied for different types of buildings (residential, public, and commercial). To assess the possibilities for the integration of this low-temperature water with on-site end-users, it is essential to understand the dynamics of water exchange in temperature-stratified storage tanks. The internal-flow hydraulic theory can be useful in dealing with the dynamics of stratified flow through submerged openings, which regulate the water exchange in the stormwater storage tank.

In Figure 2-8, a stormwater storage tank is illustrated to explain the water exchange in a storage tank. The thermal stratification takes place due to the temperature variation between stagnant water and collected stormwater in the storage tank. The collected stormwater can be considered to be relatively warm, since rainfall events occurring in urban areas not only have an air cooling effect, but also have the possibility of cooling impermeable urban surfaces by absorbing excessive heat within catchments (Janke et al., 2013). In heterogeneous fluid, the buoyancy is the product of gravity and varying density. Therefore, the layer of collected warm stormwater (less-dense) will settle at the top, and the layer of colder stormwater (denser) at the bottom of the tank.

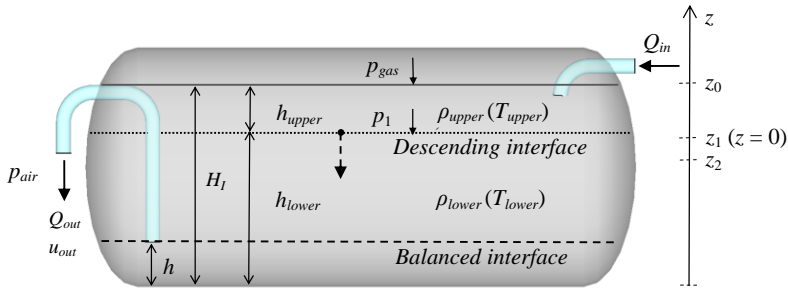


Figure 2-8. Sketch of stormwater storage tank (filling $n = 1$) with influx and outflux and notations. Thermal stratification with a descending interface is due to warm influx.

To maintain the stratification in the storage tank (as required in several practical applications), i.e. keep the upper layer from mixing with the lower layer, the warm (less-dense) stormwater is charged into the high-temperature region (T_{upper}) and colder (denser) stormwater is discharged from the low-temperature region (T_{lower}) of the storage tank. A density jump occurs at the interface due to the temperature gradient separating the warmer and colder fluid layers in the storage tank. The increase in water temperature in the storage tank is due to the random rain events. During the stormwater inflow into the storage tank, the warm upper-layer thickness h_{upper} (m) increases and the interface descends towards the discharge opening, where the colder lower-layer water is discharged. When the tank is filled with less-dense water $\rho_{upper}(T_{upper})$ to a maximal upper layer thickness ($h_{upper} = H_l - h$) and denser water $\rho_{lower}(T_{lower})$ is discharged to its minimum thickness ($h_{lower} = h$), steady state stratification is achieved. It should be noted that, when the storage tank is left idle, the temperature difference between layers decays over time due to heat transfer across the interface, approaching a thermal equilibrium in the tank. Thus, the above described condition refers to a tank filling $n = 1$ that corresponds to the one-time water exchange in the storage tank. The number of tank fillings, however, can be important in the design of a tank for the integration of this low-temperature water with on-site end-users. For instance, in terms of stormwater thermal heat usage for heating applications, further stormwater outflow from the storage tank can be associated with a loss of potential heat available for heat extraction.

Generally, the water exchange through the stormwater storage tank can be related to the stormwater in- and outfluxes of the tank. The water influx is due to the stormwater inflow (Q_{in}) into the tank, which can be characterised by the temperature and volume of rainwater that is precipitated on the catchment. The water outflux, on the other hand, is due to the stormwater outflow (Q_{out}) from the tank, which can be characterised by the temperature and volume of stormwater in the storage tank. Stormwater system parameters determined by SWMM LID may be used to determine the stormwater inflow quantities (see Publication IV). The unidirectional stratified outflow from the submerged discharge opening is essentially due to the excess hydrostatic pressure in the storage tank.

In the presence of stratification in the storage tank, the outflow rate (Q_{out}) varies due to the interface lift in the storage tank. Specifically, the unidirectional water outflow velocity (u_{out}) is time dependent, due to the gradually reducing internal pressure (due to the descent of the interface inside the tank) until the steady state stratification is achieved. The outflow velocity can be determined from the Bernoulli

equation. The Bernoulli head for a unidirectional stratified flow through the submerged discharge opening of a thermally-stratified stormwater storage tank can be expressed as:

$$\frac{u_{out}^2}{2g}(1+\Pi) = (z_1 - z_2) + \left(\frac{p_1}{\rho_{lower}g} - \frac{p_{air}}{\rho_{lower}g} \right), \quad (97)$$

where $(z_1 - z_2)$ is the elevation-head difference (m) between the discharge opening and the interface (see Figure 2-8), p_1 is the hydrostatic pressure (Pa) at the interface, and ρ_{lower} is the water density (kg m^{-3}) in the lower layer. The hydrostatic pressure at the interface in the storage tank is: $p_1 = p_{gas} + (z_0 - z_1) \rho_{upper}g$; where p_{gas} is the gas pressure (Pa) in the tank, $(z_0 - z_1)$ is the elevation difference (m) between the surface and the interface in the tank, i.e. the upper-layer thickness (h_{upper}), and ρ_{upper} is the water density (kg m^{-3}) in the upper layer. In the presence of tank ventilation, the pressures of gas and air are equal, i.e. $p_{gas} = p_{air}$.

According to Publications IV and V, the low-temperature stormwater can be considered as a carrier of thermal energy in the urban environment, because it is temporarily freely available in large quantities and is relatively warm. Therefore, the integration of a stormwater storage tank into the existing heating system of a building allows it to meet the requirements of expanded heating capacities. In addition, the proposed solution increases multi-functionality in the urban infrastructure that is essentially used to mitigate impacts from extreme climate events. It should be noted that the heat extraction from collected stormwater in the storage tank is dependent on water exchange through the tank. Thus, the determination of integrated system parameters, such as stormwater volume in the storage tank for heat extraction and the number of tank fillings due to harvested rainwater from the catchment area, require optimisation in order to utilise the locally-available resources. For this purpose, GA can be employed (see Chapter 3) for searching the dimensions of integrated-system design parameters, which are defined in the model as variables.

2.3 Ventilation

A primary purpose of windows is to provide natural light and ventilation. Natural ventilation harnesses the wind, and also the buoyancy forces associated with temperature differences between the indoor and outdoor environments, to drive air flow through a building (Hunt and Linden, 2004). Airtight and insulated building envelopes, where air movement through the building fabric (walls, ceilings, etc.) is significantly reduced, are equipped with mechanical ventilation to fulfil the comfort and energy efficiency benchmarks (Kalamees et al., 2016). According to Mayer and Antretter (2013), windows are opened to control indoor temperature and inhabitants' well-being by providing a fresh air inflow. The user behaviour of opening windows can be associated with several factors, for instance personal feeling, availability of mechanical ventilation, indoor thermal comfort and air quality (e.g. CO_2 concentration). Thus, the indoor environment of buildings requires a good understanding of the interaction of airflows through windows with HVAC systems.

Two distinctive cases, cold and hot seasons, are explained to demonstrate the evolution of stratification in a single room with mechanical ventilation. The stratified flows in buildings occur due to heating in cold seasons, where the outdoor air

temperature T_o is less than the indoor air temperature T_i , and cooling in hot seasons, where $T_o > T_i$. The density difference is mainly due to temperature differences between indoor and outdoor environments, thus, the air exchange through open windows is strongly dependent on the prevalent climate conditions. For instance, in office and public buildings, the ambient indoor temperature set-points for heating in cold seasons and cooling in hot seasons are typically considered to be 21°C and 25°C, respectively. Maintaining the indoor temperature in this range complies with the ventilation and ambient temperature requirements established for the minimum requirements for energy performance regulations (Riigi Teataja, 2012). The mixing-type ventilation, in which the fresh air supply is tempered by mixing with the indoor air, is largely implemented in cool and temperate climates (Hunt and Linden, 2004). Therefore, it is also considered in the pilot study herein. It should be noted that vertical thermal stratification in a room with a closed window is considered absent, and thus simplified to the initially well-mixed (homogeneous) condition. However, the buoyancy-driven flows between two adjacent building zones with vertical thermal stratification connected by top and bottom vents can be found in Nabi and Flynn (2015).

By opening a window, the unidirectional stratified flow through window may take place, driven by the excess pressure due to mechanical ventilation. Indoor air outflow occurs when the indoor pressure (p_i) exceeds the outdoor pressure (p_o) at window level. It should be noted that the balance between indoor and outdoor pressures may be achieved almost instantly during the opening of a window (ventilation switched off). In the case of continuously operating mechanical ventilation, the bidirectional stratified flow through a window may take place with a net barotropic flow component. This is possible due to the comparatively small excess pressure ($(p_i - p_{air}) / p_i \ll 1$) for living-room in buildings and the large opening area of windows. Therefore, the attention is focused on the bidirectional stratified flow driven by the buoyancy that dominates the air exchange through open windows in cold and hot seasons.

Figure 2-9 illustrates the bidirectional stratified flow through an open window of a single room in the cold season. Due to the buoyancy forces associated with temperature differences between indoor and outdoor environments, the warm indoor air (less-dense) exits through the upper part of the window, and the cold outdoor air (denser) enters into the room through the lower part of the window. The intruding cold outdoor air forms a gravity current that propagates along the floor towards the internal walls (Figure 2-9i). When incoming flow strikes the wall, the cold air will first surge vertically upwards, known as "sloshing", due to which mixing between the ambient air and the current may take place. Accumulation of cold air against the wall results in the transmission of a reflected wave back to the window (Figure 2-9ii) that, however, may temporarily alter the stable inflow conditions by reducing the cold air inflow rate (Q_{lower}). For relatively high windows, the effect of backflow only induces mixing in a room and modifies the ambient air, although stratified flow conditions in an opening remain more-or-less steady. Due to the temperature gradient, stratification develops in the room over time, including two distinct layers with a density jump at the interface. It can be seen from (Figure 2-9iii) that a horizontal interface separates the upper layer, which is composed of air having the initial density of the indoor air (ρ_i), from the lower layer, composed of cold outdoor air ($\rho_o > \rho_i$). During the bidirectional stratified flow, the interface elevation in a room changes, i.e. ascends towards the upper lip of the window, and the two-layer exchange flow culminates when the balanced interface is reached (Figure 2-9iv).

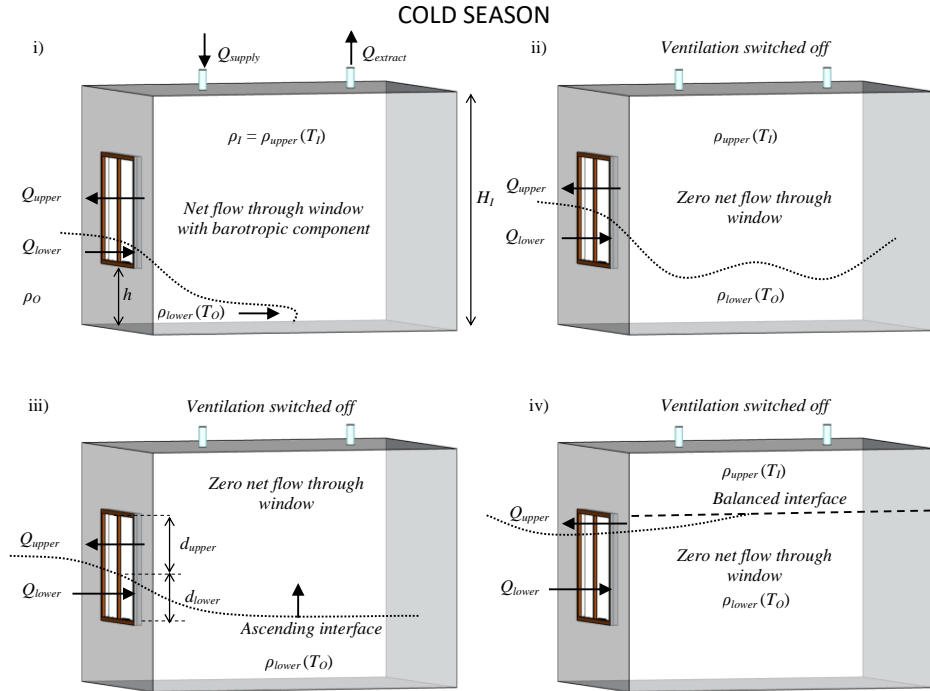


Figure 2-9. Bidirectional stratified flow through an open window of a single room in the cold season. i) Exchange flow with excess pressure due to ventilation and ii), iii), iv) buoyancy-driven exchange flow (ventilation switched off).

Figure 2-10 illustrates the bidirectional stratified flow in a hot season, where the cool indoor air (denser) exits from the lower part and the warm outdoor air (less-dense) enters from the upper part of the window. A warm gravity current forms along the ceiling (Figure 2-10i). However, due to mechanical ventilation connections in the ceiling, the upper layer warm air may mix with the cool supply and partially extract from the top if the ventilation is switched on. Internal walls bound the propagating current, and thus the warm air surges vertically downwards when striking the walls and reflects back towards the window (Figure 2-10ii). Contrary to the cold season case, the horizontal interface in the room descends towards the lower lip of the window, and the bidirectional stratified flow culminates when the balanced interface is reached.

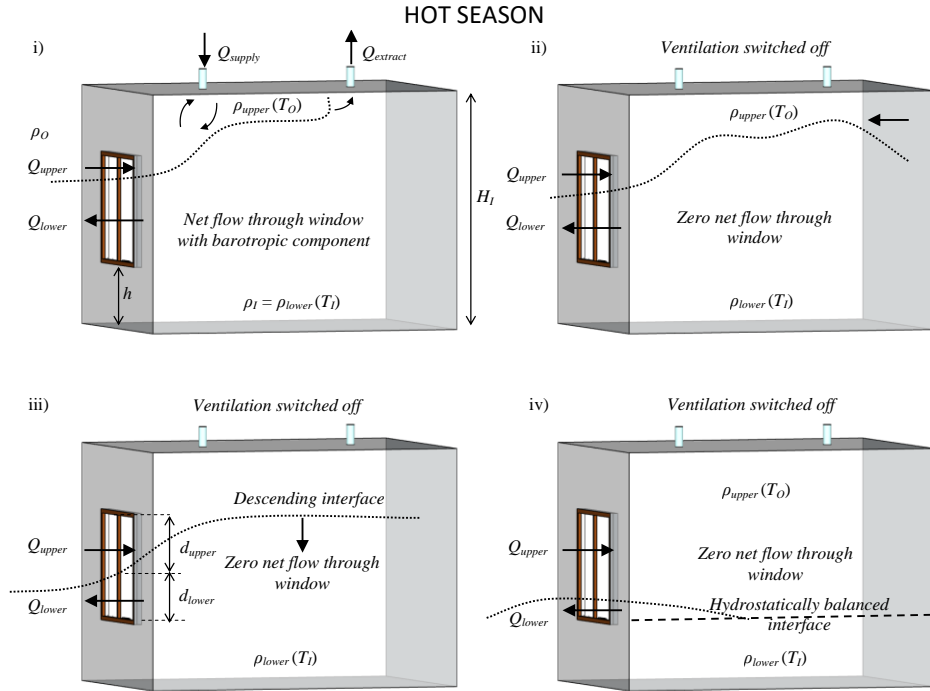


Figure 2-10. Bidirectional stratified flow through an open window of a single room in the hot season. i) Exchange flow with excess pressure due to ventilation and ii), iii), iv) buoyancy-driven exchange flow (ventilation switched off).

In the case of an open window and simultaneously operating mechanical ventilation (Figure 2-9i and 2-10i), the bidirectional stratified flow through a window may take place with a net flow with a barotropic component. This is due to the conditions when the ventilation supply and extraction flow rates are uneven. For instance, in a room that is pressurised relative to the outdoor conditions, i.e. more fresh air is supplied into a room than extracted ($Q_{supply} > Q_{extract}$). In this case, the bidirectional stratified flow is not only driven by the buoyancy due to the density difference, but also by the pressure due to the continuous excess fresh air supply ($Q_{supply} - Q_{extract}$). The excess fresh air supply magnifies the indoor air outflow rate through the window that, in the cold season, corresponds to the upper layer outflow rate (Q_{upper}) and in the hot season to the lower layer outflow rate (Q_{lower}). The effect of mechanical ventilation can be accounted for in the analytical formulae for the volumetric flow rate of bidirectional stratified flow through a rectangular opening (Equations 47 and 50) through the dimensionless flow-rates-ratio parameter (q). Thus, the ratio between the upper and lower layers' discharges (Equation 29) is $q > 1$ in a cold season, and $q < 1$ in a hot season. The upper layer (indoor air) outflow rate and the lower layer (outdoor air) inflow rate through an open window can be determined using Equations (47) and (50), respectively. However, the process parameters of stratified flow, such as hydraulic-flow coefficients and mixing quantities, should be determined in combination with the experimental or numerical results.

If the mechanical ventilation is switched off, the bidirectional stratified flow takes place as zero net flow through an open window, driven only by the buoyancy. In this case, the upper and lower layers' discharges are equal ($Q_{upper} = Q_{lower}$) and the flow-

rates-ratio parameter in Equations (47) and (50) is $q = 1$. However, the interface level in the opening varies; it ascends in the cold season, i.e. lifts from the upper lip of the window to the lower lip of the window, and descends in the hot season, i.e. lifts from the lower lip of the window to the upper lip of the window. The lifting of the interface during the bidirectional stratified flow in the cold season, as well as in hot season, is associated with the variation of the upper and lower layers' flow rates. The location of the interface in the centre of the window cross-section corresponds to the maximum exchange flow rate and sub-maximal flow conditions.

3 Optimisation method

3.1 Search techniques

Search techniques can be broadly classified into three classes (Figure 3-1): calculus-based techniques, enumerative techniques and guided random search techniques.

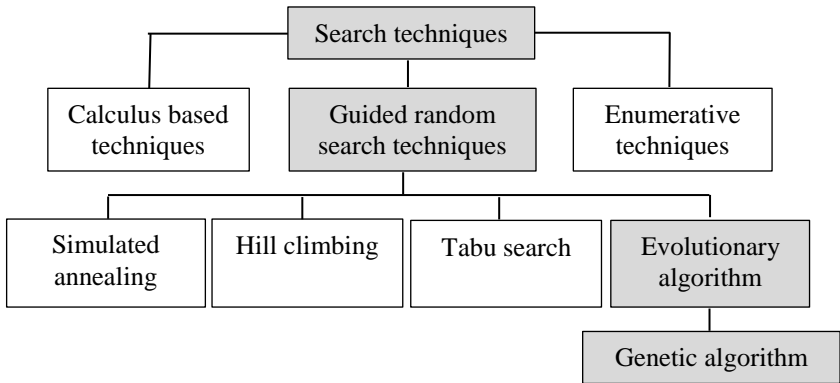


Figure 3-1. Scheme of search techniques.

The success of the optimisation is affected by the properties of the problem, formulation of the objective function, and the selection of an appropriate optimisation algorithm (Palonen, et al., 2009). Obtaining a valid, accurate model of the design problem is the most important step in optimisation (Parkinson et al., 2013). This may be, for instance, a scientific model (process modelling) or an engineering model (system modelling).

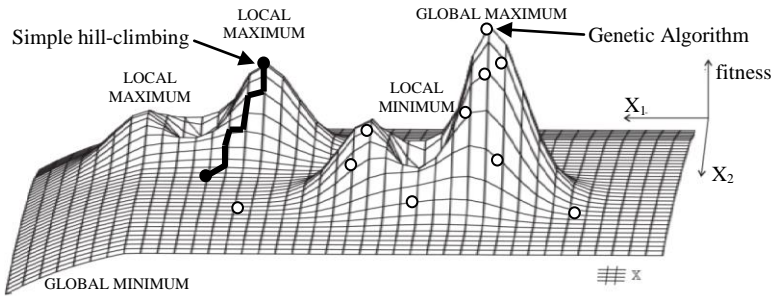


Figure 3-2. Fitness landscape with global and local optima of a two-dimensional function (Weise, 2009). Examples of simple hill-climbing finding the best local maximum and GA finding the global maximum.

Fitness landscapes (Figure 3-2) are often used to help visualise the search space of optimisation problems and to describe the possible pitfalls of the search techniques. Search landscapes can be considered as a range of mountains, where the fitness value of each design determines the height for each point. Fitness peaks (e.g. local or global maxima) represent points from which all paths downhill lead to designs with lower

fitness, and fitness valleys (e.g. local or global minima) represent regions from which paths lead uphill to designs with higher fitness.

Calculus-based methods tend to seek local extreme points (local maxima or minima), either by searching for points with slopes of zero in all directions (indirect methods), or by moving along a function in a direction with the steepest gradient, i.e. simple hill-climbing (direct methods) in Figure 3-2 (Goldberg, 1989). Direct methods seek extremes in the function space and move in a direction related to the local gradient, which finds the best local solution by climbing the steepest permissible gradient. However, indirect methods seek solutions by solving a set of equations resulting from setting the gradient of the objective function to zero. The problem with calculus based techniques is that they rely on the existence of derivatives in a function and tend to find local extremes, rather than the absolute extreme. These techniques can be used only on a restricted set of "well behaved" functions which, therefore, limits their use to very narrow problem fields. However, within their limitations, calculus-based methods can be quite effective in a small class of unimodal problems. However, their outcome may easily be just a local optimum, while the actual best solution would be a global optimum.

Enumerative techniques involve evaluating all of the possible function values of the search space one by one, in order to arrive at the optimal solution (Goldberg, 1989). Dynamic programming is a well-known example of enumerative search. Although these techniques can be useful for very small problem sizes and are simple to implement, their biggest drawback is inefficiency, since they require significant computation. Most search spaces (of even moderate size) are too large, thus it may become simply impossible to search all the points in the space.

A large number of optimisation problems are solved using a GRST (Arora, 2015). GRST are based on enumerative methods, but they use additional information about the search space to guide the search to potential regions of the search space (Goldberg, 1989). The GRSTs are useful in problems where the search space is huge, multimodal, and discontinuous, and where a near-optimal solution is acceptable.

One example of GRST is simulated annealing, which uses a thermodynamic evolution process to search for minimum energy states (Bogdanović, 2011). This method is essentially a modified version of simple hill climbing. Optimisation of a solution involves evaluating the neighbours of a state of the problem, which are new states produced through conservatively changing a given state (Bogdanović, 2011).

The Hill-Climbing with Random Restarts method is a second example devised by combining simple hill-climbing and random methods. This method aims to ascend to a peak by repeatedly moving to an adjacent state with higher fitness. The process is repeated again at another randomly-selected location until: 1) the solution is found or 2) the parameter determining the maximal number of moves between restarts is fulfilled. This method is useful for local optimum searches, since it cannot guarantee to lead to any of the existing better solutions in the search space, which limits its use for global optimum problems. However, it can arrive at optimal solutions within polynomial time for most problem spaces, when the probability theory and local sampling is implemented to direct the restarting of hill-climbing algorithms (Cohen et al., 1994).

The Tabu search is a third example, and is a heuristic method originally proposed by Glover in 1986 to allow local search methods to overcome local optima. Heuristics, i.e. approximate solution techniques, have been used since the beginnings of operations

research to solve difficult combinatorial problems (Gendreau and Potvin, 2005). One of the main components of the Tabu search is the adaptive memory (Tabu list), which creates a more flexible search behaviour. The main problem with the Tabu search is associated with a large search space and particularly high dimensionality, due to which it is easy to stay around in the same neighbourhood even with a very large Tabu list. An extensive description of the Tabu search methodology can be found in Glover and Laguna (1997).

Evolutionary algorithms are a fourth example; these are stochastic search and optimisation heuristics derived from classic evolution theory (Streichert, 2007). Evolutionary algorithms employ specific approaches based on principles of evolution found in nature, and use mechanisms such as reproduction, mutation, recombination, natural selection, and survival of the fittest. Evolutionary algorithms often perform well in approximating solutions to all types of problems, since they ideally do not make any assumption about the underlying fitness landscape (Joshi and Vakaskar, 2011). The greatest advantage of evolutionary algorithms comes from the ability to address problems that are outside of current human comprehension (Joshi and Vakaskar, 2011). Evolutionary algorithms can be applied to complex problems with discontinuous, non-differentiable, and possibly noisy target functions (Eiben and Smith, 2003). They are also robust, easy to use, and applicable to different optimisation problems.

GA is one of the most popular evolutionary algorithm that attempts to explore the entire search space in order to locate the global optimum (Goldberg, 1989). It uses biological concepts to solve optimisation problems through imitating evolutionary processes, based on the Darwinian theory of natural selection (Fang, 2007). However, there is no guarantee that such a point will be found, since there is no such criterion which can demonstrate that a global optimum has been reached. This shortcoming is also present for all other alternative search techniques. However, the GA produces not only a single optimised solution but a population of feasible and improved solutions, which enables the decision-maker to judge on the final solution choices. The main reasons to use a GA are due to its simple concept and wide range of uses (single- and multi-objective problems, hybrid and parallel applications), applicability to noisy and multiple local optima environments, and the possibility to use a large number of parameters. GAs were first introduced in 1962 by the work of John Holland on adaptive systems. His book, *Adaptation in Natural and Artificial Systems* (Holland, 1975), introduced the concept of using the mutation, selection, and crossover, simulating processes of biological evolution as a problem-solving strategy. According to Haupt and Haupt (1998), evolutionary computation is a thriving field, and GAs are used today for "solving problems of everyday interest". It is a powerful problem-solving technique of immense power and nearly unlimited application (Marczyk, 2004).

3.2 Genetic Algorithm

A GA is used for solving the optimisation problems in Publications II, IV, and V. An optimisation problem addressed by a GA is to find the best solution from all feasible solutions. An optimisation model consists of: 1) a set of design variables, 2) a set of constraints, and 3) an objective function.

Design variables represent changeable design parameters, which need to be determined in order to explore the search space (Parkinson et al., 2013). The GA adjusts the design variables in order to satisfy the objective function and constraints.

Design variables can be either continuous, i.e. take any value in the range between the lower and upper limit, or discrete variables, i.e. take predefined specified values (e.g. from a list of standard sizes). Additionally, variables may be related, i.e. once some of the design values are determined (e.g. type of material) other variables related to properties (density, strength, etc.) can be determined straightforwardly. Therefore, during the process of choosing the set of variables, it is useful to lay out the model equations and determine the order in which equations will be calculated (Parkinson et al., 2013).

Constraints representing limits within the solution must stay. In the case of equality constraints, target values must be satisfied (Parkinson et al., 2013). GA optimisation problems may have one or more constraints including inequality, equality, and/or variable bounds to be satisfied. Also, in real engineering applications, usually more than one constraint is involved in the problem (Amouzgar, 2012). Solutions that satisfy all the constraints (inequality and equality) and variable bounds are denoted as feasible solutions. On the contrary, infeasible solutions are solutions that do not satisfy all constraints and variable bounds.

The objective function is being optimised, and this function measures the effectiveness of the design. Most optimisation problems have a single objective function however, there are cases when optimisation problems have no objective function or multiple objective functions. For a single-objective optimisation problem, the optimality is the minimum, maximum, or targeted objective function. In the case of there being no particular objective to optimise, the aim of the problem is to find values for the variables that satisfy the constraints. For multi-objective optimisation problems, the criterion can be defined as Pareto optimality, since such problems involve several criteria that sometimes conflict.

In Figure 3-3 a simple flow chart of GA is presented to explain the sequence of GA steps in the optimisation process.

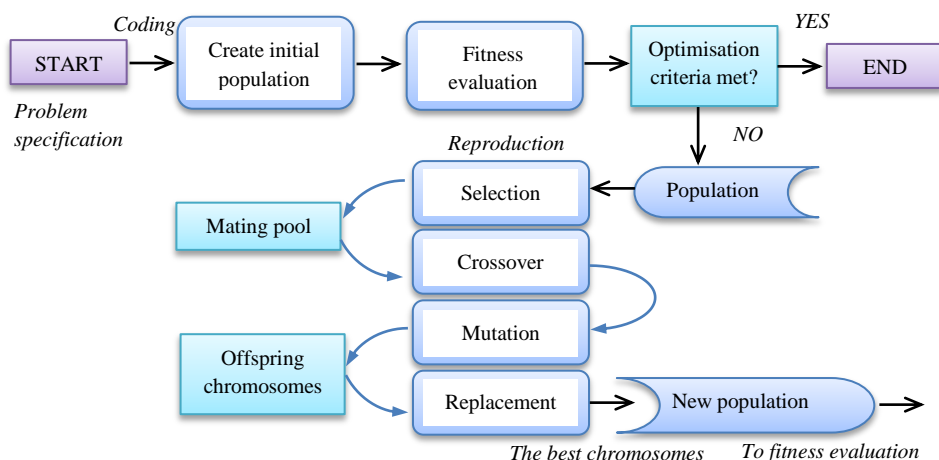


Figure 3-3. Flow chart of basic steps in GA.

In biology, genes are defined as a sequence of DNA that represents certain features of individuals. In GA, binary coding may be used, by which the design containing certain information codes as a chromosome. In most cases, GA follows the typical iteration steps by using binary or floating genes to represent design variables with fixed length

(Parkinson et al., 2013). In binary representation, the 1 and 0 sequence in the GA gene represents a unique solution. Each binary number is thought of as one chromosome of the gene, as in biology. Another possibility, and also the simplest representation, is that the value representation where the chromosome consists of the values of the design variables placed side by side. Chromosome codes may also be permutations of elements, lists of rules, program elements (genetic programming), or any data structure.

The search for solutions begins with the creation of an initial population where each individual represents a point in a search space. The GA creates a random set of designs, which can be spread evenly across the search space, allowing the entire range of possible solutions. The population size (N) specified by the designer is the number of designs in each generation. For instance, a population of 20 to 100 designs often works well (Parkinson et al., 2013).

Evaluation is the link between the GA and the optimisation problem it is solving, which encodes the chromosome and assigns its fitness. In nature, the competition among individuals results in the fittest individuals dominating over the weaker ones. GA shares the same strategy by simulating the survival of the fittest designs. Fitness, i.e. a predefined numerical measure for the problem, evaluates the designs (coded as chromosomes) in the population (Figure 3-4). Each design is analysed to evaluate the objective function (minimised, maximised, or targeted value) of the optimisation problem and constraints. In the case of no assigned constraints, the fitness is simply the value of the objective. In the contrary case, the objective and constraint values are combined into a single fitness value (Parkinson et al., 2013). The fitness can also be defined through the penalty approach and segregation approach.

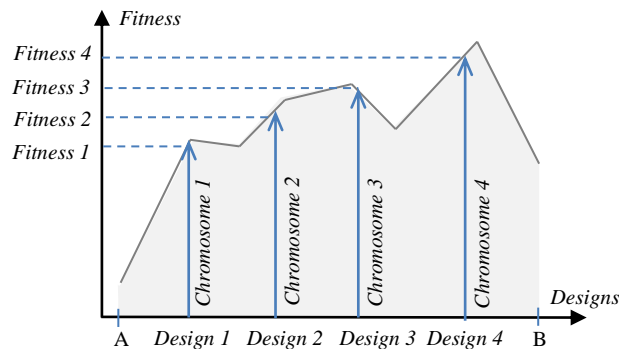


Figure 3-4. Sketch of evaluating the goodness of designs bounded by the constraints A and B.

The selection operator determines the mating pool from individuals of the current population, according to the given measure of fitness, for producing the next generation of designs. Two types of selection methods are generally used: elite and non-elite (Fang, 2007). Elite selection methods ensure that the best individuals of the current population always go to the next population. Elitism favours individuals with the best fitness and uses them to produce more designs. Two of the non-elite selection methods are roulette wheel selection and tournament selection (see Parkinson et al., 2013), which are based on the survival-of-the-fittest strategy. There are also many other methods that can be applied to select the best designs; for instance, rank selection, generational selection, fitness-proportionate selection, and steady state

selection. Note that there is no one selection method that is best for all optimisation problems, because some methods result in fast convergence, others will tend to produce a more thorough exploration of the search space (Dyer, 2008).

The crossover operator exchanges the genes of two selected individuals from the mating pool to create new offspring. The crossover can be performed at either a single point, i.e. one-point crossover, or multiple points, e.g. two-point crossover. Figure 3-5 explains a single-point crossover for swapping the genetic material between two parents with the gene length being five and with the crossover position after the second gene of the chromosome.

The mutation operator makes random gene modifications in some of the offspring's chromosomes, i.e. introduces new points in the search space that help the GA to escape from a local optimum (Rajan, 2013). The predefined mutation probability is compared with a randomly-generated number between zero and one. If the random number is greater than the mutation probability, the gene at a randomly-selected location in a chromosome is flipped to another value. For example, in Figure 3-5, the binary bit is flipped (0 with 1) at a certain position (the first gene of the second offspring).

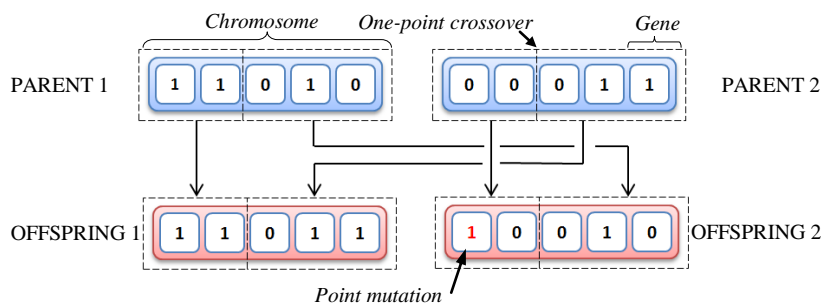


Figure 3-5. Creation of offspring with one-point crossover and point mutation (bit strings representation).

Evolution happens to a population, i.e. a new generation of individuals is created with a different set of chromosomes. In nature, individuals of the next population are much more adapted to their environment compared to their predecessors (at least most of them). The least fit members are not strong enough to survive and mate in the reproduction process. The process of selecting the most fit individuals (carrying advantageous genes) into the next generation is done by the replacement operator. There are two main types of replacement strategies: generational replacement and steady state replacement. In the case of generational replacement, the entire population is replaced by newly-generated offspring (Fogel and Fogel, 1995). In the case of steady state replacement, most fit individuals are passed directly to the next generation, while the rest of the individuals go through the selection process to fill the remaining places in the population.

The population generation process repeats until a termination condition is reached. Common terminating conditions (stopping criteria) are:

- the maximum number of generations is reached;
- predefined computation time is reached;
- the highest-level solution's fitness is reached, or further successive generations no longer produce better results;

- a solution is found that satisfies objective criteria;
- manual inspection;
- combinations of the above.

3.3 Process optimisation

In Publication II, a GA is used for searching the values of combined process parameters, which are defined in the hydraulic-flow optimisation model as variables. There are many unknown empirical parameters involved in the hydraulic modelling of real fluid flows, and it is usually necessary to perform experiments to verify the equations. The determination of unknown fluid parameters, such as discharge coefficients and emulsion density, for unidirectional stratified flow through a submerged side hole of a double-hull tank, is a challenging task. GA is one possible method that can be used for solving complex fluid flow problems. There are multiple methods for both quantitative and qualitative visualisation of fluid flows that can also be implemented to investigate the unknown process parameters, for instance CFD.

3.3.1 Physical modelling

Data from the Sintef Sealab experimental test N12 (see Tavakoli et al., 2011) is used for unidirectional oil outflow modelling from a submerged side orifice of a double-hull tank (Table 3-1).

Table 3-1. Design data for unidirectional oil spill from double-hull tank (test N12).

Main tank geometry (width, depth, height)	1.0 x 0.5 x 1.0 (m)
Ballast tank geometry (width, depth, height)	1.0 x 0.1 x 1.0 (m)
Pool geometry (width, depth, height)	5.0 x 12.0 x 3.0 (m)
Initial oil depth in main tank	$H_I = 0.89$ (m)
Initial emulsion depth in ballast tank	$H_B = 0.0$ (m)
Emulsion depth in ballast tank (balanced surface)	$H_{BB} = 0.31$ (m)
Initial water depth in pool	$H_O = 0.41$ (m)
Height of orifice lower lip	$h = 0.1$ (m)
Unidirectional oil spill duration	$t = 590$ (s)
Inner and outer orifice diameters	$d_I = d_O = 0.022$ (m)
Inner and outer orifice shapes	Circular
Density of oil (olive oil)	$\rho_{oil} = 920$ (kg m ⁻³)
Density of water at 20°C	$\rho_{water} = 988$ (kg m ⁻³)

The test started by simultaneous opening of inner and outer orifices. No oil outflow occurred during the side ballast tank filling with oil-water mixture (emulsion) down to the orifice level. The overall duration of the unidirectional flow was 590 seconds and 222 litres of oil left the main tank, from which 180 litres of oil spilled into the pool and 42 litres were retained in the ballast tank.

3.3.2 Hydraulic-flow problem

During the unidirectional oil spill from a double-hull tank, oil and water inflow into the ballast tank, i.e. space between the inner and outer walls of a tank, take place from the inner cargo tank and the pool, respectively. This results in the formation of emulsion in the ballast tank, which alters the dynamics of the unidirectional oil outflow through both orifices due to the changing emulsion density and surface lift in the ballast tank.

Therefore, the determination of discharge coefficients for the inner and outer orifices, according to the experimental results of Tavakoli et al. (2011), cannot be done in a straightforward manner. However, in combination with experimental results, this provides some quantitative information on the behaviour of: 1) oil outflow from the main tank, 2) oil capture in the ballast tank, and 3) oil spill into the pool (Figure 3-6). GA can be used for searching the values of the combined process parameters, which are defined in the optimisation model as variables. The hydraulic-flow problem involves determining the emulsion volumetric flow rate in the ballast tank that is related to the oil influxes and outfluxes of the ballast tank. The derived analytical formula for the volumetric flow rate of the unidirectional stratified flow through a submerged side opening, which makes use of the GA-found discharge coefficients and emulsion density, is used to determine the oil outflow rates for the inner (*I*) and outer (*O*) orifices in the optimisation model.

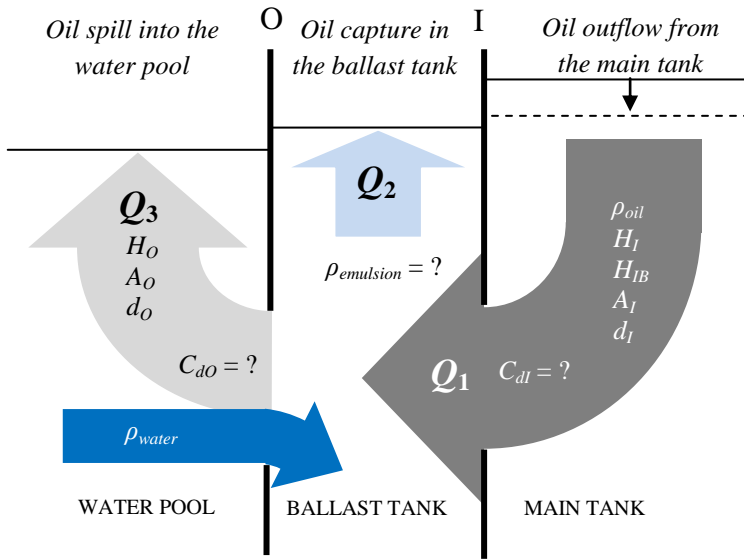


Figure 3-6. Schematic illustration of hydraulic-flow optimisation problem.

3.3.3 Setup and run of process optimisation

The optimisation is performed as an attempt to reach the target value, i.e. the emulsion flow rate into the ballast tank. The objective function of the single-objective hydraulic-flow problem is determined as:

$$Q_2(C_{dI}, C_{dO}, \rho_{emulsion}) = Q_1 - Q_3, \quad (98)$$

where Q_1 is the unidirectional oil outflow rate ($\text{m}^3 \text{s}^{-1}$) from the main tank, Q_2 is the emulsion flow rate ($\text{m}^3 \text{s}^{-1}$) in the ballast tank, and Q_3 is the unidirectional oil spill flow rate ($\text{m}^3 \text{s}^{-1}$) into the pool. The GA determines the three following design variables:

- value of the discharge coefficient C_{dI} for the inner orifice, (1);
- value of the discharge coefficient C_{dO} for the outer orifice, (1);
- emulsion density $\rho_{emulsion}$ in the ballast tank, (kg m^{-3}).

The optimisation problem has three constraints (variable bounds) to be satisfied:

- $0 \leq C_{dl} \leq 1$;
- $0 \leq C_{do} \leq 1$;
- $920 \leq \rho_{emulsion} \leq 988$.

Notations used in the hydraulic-flow optimisation model are explained in Figure 3-7.

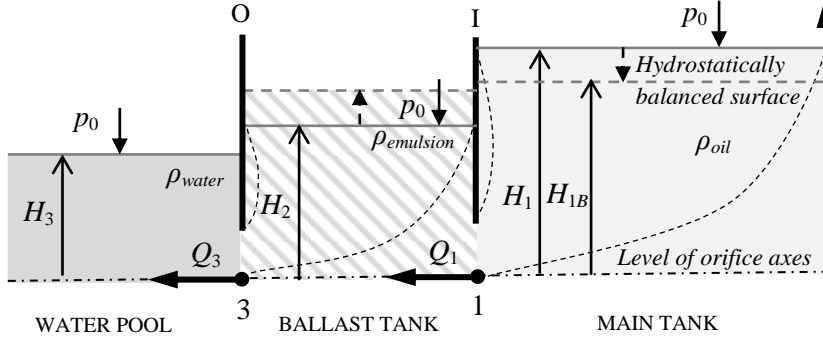


Figure 3-7. Notations of unidirectional oil spill from double-hull tank side orifice.

Equations applied in the hydraulic-flow optimisation model are listed in Table 3-2.

Table 3-2. Hydraulic-flow optimisation model equations and explanations.

Equation	Explanation
$A = \pi \frac{d_l^2}{4} = \pi \frac{d_o^2}{4} = 0.0004 \text{ (m}^2\text{)}$	Inner and outer orifice areas.
$H_3 = H_o - h - \frac{d_o}{2}$	Fluid depth above the orifice axes in the pool.
$H_1 = H_l - h - \frac{d_l}{2}$	Fluid depth above the orifice axes in the main tank.
$H_2 = H_b - h - \frac{d_l}{2}$	Emulsion depth above the orifice axes in the ballast tank.
$H_{1B} = \frac{\rho_{oil}}{\rho_{water}} H_3 = 0.33 \text{ (m)}$	Fluid depth above the orifice axes in the main tank, representing balanced surface end of unidirectional flow.
$Q_1 = 1000 C_{dl} A \sqrt{2g \left(H_1 + \frac{\rho_{emulsion}}{\rho_{oil}} H_2 \right)}$	Unidirectional oil outflow rate from the main tank.
$Q_3 = 1000 C_{do} A \sqrt{2g \left(H_2 + \frac{\rho_{water}}{\rho_{emulsion}} H_3 \right)}$	Unidirectional oil outflow rate into the pool.
$Q_2 = Q_1 - Q_3$	Emulsion flow rate in the ballast tank.

Note that the unidirectional stratified oil outflow lasted 590 seconds. The fluid depths H_1 and H_2 in the main tank and in the ballast tank, respectively, and optimisation target, emulsion flow rate Q_2 , are calculated for each time step $\Delta t = 25$ seconds (see Figure 3-8). The emulsion flow rate values are related to the captured oil volume in the ballast tank (cf Tavakoli et al., 2011). According to the experimental data, it took

approximately 25 seconds to fill the bottom part of the initially-empty ballast tank with emulsion up to the orifice level, i.e. attaining the submerged condition for the inner and outer orifices. The GA is implemented for each time step, separately inserting the values mentioned above manually.

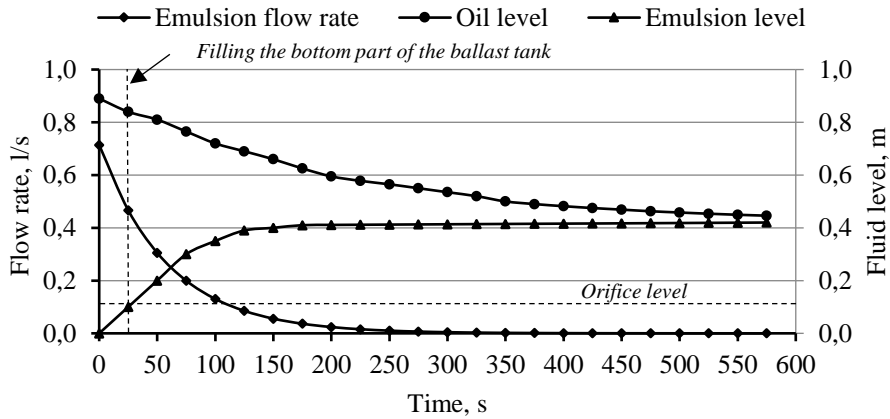


Figure 3-8. Experimental results of oil and emulsion level in the main tank and in the ballast tank, respectively, and the emulsion flow rate in the ballast tank. Curves are reproduced according to the results in Tavakoli et al. (2011).

The GA run settings for process optimisation are listed in Table 3-3.

Table 3-3. GA settings for process optimisation.

Number of chromosomes in population	12
Cross-over probability	0.8
Cross-over type	One-point
Mutation probability	0.01
Random selection probability	0.1
Constraint penalty	1e12
Absolute constraints tolerance	0
Max. number of generations	100
Convergence tolerance	0.00001
Numeric precision (digits)	6
Number of preliminary runs	4
Max. number of generations per preliminary run	10

The order of the process parameters optimisation by the GA is shown in Table 3-4.

Table 3-4. Process optimisation order.

1. Set values for GA (see Table 3-3).
2. Insert constraints for C_{dl} , C_{dO} , $\rho_{emulsion}$.
3. Set values from experimental data (see Table 3-1).
4. Calculate inner and outer orifice areas A_i and A_o .
5. Calculate water depth (H_3) in the pool.
6. Insert oil level (H_i) in the main tank from Figure 3-8

7. Insert emulsion level (H_B) in the ballast tank from Figure 3-8.
8. Calculate fluid depth (H_1) in the main tank.
9. Calculate emulsion depth (H_2) in the ballast tank.
10. Insert the emulsion flowrate (target) from Figure 3-8.
11. Get values of design variables from optimiser: C_{dl} , C_{dO} , $\rho_{emulsion}$.
12. Calculate the unidirectional oil outflow rate from the main tank.
13. Calculate the unidirectional oil outflow rate into the pool.
14. Calculate the emulsion flow rate in the ballast tank.
15. Store results.
16. Continue above procedures (6–15) for each time step.

3.3.4 Results of process optimisation

At the beginning of the oil spill, the discharge coefficients were $C_{dl} = 0.24$ and $C_{dO} = 0.06$, and during the test oil outflow decreased to $C_{dl} = 0.01$ and $C_{dO} = 0.01$ for the inner and outer orifice, respectively. The average minor head-loss coefficients for the inner orifice were $k_{1, side} = 4.30$ and $k_{2, side} = 203$ and for the outer orifice $k_{1, side} = 4.30$ and $k_{2, side} = 2499$. Both the determined discharge coefficients and the emulsion density in the ballast tank during the oil spill are presented in Figure 3-9. It should be noted that in the case of the side orifice of a double-hull tank, the discharge coefficients were relatively small compared to the results of a side orifice of the single-hull tank (mean discharge coefficient $C_d = 0.50$). Apparently, strong internal mixing is a reason for the emulsion in the ballast tank having varying density (Figure 3-9ii).

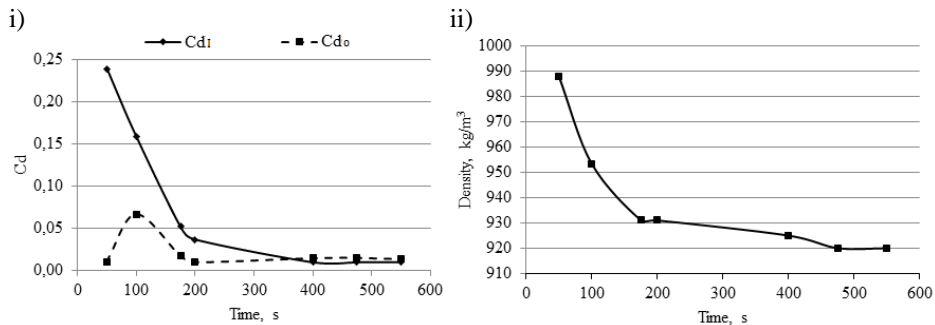


Figure 3-9. Results of GA-determined i) discharge coefficients at the inner and outer orifices and ii) emulsion density change in the ballast tank (see Publication II).

3.4 System optimisation

Complex integrated systems require guidelines for engineering design and everyday usage to meet up-to-date requirements of energy demands and safety. Finding solutions for an efficient design of built-environment integrated systems is a challenging task, and is of practical interest in the decision-making process. Often, integrated system optimisation is done implicitly, by using a combination of experience, modelling, judgement, etc.—hoping to achieve an optimal design and operation (Parkinson et al., 2013). In reality, numerous variables in the optimisation problem, and complex interactions between processes, make experience-based decision-making inefficient in terms of identifying the optimum solution. GA performs well in finding an

optimal design (or set of optimal designs) among many feasible solutions to a problem. The ability to deliver good-enough solutions for complex problems in a fast-enough computation time makes GA an attractive method for system optimisation. It should be noted that the final design essentially depends on economic conditions and the decision-maker's preference. However, the inclusion of the cumulative expenses of the optimal solutions found by GA are important for management decision analysis.

3.4.1 Engineering modelling

An apartment building, i.e. a representative of residential buildings in Publication V, is chosen to demonstrate the employment of GA for searching for the dimensions of integrated-system design parameters, such as the stormwater storage tank volume and the catchment area. On-site stormwater collection for domestic-water heating depends essentially on 1) prevalent climate conditions, 2) hot water consumption of the building, and 3) the availability of free space.

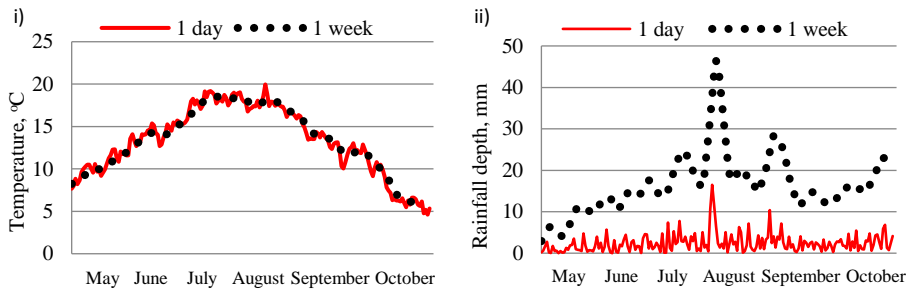


Figure 3-10. Daily mean i) rainfall-depth and ii) rainwater temperature for years 2004 to 2011. i) Calculated mean rainfall-depth over a period of one week, ii) mean rainwater temperature averaged over a period of one week.

The prevalent climate conditions exert a strong influence on local meteorological characteristics, such as rainfall intensity and temperature, that define the thermal energy of stormwater available for usage. In Publication V the rainfall data for eight years (2004–2011) measured by the Tallinn-Harku Meteorology Station (EMHI) is used to estimate the short-term mean values of the temperature and rainfall depth (integrated-system model input parameters) according to the building's functionality. The rainfall depth is calculated over the period of one week (dotted curve) using data of the daily mean rainfall depth for eight years (full curve) in Figure 3-10i. The stormwater temperatures are determined for an apartment building's duty cycle of one week (dotted curve) using the mean temperature over the eight years for each day (full curve) during the rainy season in Figure 3-10ii.

Hot water consumption depends on the functionality of the building. In an apartment building (Table 3-5), usage of hot water includes cooking, cleaning, showering, bathing, and hand washing. The daily consumption of volumetric flow rate is determined according to the hot water demand given in Kõiv and Toode (2010) where data is based on extensive experimental measurements and real hot water demands in Tallinn city. An average weekly consumption of chosen apartment building is 0.1 l s^{-1} (62.3 m^3 in one week) and it is considered that a one-week *duty cycle* represents the building inhabitants' hot water usage trends.

Table 3-5. Apartment building characteristics.

	Apartment building
Number of flats	90
Sinks	180
Showers	90
Weekly hot water consumption (q_{HW}), l s ⁻¹	0.1
<i>Duty cycle</i>	1 week

The availability of free space sets limits for the dimensions of integrated-system design parameters (catchment area and stormwater storage tank volume). Three options are available for rainwater collection for apartment building: the building's roof, parking lot area, and nearby catchments, e.g. roads and roofs (Table 3-6). Usually, apartment buildings have a flat roof, thus the roof area is determined according to the building's dimensions. The size of the parking lot area depends on the requirements for providing the parking space according to the number of flats in the apartment building. Herein, the minimum parking lot area is considered, which is 45 parking places with measurements of 2.5 x 5 (m) for 90 apartments in the existing block, i.e. 0.5 parking lots per apartment (EVS 843:2003). It is also possible to use rainwater from roads and from neighbourhood roofs, in the case of infrastructure availability.

Table 3-6. Available catchment areas for an apartment building.

Roof area, ha	0.1
Minimum parking lot area, ha	0.12
Roads and other impervious surfaces, ha	Depending on need

The stormwater storage tank volume depends on the possibility of installing an underground tank. For apartment buildings, the maximal stormwater storage tank volume is considered to be 100 m³, which is within the limits of free space for tank installation (minimum parking lot area 20.0 x 5.0 m).

3.4.2 Integrated-system model problem

The integrated-system model of stormwater collection and domestic-water heating is developed in Publication IV, and the modified model is applied for different types of buildings (residential, public, and commercial) in Publication V. The integrated system consists of 1) the rainwater harvesting area, 2) the stormwater storage tank, and 3) the hot water production system (Figure 3-11).

The aim is to find an optimal solution for constant domestic hot water production for an apartment building during a building's *duty cycle* of one week. It is considered that the hot water consumption of a building determines the required heat load while the rainfall intensity over an urban catchment and air temperature define the thermal energy of stormwater available for usage. The integrated-system model, taking use of the stormwater heat extraction equation and domestic water heat load formula, is used to determine the hot water production days (see Publication V). However, it is currently unknown how large an urban catchment area is required to harvest the necessary rainwater and how large a storage tank should be used to satisfy the apartment building demands for domestic hot water production. GA is employed to find the integrated system parameters, such as stormwater volume in storage tank for

heat extraction and number of tank fillings due to harvested rainwater from catchment area, which are defined in the optimisation model as variables.

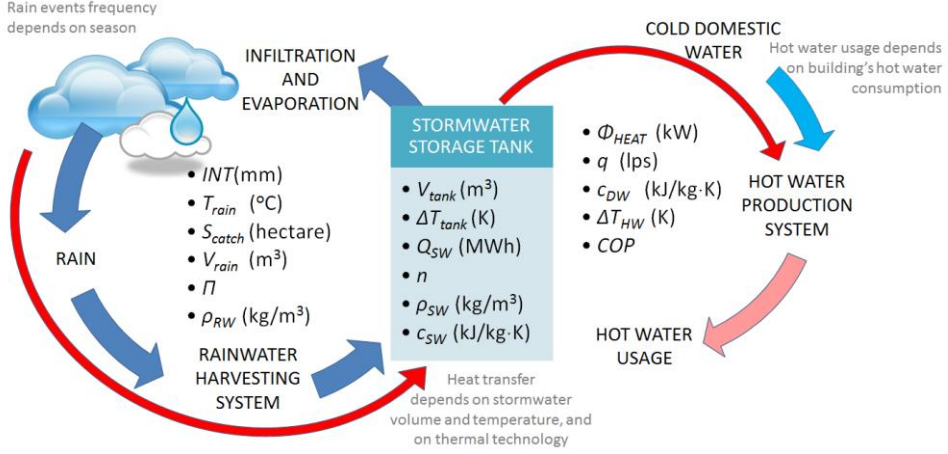


Figure 3-11. Schematic illustration of stormwater collection and domestic-water heating integrated system and notations.

3.4.3 Setup and run of system optimisation

The optimisation is performed as an attempt to reach the target value, i.e. the hot water usage days (*duty cycle*) during rainy season months using local meteorological characteristics, such as rainfall intensity and temperature. The objective function of the single-objective integrated-system problem is determined as:

$$days(n, V_{tank}) = \frac{Q_{SW}}{Q_{HW}}, \quad (99)$$

where Q_{SW} is the energy (kWh) available from the stormwater storage tank per *duty cycle*, Q_{HW} is the energy (kWh) required to warm up the domestic water from the initial temperature of 5°C to 55°C per day. GA determines the two following design variables:

- the number of tank fillings n (1);
- the stormwater volume in the storage tank V_{tank} (m³).

The optimisation problem has two constraints to be satisfied:

- $10 \leq V_{tank} \leq 100$;
- $1 \leq n \leq 10$.

The number of stormwater tank fillings required during an apartment building's *duty cycle* expresses virtually the ratio of time scales of stormwater heat extraction from the storage tank and the rainfall return period. It is considered that the heat extraction from stormwater results in the stratified flow through the storage tank that regulates the number of storage tank fillings. The minimal value $n = 1$ corresponds to the stormwater storage tank filling once a week, and the maximal value $n = 10$ corresponds to ten fillings per week. Higher values for n will expand the catchment area

vastly, which in the case of an apartment building is not feasible. For instance, in May, when the rainwater temperature and rainfall depth are rather low, the required rainwater volume at catchment to satisfy the building's needs with the maximal storage tank size of 100 m³ results in a catchment of the size of a district. Therefore, it is reasonable to limit the number of tank fillings to keep the values real.

Equations applied in the integrated-system optimisation model are listed in Table 3-7.

Table 3-7. Integrated-system optimisation model equations and explanations.

Equation	Explanation
$\Phi_{HEAT} = \frac{q_{HW} \cdot \rho_{DW} \cdot c_{DW} \cdot \Delta T_{HW}}{1000}$	The heat flux (kW) needed to warm up the domestic water, where $\rho_{DW} = 1000$ (kg m ⁻³) is the domestic water density, and $c_{DW} = 4.19$ (kJ/kg·K) is the domestic water specific heat.
$\Delta T_{HW} = T_{HW} - T_{DW}$	Domestic water temperature rise $\Delta T_{HW} \leq 50$ (K), where T_{HW} and T_{DW} are the hot and cold domestic water temperatures (°C), respectively.
$Q_{HW} = \Phi_{HEAT} \cdot 24hour$	Energy need (kWh) per day for hot water production.
$Q_{SW} = 0.28 \cdot n \cdot V_{tank} \cdot \rho_{SW} \cdot c_{SW} \cdot \Delta T_{tank} \cdot 10^{-3}$	The energy (kWh) available from the storage tank, where $\rho_{SW} = 1000$ (kg m ⁻³) is stormwater density, $c_{SW} = 4.19$ (kJ/kg·K) is stormwater specific heat.
$\Delta T_{tank} = T_{SW} - T_{cooldown}$	The excess temperature (K) available for the heat-exchange process, where T_{SW} is stormwater temperature (°C) and $T_{cooldown} = 4^{\circ}\text{C}$ is the minimum return temperature.
$S_{catch} = \frac{V_{tank} \cdot n}{INT \cdot 1000}$	Required catchment area (m ²), where INT is rainfall depth (mm).
$f_{ce} = \frac{V_{tank}}{a} + \frac{S_{catch}}{b}$	Cumulative expenses (1), where $a = 1.0$ m ³ is the stormwater-volume unit, and $b = 0.1$ ha is the catchment-area unit.

GA run settings for system optimisation are listed in Table 3-8.

Table 3-8. GA settings for system optimisation.

Number of chromosomes in population	8
Cross-over probability	0.8
Cross-over type	One-point
Mutation probability	0.01
Random selection probability	0.1
Constraint penalty	1e12
Absolute constraints tolerance	0
Max. number of generations	100

Convergence tolerance	0.00001
Numeric precision (digits)	6
Number of preliminary runs	4
Max. number of generations per preliminary run	10

The order of the integrated-system model parameters optimisation by GA is shown in Table 3-9.

Table 3-9. System optimisation order.

1. Set values for GA (Table 3-8).
2. Insert constraints for V_{tank} , n .
3. Insert the usage days (target).
4. Set values for the apartment building (Table 3-5).
5. Insert cold domestic water temperature, T_{DW} .
6. Calculate domestic water temperature rise, ΔT_{HW} .
7. Calculate heat flux needed to warm up the domestic water, Φ_{HEAT} .
8. Calculate energy needed per day for hot water production, Q_{HW} .
9. Insert averaged rainfall depth INT for a specific week from Figure 3-10i.
10. Insert averaged temperature T_{SW} for a specific week from Figure 3-10ii.
11. Calculate excess temperature available for the heat-exchange process, ΔT_{tank} .
12. Get values of design variables from optimiser: V_{tank} , n .
13. Calculate the required catchment area, S_{catch} .
14. Calculate the cumulative expenses for the integrated system, f_{ce} .
15. Store results.
16. Continue above procedures (9–15) for each week during the rainy season.

3.4.4 Results of system optimisation

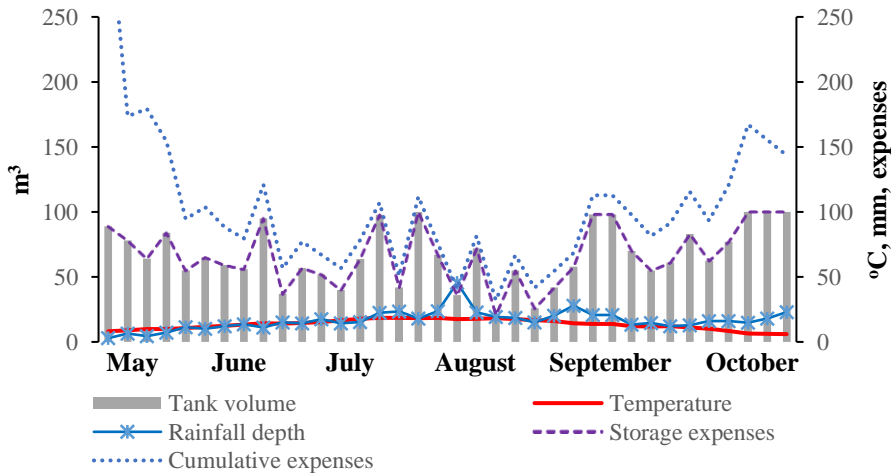


Figure 3-12. Apartment building optimal tank volume, temperature, mean rainfall-depth and expenses on dates: 5th, 10th, 15th, 20th, 25th, and 30th of the rainy months.

The GA results in Figure 3-12 confirm that the stormwater volume in the storage tank varies between 21 m³ (in mid-August, when the rainwater mean temperature is over

18°C, and one-week's rainfall depth is 19 mm) and 100 m³ (in late October, when the temperature is under 7°C, and the rainfall depth is 16 mm), during the rainy season for the apartment building. Note that the cumulative expenses in Figure 3-12 almost correspond to the storage expenses during the summer months. Peaks in the stormwater volume during several summer months in Figure 3-12 correspond to the storage tank, which is seldom filled ($n = 2-3$) during a week and, thus, represents a comparatively expensive solution. It was found that the average number of storage tank fillings is in the range of two to six during a week. Frequent filling of the storage tanks enables rapid replacement of stormwater, guaranteeing continuous hot water production. However, it is not possible to continuously charge the storage tanks during the rainfall period from May to October.

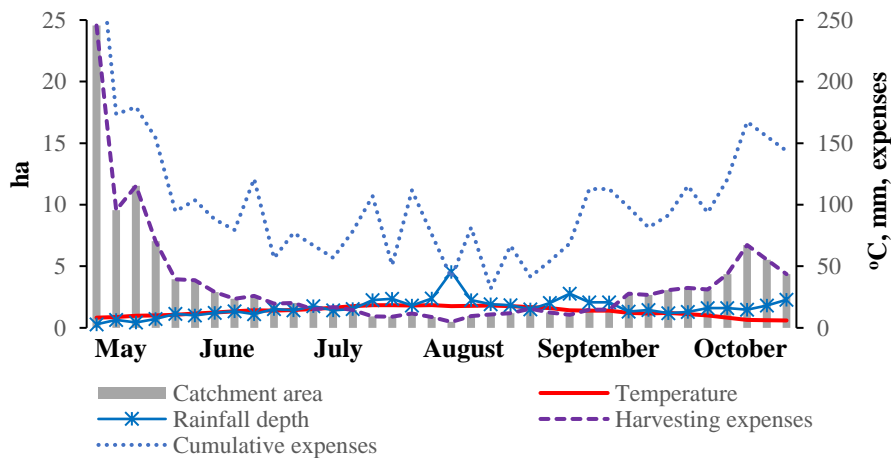


Figure 3-13. Apartment building optimal catchment area, temperature, mean rainfall-depth and expenses on dates: 5th, 10th, 15th, 20th, 25th, and 30th of rainy months.

The GA results in Figure 3-13 confirm that the catchment area varies between 0.47 ha (in early August, when the rainwater mean temperature is over 17°C, and one week's rainfall depth is 46 mm) and 24.56 ha (in early May, when the temperature is 8°C, and the rainfall depth is 5 mm). It is found that the catchment area mainly stays in the range of 0.48 ha to 3.50 ha. It was found that the building's roof and parking area catchments are not sufficient to supply the needed rainwater volume for the integrated system. The integrated system is cost effective during the period between the end of May and the beginning of October.

Inclusion of the cumulative expenses parameter of the optimal solutions found by the GA is important for management. The cumulative expenses parameter, which corresponds to the sum of two control factors: 1) stormwater storage expenses and 2) stormwater harvesting expenses, is introduced in Publication V. It is important to note that the rainwater from the area in question originating from the roof, parking lot area, and nearby catchments may differ considerably in quality. The less-polluted rainwater is preferred for collection for heat extraction, since the use of more contaminated rainwater increases the stormwater treatment expenses. The results in Figure 3-14 indicate that the optimal solutions are most expensive in May and October, when the rainwater temperature is low and a large number of tank fillings is required. This

confirms that, during the cold rainfall period months, a large amount of stormwater is needed to provide the building with the necessary thermal energy. The cost effective optimal solutions are apparent for June, July, and August, when the storage tank is seldom filled.

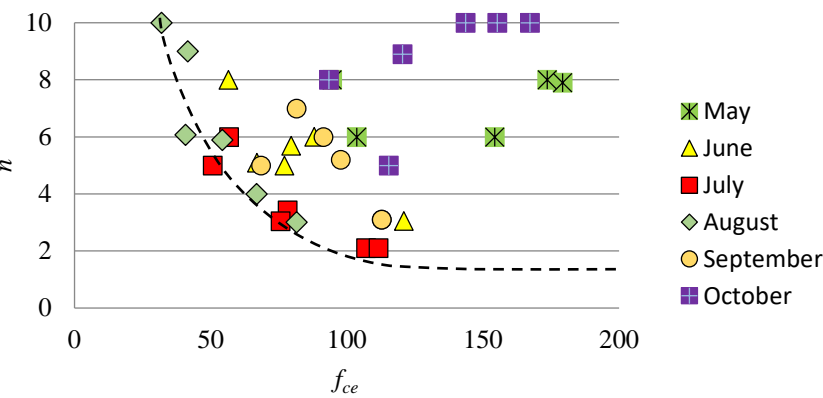


Figure 3-14. Estimated cumulative expenses parameter (f_{ce}) for a number of tank fillings (n) for the apartment building during specific rainfall periods.

4 Practical challenges

The hydraulic-theory solutions are useful in solving a number of fluid engineering problems in built environment enclosures, including: 1) risk assessment of oil spills, 2) making use of renewables e.g. employment of low-temperature water sources, and 3) energy efficiency of buildings.

In risk assessments of built environment enclosures it is important to consider risks associated with stratified flows that may have a significant environmental, financial, or health impact. Possible accidental outflows, such as leakage of hazardous fluids from damaged enclosures, may cause serious environmental consequences, the prevention of which require fast calculation tools for planning and preparing effective response strategies. Large leaks from built environment enclosures can also result in economic loss, e.g. oil lost from a damaged tanker during an accident, or preheated indoor air outflow from a building. Small unintentional leaks are mainly associated with energy losses, e.g. air leaks from airtight and insulated buildings. In order to assess the potential environmental or financial risks posed, it is essential to predict the amount and duration of fluid leakage for different enclosure configurations and leak points. Furthermore, the growing demand for energy in urban areas makes the use of local energy sources (e.g. low-temperature fluid) more attractive and economically more competitive than other renewables (Directive 2009/28/EC). For instance, heat extraction from thermally-stratified fluids in built environment enclosures, e.g. from stormwater in storage tanks or indoor air in buildings, can be seen as a potential heat source for on-site end-users. Employment of low-temperature fluids in heating systems may contribute to an increase in the energy efficiency of buildings, and increase the multi-functionality in urban infrastructure.

4.1 Risk assessment

The derived hydraulic-theory solutions are used in the oil-spill model that has been developed for oil-leak calculations from damaged tankers. The fast-operating model contributes to the project MIMIC. Publication I presents the oil-spill model that can be applied quite generally to predict the oil spill for different tank filling levels. The practical outcome of the model is the estimation of the spilled oil volume and duration for different tanker configurations and cargo oils. Publication II extends the oil-spill model for an exchange flow through a circular hole, and presents the experimentally-determined discharge coefficients that can be implemented in hydraulic models with similar opening geometry. It is demonstrated that for oil spills from complex tank configurations (e.g. double-hull tank), the process parameters of stratified flows, such as discharge coefficients and emulsion density, can be determined by implementing GA.

The oil-spill model is combined with the damage assessment model by Tabri et al. (2015) to form the ADSAM. ADSAM is a web-based tool that allows the convenient definition of an accidental scenario, and provides a report including the damage description, and the amount and duration of the oil spill. It should be noted that ADSAM is a part of a larger simulation environment that integrates: 1) statistical analysis to evaluate the relevant accidental scenarios, 2) ADSAM, and 3) Smart-Response Web-based environment consequence evaluation. In the case of real accidents, the simulation environment can be used as a tool that provides response-related awareness, i.e. presents an accidental outcome that includes the amount and

duration of oil spill, spill movement according to the actual weather conditions, and the environmental impact. The performance of this integrated simulation environment is demonstrated by simulating a number of grounding accidents close to the Port of Muuga in the Gulf of Finland (see Tabri et al., 2015). The simulation environment can be used for risk analysis studies in order to develop the measures and regulations to improve safety at sea (Heinvee, 2016). The developed integrated tool is already used by Estonian oil spill response authorities for contingency planning, training, and in emergency situations (Haapasaari et al., 2014).

Publication III presents the enhanced oil-spill model, which is used for a parametric study on the influence of winter conditions on oil outflow quantities. The dynamical effects due to mixing (emulsification) and heat exchange are parametrized for the exchange flow through a submerged opening, which affects the flow rates, outflow volumes, and process durations. The water-ice-oil mixture near the ship's hull affects the oil outflow conditions, resulting in changes of outflow duration and volume. The oil spill model extended to winter conditions contributes to the project BONUS STORMWINDS. The project has an overall objective to enhance the safety of maritime transportation in the Baltic Sea through science-based decision support and technological developments. The web-based simulation tool for estimating the volume of oil spilled in a collision or grounding accident is extended for winter conditions. According to the simulation tool results for accidental oil spill, accident location, oil properties and actual weather conditions, the Seatrack Web simulates the oil spill spreading in the sea area and the sizes of the polluted areas.

4.2 Renewables

In Publications IV and V, the low-temperature stormwater is considered to be a carrier of thermal energy in the urban environment, because it is temporarily freely available in large quantities and is relatively warm. Stormwater has a large heat capacity and, therefore, city-sized catchment volumes of collected stormwater represent a considerable potential source of thermal energy. Although the theoretically-available heat in the urban water sources is comparatively large, the practical heat recovery potential may be limited (Laanearu et al., 2017). Generally, heat extraction from low-temperature fluids is considered challenging due to the available heat extraction technology and limitations of available end-users. However, newly-developing technologies, for instance heat pumps, can provide significant opportunities for low-temperature water usage for potential end-users, such as domestic water heating and space heating in buildings, that require a heat load at a temperature slightly higher than the source.

Publication IV presents the approach of integrating the stormwater and a public building water-heating system to analyse the possibility of thermal heat usage from collected stormwater for domestic hot-water production. For productive low-temperature stormwater integration, three essential components are required: 1) an accessible catchment for stormwater harvesting, 2) a stormwater storage tank for heat extraction, and 3) the hot water production system for end-use. Publication V extends the approach for the optimal collection of stormwater through maximising the water-absorbed heat usage in relation to hot water consumption in different types of buildings (residential, public, and commercial). Finding solutions for an efficient design of built-environment integrated systems is a challenging task, and the determination of integrated system parameters (e.g. stormwater volume in the storage tank for heat

extraction, the number of tank fillings due to harvested rainwater from the catchment area) require energy-based optimisation. In order to utilise the locally-available resources, GA is consistently employed in Publication V for searching the dimensions of integrated-system design parameters. Within many possible solutions, dimensions for the stormwater storage tank and rainwater catchment area are determined for estimating the availability of stormwater thermal energy for domestic hot-water consumers.

The developed integrated model can be used as a resource assessment tool that enables energy project leaders and decision-makers to evaluate the opportunities for the employment of this low-temperature water source with end-users. One practical outcome of this assessment tool is the possibility of guiding building development in assessing whether a new building has the necessary catchment area (e.g. roof, parking area, etc.) to harvest the rainwater to support a future installation of this integrated system. Another outcome is the possibility of determining the amount of thermal energy in an existing stormwater storage tank installed to mitigate impacts from extreme climate events. Integration of nearby stormwater tanks, for instance stormwater retention tanks for flooding control, with local end-users allows the increase of multi-functionality in the urban infrastructure.

In the integrated-system model, it is considered that the hot water consumption of a building determines the required heat load, while the rainfall intensity over an urban catchment, as well as the air temperature, defines the thermal energy of stormwater available for use. In order to determine the hot water consumption of a building that defines the required heat load for heat extraction, it is important to fix a building's *duty cycle* for calculations. In the design of a thermal energy storage tank, it is important to determine tank fillings (n), which depends on the heat extraction for heating applications and available stormwater volume in the catchment.

A building's *duty cycle* is the portion of time during which the building's stormwater tank is operated according to the building functionality. Residential, public, and commercial buildings are the buildings which are mostly used in urban areas, and are most appropriate for on-site stormwater collection for the purpose of domestic water heating in terms of technological solutions and infrastructure availability. Until now, there have been no specific criteria for the selection of the building's *duty cycle*; however, an approximate method can be considered to define a building's *duty cycle*, including mains water usage trends in the building. Publication V relates the building's *duty cycle* to the period during which the building's hot-water consumption has periodicity. For instance, in the case of a residential building, the domestic hot water consumption varies daily, i.e. there is a distinct difference in consumption during business days and during the weekend, but the hot water usage-profile remains constant for different weeks throughout the rainy period. Therefore, the *duty cycle* of a residential building is considered to be one week, representing in Publication V a reference period that is considerably shorter than the rainfall period. According to the available data from Kõiv and Toode (2010), domestic hot water usage in public and commercial buildings is more smoothly distributed than that in residential buildings. Also, buildings with large catchment areas allow the harvesting of more rainwater for longer-term usage. Thus, one-week precision-determined duty cycles are used for calculations according to the importance of hot water production and the functionality of the building that includes the size and availability of catchments. In Publication V the

duty cycle of the public building is two weeks (two reference periods), and for commercial building three weeks.

While hot water consumption depends on a building usage profile, rainwater input into the stormwater system has a more random character. Prevalent climate conditions have a strong influence on thermal energy collection due to variation in rainfall intensity, temperature, and rain return period from a specific catchment. Whereas stormwater storage in tanks permits the collection of this excess thermal energy for later use in built environment applications, it is difficult to determine how many times the storage tank should be filled with stormwater to enable the necessary water exchange in a tank for heat extraction to satisfy individual building demands for domestic hot water production. CFD modelling can be useful in simulating the temperature-stratified flow in a storage tank where the heat transfer and fluid exchange takes place simultaneously. However, in Publication V, a search technique such as GA is used for finding the values of the combined process parameters. For this purpose, the rainwater harvesting period is related to a building's *duty cycle*, which corresponds to energy consumption for hot water production. In this sense, the ratio of time scales of stormwater heat extraction from a tank and the rainfall return period can be expressed virtually by the number of stormwater tank fillings required during a building's *duty cycle*. The GA finds a number of storage tank fillings corresponding to rainfall statistics and the hot water consumption of buildings. According to the results in Publication V, the maximum stormwater volume in the storage tank and frequent tank fillings are generally obtained for colder and less intense rain periods. However, smaller storage tank sizes and less tank fillings are obtained for the months when the rain temperature is high and the rain intensity is comparatively high, such as June, July, and August.

In Publication V, the complex problem of the heat-transfer process between the atmosphere and the domestic hot water system is explained by introducing the combined energy parameter Π , which is the series representation of the enthalpy change and the volume of a rain events that are available for the heat-exchange process during a rainwater harvesting period, corresponding to a building's *duty cycle*. The efficiency of thermal energy transfer between the atmosphere and a heating system can be represented by the parameter η , which determines rainwater thermal energy available for hot water production. In a lossless system, the efficiency parameter is considered to be one ($\eta = 1$). However, in a real situation, this assumption cannot be used for several reasons: rainwater loss in an urban catchment, i.e. the runoff coefficient is less than one, the stormwater system is not thermally isolated, the rain return period varies, i.e. some heat can be taken out from the tank by outflow, and due to the heat pump efficiency.

4.3 Energy efficiency

According to an established EU target (Directive 2010/31/EU), all new residential buildings to be built between 2021–2030 must comply with the nearly zero-energy performance requirements. Ensuring a proper indoor environment to avoid deterioration of indoor air quality, comfort, and health, is one official recommendation published by the European Commission (EU 2016/1318) for reaching the nearly zero-energy buildings (NZEB) by 2020. The ventilation strategy, proper system, and its use are the main factors influencing the building's indoor environment and its users comfort. Finding solutions for the right balance between indoor environmental quality

and energy use in buildings is, however, a challenging task. The buildings energy efficiency relates to many factors, for instance: air leaks in building envelope, ventilation strategy, and occupant behaviour.

Sealing the building thermal envelope enables the minimisation of air leaks and heat losses from the building. Air tightness is among the key preconditions for energy efficient constructions, which may reduce the energy performance of the buildings (Kraus and Kubekova, 2013). Typical air leakage places are at the junctions of building walls, around and through windows and doors, and penetrations through the air barrier systems (Kalamees, 2007). In heating-dominated climates, cold outdoor air infiltration and the warm indoor air exfiltration may have a significant effect on the energy consumption of the building. For instance, infiltration causes about 15–30% of the energy use of space heating, including ventilation in typical Finnish detached houses (Jokisalu et al., 2008).

Air leaks can be considered as unidirectional stratified flows through the building envelope, driven by excess pressure caused by wind, stack effect, or mechanical equipment in the building. Windows, on other hand, may be seen as relatively large air leaks in the building envelope, whereby uni- and bidirectional stratified flows are possible driven by excess pressure and buoyancy. Opening windows is a manual way to control the fresh air supply associated with building users' behaviour, indoor environment, and outdoor weather conditions. The user behaviour of opening windows is one of many energy-related occupant actions that influence the building's expected energy consumption. The hydraulic-theory solutions proposed in this thesis, in combination with knowledge acquired from Post-Occupancy Evaluation, may be used to improve the energy performance models for buildings where windows can be opened. According to Menezes et al. (2012) in-use performance of occupied buildings differ in energy use from the predicted performance. This is found to be due to unrealistic input parameters regarding occupancy behaviour and facilities management in building energy models.

Usage of operable windows for building ventilation attracts interest due to growing concerns about energy efficiency. For instance, during interim periods such as autumn and spring, when the building's heating and cooling is adjusted, opening windows can provide comfort indoors due to seasonally mild outdoor temperatures. However, operable window systems require careful integration with other building systems, such as ventilation, heating, and cooling systems to be effective and to provide the required levels of thermal comfort (Wang, 2014). The hydraulic-theory solutions may be useful in developing a fast-operating simulation model of air change calculations from operable windows, which can bind different variables, such as window location, opening shape, excess pressure due to mechanical ventilation, and indoor-outdoor environmental conditions, into one model. Determination of large air leaks, i.e. the outdoor air inflow rate and indoor air outflow rate through an open window, may be included in the ventilation calculations to avoid energy-wasting conflicts between operable windows and HVAC systems. Also, it makes it possible to determine heat losses associated with warm indoor air outflow and cold air inflow during the cold season, and enables the assessment of the cooling potential in the hot season.

Opening windows can provide a useful cooling effect to prevent overheating in hot seasons. Recent studies on summer thermal comfort in Nordic country apartment buildings (Simson et al., 2017; Maivel et al., 2014) has shown that overheating is an ongoing problem, specifically in modern newly-built buildings (built after the year

2000). This is mostly due to increased air tightness and better thermal insulation of building envelopes, usage of large windows (higher window-to-floor ratio compared to old buildings), and a growing trend of using glass as a structural element (glass-façade design). While active cooling systems can be used to avoid overheating in buildings, they increase the building's energy use and are relatively expensive (Maivel et al., 2014). The feasibility study by Gross and Hu (2011) shows that open windows may lower the risk of overheating in buildings. Operable windows, controlled by a simple temperature-based algorithm, were able to provide sufficient natural ventilation during 98.4% of the summer time (June to September), and reduced the average overheated degree hours for the entire building of an existing university dormitory in a marine west coastal climate.

The "standard use" of the building is considered in the input parameters of the energy performance calculations to verify the compliance of a building with the minimum requirements (Riigi Teataja, 2013). This, however, assumes closed windows for non-residential buildings, i.e. the cooling of rooms during the hot season by air change through open windows is not taken into account. For residential buildings, only the airing position of open windows is considered for calculating the hot season indoor temperature and energy need for space cooling (note that when the heating set-point is reached, the windows are closed). It should be underlined that comfort and energy efficiency benchmarks cannot be reached by using only natural ventilation for airtight and well-insulated buildings throughout the year. However, by a balanced combination of mechanical ventilation and automated design, savings in buildings' energy consumption can be revealed (Wang, 2014). Further research is needed before implementing the hydraulic-theory solutions for estimating the feasibility of the integration of operable windows, because this practical challenge is new and introduced for the first time in this thesis.

Summary of findings

Stratified flows are encountered in a diverse range of both natural and built environment systems. They thus have a significant influence on the physical world around us. Nevertheless, the theory of internal-flow hydraulics has not been widely applied in dealing with stratified flow engineering-problems in built environments. In this thesis, three pilot studies are introduced to demonstrate the application usefulness of the internal-flow hydraulic theory. Essentially, the strongly-coupled stratified flow cases are the focus of the pilot studies. It should be noted that the stratification of fluids in natural environments results mostly from thermal heating in the atmosphere and oceans, and salinity variations due to different water sources. In built environments, where natural and human-made environments interact, the stratification of fluids is essentially present due to temperature variations. It is demonstrated that the internal-flow hydraulic theory is also useful for connected immiscible fluids with small density differences e.g. in the case of an oil spill from built environment enclosure.

Two types of stratified flows through submerged openings are examined: uni- and bidirectional stratified flows. Whereby, unidirectional stratified flow is related to the difference between the hydrostatic pressures, and bidirectional stratified flow is related to density differences at the opening. Many built environment systems operate under a small overpressure condition, and unidirectional flow through an opening takes place firstly due to the excess pressure, and bidirectional flow follows.

The theory of internal-flow hydraulics is employed for deriving the hydraulic-theory solutions for submerged openings in built environment enclosures. The hydraulic formulae are proposed for uni- and bidirectional stratified flows through rectangular and circular openings with different orientations (side and bottom openings). The hydraulic-modelling solutions can be used to determine the fluid outflow volumes and durations of uni- and bidirectional stratified flows. The internal-flow hydraulic theory application possibilities are demonstrated in three pilot studies 1) oil spills from damaged tankers (immiscible liquid-liquid interaction with two active layer flows), 2) water exchange in a storage tank (miscible liquid-liquid stratified fluid), 3) ventilation through an open window (illustration case of miscible gas-gas interaction with two active layer flows).

It is found that in the application of developed hydraulic formulae, the process parameters need to be determined. The process parameters of stratified flows, such as discharge coefficients and mixing quantities, can be determined in combination with the experimental or numerical-modelling results. The hydraulic-theory solutions are used for determining the discharge coefficients from the available experimental results for the pilot study of oil spills. GA is used for searching the values of combined process parameters, such as discharge coefficients and mixture (emulsion) density, for the complex oil spill case (double-hull tanker). It is demonstrated that the hydraulic formulae are easy to implement and they allow different scenarios to be dealt with (flows through side and bottom openings). The oil spill pilot study demonstrates that the dynamical effects due to mixing (emulsification in the case of immiscible liquids) and heat exchange can be parametrized for uni- and bidirectional stratified flows, which affect the flow rates, outflow volumes, and process durations.

In addition to the process parameters, the system parameters are also required, which are related to the engineering design. As a pilot study, this thesis proposed a

novel approach for the integration of built environment systems that require solutions to meet the current requirements of the energy demands and safety. In the pilot study, it is considered that stormwater is the low-temperature water in urban areas, and presents a potential on-site thermal-energy source for the hot-water production in different types of buildings. It is demonstrated that a developed model of integrated systems, taking into account the stormwater heat extraction equation and domestic water heat load formula, makes it possible to determine the design parameters. The GA is consistently employed to search for the integrated-system design parameters, such as stormwater volume in the storage tank and the number of tank fillings, which are defined in the model as variables.

Practical challenges for pilot studies that make use of the hydraulic-theory solutions in solving a number of fluid engineering problems in built environment enclosures focus on 1) risk assessment of oil spills, 2) making use of renewables, and 3) energy efficiency of buildings. Apart from the pilot studies in this thesis, there are a number of stratified flow problems in the built environment for which the internal-flow hydraulic theory may prove useful.

The built environment systems require practical solutions for engineering purposes. The application of hydraulic formulae in the pilot studies are based essentially on decision-making processes, which depend on available information about the built environment enclosure. However, due to the complexity of built environments, and the lack of specific experimental results, advanced numerical models (e.g. CFD) may be used in future work for analysing specific cases of stratified flows through submerged openings (e.g. transition phase between uni- and bidirectional stratified flows in mobile enclosures). Also, CFD may be employed to gain useful information in determining mixing parameters that depend on temperature (e.g. outflow volume of emulsion in oil spills).

Conclusions

1. The hydraulic formulae based on the internal-flow hydraulic theory can be used to determine stratified flow quantities in submerged openings connecting miscible or immiscible fluids with small density differences.
2. The developed hydraulic-theory solutions can be implemented for the determination of flow rates of uni- and bidirectional flows through submerged rectangular openings. The analytical formula, including a shape factor, for the volumetric flow rate of bidirectional stratified flow makes it possible to consider the opening geometry in the determination of the flow rate.
3. The developed hydraulic-theory solutions can be implemented for the determination of flow rates of uni- and bidirectional flows through submerged circular openings.
4. The GA makes it possible to determine the process parameters such as discharge coefficients and emulsion density, which are defined as three design variables in a single-objective function for bidirectional flow through a submerged opening.
5. Experimentally-determined discharge coefficients for circular openings can be implemented in uni- and bidirectional volumetric flow rate solutions with similar opening geometry.
6. The dynamical effects due to mixing (emulsification in the case of immiscible liquids) and heat exchange can be parametrized for uni- and bidirectional stratified flows, which affect the flow rates, outflow volumes, and process durations.

7. The GA makes it possible to determine the system parameters, such as storage tank volume and catchment area, for different types of buildings, that determine the thermal heat usage possibilities by optimising a single-objective function with two design variables (number of tank fillings and stormwater volume in a storage tank).
8. It can be considered that infiltration through a building envelope corresponds to unidirectional stratified flow, and that large leaks through a building envelope correspond to bidirectional stratified flow.

List of Figures

Figure i-1. Notations: i) single-layer flow and ii) two-layer flow.	10
Figure i-2. Gravity current across the submerged sill (Carr et al., 2015). The data source: Experimental program, funded under the EU FP7 Hydralab IV Initiative, conducted in the largest rotating platform in the world; the LEGI Coriolis Platform II in Grenoble. ...	13
Figure i-3. Stratified flows of built environment storage systems. i) Oil spill from a damaged tanker. ii) Storage tank of a stormwater collection and domestic-water heating integrated system.	14
Figure i-4. Buoyancy-driven flows of miscible fluids. i) Bidirectional stratified flow through open windows. ii) Unidirectional stratified flow in a room with displacement ventilation.	15
Figure i-5. Sketch of two-layer frictional flow with a density jump between layers. The internal-flow energy head loss ΔE_{int} is positive when the flow in the fluid layers is in opposite directions, as in the case of buoyancy-driven flow.	16
Figure 1-1. Sketch of unidirectional stratified flow through the submerged side opening with less-dense fluid inside the enclosure and notations.	26
Figure 1-2. Sketch of bidirectional stratified flow through the submerged side opening with less-dense fluid inside the enclosure, and notations.	27
Figure 1-3. Sketch of a bidirectional stratified flow through the side opening of rectangular shape with less-dense fluid inside the enclosure, and notations.	28
Figure 1-4. Sketch of a bidirectional stratified flow through the side opening of circular shape (orifice) with less-dense fluid inside the enclosure and notations.	34
Figure 2-1. Sketch of single-hull oil tank with bottom orifice: (i) no damage, (ii) damage with excess hydrostatic pressure and oil spill, and (iii) damage without oil spill.	42
Figure 2-2. Charts of i) oil flow rates of unidirectional stratified flow through a bottom orifice in lab test N4, and ii) experimentally determined discharge coefficients at different orifice Reynolds numbers. The curve "experimental" is reproduced according to the results in Tavakoli et al. (2011). Curve "viscous" corresponds to the hydraulic solution with mean discharge coefficient.	43
Figure 2-3. Sketch of single-hull oil tank with side orifice: (i) no damage, (ii) damage with excess hydrostatic pressure and oil spill, (iii) damage without excess hydrostatic pressure and oil spill, and (iv) damage without horizontal density difference and no oil spill.	43
Figure 2-4. Charts of i) oil flow rates of unidirectional stratified flow through a side orifice in lab test N9 and ii) experimentally-determined discharge coefficients at different orifice Reynolds numbers. The curve "experimental" is reproduced according to the results in Tavakoli et al. (2011). Curve "viscous" corresponds to the hydraulic solution with mean discharge coefficient.	44
Figure 2-5. Chart of oil outflow rates of bidirectional stratified flow through a side orifice in lab test N9*. The curve "experimental" is reproduced according to the results in Tavakoli et al. (2011). Curve "viscous" corresponds to the hydraulic solution with mean discharge coefficient.	44
Figure 2-6. Unidirectional oil spill in summer and winter conditions with the effect of heat exchange.	46
Figure 2-7. The oil outflow rate and flow-rates-ratio parameter variation of heavy crude oil (at inner temperature 60°C and 30°C) at different emulsification rates $f=1...0.50$ for summer (18°C) and winter (-1°C) conditions..	47

Figure 2-8. Sketch of stormwater storage tank (filling $n = 1$) with influx and outflux and notations. Thermal stratification with a descending interface is due to warm influx. ...	48
Figure 2-9. Bidirectional stratified flow through an open window of a single room in the cold season. i) Exchange flow with excess pressure due to ventilation and ii), iii), iv) buoyancy-driven exchange flow (ventilation switched off).	51
Figure 2-10. Bidirectional stratified flow through an open window of a single room in the hot season. i) Exchange flow with excess pressure due to ventilation and ii), iii), iv) buoyancy-driven exchange flow (ventilation switched off).	52
Figure 3-1. Scheme of search techniques.	54
Figure 3-2. Fitness landscape with global and local optima of a two-dimensional function (Weise, 2009). Examples of simple hill-climbing finding the best local maximum and GA finding the global maximum.	54
Figure 3-3. Flow chart of basic steps in GA.	57
Figure 3-4. Sketch of evaluating the goodness of designs bounded by the constraints A and B.	58
Figure 3-5. Creation of offspring with one-point crossover and point mutation (bit strings representation).	59
Figure 3-6. Schematic illustration of hydraulic-flow optimisation problem.	61
Figure 3-7. Notations of unidirectional oil spill from double-hull tank side orifice.	62
Figure 3-8. Experimental results of oil and emulsion level in the main tank and in the ballast tank, respectively, and the emulsion flow rate in the ballast tank. Curves are reproduced according to the results in Tavakoli et al. (2011).	63
Figure 3-9. Results of GA-determined i) discharge coefficients at the inner and outer orifices and ii) emulsion density change in the ballast tank (see Publication II).	64
Figure 3-10. Daily mean i) rainfall-depth and ii) rainwater temperature for years 2004 to 2011. i) Calculated mean rainfall-depth over a period of one week, ii) mean rainwater temperature averaged over a period of one week.	65
Figure 3-11. Schematic illustration of stormwater collection and domestic-water heating integrated system and notations.	67
Figure 3-12. Apartment building optimal tank volume, temperature, mean rainfall-depth and expenses on dates: 5th, 10th, 15th, 20th, 25 th , and 30th of the rainy months.	69
Figure 3-13. Apartment building optimal catchment area, temperature, mean rainfall-depth and expenses on dates: 5th, 10th, 15th, 20th, 25 th , and 30th of rainy months. ..	70
Figure 3-14. Estimated cumulative expenses parameter (f_{ce}) for a number of tank fillings (n) for the apartment building during specific rainfall periods.	71

List of Tables

Table i-1. Interaction of fluids in buoyancy-driven flows..... 12

Table i-2. Uni- and bidirectional stratified flows of miscible and immiscible fluids in the natural environment (NE) and built environment (BE) for small-density-difference cases. 12

Table 2-1. Experimental results of lab tests by Tavakoli et al. (2011). 42

Table 3-1. Design data for unidirectional oil spill from double-hull tank (test N12)..... 60

Table 3-2. Hydraulic-flow optimisation model equations and explanations. 62

Table 3-3. GA settings for process optimisation. 63

Table 3-4. Process optimisation order. 63

Table 3-5. Apartment building characteristics. 66

Table 3-6. Available catchment areas for an apartment building..... 66

Table 3-7. Integrated-system optimisation model equations and explanations. 68

Table 3-8. GA settings for system optimisation. 68

Table 3-9. System optimisation order..... 69

References

- Alves, T.M., Kokinou, E., Zodiatis, G., Lardner, R., Panagio-takis, C., Radhakrishnan, H. (2015). Modelling of oil spills in confined maritime basins: The case for early response in the Eastern Mediterranean Sea. – *Environmental Pollution*, 206, 390-399. doi:10.1016/j.envpol.2015.07.042
- Amouzgar, K. (2012). Multi-Objective Optimization using Genetic Algorithms: Master's Thesis. Jönköping: Jönköping University, School of Engineering. DiVA <http://hj.diva-portal.org/smash/get/diva2:570751/FULLTEXT01.pdf> (05.04.2017)
- Arita, M., Jirka, G.H. (1987) Two-layer model of saline wedge. I: entrainment and interfacial friction. – *Journal of Hydraulic Engineering*, 113(10), 1229-1248.
- Armi, L. (1986). The hydraulics of two flowing layers with different densities. – *Journal of Fluid Mechanics*, 163, 27–58.
- Armi, L., Farmer, D. M. (1986). Maximal two-layer exchange through a contraction with barotropic net flow. – *Journal of Fluid Mechanics*, 164, 27–51.
- Arora, K.R. (2015). Optimization Algorithms and Applications. Boca Raton: CRC Press Taylor & Francis Group.
- Bogdanović, M. (2011). On Some Basic Concepts of Genetic Algorithms as a Meta-Heuristic Method for Solving of Optimization Problems. – *Journal of Software Engineering and Applications*, 4, 482-486. doi: 10.4236/jsea.2011.480 55
- Bryden, H. L., Kinder, T. H. (1990). Steady two-layer exchange through the Strait of Gibraltar. – *Deep Sea Research Part A. Oceanographic Research Papers*, 38, S445-S463.
- Carr, M., Cuthbertson, A., Laaneau, J., Sommeria, J., Kean, J., Lilover, M.-J., Kollo, M., Berntsen, J., Thiem, Ø., Viboud, S. (2015). Experimental studies of internal and near-bed dynamics of restricted exchange flows. – *E-proceedings of the 36th IAHR World Congress, Hague, Netherlands, 28 June - 3 July 2015, International Association for Hydro-Environment Engineering and Research*, 1–4.
- Çengel, Y.A., Cimbala, J.M. (2010). Solutions Manual for Fluid Mechanics: Fundamentals and Applications. Second Edition. New York: McGraw-Hill.
- Cohen, W.W., Greiner, R., Schuurmans, D. (1994). Probabilistic hill-climbing in Computational learning theory and natural learning systems (Volume II). / ed. Hanson, S. J., Kearns, M. J., Petsche, T., Rivest, R. L. Cambridge: MIT Press.
- Commission Recommendation (EU) 2016/1318 of 29 July 2016 on guidelines for the promotion of nearly zero-energy buildings and best practices to ensure that, by 2020, all new buildings are nearly zero-energy buildings. – Official Journal of the European Union 2.8.2016 L 208/46 EN (01.10.2017)
- Cuthbertson, J.S.A., Laaneau, J., Carr, M; Sommeria, J., Viboud, S. (2017). Blockage of saline intrusions in restricted, two-layer exchange flows across a submerged sill obstruction. – *Environmental Fluid Mechanics*, 1–31.10.1007/s10652-017-9523-2 [in press]
- Cuthbertson, A.J., Laaneau, J., Davies, P.A. (2006). Buoyancy-driven two-layer exchange flows across a slowly sub-merging barrier. – *Environmental Fluid Mechanics*, 6(2), 133-151.
- Dalziel, S. B. (1992). Maximal exchange in channels with nonrectangular cross sections. – *Journal of Physical Oceanography*, 22, 1188-1206.

- Dalziel, S. B. (1991). Two-layer hydraulics: a functional approach. – *Journal of Fluid Mechanics*, 223, 135-163.
- Dalziel, S. B., Lane-Serff, G. F. (1991). The hydraulics of doorway exchange flows. – *Building and Environment*, 26, 121-135.
- Dalziel, S. B. (1990). Rotating two-layer sill flows. In: Pratt, L.J. ed – *The Physical Oceanography of Sea Straits. NATO-ASI Ser., Kluwer Academic Publishers, Dordrecht*, 587.
- Dalziel, S. B. (1988). Summary: two-layer hydraulics: maximal exchange flows: PhD Thesis. Cambridge: University of Cambridge. http://www.damtp.cam.ac.uk/lab/people/sd/papers/1988/Thesis_Dalziel.pdf (02.06.2017)
- Directive 2010/31/EU of the European Parliament and of the Council of 19 May 2010 on the energy performance of buildings. – Official Journal of the European Union 18.6.2010.L 153/13. (01.10.2017)
- Directive 2009/28/EC of the European Parliament and of the Council of 23 April 2009 on the promotion of the use of energy from renewable sources and amending and subsequently repealing Directives 2001/77/EC and 2003/30/EC. – Official Journal of the European Union 5.6.2009. L 140/16. (01.10.2017)
- Dyer, D.W. (2008). Evolutionary computation in Java. A practical guide to the watchmaker framework. <http://watchmaker.uncommons.org/manual/> (03.07.2017)
- Ehlers, S. (2009). Material Relation to Assess the Crashworthiness of Ship Structures : PhD Thesis. Espoo : Helsinki University of Technology. ISBN 978-952-248-143-6
- Eiben, A.E., Smith, J.E. (2003). Introduction to Evolutionary Computing. Berlin Heidelberg: Springer.
- Estonian Centre for Standardization, 2003. Town streets : EVS 843: 2003
- Estonian Meteorology and Hydrology Institute (EMHI), 2011. Monthly and annual report (in Estonian).
- Evers, M., Jonoski, M., Maksimovič, Č., Lange1, L., Ochoa Rodriguez, S., Teklesadik, A., Cortes Arevalo, J., Almoradie, A., Eduardo Simões N., Wang, L., Makropoulos, C., (2012). Collaborative modelling for active involvement of stakeholders in urban flood risk management. – *Natural Hazards and Earth System Sciences*, 12, 2821–2842. doi:10.5194/nhess-12-2821-2012
- Fang, R., Nianping, L. (2012). Comparison of Wind-driven Natural Ventilation for Different Windows Placed in a Single Room Opening. – *The International Journal of Ventilation, (Special Edition: Towards Low Energy Buildings - Exploiting Ventilation)*, 11(2), 193-203. doi:10.1080/14733315.2012.11683981
- Fang, X. (2007). Engineering design using genetic algorithms : PhD Thesis. Ames : Iowa State University. – *Retrospective Theses and Dissertations* <http://lib.dr.iastate.edu/cgi/viewcontent.cgi?article=16942&context=rttd> (22.04.2017)
- Fannelop, T. K. (1994). Fluid Mechanics for Industrial Safety and Environmental Protection, 5, 1-523. / eBook ISBN: 9780444597847 (08.08.2017)
- Farmer, D.M., Armi, L. (1986). Maximal 2-Layer Exchange over a Sill and through the Combination of a Sill and Contraction with Barotropic Flow. – *Journal of Fluid Mechanics*, 164, 53-76. doi: 10.1017/s002211208600246x
- Fogel, G.B., Fogel, D.B. (1995). Continious evolutionary programming: analysis and experiments. – *Cybernetics and Systems, An International Journal*, 26(1), 79-90. doi: 10.1080/01969729508927488

- Gendreau, M., Potvin, J-Y. (2005). Tabu search. / ed. Burke, E.K., Kendall, G. Search Methodologies – Introductory Tutorials in Optimization and Decision Support Techniques, 165–186. New York : Springer.
- Glover, F.W., Laguna, M. (1997). Tabu Search. New York : Springer Science + Business Media.
- Gill, A. E. (1977). The hydraulics of rotating-channel flow. – *Journal of Fluid Mechanics*, 80, 641–671. doi: 10.1017/S0022112077002407
- Goldberg, D., Richardson, J. (1989). Genetic Algorithms in Search, Optimization and Machine Learning. Boston : Addison-Wesley Longman Publishing Co.
- Gross, S., Hu, H. (2011). A feasibility study of natural ventilation in a midrise student dormitory building. – *Proceedings of Building Simulation 2011: 12th Conference of International Building Performance Simulation Association, Sydney, 14-16 November*.
- Gu and Lawrence, (1995). Analytical solution for maximal frictional two-layer exchange flow. – *Journal of Fluid Mechanics*, 543, 1-17. doi: 10.1017/S0022112005006002
- Gualtieri, C., Mihailovic, D.T. (2012). Fluid Mechanics of Environmental Interfaces, Second Editions. New York : Taylor & Francis Group.
- Haapasaari, P., Dahlbo, K., Aps, R., Brunila, O-P., Fransas, A., Goerlandt, F., Hänninen, M., Jönsson, A., Laurila-Pant, M., Lehtikainen, A., Mazaheri, A., Montewka, J., Nieminen, E., Nygren, P., Salokorpi, M., Tabri, K., Viertola, J. (2014). Minimizing Risks of Maritime Oil Transportation by Holistic Safety Strategies (MIMIC) Final Report. Kotka Maritime Research Association. <http://www.merikotka.fi/wp-content/uploads/2014/07/MIMIC-Final-report.pdf> (21.08.2017)
- Haupt, R.L., Haupt, S.E. (1998). Practical Genetic Algorithms. New York : John Wiley & Sons, Inc.
- Helfrich, K.R. (1995). Time-Dependent Two-Layer Hydraulic Exchange Flows. – *Journal of Physical Oceanography*, 25, 359-373. doi: 10.1175/1520-0485(1995)025<0359:TDLHE>2.0.CO;2
- Heinvee, M. (2016). The Rapid Prediction of Grounding Behavior of Double Bottom Tankers : PhD Thesis. Tallinn : Tallinn University of technology. – *TTÜ Digikogu* <https://digi.lib.ttu.ee/i/?6211> (17.04.2017)
- Holland, J.H. (1975) Adaptation in natural and artificial systems: an introductory analysis with applications to biology, control, and artificial intelligence. Ann Arbor : University of Michigan Press.
- Hou, Q., Tijsseling, A.S., Laaneau, J., Annus, I., Koppel, T., Bergant, A., Vučovic, Anderson, A., Westende, J.M.C. (2014). Experimental Investigation on Rapid Filling of a Large-Scale Pipeline. – *Journal of Hydraulic Engineering*, 140(11). doi: 10.1061/(ASCE)HY.1943-7900.0000914
- Hunt, G.R., Linden, P.F. (2004). Displacement and mixing ventilation driven by opposing wind and buoyancy. – *Journal of Fluid Mechanics*, 527, 27-55. doi: 10.1017/S0022112004002575
- Hunt, G.R., Linden, P.F. (2001). Steady-state flows in an enclosure ventilated by buoyancy forces assisted by wind. – *Journal of Fluid Mechanics*, 426, 61-72.
- Hunt, G.R., Linden, P.F. (1999). The fluid mechanics of natural ventilation – displacement ventilation by buoyancy-driven flows assisted by wind. – *Building and Environment*, 34, 707-720.

- Janke, B.D., Herb, W.R., Mohseni, O., and Stefan, H.G. (2013). Case Study of Simulation of Heat Export by Rainfall Runoff from a Small Urban Watershed Using MINUHET. – *Journal of Hydrologic Engineering*, 18 (8), 995–1006.
- Jokisalo, J., Kurnitski, J., Korpi, M., Kalamees, T., Vinha, J. (2009). Building leakage, infiltration, and energy performance analyses for Finnish detached houses. – *Building and Environment*, 44(2), 377-387. doi: 10.1016/j.buildenv.2008.03.014
- Joshi, K.D., Vakaskar, D.C. (2011). Evolutionary Algorithms: Symbiosis of its Paradigms. – *National Conference on Recent Trends in Engineering & Technology, B.V.M. Engineering College, V.V.Nagar, Gujarat, India, 13-14 May 2011.*
- Kalamees, T., Thalfeldt, M., Zelenski, M., Meos, H., Laas, M., Kurnitski, J., Kuusk, K. (2016). – *The 14th international conference of Indoor Air Quality and Climate, Indoor Air 2016. Ghent, Belgium, 3-8 July 2016, Proceedings, 1-8. IA2016_PaperID-59_Full_Paper_Final.pdf (24.08.2017)*
- Kalamees, T. (2007). Air tightness and air leakages of new lightweight single-family detached houses in Estonia. – *Building and Environment*, 42(6), 2369-2377. doi: 10.1016/j.buildenv.2006.06.001
- Kraus, M., Kubeková, D. (2013). Airtightness of Energy Efficient Buildings. – *1st Annual International Conference on Architecture and Civil Engineering, Singapore: Global Science and Technology Forum, 2013, 29 - 35. ISSN 2301- 394X. doi: 10.5176/2301 -394X_ACE13.10*
- Kundu, P.K., Cohen, I.M., Dowling, D.R. (2011). *Fluid Mechanics*, 5th Edition. Oxford : Academic Press, 2011.
- Kõiv, T.A., Toode, A. (2010). *Hot water usage in buildings*. Tallinn: TUT Press.
- Laanearu, J., Borodinecs, A., Rimeika, M., Palm, B. (2017). A review on potential use of low-temperature water in the urban environment as a thermal-energy source. – *Proceedings of 3rd International Conference Innovative Materials, Structures and Technologies (IMST 2017)* [in press]
- Laanearu, J., Vassiljev, A., Davies, P. (2010). Modelling of exchange flow in horizontal channels with quadratic-shape cross sections: Pärnu river mouth case study. – *First Iahr European Division Congress, 4-6 May, 2010, Edinburgh, United Kingdom. CD-ROM. Heriot Watt University, Edinburgh, Scotland, UK: National Telford Institute, 18, 6.*
- Laanearu, J., Davies, P.A. (2007). Hydraulic control of two-layer flow in quadratic type channels. – *Journal of Hydraulic Research*, 45(1), 3-12.
- Laanearu, J., Lips, U., Lundberg, P. (2000). On the application of hydraulic theory to the deep-water flow through the Irbe Straight. – *Journal of Marine Systems*, 25(3-4), 323-332. doi:10.1016/S0924-7963(00)00025-7
- Lin, Y.J.P., Linden, P.F. (2002). Buoyancy-driven ventilation between two chambers. – *Journal of Fluid Mechanics*, 463, 293–312.
- Linden, P.F., Lane-Serff, G.F., Smeed, D.A. (1990). Emptying filling boxes: the fluid mechanics of natural ventilation. – *Journal of Fluid Mechanics*, 212, 309-335. doi: 10.1017/S00222112090001987
- Maivel, M., Kurnitski, J., Kalamees, T. (2015). Field survey of overheating problems in Estonian apartment buildings. – *Architectural Science Review*, 58(1), 1-10. doi: 10.1080/00038628.2014.970610
- Marczyk, A. (1994). *Genetic Algorithms and Evolutionary Computation*. <http://www.talkorigins.org/faqs/genalg/genalg.html> (21.05.2017)

- Mayer, C., Antretter, F. (2013). User behaviour regarding natural ventilation – state of the art and research needs. – *9th Nordic Symposium on Building Physics – NSB 2011*, 3, 1119-1126. *Fraunhofer-Institut für Bauphysik, Holzkirchen, Germany*.
- Menezes, A.C.K, Cripps, A., Bouchlaghem, D., Busswell, R.A. (2012). Predicted vs. actual energy performance of non-domestic buildings: using post-occupancy evaluation data to reduce the performance gap. – *Applied Energy*, 97, 355-364. doi: 10.1016/j.apenergy.2011.11.075
- Morton, B.R., Taylor, G., Turner, J. S. (1956). Turbulent Gravitational Convection from Maintained and Instantaneous Sources. – *Proceedings of the Royal Society of London*, 24 Jan. 1956. *Series A, Mathematical and Physical Sciences*, 234(1196), 1-23.
- Oldekop, N., Liiv, T. (2013). Measurement of the Variation of Shear Velocity on Bed during a Wave Cycle. – *Journal of Earth Science and Engineering*, 3, 322-330.
- Palonen, M., Hasan, A., Sirenet K., (2009). A Genetic Algorithm for optimisation of building envelope and HVAC system parameters. – *Eleventh International IBPSA Conference Glasgow, Scotland, July 27-30, 2009*. http://www.ibpsa.org/proceedings/bs2009/bs09_0159_166.pdf (07.06.2017)
- Parkinson, A.R., Ballin, R.J. and Hedengren, J.D. (2013). Optimization methods for engineering design. – Applications and theory. http://flowlab.groups.et.byu.net/me575/textbook/optimization_book.pdf (22.05.2017)
- Rajan, K. (2013). Adaptive techniques in genetic algorithm and its applications : PhD thesis. Telangana : Mahatma Gandhi University. – Shodhganga INFLIBNET Centre <http://hdl.handle.net/10603/21381> (11.09.2017)
- Ravlic, N., Gjetvaj, G. (2003). Modelling of stratified flow over topography in semi-deep coastal channels. – *Transactions on Ecology and the Environment*, 65, 487-496. WIT Press, www.witpress.com, ISSN 1743-3541
- Riigi Teataja (2013). Methodology for calculating the energy performance of buildings. – Estonia State Gazette. <https://www.riigiteataja.ee/en/eli/520102014002/> (27.05.2017)
- Riigi Teataja (2012). Minimum requirements for energy performance. – Estonia State Gazette. <https://www.riigiteataja.ee/en/eli/520102014001/consolide> (27.05.2017)
- Simecek-Beatty, D.A., Lehr, W.J., Lankford, J.L., (2005). Leaking tank experiments for heavy oils. – *Proceedings of International Oil Spill Conference, IOSC 2005, Miami Beach, FL, United States, 15–19 May 2005, Code 67046*. 4293–4297.
- Simson, R., Kurnitski, J., Maivel, M. (2017). Summer thermal comfort: compliance assessment and overheating prevention in new apartment buildings in Estonia. – *Journal of Building Performance Simulation*, 10(4), 378-391. doi: 10.1080/19401493.2016.1248488
- Streichert, F. (2007). Evolutionary Algorithms in Multi-Modal and Multi-Objective Environments : PhD Thesis. Logos Verlag Berlin ISBN 978-3-8325-1552-2
- Tabri, K., Aps, R., Mazaheri, A., Heinvee, M., Jönsson, A., Fetissov, M. (2015). Modelling of structural damage and environmental consequences of tanker grounding. – *Analysis and Design of Marine Structures V: 5th International Conference on Marine Structures, 25–27 March 2015, Southampton UK*. Ed. C. Guedes Soares and R. Ajit Sheno. Taylor & Francis, 703–710.

- Tavakoli, M.T., Amdahl, J., Leira, B.J. (2011). Experimental investigation of oil leakage from damage ships due to collision and grounding. – *Ocean Engineering*, 38(17-18), 1894-1907.
- Tavakoli, M.T., Amdahl, J., Leira, B.J. (2010). Analytical and numerical modelling of oil spill from a side damaged tank. – *5th International Conference on Collision and Grounding of Ships, 10-14 June 2010, Helsinki, Finland*.
- Tavakoli, M., Amdahl, J., Ashrafian, A., Leira, B., (2008). Analytical predictions of oil spill from grounded cargo tankers. – *Proceedings of the 27th International Conference on Offshore Mechanics and Arctic Engineering, 15-20 June 2008, Estoril, Portugal*.
- Tavakoli, M.T., Amdahl, J., Alsos, H.S., Klæbo, F., (2007). Analysis of Supply Vesselstern impacts with an FPSO. – *Proceedings of 4th ICCGS, Hamburg, Germany. Sitert av 15 - Beslektede artikler*.
- Thomas, L.P., Marino, B.M., Tovar, R., Linden, P.F. (2008). Buoyancy-driven flow between two rooms coupled by two openings at different levels. – *Journal of Fluid Mechanics*, 594, 425–443. doi:10.1017/S0022112007009123
- Wang, L. (2014). Window Operation and Its Impacts on Thermal Comfort and Energy Use. – *Proceedings of the 8th International Symposium on Heating, Ventilation and Air Conditioning. Lecture Notes in Electrical Engineering*, 262. Springer, Berlin, Heidelberg. doi: 10.1007/978-3-642-39581-9_26
- Weise, T. (2009). Global Optimization Algorithms – Theory and Application. <http://www.it-weise.de/projects/book.pdf> (07.04.2017)
- Whitehead J.A., Leetmaa, A., Know, R.A. (1974). Rotating hydraulics of straight and sill flows. – *Geophysical Fluid Dynamics*, 6, 101-125.
- Winters, K.B., Seim, H.E. (2000). The role of dissipation and mixing in exchange flow through a contracting channel. – *Journal of Fluid Mechanics*, 407, 265-290. doi: 10.1017/S0022112099007727
- Wirth, A. (2017). A Guided Tour Through Buoyancy Driven Flows and Mixing. Master. Buoyancy Driven Flows and Mixing. France : HAL Id: cel-01134112, 2017.
- Xie, H., Yapa, P. D., Nakata, K. (2007). Modelling emulsification after an oil spill in the sea. – *Journal of Marine Systems*, 68(3–4), 489–506. doi: 10.1016/j.jmarsys.2007.02.016
- Yan, J., Zhang, Y., Zhang, J., Yang, X. (2011). The method of urban rain-flood utilization based on environmental protection. – *Energy Procedia*, 5, 403–407. doi: oi.org/10.1016/j.egypro.2011.03.069

Acknowledgements

This work was carried out at the Department of Civil Engineering and Architecture at the Tallinn University of Technology. The financial support was provided during this work by the BONUS+STORMWINDS project ("Strategic and operational risk management for wintertime maritime transportation system"), Institutional Research Funding project IUT19-17 ("Dynamical processes in hydraulic networks, marine structures and sea environment"), Estonian Science Foundation Research Grant project ETF8718 ("Numerical model to assess the structural damage in ship grounding considering motion dynamics"), and project VE591 ("Dynamics of restricted exchange flows in coastal inlets (HylV-CNRS-Carr)"). I am particularly grateful for this financial support, which allowed me to participate in several scientific conferences: MARSTRUCT 2013, CLIMA 2013, and MARSTRUCT 2017.

I owe my deepest gratitude to my Tallinn University of Technology supervisor, Associate Professor Janek Laanearu, who suggested this topic for me. His continuous encouragement, enthusiasm and constructive comments have been a great motivator throughout my studies. His guidance into the world of stratified flows and suggestions to use a genetic algorithm has been essential during this work.

I sincerely thank Professor Hendrik Voll for his inspirational talks about academic studies that encouraged me to pursue my PhD. I also express my warmest gratitude to Doctor Kristjan Tabri, Professor Teet-Andrus Kõiv, Senior Researcher Anatoli Vassiljev, and late Professor Tiit Koppel for their valuable suggestions and discussions.

This thesis was made possible through the help and support from my family. My mother, Marina, and late grandmother, Nina, have been beside me supporting my dreams and goals. My husband, Madis has been extremely loving, encouraging, and motivating throughout these years and my son, Mathias has given me much happiness and energy that kept me going. My parents-in-law, Heidi and Tiit, and grandmother-in-law, Maiu, deserve special thanks for being there in my time of need. Thank you for believing in me, being delighted with my achievements, and sharing my dream!

Thank you to my second family, my teammates from TTÜ Tantsutüdrukud ja Saltopoisid, who came alongside my journey, shared a lot of love and introduced me to the science of cheerleading. Thank you to my colleagues from FILTER AS for sharing valuable practical knowledge and making my work-life truly extraordinary.

Lühikokkuvõte

Ühe- ja kaheasuuniline stratifitseeritud voolamine konstruktsioonipiirde uputatud avades

Stratifitseeritud voolamine (st tiheduse järgi kihistunud voolamine) mõjutab oluliselt tehiskeskkonna kasutamise tingimusi. Mitmed vedeliku voolamisega seotud insenertehnilised probleemid on motiveerinud arendama nii ühe- kui ka kaheasuunalise stratifitseeritud voolamise matemaatiliselt lihtsaid mudeleid ehitiste ja laevade jaoks. Arvutuslikud probleemid on seotud peamiselt mitte-homogeense vedeliku (või gaasi) voolamise määramisega süsteemides, mis koosnevad keerulistest geomeetrilistest elementidest, ning mille mõõtmised võivad varieeruda. Uputatud konstruktsioonipiirde avade, mille kaudu erineva tihedusega vedelikud (või gaasid) voolavad, orientatsioon, kuju ja suurus võib olla erinev, ning need määravad tingimused dünaamilistele protsessidele. Stratifitseeritud voolamine uputatud avas võib sõltuda nii vedelike pinnakõrguste erinevusega määratud hüdrostaatilise rõhu erinevusest avas (st veepinnast tingitud voolamine) kui ka tiheduse erinevusest avas (st ujuvusest tingitud voolamine). Lisaks võib tehiskeskkonna süsteemi asend olla nii vertikaalselt fikseeritud (nt ruum hoones või maa-alune sademeveemahuti) kui ka vertikaalselt fikseerimata (nt õlitank lekkivas tankeris). Näiteks vigastatud õlitankeri vertikaalne liikumine, mis on seotud kargovedeliku lekkega ülevalpool hüdrostaatilise rõhu tasakaalu punkti laevakeres, vähendab süvist, ja mis on seotud laeva ujuvuse kaoga, suurendab süvist. Stratifitseeritud voolamise dünaamikat võib oluliselt mõjutada ka erineva tihedusega vedelike kokkupuutekihi kiirusnihetest sõltuv segunemine. Ühe näitena võib tuua ruumi loomuliku ventilatsiooni, mis toimib koos mehaanilise ventilatsiooniga, ning mille jaoks õhuvahetusel läbi avatud akna võib esineda hõõrdepingega kaasnev mitmeasuuniline voolamine. Teise näitena võib esitada õilekke tankerist, mille jaoks õli voolamine läbi uputatud ava on seotud emulsiooni tekkimisega (e „lahustumatute“ vedelike segunemine voolamisel).

Praktiliste rakenduste jaoks võib ühe- ja kaheasuunalise stratifitseeritud voolamise vooluhulkade arvutamiseks uputatud avas kasutada väikeses tiheduse erinevuse järgi lihtsustatud voolamise hüdraulika valemeid, mis võtavad arvesse vooluhulgategureid. Seejuures, stratifitseeritud voolamise protsessiparameetrid, nagu näiteks voolutakistuse ja segunemise tegurid, tuleb määrata eksperimentaalsete andmete põhjal või kasutades numbrilisi arvutustulemusi. Selle jaoks võib kasutada otsimismeetodit nagu näiteks Geneetiline Algoritm. Geneetiline Algoritm võimaldab otsida väärtusi kombineeritud protsessiparameetritele, mis voolamise hüdraulika valemitega on defineeritud kui muutujad. Piirikihi dünaamilised efektid ühe- ja kaheasuunalise voolamise jaoks läbi uputatud ava erinevad oluliselt. Kui üheasuunalisel stratifitseeritud voolamisel sõltub vooluhulgategur peamiselt voolamise ahenemisest avas ja voolamise eraldumisest ava servadel, siis kaheasuunalisel stratifitseeritud voolamisel sõltub vooluhulgategur hõõrdepingetest nii voolamise piirikihis kui ka vedelike kokkupuutekihis. Mitmetes praktilistes rakendustes sõltub voolamise dünaamika ka soojusvahetusest, mille määrab temperatuuri muutus. Näitena võib tuua eelsoojendatud vedeliku jahtumise uputatud avas kokkupuutel väliskeskkonnaga, mis omakorda võib suurendada takistust väljavoolule või isegi põhjustada ummistumise.

Kaasaegsete insenerlahenduste otsimine integreeritud tehiskeskkonna süsteemidele on kompleksne ülesanne ning pakub praktilist huvi otsustusprotsessis. Kaasaegsete energiatõhususnõuetele vastamine on üks peamistest põhjustest, miks uute

rakendusvõimaluste otsimiseks hoonetele võtta kasutusele alternatiivsed energia ressursid (nt madalatemperatuurilise vee soojusenergia). Lokaalselt kättesaadava energia ressursi tarvitamiseks on vajalik rakendada otsimismeetodeid integreeritud süsteemide parameetrite määramiseks (nagu nt. sademevee ja hoone tarbevee süsteemi jaoks on vajalik arvutada sademevee kogus, mahuti täitmiste arv soojuse eraldamiseks, jne). Selleks, et otsida disainiparameetrite väärtusi, mis on integreeritud süsteemi mudelis defineeritud kui muutujad, võib järjepidevalt rakendada Geneetilist Algoritmi. Seejuures, soojuse eraldamine mahutist, milles on olemas nii soojem kui ka külmem vesi, sõltub oluliselt temperatuuri järgi stratifitseeritud voolamisest. Hoonete soojusjuhtivus võib oluliselt sõltuda vedelike (või gaaside) voolamisega seotud konveksioonist. Seetõttu, on tehiskeskkonnas oluline modelleerida temperatuuri järgi stratifitseeritud voolamist. Stratifitseeritud voolamise dünaamikaga seotud probleemide lahendamiseks uputatud avades, mis kontrollivad massi ja energia vahetust tehiskeskkonnas, võib rakendada sisevoolamise hüdraulika teooriat.

Käesoleva töö uudsus seisneb stratifitseeritud voolamise tingimustega seotud insenertehniliste probleemide lahendamises erinevate tehiskeskkondade jaoks. Voolamise hüdraulika valemid on tuletatud nii ühe- kui ka kahesuunalise stratifitseeritud voolamise jaoks uputatud avas. Ideaalvedeliku voolamise analüütilisi valemite on rakendatud protsessiparameetrite arvutamiseks teadusajakirjanduses avaldatud eksperimentaalsete tulemuste alusel. Vedelike (või gaaside) segunemisest (ka emulsiooni moodustumine „lahustumatute“ vedelike voolamise koostoimel) ja soojusvahetusest sõltuvat stratifitseeritud voolamise dünaamilisi efekte on kasutatud voolamise hüdraulika valemite eriparameetrite määramiseks, mis täpsustavad uputatud ava arvutustes vooluhulkasid, väljavoolu koguseid ja protsessi aega. Süsteemi disainiparameetrite väärtuseid on kasutatud integreeritud süsteemi kasutusvõimaluste selgitamiseks.

Esiteks, on näidatud, et kvaasistatsionaarse voolamise modelleerimise meetodit võib rakendada ajast sõltuvate suuruste määramiseks voolamise jaoks uputatud avades. Voolamise hüdraulika valemid on tuletatud vedelike (või gaaside) väikese tiheduse erinevuse lähenduses nii ühe- kui ka kahesuunalise stratifitseeritud voolamise jaoks uputatud avades, mis võivad olla nii nelinurkse kui ka ümara kujuga. Publitseeritud mudelbasseini õilekke katsetulemusi on kasutatud uputatud avade vooluhulgategurite arvutamiseks. Geneetilist Algoritmi on rakendatud takistustegurite ja vee-õlisegu (emulsiooni) tiheduse arvutamiseks voolamisel läbi uputatud ava. On näidatud, et voolamise hüdraulika mudeleid on lihtne kasutada ning rakendada erinevate laevaõnnetuste stsenaariumite jaoks.

Teiseks on välja arendatud tehiskeskkonna süsteemide (linna sademevee ja hoone tarbevee süsteemi) integreeritud mudel, mis kasutab veesoojuse eraldamise valemit ja tarbevee soojuskoormuse valemit, et määrata süsteemi disainiparameetrid. Geneetilist Algoritmi on kasutatud sademevee mahuti suuruse ja linnavalgala pindala otsimiseks paljude võimalike lahendite hulgast. Sademevett on vaadeldud kui madalatemperatuurilist vett linnaalal, mis esindab kohapeal olemasolevat soojusenergia allikat sooja tarbevee tootmiseks erinevat tüüpi hoonetes (korterelamu, büroohoone ja kaubanduskeskus). Välja on pakutud sademevee ja tarbevee integreeritud süsteemi toimimise optimaalsed lahendused, mis võimaldavad soojusenergiat eraldada sademevee mahutist tarbevee kütteks Läänemere piirkonnas vihmaperioodil.

Tehiskeskonna süsteemide kasutamiseks on vajalikud lahendused, mis vastavad kaasaegsetele energiatõhususe ja ohutuse nõuetele. Stratifitseeritud voolamise dünaamika tehiskeskkonnas sõltub oluliselt temperatuuri muutustest ja erinevate vedelike (või gaaside) koostoimest voolamisel. Tänapäevani piirab sisevoolamise hüdraulika valemite kasutamist tehiskeskkonnas stratifitseeritud voolamise eksperimentaalsete andmete puudulikus. Voolukiiruse ja rõhu andmed on vajalikud ühe- ja kahesuunalise stratifitseeritud voolamise modelleerimise jaoks uputatud avades. Seetõttu on vajalikud uued eksperimentaalsed tulemused ja samuti arvutusliku vedelikudünaamika (CFD) modelleerimise tulemused. See võimaldaks universaalsemalt kasutada käesolevas töös välja arendatud stratifitseeritud voolamise hüdraulika mudeleid hoonetes ja laevades.

Abstract

Uni- and Bidirectional Stratified Flows in Submerged Openings of Built Environment

Stratified flows are common phenomena in the built environment. A number of fluid engineering problems have motivated the modelling of uni- and bidirectional stratified flows in buildings and ships. This encompasses the flow of heterogeneous fluid in a complex geometric system involving a wide range of length scales. Distinctive characteristics of the submerged openings, connecting two fluids with different density, are due to the orientation, shape, and size, which determine stratified-flow dynamics under variable conditions. Stratified flows through submerged openings are essentially due to excess hydrostatic pressure (i.e. surface-slope driven) and density difference (i.e. buoyancy driven). In addition, the built environment systems can be either vertically fixed (e.g. a room in a building or underground stormwater tank), or vertically unfixed (e.g. the oil tank of a damaged ship). For instance, the vertical motion of a damaged tanker may be due to weight loss (upward motion) and buoyancy loss (downward motion). The stratified flow dynamics can be also dependent on shear-produced mixing between interacting fluids. As an example, natural ventilation of a room with mechanical ventilation may include exchange flow through an open window that experience entrainment of counter-flowing miscible fluids. Another example is an oil spill from a damaged tanker that represents immiscible fluid flow through the hole of a breached hull, which may result in the formation of emulsion.

In practical applications, the flow rates of uni- and bidirectional stratified flows through submerged openings can be calculated using the hydraulic-theory solutions that use the discharge coefficients. However, the process parameters of stratified flow, such as hydraulic-flow coefficients and mixing quantities, should be determined in combination with the experimental or numerical results. For this purpose, a genetic algorithm can be used for searching the values of the combined process parameters, which are defined in the hydraulic-theory solutions as variables. The dynamical effects due to the presence of boundary layers can differ significantly in the uni- and bidirectional stratified flows through submerged opening. As the discharge coefficient in unidirectional stratified flow is essentially related to flow contraction and separation at the opening edges, then this coefficient in bidirectional flow is related to both boundary and interfacial stresses. Also, the temperature variations due to heat transfer can affect the stratified flow dynamics. For instance, the fluid cooling during outflow from the pre-heated built environment enclosure can result in flow conditions associated with a restricted outflow or even blockage of the flow.

Moreover, finding solutions for an efficient design of the built environment integrated systems is a challenging task, and is of practical interest in decision-making processes. Energy efficiency benchmarking is the key reason to seek alternative on-site resources (e.g. thermal energy of low-temperature water) for buildings. The determination of integrated system parameters (e.g. stormwater volume in a tank for heat extraction, the number of tank fillings due to harvested rainwater from a catchment area, etc.) requires optimisation in order to utilise the locally-available resources. For this purpose, GA can be consistently employed for searching the integrated-system design parameters, which are defined in the model as variables. However, the heat extraction is dependent on stratification in a storage tank, where warmer and colder fluid is present due to temperature variations. The heat transfer

and fluid exchange in the built environment system may be altered by the convective flows. Therefore, it is essential to understand the fluid dynamics of temperature-stratified flow. The internal-flow hydraulics theory is useful in dealing with the dynamics of stratified flow through submerged openings, which regulate the mass and energy changes in the built environment enclosure.

The novelties of this thesis correspond to the different aspects of fluid engineering problems in built environments. The hydraulic formulae for submerged openings are developed for the cases of uni- and bidirectional stratified flows. These analytical formulae are used to determine the discharge coefficients from the available experimental results. The dynamical effects due to mixing (formation of emulsion in the case of immiscible liquids) and heat exchange are parametrized for the exchange flow through submerged openings, which affect the flow rates, outflow volumes, and process durations. Optimal solutions for design parameters are used for an efficient design of integrated systems.

Firstly, the quasi-steady modelling approach is used to determine the time-dependent quantities of flows through submerged openings. For this purpose, the hydraulic-theory solutions in the approximation of small density differences are derived for uni- and bidirectional stratified flows through submerged openings of rectangular or circular shape. A GA is used for searching the values of combined process parameters such as flow-resistance factors and water-oil mixture (i.e. emulsion) density in the oil spill. It is demonstrated that the hydraulic-flow models are easy to implement and that they are able to deal with different scenarios.

Secondly, it is demonstrated that a developed model of integrated systems, making use of the stormwater heat extraction equation and domestic water heat load formula, makes it possible to determine the design parameters. A GA is used for searching the dimensions of integrated systems design parameters such as the stormwater storage tank volume and the catchment area. It is considered that stormwater is the low-temperature water in urban area, and presents a potential on-site thermal-energy source for hot-water production in different types of buildings. Therefore, an optimal solution of the stormwater and domestic-water integrated system is proposed to investigate the heat extraction from stormwater storage tanks for domestic water production during the rainy season of the Baltic Sea region.

The built environment systems require the solutions to meet the current requirements for energy demands and safety. The dynamics of stratified flows in built environment enclosures are essentially dependent on temperature variations and the presence of different fluids. At present, the lack of stratified-flow experimental results restricts the usage of the hydraulic formulae for the modelling of uni- and bidirectional stratified flows through submerged openings in built environments. However, the data of velocity and pressure distributions are important for stratified flow modelling in submerged openings. Therefore, the new experimental results, as well as Computational Fluid Dynamics (CFD) modelling, are necessary for future work. This makes it possible to more universally apply the herein-developed stratified flow hydraulic-modelling solutions in solving fluid engineering problems in buildings and ships.

Appendix 1

PUBLICATION I

Sergejeva, M., Laanearu, J., Tabri, K. (2013). Hydraulic modelling of submerged oil spill including tanker hydrostatic overpressure. – *Proceedings of 4th International Conference on Marine Structures, MARSTRUCT 2013, 25–27 March 2013, Espoo, Finland. Taylor & Francis, 209–217.*

Hydraulic modelling of submerged oil spill including tanker hydrostatic overpressure

M. Sergejeva, J. Laanearu & K. Tabri

Department of Mechanics, Tallinn University of Technology, Tallinn, Estonia

ABSTRACT: Internal hydraulic theory is employed to deal with submerged oil leak from damaged tank of single- or double-hull tanker. Variable locations and sizes of damage opening are considered to calculate the oil-spill volumes and durations. The exchange-flow solutions are presented for the side-hull damage opening in the case of balanced and un-balanced hydrostatic-pressure situations. The hydrostatic overpressure is associated with the initial uni-directional oil outflow that can fill the ballast tank in the case of double-hull tanker. In the case of balanced internal and external hydrostatic pressures, the internal flow through the side hole is bi-directional, with the upper-layer less-dense liquid (oil) flowing against the direction of the lower-layer denser liquid (sea water). The time-dependent oil outflow through the bottom damage results from the reduction of internal hydrostatic pressure in the tank as compared to the external hydrostatic pressure due to the sea level.

1 INTRODUCTION

Ship collision and groundings are still one of the major types of accidents in maritime transportation yielding to significant consequences. Looking at the IMO data shows that the share of collision accidents alone is about 20% of all serious and very serious accidents (Ehlers 2009). For example, in the Gulf of Finland, there are on average 20-30 collision or grounding accidents per year making it one of the riskiest regions in maritime traffic (Kujala et al. 2009).

A ship participating in collision or grounding accident is often damaged to extent where its inner hull or tank bottom is breached. Therefore, ship collision and grounding accidents are the main reasons for large scale oil spills. A comprehensive analysis of possible collision and grounding accidents for a certain ship or for a certain sea region, should not only assess the structural damage, but should also include the duration and extent of a possible oil spill. This would allow to understand the nature of accidents and to develop risk control options accordingly. This paper proposes a simulation model that allows evaluating the extent and duration of oil spill in collision and grounding accidents once the ship dimensions and the description of damage are obtained.

When two liquids of different densities are connected at damage opening, the exchange flow can

take place. Under balanced internal and external hydrostatic pressure, the internal flow through a tank side-hole is bi-directional, with the upper less-dense liquid (oil) flowing against the direction of the lower denser liquid (sea water). During this process, the oil in the tank is replaced by the inflowing water until the oil interface is ascending above the upper lip of the opening. In addition to the oil amount also the duration of the oil spill is an important parameter, which depends also on the oil and sea-water interactions. In the case of internal overpressure for the side damaged tank the unidirectional oil outflow is expected at the beginning of oil spill process. Hydrostatic balance between the liquids of different density deletes the net barotropic component from the oil outflow layer. The oil outflow through the side damage is essentially bi-directional under hydrostatic balance situation. However, the uni-directional internal flow is mainly possible for the bottom hole, with the less-dense liquid (oil) that is flowing out from the tank under comparatively high internal hydrostatic overpressure. The internal hydrostatic under-pressure situation would result in the sea-water intake. Loading procedure of oil tankers requires that the internal pressure in tank is larger compared to the external pressure (see Tavakoli et al. 2011).

The aim of the present study is to demonstrate how the internal hydraulics theory can be applied for the modelling of stratified bi-directional flow of

connected liquids of different densities and hydrostatic pressures. Hydraulic control is the generic principle that can be used to determine internal-flow dynamics through an opening due to internal pressure gradient. The functional approach of this theory has been used in some engineering applications (Dalziel & Lane-Serff 1991). The Bernoulli type analytical solutions of internal flow are used in Tavakoli et al. (2010). For this purpose the hydraulics model for exchange flow, proposed by Laanearu & Davies (2007) for the quadratic constrictions, is used for the submerged oil leak from damaged tank. Regarding the geometric shape of the flow, the internal flow has one horizontal (length) maximum (l_0) and one vertical (depth) maximum (d_0) (both not necessary located at the centre lines of the hole). The areal shapes of flow are then classified quantitatively by the value of shape factor ξ (≥ 1), representing the ratio of equivalent area ($l_0 \times d_0$) to the actual area A of the damage opening. While in the case of single-layer flow the hydraulic modelling is usually simplified for the maximum transport and its application requires the calibrating procedure of discharge coefficient. In the case of two-layer flow several internal-flow regimes represent maximum transport (Armi 1986) and the total two-layer sheared flow resistance is due to the flow separation from the hole edges and also due to the dynamical interaction (mixing) between the coupled liquids. The stratified bi-directional flow is parameterized by the densimetric Froude-numbers (F_1^2) and (F_2^2) corresponding to the upper- and lower-layer hydraulic regime, respectively. The internal-flow solutions are parameterized by the combined Froude number ($G^2 = F_1^2 + F_2^2$).

A simulation model is developed in present study for the oil-leak calculations in uni- and bi-directional flow cases. The model can be applied quite generally to predict the oil spill for different tank filling levels. The practical outcome of the model is the estimation of the volume of spilled oil and duration for the spilling of different tanker configurations and cargo oils. In the first chapter the general system of a tanker is presented. In the next section general principles of internal-flow hydraulics are briefly explained and some numerical examples are presented for the exchange flow with non-linear filling of tank. In the third chapter the hydraulic formulae are applied to the system under unbalanced and balanced external and internal hydrostatic-pressure situations in the side damage case. The hydraulic formulae are applied to the system with the overpressure and bottom damage in the fourth chapter. The proposed model herein is used to simulate the model-scale experiment results by Tavakoli et al. (2011) to estimate the spilled and retained oil for the cases of bottom and side holes in the single and double hull situations. The validation of the method and overall results established are concluded and discussed in the last chapter.

2 SYSTEM DESCRIPTION

The most tankers are loaded such that the internal pressure due to oil level in the tank is larger than the external pressure due to the sea level. Thus, uni- or bi-directional oil spills are possible from the damaged tank. The uni-directional oil outflow results from the high internal hydrostatic pressure-head (Δ_I) as compared to the external hydrostatic pressure-head ($\rho_2 / \rho_1 \Delta_O$). In the case of the balanced internal and external hydrostatic pressure situation the oil flow is due to density difference between the cargo oil density ρ_1 and the sea-water density ρ_2 ($\rho_2 > \rho_1$). If the tanker carries substantially less cargo oil such that hydrostatic balance is established at- or several meters above the tank bottom, water enters the ship through the hole in the hull as long as the highest point of damage is below the hydrostatic balance level (National Research Council 1991).

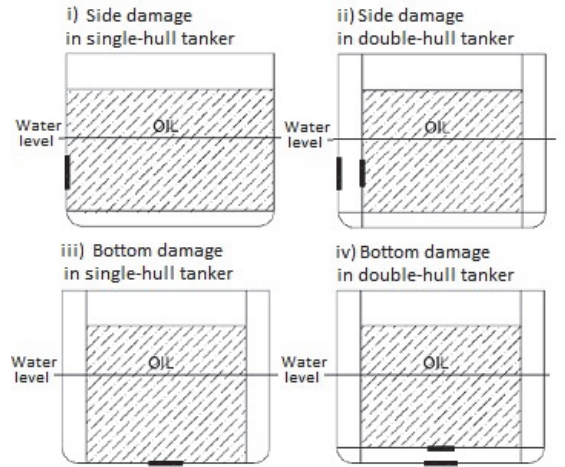


Figure 1. Submerged damages of the single- and double-hull tankers: i) side hole of single-hull tank, ii) side hole of double-hull tank, iii) bottom hole of single-hull tank and iv) bottom hole of double-hull tank.

Four cases of the single- and double-hull tank damages are studied in this paper as sketched in Figure 1. Side damages in Figure 1 i) & ii) correspond to the submerged oil-leak from the single- and double-hull holes, respectively. Bottom damages in Figure 1 iii) & iv) correspond respectively to the submerged oil-leak from the single- and double-hull holes. The central case under investigation herein is the balanced internal and external hydrostatic pressure situation i.e. $(\Delta_I + z_a) = \rho_2 / \rho_1 (\Delta_O + z_a)$ with Δ_I and Δ_O representing the inside and outside height of liquid above the hole upper lip, respectively, and the parameter z_a is a quantity that depends from the hole orientation. The uni-directional oil-flow from the side-damaged tank occurs if the unbalanced internal and external hydrostatic pressure situation exists. In the case of the hydrostatic overpressure condition

i.e. $(\Delta_I + z_a) > \rho_2 / \rho_1 (\Delta_O + z_a)$, only the uni-directional oil-spill from the damaged tanker can occur. Thus the difference between the sea level outside and the oil level inside of the tank, and the difference between the liquid densities, determine the oil-leak dynamics after accident.

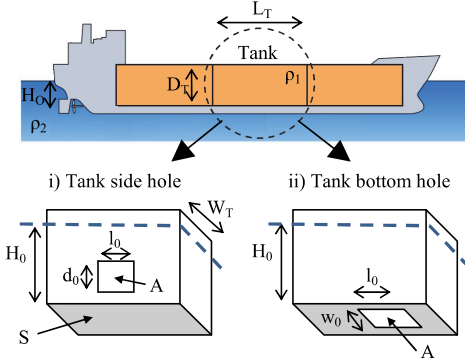


Figure 2. Schematic representation of the system: i) tank side opening and ii) tank bottom opening.

Typical tanker contains several cargo tanks (see Figure 2), which can be damaged in accident. Denoting the dimensions of a single tank as length (L_T), width (W_T) and depth (D_T), which define the tank volume $V_T = L_T \times D_T \times W_T$. The oil volume in the tank can differ from the tank volume because of the partial filling to satisfy the safety requirements. Here we assume that the oil-filled tank is of rectangular shape and the oil surface area is determined by $S_T = L_T \times W_T$ (see Figure 2). Double-side and bottom tank ballast volumes are defined herein as V_{ds} and V_{db} , respectively. The area of the damage opening in the tank structure is denoted with A . Equivalent dimensions of side damage (see Figure 2 inset i)) are characterized by the depth d_0 and the length l_0 . The area of the side opening is thus $A = d_0 \times l_0$. Hole equivalent dimensions for the bottom damage (see Figure 2 inset ii)) are characterized by width w_0 and length l_0 and the area is $A = w_0 \times l_0$. However, the area of the damage opening in outer and inner hull in the case of double-hull can differ. Henceforth, the sub-indexes O and I are used for the system parameters defined of *outer*- and *inner*-skin, respectively. The vessels collision in the offshore region results with the side damage having hole with different opening area, vertical position and shape. The bottom damages have fixed vertical position in the system.

The set of model parameters such as oil outflow volume V_T , volumetric flux Q_T and oil outflow time T_T are made non-dimensional by the following volume, flux and time scales.

$$V_{SCALE} = L_T \cdot H_0 \cdot W_T, \quad (1a)$$

$$Q_{SCALE} = A \cdot \sqrt{2g \cdot H_0}, \quad (1b)$$

$$T_{SCALE} = \frac{V_{SCALE}}{Q_{SCALE}}. \quad (1c)$$

The ship draft is denoted by H_0 . (Example tanker scales are: $H_0 = 17.8$ m, $L_T = 50$ m, $W_T = 26.5$ m.)

3 INTERNAL-FLOW HYDRAULICS

An aim of the internal-hydraulics model calculations is to determine the oil outflow volumes and durations for the different side-hole areas A and depths Δ . It is considered that the oil-leak takes place through a hull equivalent-size hole, which connects the less-dense liquid (oil) of density ρ_1 in the tank and the denser liquid (water) of density ρ_2 in the sea. The oil surface is considered to be under atmospheric pressure (p_0) and its vertical position can differ from that of outside sea water. The balanced internal and external hydrostatic pressure situation is represented by $(\Delta_I + d_0 / 2) = \rho_2 / \rho_1 (\Delta_O + d_0 / 2)$. In this paper the bi-directional flow is considered only for the side damage opening. In this central case the internal flow through a side-hole is bi-directional, with the upper-layer less-dense liquid (oil) flowing against the direction of the lower-layer denser liquid (sea water) (see Figure 3). The oil outflow through the bottom damage opening is considered to be uni-directional. The Pascal's Law of connected vessels of different density liquids apply in both cases.

An essential consideration in the theoretical analyses of the two-layer flow is existence of critical-flow sections. The maximal exchange-flow approximation requires that two controls exist simultaneously (Armi 1986). For instance in the case of the double-hull tanker it is distinct to locate the control section positions in the inner and outer holes of tanker hulls, yielding maximal transport estimate for the exchange flow. The flow through the single-hull tank side damage can only be sub-maximal i.e. is controlled only by single flow section. However, the sub-maximal solutions for exchange flow are mainly exploited in the present study, and this is justified by the damaged character where tank inner hull is always less breached. In the internal hydraulics theory the internal-head parameter $K_i = (B_2 - B_1) / g'$ is represented by the difference of the Bernoulli heads in lower (B_2) dense and upper (B_1) less-dense layer. The reduced gravity $g' = g(1 - r)$ is fixed by the density ratio $r = \rho_1 / \rho_2$. The internal flow regime is parameterized by the combined Froude number G^2 . According to Laaneau & Davies (2007) the composite Froude-number equation and the internal-head equation for the exchange flow, respectively, are given as

$$G^2 = \xi \frac{u_1^2}{g'} \frac{d_2^{\xi-1}}{D^{\xi} - d_2^{\xi}} + \xi \frac{u_2^2}{g' d_2}, \quad (2)$$

$$K_i = \left(\frac{\xi D^{(\xi-1)}}{l_0} \right)^2 K_{ii} \left[\left(\frac{1}{d_2^\xi} \right)^2 - \frac{q^2}{(D^\xi - d_2^\xi)^2} \right] + d_2 + h \quad (3)$$

The volumetric-flux parameter (determined here by the flow rate in the lower dense layer) is $K_{ii} = Q_2^2 / (2g')$. The ratio of upper layer (Q_1) and lower layer (Q_2) discharges is expressed conveniently in terms of the parameter $q^2 = Q_1^2 / Q_2^2$. The velocity of upper (1) less-dense and lower (2) dense liquids are u_1 and u_2 , respectively. The net velocity is defined by $u_n = u_1 - u_2$. The lower water-layer depth is d_2 and the upper oil-layer depth can be determined by the relationship $d_2 = d_0 - d_1$, where the depth maximum of the hole is d_0 (see Figure 2 inset i). The maximum length of the hole is l_0 . It should be mentioned that the actual hole-area A can be related to the equivalent depth and width (d_0, l_0) only by fixing the hole shape i.e. the shape factor ξ . The rectangular-shape hole represents the limiting case with the shape factor $\xi = 1$, and it will be most exploited in the present study. For instance, the triangular-shape hole corresponds to the "quadratic-shape" hole with the shape factor $\xi = 2$ and the circular-shape hole has the shape factor $\xi = 4 / \pi$ due to similarity principle $\xi = l_0 \times d_0 / A$. (For instance in the case of the environmental engineering study on river channel flow, the maximum width is at surface, maximum depth is at *Thalweg* and the shape parameter ξ was 1.8 in Laanearu et al. (2011).) In the case of single-hull tank the equations (2) and (3) can be evaluated directly to estimate the sub-maximal exchange through a hole, and in the case of double-hull tank the equations (2) and (3) should be evaluated separately for inside- and outside-hull holes, and the combined solution of the four equations can be employed to work out numerically the maximal exchange-flow flux. It should be mentioned that Equations (2) and (3) can be applied quite generally to predict the layer depths of the out- and inflowing fluids for sub-maximal exchange with the inner-hull control only.

3.1 Exchange flow

The oil spill from the single-hull tank side hole is schematically represented in Figure 3. The exchange flow through side hole is determined by the model parameters, such as the hole areal size $A = d_0 \times l_0$ ($\xi = 1$), the stratification that is given by the reduced gravity g' , and the system parameters, such as oil thickness ($H_I = h_I + d_{0I} + \Delta_I$) inside of the tank and the sea-water relative thickness ($H_O = h_O + d_{0O} + \Delta_O$) outside of the tank. In the case of balanced internal and external hydrostatic pressure situation ($(\Delta_I + d_0 / 2) = \rho_2 / \rho_1 (\Delta_O + d_0 / 2)$) the oil thickness H_I is a dynamical parameter, which depends only on the parameter h_I during the bi-directional-flow process. The sea-water thickness H_O (and h_O) is assumed to be constant and fixed by the ship draft.

The hull thickness in the case of single-hull tank is considered negligible. During tanker emptying process the oil with the depth $h_I(t)$ below the lower lip of hole is regulated by the sea-water amount inside of the tank, and the sea-water depth h_O below the lower lip of hole is dependent on the sea-water intake depth outside (what in the present model calculations is fixed by the tank bottom).

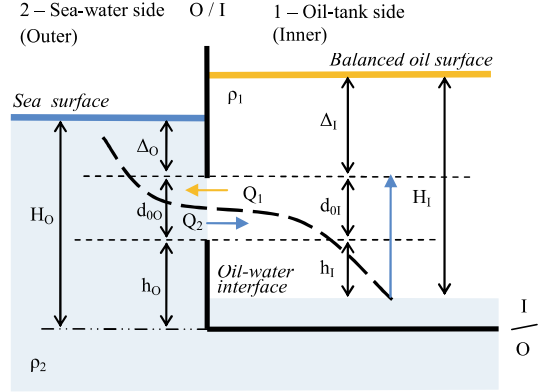


Figure 3. Sketch of the bi-directional flow through the single-hull side damage hole and notations.

3.2 Application example

The oil-spill dynamics for the dimensionless cases of hole size ($A / (L \times H_O)$): with $A = (5 \times 5) \text{ m}^2$, $(4 \times 4) \text{ m}^2$ and $(3 \times 3) \text{ m}^2$, and with the hole lower lip dimensionless depth $(\Delta_O + d_0) / H_O$: with $(\Delta_O + d_0) = (5 + 5) \text{ m}$, $(10 + 4) \text{ m}$ and $(15 + 3) \text{ m}$ from the oil level inside of the tanker, respectively, is shown by full curves in Figure 4.

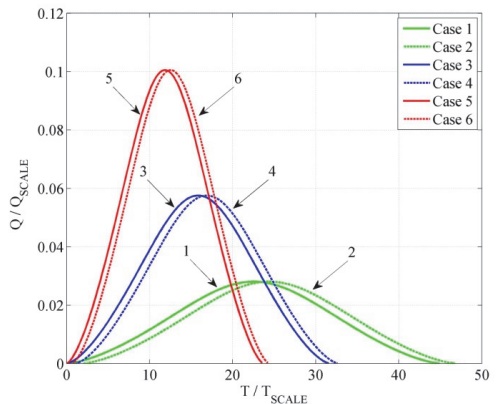


Figure 4. Bi-directional flow with the oil outflow volumetric flux equal to the sea-water inflow volumetric flux ($q^2 = 1$) for different dimensionless hole sizes ($A / (L_T \times H_O)$) and the dimensionless depths. Case 1: Balanced system, $3 \times 3 \text{ m}^2$, $\Delta_I = 15 \text{ m}$; Case 2: Overpressure, $3 \times 3 \text{ m}^2$, $\Delta_I = 14 \text{ m}$; Case 3: Balanced system, $4 \times 4 \text{ m}^2$, $\Delta_I = 10 \text{ m}$; Case 4: Overpressure, $4 \times 4 \text{ m}^2$, $\Delta_I = 9 \text{ m}$; Case 5: Balanced system, $5 \times 5 \text{ m}^2$, $\Delta_I = 5 \text{ m}$; Case 6: Overpressure, $5 \times 5 \text{ m}^2$, $\Delta_I = 4 \text{ m}$.

The non-linear emptying of the initially oil-filled tank is associated with the changing oil outflow flux, having peak value in the case of equal liquids depths at hole i.e. $d_1 = d_2$. It can be recognized from the results in Figure 4 that comparatively large holes correspond to high peak volumetric flux, and comparatively deeply submerged holes correspond to larger outflow time. Also solution curves for the oil leak in the cases of un-balanced hydrostatic pressure situations are included in Figure 4 with dashed curves. The peak fluxes are "right-ward" shifted due to the uni-directional oil outflow in the case of hydrostatic overpressure condition at beginning. The exchange flow analytical calculations by Tavakoli et al. (2010) were limited to the maximum oil outflow flux, which is employed essentially in the estimation of shortest oil outflow duration below.

4 SIDE DAMAGE: ANALYTICAL MODEL

4.1 Uni-directional flow

The uni-directional leak from the side-damaged tank occurs if the unbalanced internal and external hydrostatic pressure situation exists. Herein the example calculations are given for the oil outflow through the rectangular-shape hole ($\xi = 1$). In the model calculations the oil thickness H_I is a dynamical parameter that depends on the parameter $\Delta_I(t)$ during the uni-directional flow process (cf Figure 4). The sea-water thickness H_O (and Δ_O) is assumed to be constant and fixed by the ship draft. In the hydraulic model calculation the uni-directional oil outflow volumetric flux is determined by the standard Torricelli's formula

$$Q_1 = C_d A \sqrt{2g((\Delta_1 + d_0/2) - \rho_2/\rho_1(\Delta_0 + d_0/2))}, \quad (4)$$

where C_d is the discharge coefficient. The time-dependent oil outflow through the side hole results from the reduction of internal pressure due to descending of oil surface in the tank as compared to the sea level of fixed position i.e. $H_O = \text{const.}$

In the case of single-hull side hole the oil outflow duration and volume with changing internal pressure can be calculated by the analytical formulae:

$$T_{oil} = \frac{2S}{A \sqrt{2g}} \frac{1}{C_d} \sqrt{V_{oil}/S}, \quad (5a)$$

$$V_{oil} = \left(\left(\Delta_I + \frac{d_0}{2} \right) - \frac{\rho_2}{\rho_1} \left(\Delta_O + \frac{d_0}{2} \right) \right) S. \quad (5b)$$

The total oil outflow volume for uni-directional flow is fixed due to the difference in the hydrostatic pressure of the oil and water columns relative to the hole axis. The total oil outflow duration for uni-directional flow is dependent on the discharge coef-

ficient, and the shortest duration is associated with the inviscid case i.e. $C_d = 1$.

The oil spill uni-directional flow calculations for different side dimensionless holes $A / (H_O \times L_T)$ (with the actual areal sizes of $A = 1 \times 1 \text{ m}^2, 2 \times 2 \text{ m}^2, 3 \times 3 \text{ m}^2, 4 \times 4 \text{ m}^2$) of the single-hull tank and inviscid case are concluded in Table 1.

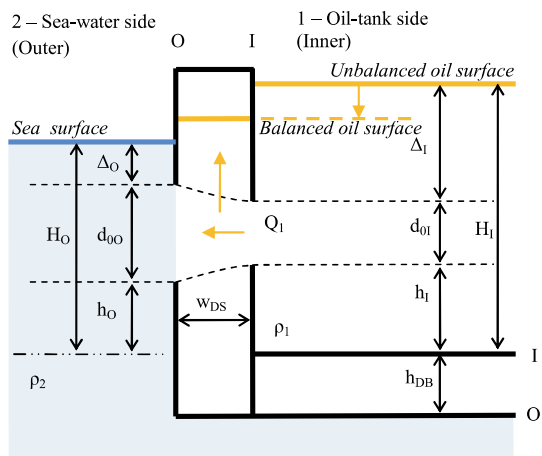


Figure 5. Sketch of the uni-directional flow through the double-hull side damage hole and notations. Non-ventilated side ballast volume V_{DS} is available for the initial oil volume loss.

In the case of double-hull tank, however, the Torricelli's Formula should be integrated with the side ballast volume V_{DS} . Several limitations of the double-hull volume may apply due to the tanker construction (see Figure 5). The time-dependent oil outflow duration and volume can be calculated by modified analytical formulae:

$$T_{oil} = \frac{2S}{A \sqrt{2g} C_d} \sqrt{V_{oil}^*/S}, \quad (6a)$$

$$V_{oil}^* = \left(\left(\Delta_I^* + \frac{d_0}{2} \right) - \frac{\rho_2}{\rho_1} \left(\Delta_O + \frac{d_0}{2} \right) \right) S, \quad (6b)$$

where Δ_I^* is fixed by the relationship $\Delta_I^* = \Delta_I - V_{DS}/S$. Here the ballast volume V_{DS} that is available for the oil, is dependent on the trapped air pillow i.e. non-ventilation condition apply. It should be mentioned here that in the case of submerged and low-positioned damage no oil outflow may occur from the tanker, because the oil outflow volume available due to the high internal overpressure condition may be smaller as compared to the side ballast volume V_{DS} . In such case the oil outflow from the tanker is determined only by the bi-directional flow. The oil spill uni-directional flow calculations for different side holes of dimensionless areas $A / (H_O \times L_T)$ (with the actual areal sizes of $A = 1 \times 1 \text{ m}^2, 2 \times 2 \text{ m}^2, 3 \times 3 \text{ m}^2, 4 \times 4 \text{ m}^2$) of the double-hull tank and viscid case ($C_d = 1.0$) are also concluded in Table 1.

4.2 Bi-directional flow

The bi-directional flow through the double-hull tank side hole is sketched in Figure 6.

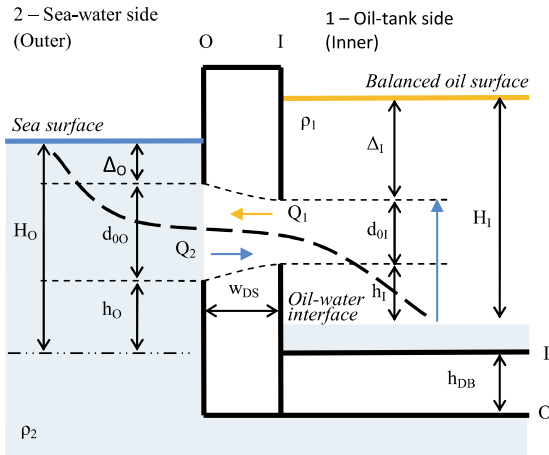


Figure 6. Sketch of the bi-directional flow through the double-hull side damage hole and notations. Non-ventilated side ballast volume V_{DS} is filled during the uni-directional flow.

An essential consideration in the theoretical analysis of the two-layer internal hydraulics is existence of critical-flow sections. Several sub-maximal flow regimes are possible by maximising the exchange flow through the side hole of damaged tank. The critical-flow solutions corresponding to the sub-maximal flow can be determined by using the implicit-function differentiation theorem as applied to Equation (3) with respect to the lower layer depth variable d_2 . The result corresponds to the composite Froude number formula $G^2 = F_1^2 + F_2^2 = 1$. The seawater volumetric flux maximum of bi-directional flow is given by the formula

$$Q_2^2 = \frac{g' w_0^2 d_0^3}{\xi^3} \left[\left(\frac{d_0}{d_2} \right)^{2\xi+1} - \frac{q^2 (d_2/d_0)^{(\xi-1)}}{(1 - (d_2/d_0)^\xi)^3} \right]^{-1}. \quad (7)$$

The oil-leak volumetric flux of bi-directional flow is determined by $Q_1^2 = q^2 Q_2^2$. It should be noted that the sea-water volumetric flux by Equation (7) has a single maximum associated with the fully controlled flow at the oil-interface position $d_1 = d_2$ in hole. In the case of balanced internal and external hydrostatic pressure situation the upper-layer less-dense liquid (oil) is flowing against the direction of the lower-layer denser liquid (sea water) without net flux i.e. $Q_n = Q_1 - Q_2 = 0$.

The oil spill bi-directional flow calculations for different side holes dimensional areas A ($H_O \times L_T$) (with the actual areal sizes of $A = 1 \times 1 \text{ m}^2, 2 \times 2 \text{ m}^2, 3 \times 3 \text{ m}^2, 4 \times 4 \text{ m}^2, 5 \times 5 \text{ m}^2$) of the single- and double-hull tank are also concluded in Table 1.

Table 1. Side damage oil spill analytical calculations.

A / A _{SCALE}	Δ_1 / H ₀	Single hull unidirectional		Single hull bi-directional	
		V _{SPILL} / V _{SCALE}	T _{SPILL} / T _{SCALE}	V _{SPILL} / V _{SCALE}	T _{SPILL} / T _{SCALE}
0.0011	1.40	0.31	1.11	0.07	4.39
0.0045	1.12	0.35	1.19	0.35	15.37
0.0101	0.84	0.40	1.26	0.63	22.57
0.0180	0.56	0.44	1.33	0.91	28.22
		Double-hull unidirectional		Double-hull bi-directional	
0.0011	1.40	0.23	0.95	0.07	4.39
0.0045	1.12	0.29	1.08	0.35	15.37
0.0101	0.84	0.36	1.19	0.63	22.57
0.0180	0.56	0.42	1.29	0.91	28.22

5 BOTTOM DAMAGE: ANALYTICAL MODEL

5.1 Uni-directional flow

The uni-directional leak from the bottom-damaged tank occurs if the un-balanced internal and external hydrostatic pressure exists. In the case of hydrostatic overpressure i.e. $\Delta_l > \rho_2 / \rho_1 \Delta_o$ (with $\rho_2 > \rho_1$), only the uni-directional oil-spill from the damaged tanker can take place. Here the example calculations are given for the oil outflow through the rectangular-shape hole ($\xi = 1$). In the case of double-hull tanker the inside hull rectangular-shape hole area $A_l = w_{0l} \times b_{0l}$ is set equal to the outside hull area $A_o = w_{0o} \times b_{0o}$ i.e. $A = A_l = A_o$. It should be mentioned that in the model calculations similar to the uni-directional flow through the side hole the oil thickness H_l is a dynamical parameter, which depends directly from the parameter $\Delta_l(t)$ during the uni-directional-flow process (see Figure 7). The seawater thickness H_o is assumed to be constant and fixed by the ship draft. In the model calculation the uni-directional oil outflow flux is determined by the standard Torricelli's Formula:

$$Q_1 = C_d A \sqrt{2g(\Delta_1 - \rho_2/\rho_1 \Delta_0)}, \quad (8)$$

where C_d is the discharge coefficient. The time-dependent oil outflow through the bottom hole results from the reduction of internal pressure due to descending of the oil surface in the tank as compared to the sea level of fixed position i.e. $H_O = \text{const.}$

In the case of single-hull bottom hole the time-dependent oil outflow duration and volume can be calculated by the straightforward analytical formulae:

$$T_{oil} = \frac{2S}{A\sqrt{2g}} \frac{1}{C_d} \sqrt{V_{oil}/S}, \quad (9a)$$

$$V_{oil} = \left(\Delta_I - \frac{\rho_2}{\rho_1} \Delta_O \right) S. \quad (9b)$$

The total oil outflow volume for uni-directional flow is fixed due to the difference in the hydrostatic pressure of the oil and water columns relative to the tank bottom. The total oil outflow duration for uni-directional flow is dependent on the discharge coefficient, and the shortest duration is associated with the inviscid case i.e. $C_d = 1$. The oil spill uni-directional flow calculations for different bottom holes of dimensionless areal sizes $A / (H_O \times W_T)$ (with the actual areal sizes of $A = 1 \times 1 \text{ m}^2, 2 \times 2 \text{ m}^2, 3 \times 3 \text{ m}^2, 4 \times 4 \text{ m}^2, 5 \times 5 \text{ m}^2$) of the single-hull tank and inviscid case are concluded in Table 2.

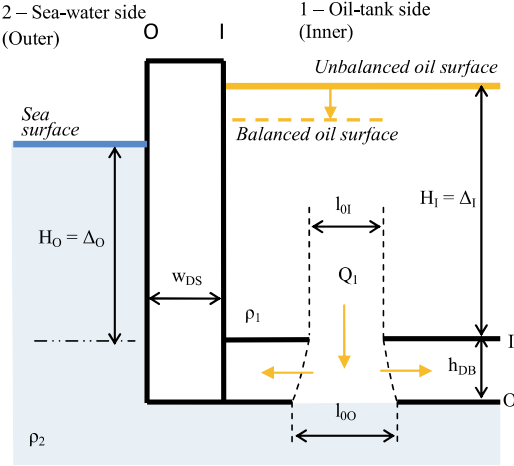


Figure 7. Sketch of the uni-directional flow through the double-hull bottom damage hole and notations. The initial oil volume loss is due to the bottom ballast of volume V_{DB}

In the case of double-hull tank, however, the Torricelli's Formula should be integrated with the bottom ballast volume V_{DB} , which is available for the oil volume loss. Several limitations of the double-hull volume may apply due to the tanker construction (see Figure 7). In this case the oil outflow duration and volume can be calculated by modified analytical formulae:

$$T_{oil} = \frac{2S}{A \sqrt{2g}} \frac{1}{C_d} \sqrt{V_{oil}^* / S}, \quad (10a)$$

$$V_{oil}^* = \left(\Delta_I^* - \frac{\rho_2}{\rho_1} \Delta_O \right) S. \quad (10b)$$

where Δ_I^* is fixed by the relationship $\Delta_I^* = \Delta_I - V_{DB} / S$. It should be mentioned here that no oil outflow occurs from the tanker if the bottom ballast volume V_{DB} is large enough as compared to the oil outflow volume available due to the internal overpressure.

The oil spill uni-directional flow calculations for different bottom holes of dimensionless areas $A / (H_O \times W_T)$ (with the actual areal sizes of $A = 1 \times 1 \text{ m}^2, 2 \times 2 \text{ m}^2, 3 \times 3 \text{ m}^2, 4 \times 4 \text{ m}^2, 5 \times 5 \text{ m}^2$) of the

double-hull tank and inviscid case are concluded in Table 2.

Table 2. Bottom damage oil spill calculations.

A / A _{SCALE}	Δ_I / H ₀	Single hull unidirectional		Double hull unidirectional	
		V _{SPILL} / V _{SCALE}	T _{SPILL} / T _{SCALE}	V _{SPILL} / V _{SCALE}	T _{SPILL} / T _{SCALE}
0.0021	1.40	0.30	1.10	0.064	0.51
0.0085	1.12	0.30	1.10	0.064	0.51
0.0191	0.84	0.30	1.10	0.064	0.51
0.0339	0.56	0.30	1.10	0.064	0.51
0.0530	0.28	0.30	1.10	0.064	0.51

6 DISCUSSION

Here the developed method is compared due the hydraulic characteristics with the model-scale experiments by Tavakoli et al. (2011). Due to flow separation effects at hole, the real discharge is lower than the maximal discharge. For instance, the discharge coefficient that is estimated for the uni-directional flow through single bottom puncture (C1, diameter = 2.2 cm) was found to be 0.67 in Tavakoli et al. (2011). The model-scale experiment discharge coefficient was found to be 0.68 in the case of single side puncture (S1, diameter = 2.2 cm). In the simulation model proposed, the case of the side hole below the waterline 0.4 meter and overpressure-head with 0.27 m the discharge coefficient of circular hole was estimated to be $C_d = 0.77$. This small discrepancy found is apparently due to *vena contracta* of the streamlines at the puncture, reported in Tavakoli et al. (2011). With the equal hydrostatic pressures on both sides of the hole, the bi-directional flow occurred in the model-scale experiment of Tavakoli et al. (2011). In the two-layer phase, the oil surface was constant and the oil-water interface ascended in the cargo tank. The two-layer flow in the experiment continued for approximately 5 h and finally stopped when the hole was covered by water on both sides. In the two-layer model proposed herein the circular hole is approximated by the shape factor $\xi = 4 / \pi$. The model calculation for the bi-directional inviscid flow under same initial and boundary conditions proved that the oil outflow from the cargo tank lasted 1,53 h. This proves well that the total two-layer sheared flow resistance through the circular hole (S1) of area 3.8 cm^2 was due to the flow separation from the hole edges and also due to the dynamical interaction (mixing) between oil and water. The total oil outflow volume was also found to correspond with a model-scale experiment by Tavakoli et al. (2011). The oil outflow of the simulation model can be: i) uni-directional, ii) bi-directional and iii) retained in the ballast. Calculated spilled oil and retained oil volumes are presented and compared with the model-scale experimental results by Tavakoli et

al. (2011) in Table 3. The model-scale experimental tank was built with a horizontal section of $100 \times 50 \text{ cm}^2$ and height of 100 cm. The water level was 47 cm and the oil level varied between 70 – 85 cm in the model-scale tank experiments. The largest puncture at bottom (C_1) and side (S_1) had diameter of 2.2 cm ($A = 3.8 \text{ cm}^2$).

Table 3. Modelled spilled and retained oil percentages. Tavakoli et al. (2011) experimental results in parentheses.

Design	Hole	Spilled oil (%)	Retained oil (%)
Single bottom	C_1	36.3 (34)	0 (0)
Single side hole	S_1	45.7 (57)	0 (0)
Double bottom	C_1	28.3 (26)	11.7 (35)
Double side	S_1	34.9 (40)	10.8 (19)

7 CONCLUSIONS

The aim of present study was to demonstrate how the internal hydraulics theory can be applied for the modelling of submerged oil spill. The practical outcome of the model was estimation of the volume and duration of spilled oil from damaged tanker. In the case of un-balanced internal and external hydrostatic pressure situation the initial flow through the holes was uni-directional and after establishment of the balanced hydrostatic pressure situation at the side hole axis the bi-directional flow followed. However, distinction between the single- and double-hull tankers was done due to the ballast volume, associated with the oil loss.

A numerical model was used to calculate the stratified flow through the side hole with the non-linear water filling of initially oil-filled tank. This numerical solution was restricted to the zero net-flow ($u_n = u_1 - u_2 = 0$). This case represented realistic situation with the bi-directional flow starting and ending with the zero oil outflow volumetric flux. This condition corresponds to the uni-directional flow situation that was ended after oil surface inside of the tank was descended to the balanced hydrostatic pressure level and before the oil interface was ascended above the hole upper lip. The oil outflow flux maximum ($Q_1 = Q_2 \rightarrow \max.$) was associated with the oil interface position at hole of the equal liquid depths i.e. $d_1 = d_2$.

The oil uni-directional outflow velocity was time dependent due to gradually reducing internal pressure (due to descending of the oil surface inside of the tank), and was associated with the non-linear emptying of the oil-filled tank until the balanced internal and external hydrostatic pressure situation was established. The linear emptying of the oil-filled tank was associated with bi-directional flow through the side hole, which was fixed to the maximum volumetric flux without net flow. In all simulation

model solutions the oil-water interface was ascending from tank bottom to the upper-lip of hole.

To conclude the study it should be mentioned that the developed simulation model can be applied also in the cases of not submerged single- and double hull side holes. The uni-directional flow phase in this case corresponds to the oil surface descending until the sea level, and occurs without the oil loss into ballast volume for the double-hull tanker case.

8 ACKNOWLEDGEMENTS

This research work has been financially supported by Estonian Science Foundation (grant agreement ETF8718) and by Central Baltic Interreg IV program through MIMIC project (“Minimizing risks of maritime oil transport by holistic safety strategies”). This help is here kindly appreciated

9 REFERENCES

- Armi, L. 1986. The hydraulics of two flowing layers of different densities. *Journal of Fluid Mechanics*: 163: 27-58.
- Cuthbertson, A.J., Laanearu, J. & Davies, P.A. 2006. Buoyancy-driven two-layer exchange flows across a slowly submerging barrier. *Environ. Fluid Mech.*:6 No 2(19): 133-151.
- Dalziel, S. B. & Lane-Serff, G. F. 1991. The hydraulics of doorway exchange flows. *Building and Environment*: 26: 121-135.
- Ehlers, S. 2009. Material Relation to Assess the Crashworthiness of Ship Structures, Doctoral Dissertation, Helsinki University of Technology, available at: <http://lib.tkk.fi/Diss/2009/isbn9789522481443/>
- Ehlers, S. Tabri, K. 2012. A combined numerical and semianalytical collision damage assessment procedure, *Marine Structures*: 28(1): 101-119.
- Kujala, P., Hanninen, M., Arola, T., Ylitalo, J. 2009. Analysis of the marine traffic safety in the Gulf of Finland. *Reliability Engineering & System Safety*: 94(8): 1349-1357.
- Laanearu, J. & Davies, P. A. 2007. Hydraulic control of two-layer flow in quadratic type channels. *Journal of Hydraulic Research*: 45(1): 3-12.
- Laanearu, J., Vassiljev, A. & Davies, P. A. 2011. Hydraulic modelling of stratified bi-directional flow in a river mouth. *Engineering and Computational Mechanics I*: 164(EM4): 207-216.
- Tavakoli, M. T., Amdahl, J. & Leira, B. J. 2010. Analytical and numerical modelling of oil spill from a side damaged tank. *5th International Conference on Collision and Grounding of Ships, Helsinki, 10-14 June 2010*.
- Tavakoli, M. T., Amdahl, J. & Leira, B. J. 2011. Experimental investigation of oil leakage from damage ships due to collision and grounding. *Ocean Engineering*: 38(17-18): 1894-1907.
- Zhu, Z. Z., Fouli, H. & Okyere, A. Y. 2001. Exchange flow through opening. *Journal of Hydraulic Research*: 40(3): 341-350.
- Zhu, D. Z. 2003. Hydraulic control of exchange flows. *Journal of Hydraulic Research*: 41(5): 503-511.

Appendix 2

PUBLICATION II

Kollo, M., Laanearu, J., Tabri, K. (2017). Hydraulic modelling of oil spill through submerged orifices in damaged ship hulls. – *Ocean Engineering*, 130, 385–397. doi: 10.1016/j.oceaneng.2016.11.032



Hydraulic modelling of oil spill through submerged orifices in damaged ship hulls



Monika Kollo^{a,*}, Janek Laanearu^b, Kristjan Tabri^b

^a Faculty of Civil Engineering, Tallinn University of Technology, Ehitajate tee 5, Tallinn 19086, Estonia

^b Department of Mechanics, Tallinn University of Technology, Ehitajate tee 5, Tallinn 19086, Estonia

ARTICLE INFO

Keywords:

Oil spill
Ship accident
Stratified flow
Hydraulic model
Discharge coefficient
Genetic Algorithm

ABSTRACT

Hydraulic models for one- and two-layer flows are combined in different oil spill scenarios for tanker accidents. Four oil spill model versions are used to determine oil-leak quantities in six test cases. Five test cases are verified by comparison to the laboratory results of Tavakoli et al. (2011). One test case is presented as a demonstration of the modelling approach developed here. In the hydraulic modelling, it was found that a descending oil surface in the leaking tank yields a unidirectional flow, while an ascending oil-water interface shows a bidirectional flow. Oil spill volumes and durations confirm that oil outflow depends strongly on flow separation and mixing at the submerged orifices. As a corollary of this work, discharge coefficients are determined from the experimental verification of the hydraulic models. An optimisation algorithm was employed to determine the head losses of a stratified flow through the double-hull tank hole.

1. Introduction

Ship collisions and groundings are major accident types in maritime transportation (EMSA, 2010, 2014). Depending on the ship type and extent of damage, such accidents can result in human casualties, adverse environmental effects and/or financial loss. Oil slick in offshore regions, such as the Gulf of Mexico, the Strait of Sicily, the Baltic and the Mediterranean Sea, can reveal complicated dynamics. Due to the distances to the shore where civil protection teams and clean-up equipment are located, oil spills are difficult to manage (Cucco et al., 2012; Soomere et al., 2014; Melaku et al., 2015). According to Alves et al. (2015), oil slick movement in the Eastern Mediterranean Sea is strongly affected by bathymetric, meteorological, oceanographic, and geomorphological conditions. Accidents involving oil tankers can result in adverse environmental effects if structural damage to the ship hull occurs at such a location that compartments containing oil are breached, leading to significant spills (Soomere et al., 2010, 2014; Alves et al., 2014, 2015, 2016; NEREIDS Project). Thus, to assess potential environmental risks, it is essential to understand possible consequences of accidental breaches in tanker hulls. Furthermore, in addition to the typical trajectories of oil slick movement it is necessary to be able to predict the amount of potential oil spilt for different hull configurations and breach points. The oil spill model presented here is a part of the accidental damage and spill assessment model (ADSAM), which was devised to estimate rapid oil spill scenarios for hull collisions

and grounding damage. The ADSAM model predicts structural damage and evaluates the spill volume and duration in situations where only limited data are available for ships involved in maritime accidents. In this regard, the ADSAM model is well suited for a risk analysis approach whereby large numbers of scenarios can be analysed using limited available data. An integrated model of this kind is proposed in Tabri et al. (2015).

When modelling oil-outflow dynamics from a leaking tank, it is essential to use tools that are capable of modelling flow to density variations, hydrostatic driving pressure, viscosity and mixing and hull-damage characteristics (e.g., orifice location, size and shape). Oil emulsification plays a significant role in modelling oil slick trajectory (Alves et al., 2015), as emulsion with 80% water content may end up with a volume that is five-times the spilled volume of parent oil (Xie et al., 2007). In the formation of emulsions resulting from the physical mixing promoted by turbulence at the sea surface, the density and viscosity of a liquid is constantly changing. Nevertheless, such investigations of oil outflows from leaking tanks (e.g., Simecek-Betty et al., 2005; Tavakoli et al., 2011) are scarce. Published models are limited to calculating the final outflow (i.e., oil spill) volume, with little or no consideration of variations in the outflow dynamics with time. An engineering modelling tool based on the internal-flow hydraulic formulae (Sergejeva et al., 2013) can be applied to determine integrated parameters in oil spill scenarios. However, a Computational Fluid Dynamics (CFD) tool for rapid assessment of oil spill accidents

* Corresponding author.

E-mail addresses: monika.kollo@ttu.ee (M. Kollo), janek.laanearu@ttu.ee (J. Laanearu), kristjan.tabri@mec.ee (K. Tabri).

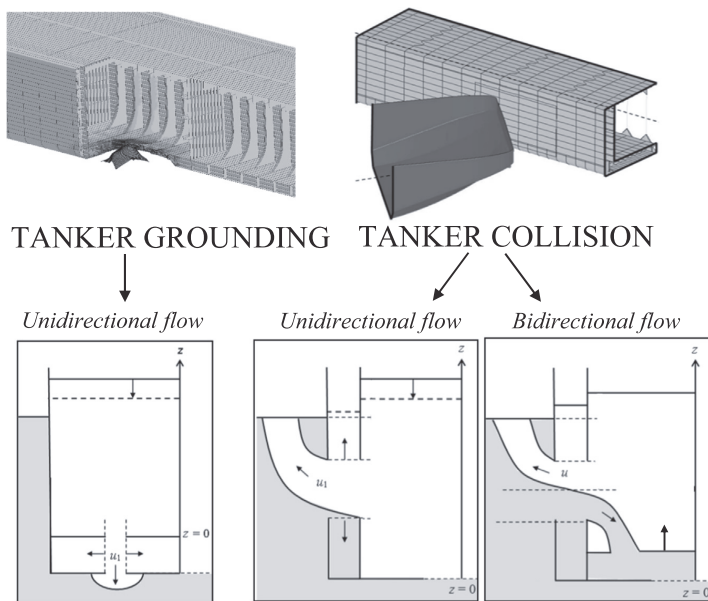


Fig. 1. Oil spill scenarios of grounding and collision for a double-hull tanker.

can be computationally demanding (Tavakoli et al., 2012). Thus, the use of stratified-flow hydraulic models is justified for the fast prediction of multiphase flow quantities. CFD analysis can be useful in validating more complicated spill cases where decision-based models are uncertain (e.g., due to the dynamics of a multiphase flow process).

Oil spills encompass the flow of two immiscible liquids in a complex geometric system that involves a wide range of length scales. Hydraulic formulae relevant for a stratified *unidirectional* flow through a hole can be readily obtained by considering the density difference between the liquids and excess hydrostatic pressure as the main driving forces. However, a realistic oil outflow rate can also be estimated by using the coefficient of discharge. Without excess hydrostatic pressure, a *bidirectional* flow occurs, whereby oil flows out from a leaking tank and seawater flows in the opposite direction (Fig. 1). Two-layer flow dynamics are predominantly solved numerically because no analytical solutions for non-rectangular holes are readily available for particular applications. However, hydraulic models can be adapted to the changing hydrostatic pressure and they provide satisfactory results in quasi-stationary conditions (Cuthbertson et al., 2006).

In the present study, a novel analytical solution for an exchange flow through a circular hole (orifice) is introduced. We emphasise that the oil-water exchange flow rate at the hole depends on the flow separation at the edges of the hole and the dynamical interaction of superimposed layers (e.g., mixing). The following hypotheses are proposed for the modelling of oil spills:

- discharge formulae allow the determination of oil outflow volumes;
- continuity formulae allow the determination of oil outflow durations;
- *unidirectional* oil outflow can be characterised by a quasi-stationary condition;
- *bidirectional* flow with oil outflow can be characterised by a stationary condition;
- a transitional stage between a *unidirectional* and a *bidirectional*

flow is absent without a tank lift;

- discharge coefficients can be determined from available experimental data;
- the Genetic Algorithm predicts density and viscosity variations for a *bidirectional* flow associated with an oil outflow.

Results obtained from the physical modelling of oil outflows from the single- and double-hull test tank allow for the validation of the hydraulic models in terms of their geometric, kinematic and dynamic similarity with ship accidents (Tavakoli et al., 2011). In particular, the experimental conditions of different Tavakoli's lab tests can be used to build different versions of oil spill models. Changes in the oil surface (i.e., air-oil interface) and oil-water interface level in a leaking tank, with a fixed water level outside the tank, can be directly used to validate the results of the proposed hydraulic models. The dynamical interaction between immiscible liquids can result in changes of outflowing liquid density and viscosity. The aim of this study is to use hydraulic models to help interpret the complicated nature of oil-outflow dynamics from a tank. However, in different accident scenarios the fluids will still behave in a similar way. It should be mentioned here that the proposed internal-flow hydraulic models can be further used to determine the mixed-layer depth (associated with the emulsification of an outflowing liquid) and can be implemented to complement the oil spill mitigation procedures compiled for NEREIDS (Alves et al., 2015).

This paper is organised as follows. First, the hydraulic framework based on the quasi-steady flow equations for one- and two-layer hydraulic modelling is introduced together with the internal hydraulic formulae for *unidirectional* and *bidirectional* flows through orifices. Four oil spill models corresponding to oil outflow through the side or bottom orifice of single- or double-hull tankers are presented for two scenarios: grounding and collision. Next, modified and novel analytical formulae are used to determine the discharge coefficients, according to the experiments by Tavakoli et al. (2011). An optimisation algorithm is employed to determine the internal-flow head losses from the flows

through the orifices of the double-hull tank. Finally, a demonstration case of the developed hydraulic models is presented.

2. Hydraulic modelling

Holes in ship hulls usually result from ship collisions, whereas tanker grounding can result in a bottom leak. A stratified flow through submerged holes takes place when the liquids on both sides of the hull have different densities. Stratified flows are usually modelled as a homogeneous layer with inviscid liquids subjected to a hydrostatic pressure distribution. The Bernoulli equations of the homogeneous layer are also used in the modelling of stratified flows at orifices (cf. Tavakoli et al., 2012). However, in the Bernoulli's approach, coupling between superimposed layers is absent and simplified treatment of the internal-flow energy complicates the modelling (Armi, 1986). In the case of oil and water, the hydraulically driven flows can be limited to a small density difference between the layers. Through the holes, two types of stratified flows, *unidirectional* and *bidirectional*, are possible and can be related to two "key parameters": the difference between the water level outside and the oil level inside the tank and the difference in liquid density. In practice, the higher the oil tanker is loaded, the larger the pressure will be inside the vessel and its difference to the seawater pressure outside the hull. Thus, oil leaks out once the tank structure is breached. If the tanker carries substantially less oil, such that the hydrostatic balance is attained above the oil-tank bottom, outside water tends to enter the tank as long as the highest point of damage is below the hydrostatic balance level (National Research Council, 1991).

2.1. Unidirectional flow

A tanker can be loaded with an oil level above the seawater level. In the case of excess hydrostatic pressure at the level of the hole, stratified flows through the hole are *unidirectional*. Oil outflow through the hole occurs when the inside pressure (p_i) exceeds the outside pressure (p_o). The oil level descends in the leaking tank during the *unidirectional* outflow, resulting in a decrease in the weight of the ship. Therefore, the ship's buoyancy increases (i.e., oil level descending speed is reduced and the *unidirectional* outflow of oil is virtually magnified). Excess hydrostatic pressures can also result from a relatively high oil level (Δ_i) and gas pressure (p_{gas}) in a ductless tank, as compared to the water level (Δ_o) and air pressure (p_{air}) on the sea surface. Here, the density of oil (ρ_{oil}) is considered to be slightly lower than seawater (ρ_{water}) (i.e., corresponding to the condition $(\rho_{water} - \rho_{oil})/\rho_{water} < 1$). The vertical pressure gradient varies according to the liquid density and the hydrostatic excess pressure point at the tanker hull may be positioned to a certain depth below the waterline. Bernoulli's equation for a *unidirectional* stratified flow through the hole can be expressed as:

$$\frac{u_{oil}^2}{2g}(1 + \Pi) = (z_o - z_i) + \left(\frac{p_{gas}}{\rho_{oil}g} - \frac{p_o}{\rho_{oil}g} \right) \& p_o < p_i, \quad (1)$$

where the elevation-head difference is $z_o - z_i = \Delta_i + d_o/2$ and the pressure-head difference is $(p_{gas} - p_o)/\rho_{oil}g = (p_{gas} - p_{air})/\rho_{oil}g - \rho_{water}(\Delta_o + d_o/2)/\rho_{oil}$. In the presence of oil tank ventilation, the pressures of gas and air are equal (i.e., $p_{gas} = p_{air}$) and the pressure-head difference is simplified as $(p_{gas} - p_o)/\rho_{oil}g = -\rho_{water}(\Delta_o + d_o/2)/\rho_{oil}$. The internal-flow head loss in Eq. (1) is represented by the sum of the local head-loss coefficients $\Pi = \sum_i k_i$.

The *unidirectional* stratified flow through the hole in the hull side is depicted in Fig. 2i. It should be mentioned that, when the hydrostatic excess pressure point is positioned below the hull bottom, then the conditions described above would apply to the *unidirectional* flow through a hole in the hull bottom. Hence, the description is limited

only to the side-hull case.

According to continuity, the oil outflow rate can be calculated by the formula of a *unidirectional* flow:

$$Q_{oil} = u_{oil}A_0, \quad [\text{Formula for a unidirectional flow}] \quad (2)$$

where u_{oil} is the oil outflow velocity and $A_0 = \pi d_o^2/4$ is the area of the orifice. It should be emphasised that, in the case of a bottom hole, oil outflow stops when the hydrostatic balance is attained between the oil surface in the tank and the sea surface outside, at the level of the hole. However, in the case of a side hole, *bidirectional* flow follows when the *unidirectional* flow wanes down to a hydrostatically balanced situation. During the final stage of the oil level descent, a barotropic net exchange flow is possible due to a transitional stage between the *unidirectional* and *bidirectional* flows. This transitional stage can be essentially ignored in a vertically fixed tank (Tavakoli et al., 2011). Due to the tanker's buoyancy loss, whenever significant vertical movements occur, the difference between oil and water surfaces changes. Thus, the water inflow into the leaking tank is magnified during the *bidirectional* flow.

2.2. Bidirectional flow

The *bidirectional* flow through the hole is depicted in Fig. 2ii. At small density differences and equal pressures at the water and oil surface, the equations governing a two-layer flow are as follows:

$$E_{upper} = \frac{1}{2}\rho_{oil}u_{upper}^2 + p_1 + \rho_{oil}g(d_{upper} + d_{lower} + h), \quad (3)$$

$$E_{lower} = \frac{1}{2}\rho_{water}u_{lower}^2 + p_2 + \rho_{oil}gd_{upper} + \rho_{water}g(d_{lower} + h), \quad (4)$$

where $p_1 = p_i$ and $p_2 = p_o$ are the pressures at the upper lip inside (I) and outside (O) the side hole, respectively. The vertical size of the hole corresponds to the diameter d_o and the centre-line depths of the lighter (ρ_{oil}) and heavier (ρ_{water}) liquid layer are d_{upper} and d_{lower} , respectively. Flow velocities in the upper and lower layer are u_{upper} and u_{lower} , respectively and h is defined as the hole's lower lip height measured from the bottom of the oil-tank. Here, the upper layer flow in the hydraulic model corresponds to the oil flow ($u_{upper} = u_{oil}$) and the lower layer flow to the water flow ($u_{lower} = u_{water}$).

In the modelling of two-layer flows it is common to define the internal-flow energy equation:

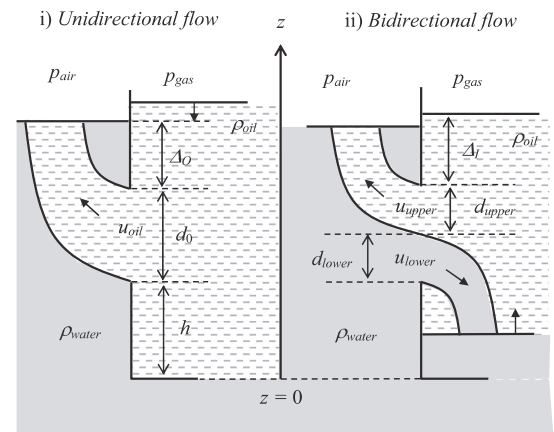


Fig. 2. Unidirectional (i) and bidirectional (ii) stratified flow schematics and notations for a hole in the side plate, corresponding to the ship-hull wall.

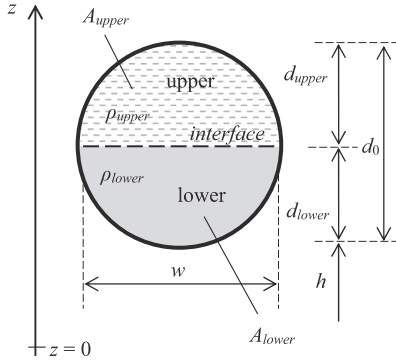


Fig. 3. Notations and sketch of a two-layer flow through the orifice.

$$E_{int} \equiv \frac{E_{lower} - E_{upper}}{\rho_{water} g'}. \quad (5)$$

A stratified flow through the orifice is illustrated in Fig. 3. Due to the changing depths of the layers, the interfacial width (w) of the two-layer flow is not constant at the orifice. The maximal interface width occurs in the middle of the hole (i.e., $w_{max} = d_0$). According to $A_0 = \pi(d_0^2/4) = A_{upper} + A_{lower}$, the area of the orifice is related to the upper and lower layer areas.

The internal-flow energy equation is given by:

$$E_{int} = \left(\frac{u_{lower}^2}{2g'} - \frac{u_{upper}^2}{2g'} \right) + d_{lower} + h. \quad (6)$$

The flow velocities of the upper and lower layer are defined as the flow rates per flow area of each of the layers:

$$u_{lower} = \frac{Q_{lower}}{A_{lower}}; u_{upper} = \frac{Q_{upper}}{A_{upper}} = \frac{Q_{upper}}{(A - A_{lower})}. \quad (7)$$

Inserting the flow velocities of the layers into Eq. (4) and using the following parameters for the flow rate: $K = Q_{lower}^2/2g'$ and the ratio of flow rates: $q^2 = Q_{upper}^2/Q_{lower}^2$, the internal-flow energy Eq. (6) is expressed as:

$$E_{int} = K \left(\frac{1}{A_{lower}^2} - \frac{q^2}{(A - A_{lower})^2} \right) + d_{lower} + h. \quad (8)$$

Particular attention is now given to the hole, where its interfacial width is a function of the layer depth, as indicated in Fig. 3. The area of a lower layer expressed by the dimensionless thickness of the lower layer $d^* = d_{lower}/d_0$ is given by an empirical expression:

$$A_{lower}(d^*) = \frac{1}{8} \pi d_0^2 \left[1 + \frac{2}{\pi} \arcsin(2d^* - 1) + \frac{4}{\pi} (2d^* - 1) \sqrt{d^* - d^{*2}} \right]. \quad (9)$$

The dimensionless area of the lower layer is defined as $A^* = A_{lower}/A_0 = 4A_{lower}/(\pi d_0^2)$. The interface width of a two-layer flow at the orifice is defined as $w(d^*) = 2d_0 \sqrt{d^* - d^{*2}}$. The interface width of the two-layer flow per definition is the lower layer's upper width(w), which is equal to the lower width of the upper layer. The dimensionless lower-layer area is given by:

$$A^* = \left[\frac{1}{2} + \frac{1}{\pi} \arcsin(2d^* - 1) + \frac{2}{\pi} (2d^* - 1) \sqrt{d^* - d^{*2}} \right]. \quad (10)$$

The non-dimensional form of the internal-flow energy (Eq. (6)) for the two-layer flow through the orifice is:

$$E_{int}^* = \frac{16}{\pi^2} K^* \left(\frac{1}{A^{*2}} - \frac{q^2}{(1 - A^*)^2} \right) + d^* + h^*, \quad (11)$$

where the following dimensionless quantities are used:

$$E^* = \frac{E_{int}}{d_0}; K^* = \frac{Q_{lower}^2}{2g' d_0^3}; A^* = \frac{A_{lower}}{A_0}; d^* = \frac{d_{lower}}{d_0}; h^* = \frac{h}{d_0}; q^2 = \frac{Q_{upper}^2}{Q_{lower}^2}.$$

The maximal flow rate can be derived from the dimensionless internal-flow energy Eq. (11) by applying the implicit function differentiation theorem to the dimensionless lower-layer depth (d^*):

$$\frac{\partial E_{int}^*}{\partial d^*} = 0, \quad (12)$$

where the resulting function is as follows:

$$\frac{\partial E_{int}^*}{\partial d^*} = \frac{16}{\pi^2} K^* \left(-\frac{2}{A^{*3}} \frac{\partial A^*}{\partial d^*} - \frac{2q^2}{(1 - A^*)^3} \frac{\partial A^*}{\partial d^*} \right) + 1.$$

The upper-layer flow rate can be determined by the formula:

$$Q_{upper} = \left[\frac{g' \pi^2 d_0^5 q^2}{8} \left(\frac{2}{A^{*3}} \frac{\partial A^*}{\partial d^*} + \frac{2q^2}{(1 - A^*)^3} \frac{\partial A^*}{\partial d^*} \right) - 1 \right]^{1/2}, \quad (13)$$

[Formula for a *bidirectional* flow of oil outflow]

where the following function applies:

$$\frac{\partial A^*}{\partial d^*} = \frac{2}{\pi} \frac{1}{\sqrt{1 - (2d^* - 1)^2}} + \frac{4}{\pi} \sqrt{d^* - d^{*2}} + \frac{1}{\pi} \frac{(2d^* - 1)}{\sqrt{d^* - d^{*2}}} (1 - 2d^*). .$$

The upper layer flow rate (Eq. (13)) corresponds to the oil flow rate and will henceforth be used in the *bidirectional* flow with oil outflow calculations. The lower layer flow rate is determined by $Q_{lower} = Q_{upper}/q$. Due to their continuity, the flow rates in the lower and upper layer are related to the flow velocities and layer areas according to $Q_{lower} = u_{lower} A_{lower}$ and $Q_{upper} = u_{upper} A_{upper} = u_{upper} (A_0 - A_{lower})$, respectively.

2.3. Optimisation by the Genetic Algorithm

Discharge coefficients are essential to evaluate the test cases below according to the introduced inviscid analytic formulae. For this purpose, the Genetic algorithm (GA) technique is useful. The GA technique has limited use for finding the global optimum. Other optimisation methods and population-based heuristic algorithms, such as the Bat Algorithm and Particle Swarm Optimisation, can be applied to find target values (cf. Koffka and Ashok, 2012). The optimisation is performed as an attempt to reach the target value (retained oil-water flow rate). The problem is solved as follows:

$$C(X) = \left[1000 A \left(C_{dl} \sqrt{2g \left(H_I - \frac{\rho_{emulsion}}{\rho_{oil}} H_E \right)} - C_{do} \sqrt{2g \left(H_E - \frac{\rho_{water}}{\rho_{emulsion}} H_O \right)} \right) \right], \quad (14)$$

where H_I , H_E and H_O are heights above the orifice axis of oil, emulsion and sea water, respectively. The target value $C(X) \rightarrow 0$ is the difference between the oil outflow rate from the cargo and the spilled oil rate. In other words, the target value is the retained oil-water flow rate (Q_E) in the ballast tank. The three designed variables are composed in the optimisation model: (1) C_{dl} , the coefficient of discharge for the inner orifice, (2) C_{do} , the coefficient of discharge for the outer orifice and (3) $\rho_{emulsion}$, the emulsion density in the ballast tank, $X = [C_{dl} C_{do} \rho_{emulsion}]$. Possible variation ranges for the coefficients of discharge were determined to be $0.01 \leq C_d \leq 1$ and for the oil-water mixture density $\rho_{oil} \leq \rho_{emulsion} \leq \rho_{water}$.

2.4. SPILL MODEL 1: Bottom orifice of a single-hull tank

At the hydrostatic excess pressure, the *unidirectional* oil flow starts

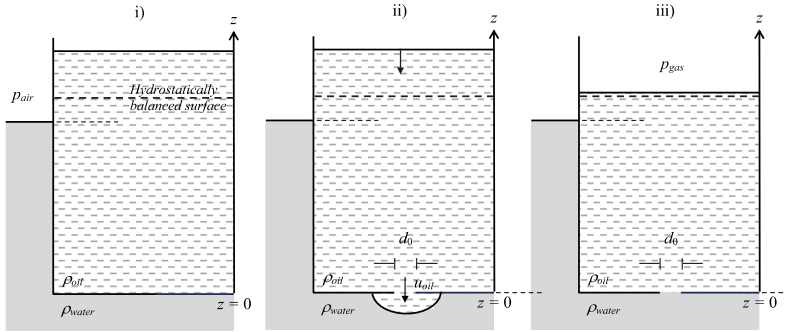


Fig. 4. Oil tank illustration for a single-hull bottom orifice: (i) no damage, (ii) damage with excess hydrostatic pressure and oil spill and (iii) damage without oil spill.

through the bottom hole and the oil outflow stops when the hydrostatic balance is attained (Fig. 4). The total oil spill can be calculated by the following model function:

$$Q_{oil\ spill} = \begin{cases} 0 & \text{no damage} \\ \text{unid. flow (Eq. 2)} & \text{damage with excess hydrostatic pressure} \\ e & \text{damage without excess hydrostatic pressure} \\ 0 & \text{damage without excess hydrostatic pressure} \end{cases} \quad (15)$$

The total oil spill volume (V_{oil}) and outflow duration (T_{oil}) in the case of the single-hull bottom orifice can be calculated by the following formulae:

$$V_{oil} = \left(\Delta_l - \frac{\rho_{water}}{\rho_{oil}} \Delta_o \right) S, \quad (16)$$

$$T_{oil} = \frac{2S}{A_0 \sqrt{2g}} \frac{1}{C_d} \sqrt{V_{oil}/S}, \quad (17)$$

where S is the oil surface area in the tank and C_d is the discharge coefficient (Sergejeva et al., 2013).

2.5. SPILL MODEL 2: Side orifice of a single-hull tank

After the ship collision, oil outflow through side damage continues under a hydrostatic balance (see Fig. 5). The oil outflow stops when the

tank is filled with seawater up to the orifice level. The total oil spill can be calculated by the following model function:

$$Q_{oil\ spill} = \begin{cases} 0 & \text{no damage} \\ \text{unid. flow (Eq. 2)} & \text{damage with excess hydrostatic pressure} \\ e & \text{damage without excess hydrostatic pressure} \\ \text{bid. flow (Eq. 13)} & \text{damage without excess hydrostatic pressure} \\ 0 & \text{damage without horiz. density difference} \\ ce & \end{cases} \quad (18)$$

The total oil spill volume (V_{oil}) and outflow duration (T_{oil}) in the case of the single-hull side orifice can be calculated by the following two formulae:

$$V_{oil} = \left(\left(\Delta_l + \frac{d_0}{2} \right) - \frac{\rho_{water}}{\rho_{oil}} \left(\Delta_o + \frac{d_0}{2} \right) \right) S, \quad (19)$$

$$T_{oil} = \frac{2S}{A_0 \sqrt{2g}} \frac{1}{C_d} \sqrt{V_{oil}/S}. \quad (20)$$

2.6. SPILL MODEL 3: Bottom orifice of a double-hull tank

Upon double-hull ship grounding, oil spills do not occur until the

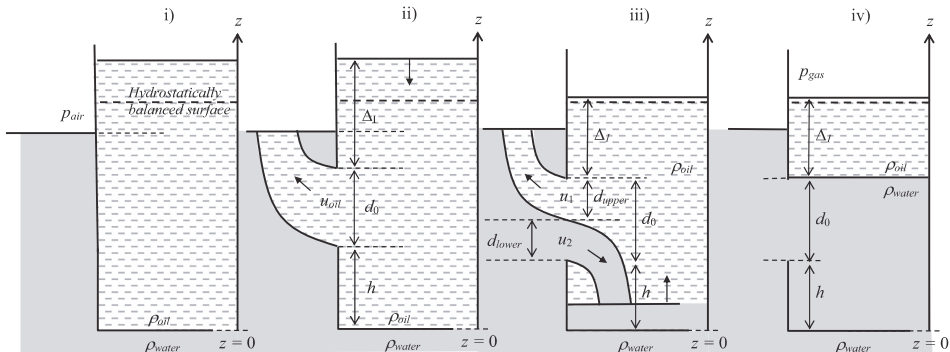


Fig. 5. Oil tank illustration for the single-hull side orifice: (i) no damage, (ii) damage with excess hydrostatic pressure and oil spill, (iii) damage without excess hydrostatic pressure and oil spill and (vi) damage without horizontal density difference and no oil spill.

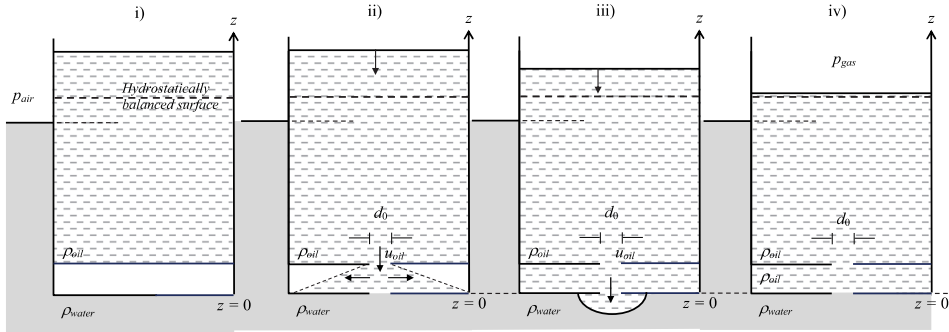


Fig. 6. Oil tank illustration for the double-hull bottom orifice: (i) no damage, (ii) damage with excess hydrostatic pressure and filling of bottom ballast tank, (iii) damage with excess hydrostatic pressure and oil spill and (iv) damage without horizontal density difference and no oil spill.

bottom ballast tank is filled with oil. The *unidirectional* oil outflow starts when excess hydrostatic pressure occurs after the bottom ballast tank is filled with oil (Fig. 6). Oil outflow stops when the hydrostatic balance is attained. The total oil spill can be calculated by the following model function:

$$Q_{oil\ spill} = \begin{cases} 0 & \text{no damage} \\ 0 \text{ (Filling of bottom ballast tank)} & \text{damage with excess hydrostatic pressure} \\ \text{unid. flow (Eq. 2)} & \text{damage with excess hydrostatic pressure} \\ 0 & \text{damage without excess hydrostatic pressure} \end{cases} \quad (21)$$

The total oil spill volume (V_{oil}^*) and outflow duration (T_{oil}) in the case of the double-hull bottom orifice can be calculated as follows:

$$V_{oil}^* = \left(\Delta_j^* - \frac{\rho_2}{\rho_1} \Delta_o \right) S, \quad (22)$$

$$T_{oil} = \frac{2S}{A_0 \sqrt{2g}} \frac{1}{C_d} \sqrt{V_{oil}^* / S} \quad (23)$$

where $\Delta_j^* = \Delta_j - V_{DB}/S$ and V_{DB} is the oil-filled bottom ballast volume.

2.7. SPILL MODEL 4: Side orifice of a double-hull tank

Upon side damage of a double-hull tank, no oil outflow occurs until the side ballast tank is filled with oil down to the level of damage. The *unidirectional* oil outflow starts when excess hydrostatic pressure occurs after the side ballast tank is filled with oil down to the level of hull damage. The oil outflow continues when the hydrostatic balance is attained (Fig. 7) and the outflow stops when the tank is filled with seawater up to the orifice level. The total oil spill can be calculated by the following model function:

$$Q_{oil\ spill} = \begin{cases} 0 & \text{no damage} \\ 0 \text{ (Filling of side ballast tank)} & \text{damage with excess hydrostatic pressure} \\ \text{unid. flow (Eq. 2)} & \text{damage with excess hydrostatic pressure} \\ \text{bid. flow (Eq. 13)} & \text{damage without excess hydrostatic pressure} \\ 0 & \text{damage without horizontal density difference} \end{cases} \quad (24)$$

The total oil spill volume (V_{oil}^*) and duration (T_{oil}) in the case of the double-hull side orifice can be calculated as follows:

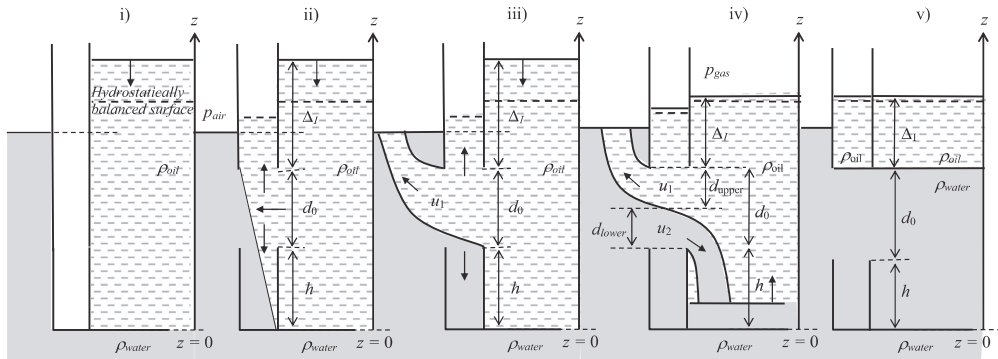


Fig. 7. Oil tank illustration for the double-hull side orifice: (i) no damage, (ii) damage with excess hydrostatic pressure and partial filling of the side ballast tank, (iii) damage with excess hydrostatic pressure and oil spill, (iv) damage without excess hydrostatic pressure and oil spill and (v) damage without horizontal density difference and no oil spill.

Table 1

Experimental results of test scenarios by Tavakoli et al. (2011).

Test no	Hull Design	Scenario	Orifice	H_I (m)	H_O (m)	$T_{ballast}$ (s)	T_{total} (s)	V_{total} (l)	$V_{ballast}$ (l)	V_{basin} (l)
N4	Single	Grounding	C1	0.80	0.47	–	460	138	–	138
N9	Single	Collision	S1	0.80	0.40	–	385	145	–	145
N9*	Single	Collision	S1	0.51	0.40	–	18600	50	–	50
N10	Double	Grounding	C2, C2	0.85	0.47	230	1230	171	60	111
N12	Double	Collision	S1, S1	0.89	0.41	590	590	222	42	180
DC*	Double	Collision	S1, S1	–	–	–	–	–	–	–

* bidirectional flow.

$$V_{oil}^* = \left(\left(\Delta_l^* + \frac{d_0}{2} \right) - \frac{\rho_{water}}{\rho_{oil}} \left(\Delta_o + \frac{d_0}{2} \right) \right) S, \quad (25)$$

$$T_{oil} = \frac{2S}{A_0 \sqrt{2g}} \frac{1}{C_d} \sqrt{V_{oil}^*/S}, \quad (26)$$

where $\Delta_l^* = \Delta_l - V_{DS}/S$ and V_{DS} is the side-ballast volume filled with oil.

3. Experimental system

According to Tavakoli et al. (2011), the lab tank in the Sintef Sealab (Trondheim, Norway) consisted of a large rectangular tank with dimensions 1.0 m × 0.5 m × 0.5 m (i.e., its total volume was 0.25 m³). The tank was built at 1/3 scale of an existing Floating Production,

Storage and Offloading unit (FPSO) to achieve geometric similarity with a ship oil tank. The lab tank was made of watertight plywood and transparent Plexiglas. The lab tank was placed in the pool with dimensions of 12 m × 5 m × 3 m. The pool was filled with water at a temperature of 15–20 °C, which corresponds to a kinematic viscosity of 1 cSt and a density of 998 kg/m³. In the experiments, olive oil was chosen to represent the oil due to its properties akin to cargo oil: a kinematic viscosity of 81 cSt and a density of 920 kg/m³.

In this study, data from the Sintef Sealab experimental tests (Table 1) were used for the oil outflow modelling from the submerged orifices. Similarly, two scenarios were investigated for single- and double-hull tanks: (1) grounding case, with the orifice in the bottom plate and (2) collision case, with the orifice in the side plate.

Fig. 8 provides an illustrative reproduction of the experimental

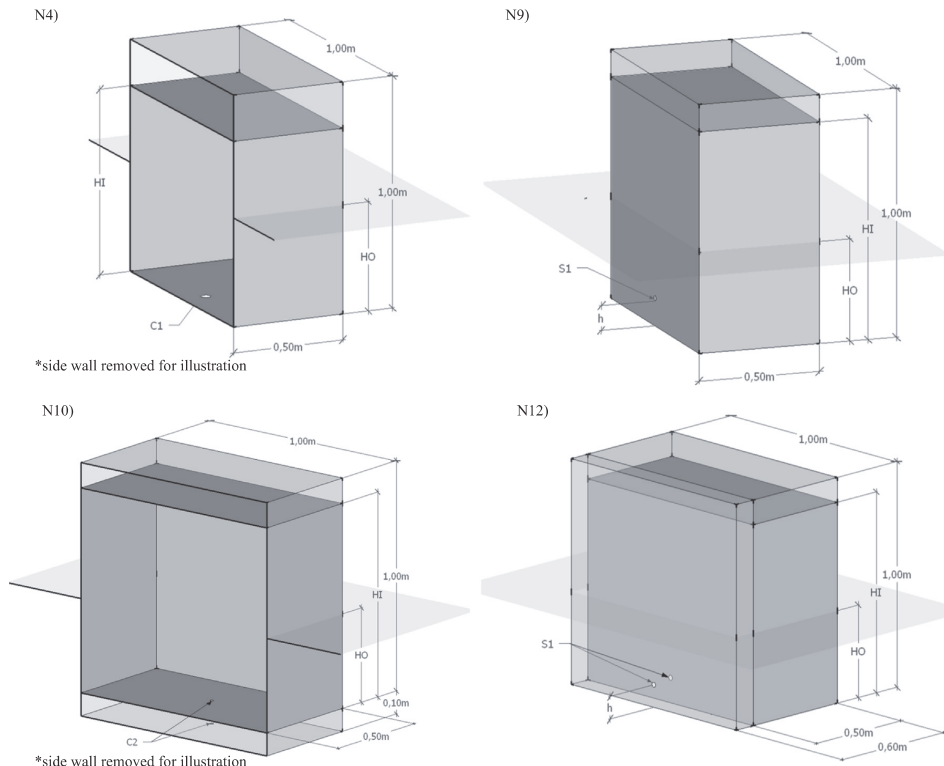


Fig. 8. Oil tank illustration for different test scenarios: N4= grounding case with bottom orifice in the single-hull tank, N9= collision case with side orifice in the single-hull tank, N10= grounding case with the bottom orifice in the double-hull tank and N12= collision case with the side orifice in the double-hull tank.

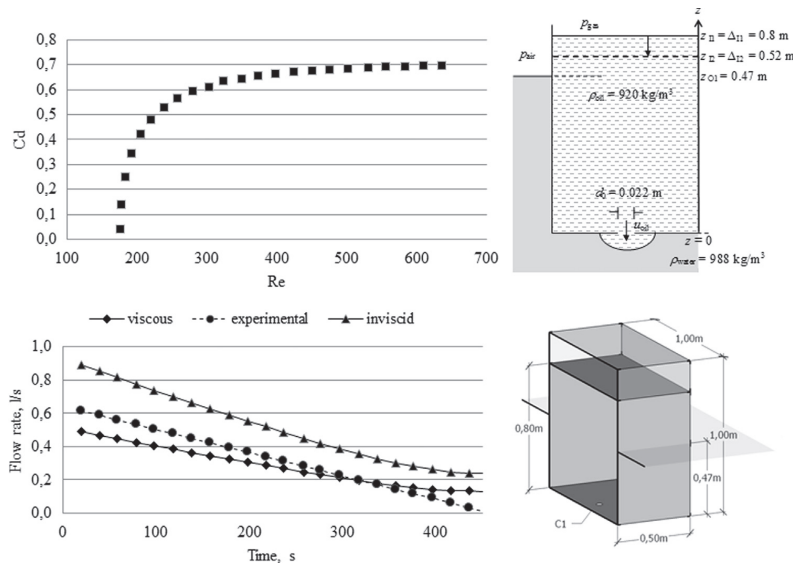


Fig. 9. Oil tank illustration for a *unidirectional* flow in the lab test N4 (orifice C1 case) with charts of experimentally determined discharge coefficients at different orifice Reynolds numbers and oil flow rates of *unidirectional* flow.

apparatus, where orifices S1, C1 and C2 have diameters of 2.2 cm, 2.2 cm and 1.6 cm, respectively. The holes were drilled in the side and bottom plates of the tank. The side orifice was located in the side plate with a lower lip height $h = 0.1$ m above the tank inner bottom. The bottom orifice was located at the centre of the bottom plate. In both cases (i.e. double side and double bottom) the orifices in the inner and outer plates had the same size. The oil level inside the tank was measured using a metric ruler (resolution of 1 mm) attached to the side of the tank and the time (t) was measured using a stopwatch (with an accuracy of 1 s). In both cases, the two "key parameters" that determine the oil outflow dynamics after opening of the orifice were the difference between the water level ($H_O = \Delta_O + d_0 + h$) outside and the oil level ($H_I = \Delta_I + d_0 + h$) inside the tank and the difference between the liquid densities.

4. Results

4.1. TEST CASE 1: Unidirectional flow through the bottom orifice of a single-hull tank

The initial condition (see Table 1) of the *unidirectional* oil outflow in a single-hull bottom-leaking tank is presented in Tavakoli et al.'s (2011) lab test N4. The excess hydrostatic pressure is introduced via the higher oil level inside the tank (Fig. 9). A total of 138 l of oil leaked into the pool over 460 s. The determined discharge coefficient $C_d = 0.64$. However, the experimental data indicate that the C_d value changes (in the range $C_d = 0.55 \dots 0.7$) during the *unidirectional* oil outflow, as a function of the orifice Reynolds number, $Re_{orifice} = \sqrt{2g((\Delta_I + d_0/2) - \rho_{water}/\rho_{oil}(\Delta_O + d_0/2))} d_0/\nu_{oil}$, where the kinematic viscosity of the oil is ν_{oil} . The estimated minor head-loss coefficient $k_{1,bottom} = 4.94$. The determined discharge coefficients at different orifice Reynolds numbers are presented in Fig. 9.

4.2. TEST CASE 2: Unidirectional flow through the side orifice of a single hull tank

The initial condition (Table 1) of the *unidirectional* oil outflow in a

single-hull side-damaged tank is presented in the lab test N9. The excess hydrostatic pressure is introduced via a higher oil level inside the tank (Fig. 10). In the first stage, the total oil outflow volume for the *unidirectional* flow results from the excess hydrostatic pressure at the orifice level. In the first stage, 145 l of oil leaked into the pool over 385 s. The experimental data indicated that the C_d value changed during the *unidirectional* oil outflow according to the orifice Reynolds number. The mean discharge coefficient $C_d = 0.50$ and the mean minor head-loss coefficient $k_{1,side} = 4.30$. The discharge coefficients determined experimentally at different orifice Reynolds numbers are presented in Fig. 10.

4.3. TEST CASE 2: Bidirectional flow through the side orifice of a single-hull tank

The initial condition (see Table 1) of the *bidirectional* flow of oil outflow, following the *unidirectional* oil outflow, in the case of a single-hull side-damaged tank is presented in lab test N9. The adjusted oil level inside the tank leads to the balanced hydrostatic pressure situation. The corresponding experimental setup of the *bidirectional* stratified flow in the experimental apparatus is illustrated in Fig. 11. The *bidirectional* flow occurs with the ascending oil-water interface. The total oil outflow volume for the *bidirectional* flow is fixed by the oil-water interface at the orifice level. In the second stage, 50 l of oil leaked into the pool over 18,600 s. The total oil outflow from the side orifice was 195 l over 18,985 s. However, in the case of the *bidirectional* flow, the discharge coefficient cannot be determined in a straightforward manner. Only by assuming the maximal two-layer exchange flow conditions (i.e., the interfacial depth $d_{lower} = d_0/2$) can the oil outflow rate be determined. Making use of the ascending oil-water depth during the *bidirectional* flow, the discharge coefficient $C_d = 0.22$. It was found that the discharge coefficient is considerably smaller than the C_d values for the first-stage oil outflow. The corresponding mean minor head-loss coefficients are $k_{1,side} = 4.30$ and $k_{2,side} = 16.27$.

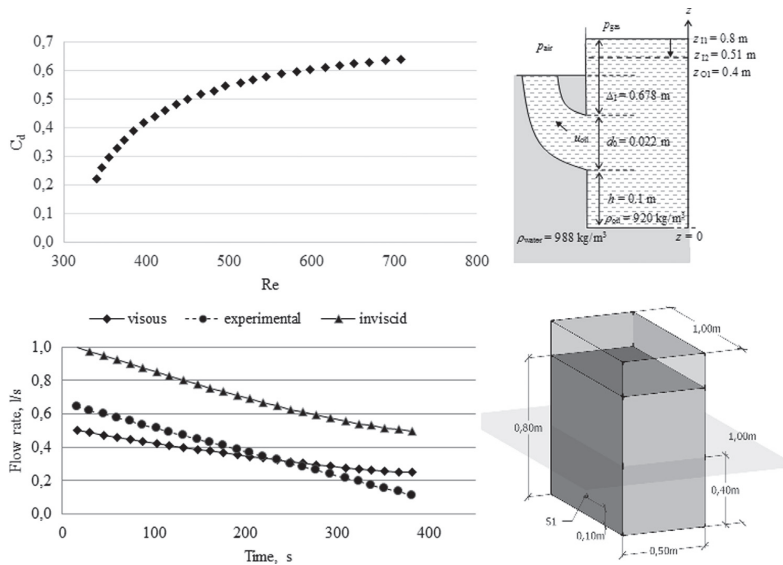


Fig. 10. Oil tank illustration for a *unidirectional* flow during the first stage in the lab test N9 (orifice S1 case) with charts of experimentally determined discharge coefficients at different orifice Reynolds numbers and oil flow rates.

4.4. TEST CASE 3: Unidirectional flow through the bottom orifice of a double-hull tank

The initial condition (Table 1) of *unidirectional* stratified flow during the double-hull bottom leakage is presented in lab test N10, where excess hydrostatic pressure is introduced due to the higher oil level inside the tank (Fig. 12). The oil outflow from the tank can be divided into two stages. In the first stage, the *unidirectional* oil outflow occurs as the oil level descends, which results in a high inner

hydrostatic pressure-head (Δ_I) as compared to the outer hydrostatic pressure-head ($\rho_o/\rho_I\Delta_O$). In Tavakoli et al.'s (2011) test run, after simultaneous opening of the inner and outer orifices of the tank hull, the ballast tank was filled for 230 s. Moreover, water inflow into the ballast tank was detected together with the oil inflow. In the second stage, emulsion outflow took place (i.e., the oil and water mixture flowed into the basin until the hydrostatic balance was attained at the bottom level). In the first stage, 111 l of oil leaked into the pool for 1230 s. The mean discharge coefficient $C_{d1} = C_{d2} = 0.54$ characterised

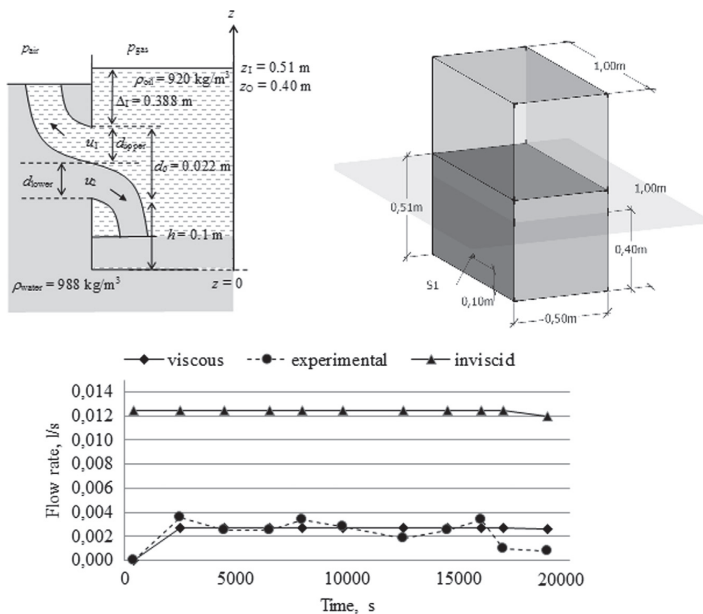


Fig. 11. Oil tank illustration for *bidirectional* flow during the second stage of lab test N9 (orifice S1 case) with a chart of oil flow rates.

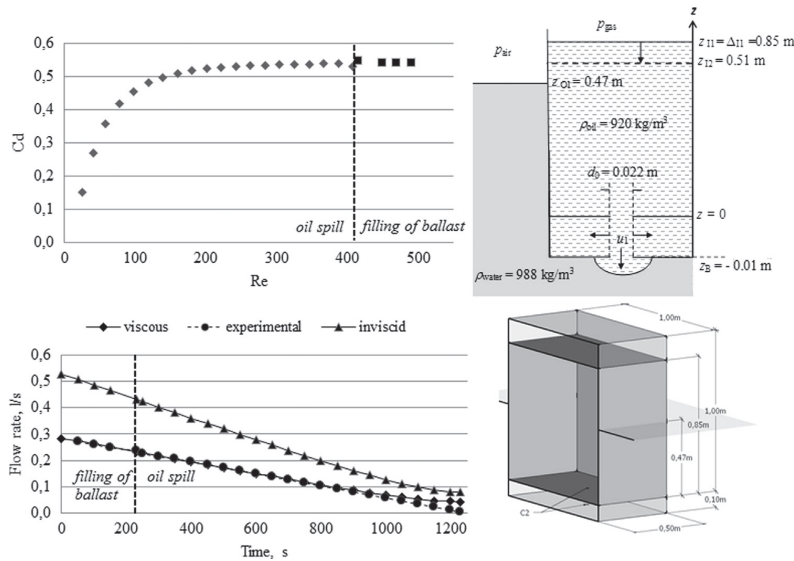


Fig. 12. Oil tank illustration for a unidirectional flow in lab test N10 (orifice C1 case) with charts of experimentally determined discharge coefficients at different orifice Reynolds numbers and oil flow rates.

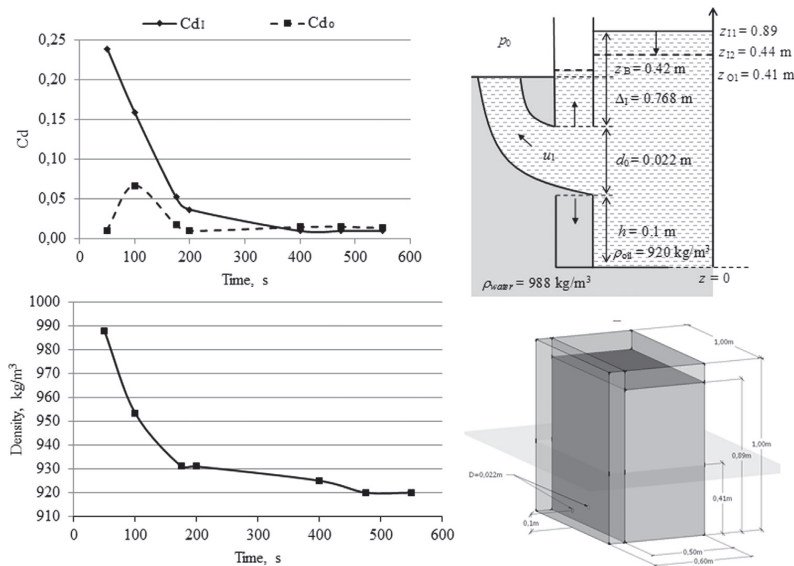


Fig. 13. Oil tank illustration for a unidirectional flow during the first stage in the lab test N12 (orifice S1 case) with charts of GA-determined discharge coefficients at the inner and outer orifices and oil-water mixture density in the ballast tank.

both stages. The mean minor head-loss coefficients were $k_{1,bottom} = 2.43$ and $k_{2,bottom} = 5.54$. The mean discharge coefficients at different orifice Reynolds numbers are presented in Fig. 12.

4.5. TEST CASE 4: Unidirectional flow through the side orifice of a double-hull tank

The initial condition (Table 1) and the experimental setup of the lab test N12 are shown in Fig. 13. In Tavakoli et al.'s (2011) test, the run was started by opening the inner and outer orifices on both sides of the

ballast tank and terminated as soon as the oil level in the cargo tank was constant for five minutes. This corresponds to the oil outflow during the first stage but excludes the second stage, due to density differences. The water flow was terminated in Tavakoli et al.'s (2011) test (i.e., hydrostatic equilibrium was attained between the emulsion in the ballast tank and the water in the pool). The hydrostatic oil pressure at the inner opening (S1) was greater than that of the emulsion; as a result, the unidirectional flow increased the hydrostatic pressure inside the ballast tank. Consequently, emulsion in the ballast tank was pushed into the basin. In the case of a double-hull tank, an optimisation

Table 2

Head loss coefficients corresponding to the test scenarios of Tavakoli et al. (2011).

Test nr	Hull Design	Scenario	Orifice	C_{dI}	C_{dO}	$k_{1,bottom}$	$k_{2,bottom}$	$k_{1,side}$	$k_{2,side}$	Re
N4	Single	grounding	C1	0.55	–	4.94	–	–	–	180–640
N9	Single	collision	S1	0.50	–	–	–	4.30	–	340–700
N9*	Single	collision	S1	0.22	–	–	–	4.30	16.27	–
N10	Double	grounding	C2, C2	0.54/ 0.54	–	2.43	5.54	–	–	25–500
N12	Double	collision	S1, S1	0.07	0.02	–	–	4.30/ 4.30	203/ 2499	90–730
DC*	Double	collision	S1, S1	0.15	–	–	–	4.30	16.27	–

* Bidirectional flow.

jet from the leaking tank. At hydrostatic equilibrium ($p_o = p_l$), the hydraulic model presented for a *bidirectional* stratified flow through an orifice can be applied in a straightforward manner until the oil level in the tank is higher than the upper lip of the orifice. If the oil level is below the upper lip of the orifice, the shape factor should be considered through the "quadratic-type" opening with the free surface, as in the calculation of *bidirectional* stratified flow (Laanearu and Davies, 2007).

5.3. Lift effect in hydraulic modelling

In the present study, the calculations of oil spill volumes and durations are limited to a vertically fixed tank. However, the proposed analytical solutions can be adapted to determine oil spill from a tanker where vertical motion is present. In this regard, the ship vertical displacement determines the relative motions of the oil surface and oil-water interface in the leaking tank during oil spills. The excess hydrostatic pressure introduced by a higher oil surface level is associated with the upward displacement of a tanker due to oil weight reduction in the tank and should also magnify the oil outflow rate. By contrast, in the *bidirectional* flow, the ship buoyancy is lost and thus downward displacement can occur. During the ship lift, the oil spill rate depends on the net barotropic two-layer flow component associated with excess hydrostatic pressure. When the ship vertical displacement corresponds to sinking, the water inflow into the tank should be magnified and the oil outflow should be reduced during *bidirectional* flow.

5.4. Internal-flow head losses and discharge coefficients

As expected, the actual discharges through the orifices are smaller than the inviscid hydraulic models predict. This is due to the internal-flow head losses associated with the boundary and shear stresses. The head losses per definition $C_d = Q_{inviscid}/Q_{actual}$ (Laanearu et al., 2014) are dependent on the coefficient of discharge. It was found that these discharge coefficients differ significantly for the *unidirectional* and *bidirectional* stratified flows of the leaking tank. The discharge coefficient C_d and the corresponding resistance coefficients k for the different grounding and collision scenarios are presented in Table 2. The experimental data reveal that the estimated C_d values vary during the *unidirectional* flows, according to the orifice Reynolds number, in the range 25...730. The estimated discharge coefficients for the *unidirectional* flow through side and bottom orifices with the same size have similar values $C_d \approx 0.5$. This comparatively large discharge coefficient for the case of a one-layer flow corresponds to the resistance due to flow separation. Apparently, a similar discharge coefficient ($C_d = 0.54$) is also obtained in the case of a *unidirectional* flow through the double-hull bottom. The reason for this may be that during the first stage, the air release from the ballast tank does not significantly change the oil outflow dynamics. In contrast, in the case of a double-hull side breach that included the emulsion in the ballast tank, relatively small discharge coefficients were found ($C_d = 0.07$ and $C_d = 0.02$). In the second stage, with a *bidirectional* flow, the discharge coefficient is comparatively larger ($C_d = 0.22$). The discharge coefficient in the demonstration case was determined from the specific formula where

the resistance coefficients k_1 and k_2 from the single hull side scenario were applied (see Table 2). According to the principle of dynamical similarity of oil spills, the usage of C_d values in ship accident scenarios should belong to the same Reynolds number range as in the lab experiments by Tavakoli et al. (2011).

6. Conclusions

The developed hydraulic modelling approaches can be used in the assessment of oil spill scenarios for ship accidents: collision and grounding. The hydraulic modelling is also suited to the creation of worst-case scenarios for oil spills.

The experimental results of Tavakoli et al. (2011) form a useful database for detailed analyses of oil spill volume and duration through breached single- and double-hull tanks.

In the case of a single-hull tank, oil outflow corresponds to the oil spill and in the case of a double-hull tank the ballast tank reduces oil spill volume and duration.

The oil outflow from the leaking tank with a double-hull yields the formation of emulsion. The GA helps to determine the continuously changing viscosity and density of the multiphase flow process.

Hydraulic models for one- and two-layer flows were modified to consider the stratification and breached hull geometry (orifice).

In the hydraulic modelling, the descending oil surface in the leaking tank yields a *unidirectional* flow. The *unidirectional* oil outflow takes place under changing hydrostatic pressure, which results in flow rate reduction during the first stage of oil spill.

In the hydraulic modelling, the ascending oil-water interface corresponds to a *bidirectional* flow. The *bidirectional* flow through the orifice takes place under constant hydrostatic pressure, which results in a constant flow rate during the second stage of oil spill.

The discharge coefficients determine the discrepancies of the oil spill volume and duration as compared to the inviscid-flow prediction.

To apply the hydraulic modelling approaches, it is necessary to determine discharge coefficients experimentally for a wide range of orifice Reynolds numbers.

The transitional stage between the *unidirectional* and *bidirectional* flow, where the oil surface and the oil-water interface are mobile, is not addressed in the present work. In fact, the experimental results of Tavakoli et al. (2011) confirm the absence of this transitional stage for a leaking tank without lift.

In practical applications, the continuous calculation of *unidirectional* and *bidirectional* flow for oil spills should be performed. For this purpose, the oil spill model functions can be applied, which make use of the discharge coefficients depending on the orifice Reynolds number.

The ship vertical displacement determines the relative motions of the oil surface and oil-water interface with respect to sea surface changes and the oil outflow rate.

Acknowledgements

This research work has been financially supported by the Estonian Ministry of Education and Research (IUT 19–17 and grant agreement ETF8718) and by Central Baltic Interreg IV program through MIMIC

project ('Minimizing risks of maritime oil transport by holistic safety strategies').

References

- Alves, T.M., Kokinou, E., Zodiatis, G., 2014. A three-step model to assess shoreline and offshore susceptibility to oil spills: the South Aegean (Crete) as an analogue for confined marine basins. *Mar. Poll. Bull.* 86 (1–2), 443–457.
- Alves, T.M., Kokinou, E., Zodiatis, G., Lardner, R., 2016. Hindcast, GIS and susceptibility modelling to assist oil spill clean-up and mitigation on the southern coast of Cyprus (Eastern Mediterranean). In: De Dominicis, M., Ribotti, A. (Eds.), *Physical, Chemical and Biological Observations and Modelling of Oil spills in the Mediterranean Sea. Deep-Sea Res. II*, in press https://www.researchgate.net/publication/281714208_Hindcast_GIS_and_susceptibility_modelling_to_assist_oil_spill_clean-up_and_mitigation_on_the_southern_coast_of_Cyprus_Eastern_Mediterranea.
- Alves, T.M., Kokinou, E., Zodiatis, G., Lardner, R., Panagiotakis, C., Radhakrishnan, H., 2015. Modelling of oil spills in confined maritime basins: the case for early response in the Eastern Mediterranean Sea. *Environ. Poll.* 206, 390–399.
- Armí, L., Farmer, D.M., 1986. Maximal two-layer exchange through a contraction with barotropic net flow. *J. Fluid Mech.* 164, 27–51.
- Armí, L., 1986. The hydraulics of two flowing layers with different densities. *J. Fluid Mech.* 163, 27–58. <http://dx.doi.org/10.1017/s0022112086002197>.
- Cucco, A., Sinerchia, M., Ribotti, A., Olita, A., Fazioli, L., Perilli, A., Sorgente, B., Borghini, M., Schroeder, K., Sorgente, R., 2012. A high-resolution real-time forecasting system for predicting the fate of oil spills in the Strait of Bonifacio (Western Mediterranean Sea). *Mar. Poll.* 64, 1186–1200.
- Cuthbertson, A.J.S., Laaneau, J., Davies, P.A., 2006. Buoyancy-driven two-layer exchange flows across a slowly submerging barrier. *Environ. Fluid Mech.* 6 (2), 133–151.
- EMSA, 2010. Maritime Accident Review 2010. Available at: (<http://www.emsa.europa.eu/emsa-documents/latest/item/1219-maritime-accident-review-2010.html>). Retrieved 03.03.2015.
- EMSA, 2014. Annual overview of marine casualties and incidents 2014. Available at: (<http://www.emsa.europa.eu/emsa-documents/latest/item/2303-annual-overview-of-marine-casualties-and-incidents-2014.html>). Retrieved 03.03.2015.
- Koffka, K., Ashok, S., 2012. A comparison of BA, GA, PSO, BP and LM for training feed forward neural networks in e-Learning context. *IJISAE* 7, 23–29.
- Laaneau, J., Cuthbertson, A.J.S., Davies, P.A., 2014. Dynamics of dense gravity currents and mixing in an up-sloping and converging vee-shaped channel. *J. Hydraul. Res.* 52 (1), 67–80. <http://dx.doi.org/10.1080/00221686.2013.841779>.
- Laaneau, J., Davies, P.A., 2007. Hydraulic control of two-layer flow in quadratic type channels. *J. Hydraul. Res.* 45 (1), 3–12.
- National Research Council, 1991. *Tanker Spills – Prevention by Design*. National Research Council, National Academy Press, Washington, DC.
- NEREIDS Project. Available at: (<http://www.nereids.eu>).
- Melaku, C.D., Solidoro, C., Bandelj, V., Quattrocchi, G., Sorgente, R., Olita, A., Fazioli, L., Cucco, A., 2015. Assessment of oil slick hazard and risk at vulnerable coastal sites. *Mar. Poll. Bull.* 94 (1–2), 84–95.
- Sergejeva, M., Laaneau, J., Tabri, K., 2013. Hydraulic modelling of submerged oil spill including tanker hydrostatic overpressure. In: *Proceedings of the 4th International Conference on Marine Structures, MARSTRUCT 2013*: Espoo, Finland; 25–27 March.
- Simcecek-Beatty, D.A., Lehr, W.J., Lankford, J.L., 2005. Leaking tank experiments for heavy oils. In: *Proceedings of International Oil Spill Conference, IOSC 2005*, Miami Beach, FL; United States; 15–19 May; Code 67046. 4293–4297.
- Soomere, T., Viikmäe, B., Delpêche, N., Myrberg, K., 2010. Towards identification of areas of reduced risk in the Gulf of Finland, the Baltic Sea. *Proc. Est. Acad. Sci.* 59, 156–165.
- Soomere, T., Döös, K., Lehmann, A., Meier, M., E., Murawski, J., Myrberg, K., Stanev, E., 2014. The potential of current- and wind-driven transport for environmental management of the Baltic Sea. *AMBIO* 43, 94–104.
- Tabri, K., Aps, R., Mazaheri, A., Heinvee, M., Jönsson, A., Fetissov, M., 2015. Modelling of structural damage and environmental consequences of tanker grounding. In: *Analysis and Design of Marine Structures V: Proceedings of the 5th International Conference on Marine Structures*, Southampton, UK; 25–27 March.
- Tavakoli, M.T., Amdahl, J., Leira, B.J., 2011. Experimental investigation of oil leakage from damage ships due to collision and grounding. *Ocean Eng.* 38 (17–18), 1894–1907.
- Tavakoli, M.T., Amdahl, J., Leira, B.J., 2012. Analytical and numerical modelling of oil spill from a side tank with collision damage. *Ships Offshore Struct.* 7 (1), 73–86.
- Xie, H., Yapa, P.D., Nakata, K., 2007. Modeling emulsification after an oil spill in the sea. *J. Mar. Syst.* 68 (3–4), 489–506.

Appendix 3

PUBLICATION III

Sergejeva, M., Laanearu, J., Tabri, K. (2017). On parameterization of emulsification and heat exchange in the hydraulic modelling of oil spill from a damaged tanker in winter conditions. – *Proceedings of 6th International Conference on Marine Structures, MARSTRUCT 2017, 8 – 10 May 2017, Lisbon Portugal*. doi: 10.1201/9781315157368-7

On parameterization of emulsification and heat exchange in the hydraulic modelling of oil spill from a damaged tanker in winter conditions

M. Sergejeva, J. Laanearu & K. Tabri

Department of Mechanics, Tallinn University of Technology, Tallinn, Estonia

ABSTRACT: A parametric study of hydraulic analysis of oil spill from a damaged tanker in winter conditions is presented. The oil-spill model is extended to account the effects of emulsification and heat exchange. The emulsification is associated with an interfacial mixing and transfer of mass and momentum between the counter-flowing layers. Therefore, the effect of emulsification is included only for bidirectional stratified flow, whereby oil flows out from a leaking tank and seawater flows in opposite direction. The effect of heat-exchange is considered in both cases i.e. uni- and bidirectional stratified flows. For these purposes two key parameters are introduced i) the seawater inflow-rate reduction parameter f and ii) the thermal expansion coefficient α . The water-ice-oil mixture near the ship hull affects the oil outflow conditions, resulting in changes of outflow duration and volume. The extended hydraulic model is tested to consider the outside temperature variations between summer and winter conditions.

1 INTRODUCTION

Oil spills in winter conditions can reveal different outflow characteristics as compared to spill situations without large temperature gradients, corresponding to summer conditions. For instance, in the presence of ice, the oil may be frozen and captured in growing ice or spread below an ice sheet. The sea ice results in lowest possible water temperatures near the sea surface. The temperature variations due to the warm inside and cold outside fluids can affect the oil outflow volume and duration in tanker accidents. Therefore, the winter conditions influence significantly the spill situation. It is essential to identify the key factors in spill operations in cold seas such as the Baltic Sea, and also the Arctic.

Ship collisions and groundings are major accident types in maritime transportation (EMSA 2010, 2014). Also in e.g. the Northern Baltic Sea during winter conditions, these are the most frequently occurring accident types (Goerlandt et al., 2017). Depending on the ship type and extent of damage, such accidents can result in human casualties, adverse environmental effects and/or financial loss. Accidents involving oil tankers can result in adverse environmental effects if a structural damage to the ship hull occurs at a location where compartments containing oil are breached, leading to significant spills. A recent risk analysis of winter navigation risks in the Finnish waters indicates that major oil spills in ice conditions are most likely

from collisions, but outside the ice season, groundings pose a higher risk (Valdez Banda et al., 2015). To assess potential environmental risks posed, it is essential to understand possible consequences of accidental breaches in tanker hulls. Furthermore, it is also important to be able to predict the amount of potential oil spill for different hull configurations and breach points and typical trajectories of oil slick movement. Risk and oil spill consequence models have been proposed to assess risks of wintertime collision accidents (Valdez Banda et al., 2016, Goerlandt and Montewka 2014), but these state-of-art models do not take the oil outflow dynamics, nor the specific effects on cold temperatures on this phenomenon into account, while these may have significant effects. The oil-spill model presented here is a part of the Accidental Damage and Spill Assessment Model (ADSAM) to estimate fast possible oil spill scenarios from hull collision and grounding damage (Tabri et al., 2015).

When modelling oil outflow dynamics in winter conditions, in addition to hydrostatic driving pressure and hull-damage characteristics, it is essential to include changes of liquids physical properties (density and viscosity) due to temperature variations. It is important to consider the heat-exchange modified shear-induced mixing processes in stratified flows. Turbulent fluxes within the strong interfacial shear layer between fluids can result in significant interfacial mixing and transfer of mass and momentum between the layers. Oil emulsification plays a significant role in the modelling of oil

slick trajectory (see Alves et al., 2015), as emulsion with an 80% water content may have a volume that is five times the spilled volume of a parent oil (Xie et al., 2007). In the formation of emulsions due to the physical mixing promoted by turbulence at the sea surface, the density and viscosity of a liquid is constantly changing. In winter conditions the oil-water emulsion may be frozen and captured in growing ice or spread below an ice sheet.

The study presents the enhanced internal-flow hydraulic model, which is used for a parametric study on the influence of the winter conditions on oil spill outflow quantities. The Computational Fluid Dynamics (CFD) analysis could also be used for this purpose. However, a CFD tool (see Tavakoli et al., 2012) for a rapid assessment of oil-spill accidents can be also computationally demanding. Thus, the use of a hydraulic model is well justified for fast prediction of multiphase-flow quantities. Usually the oil spills encompass the flow of two immiscible liquids in a complex geometric system, involving a wide range of length scales. Recently the analytical solutions of uni- and bidirectional stratified flows through a circular hole (orifice) were introduced in Kollo et al. (2016). In the present study the flow separation at hole edges and the dynamic interaction of superimposed layers (e.g. mixing), the uni- and bidirectional stratified flow rates at the hole are also depend on large temperature differences.

The hydraulic framework based on the quasi-steady- and steady-flow equations is firstly introduced, focusing on the modelling of uni- and bidirectional flows through the submerged orifice, respectively. Next, the oil-spill model of stratified flow is extended to account the effects of emulsification and heat exchange. Thus the extended hydraulic model is tested for a parametric cases to figure out the influence of the winter conditions on oil-spill quantities. Finally, the overall results are concluded and discussed.

2 HYDRAULIC THEORY

2.1 Unidirectional stratified flow

Oil outflow occurs when the inside pressure (p_i) in a cargo tank exceeds the outside pressure (p_o) at the level of a submerged hole. Excess hydrostatic pressures can also result from a relatively high oil level (Δ_l) and gas pressure (p_{gas}) in a ductless tank, as compared to the water level (Δ_o) and air pressure (p_{air}) on the sea surface. Here, the density of oil (ρ_{oil}) is considered to be slightly less than that of sea-water density (ρ_{water}), i.e., corresponding to the condition $(\rho_{water} - \rho_{oil})/\rho_{oil} \ll 1$. In case of a unidirectional stratified flow through hole and $p_{gas} > p_o$, the Bernoulli's equation can be expressed as:

$$\frac{u_{oil}^2}{2g}(1 + \Pi) = (z_0 - z_1) + \left(\frac{p_{gas}}{\rho_{oil}g} - \frac{p_o}{\rho_{oil}g} \right), \quad (1)$$

where $z_0 - z_1 = \Delta_l + d_o/2$ is the elevation-head difference; and $(p_{gas} - p_o)/\rho_{oil}g = (p_{gas} - p_{air})/\rho_{oil}g - \rho_{water}(\Delta_l + d_o/2)$ is the pressure-heads difference. In the presence of ventilation, the gas pressure is the air pressure, i.e. $p_{gas} = p_{air}$, and the pressure-heads difference is simplified to $(p_{gas} - p_o)/\rho_{oil}g = -\rho_{water}(\Delta_o + d_o/2)/\rho_{oil}$. The internal-flow head loss in Equation 1 is represented by the sum of local head-loss coefficients $\Pi = \sum k_i$. The unidirectional stratified flow through the submerged hole with diameter d_o is depicted in Figure 1(ii). However, the same conditions as described above will apply to the hole in the hull bottom. Therefore, the description herein is limited only to the side-hull case.

The unidirectional oil outflow rate can be calculated by the formula:

$$Q_{oil} = u_{oil} A_o, \quad (2)$$

where u_{oil} = oil outflow velocity; and A_o = the area of orifice. It is important to emphasize that in the case of a bottom hole, oil outflow stops when the hydrostatic balance is attained at the submerged hole level between the oil surface in the tank and the sea surface outside. However, in the case of a side hole, the bidirectional stratified flow follows when the unidirectional stratified flow spins down in a hydrostatically balanced situation (cf. Tavakoli et al., 2011). It should be noted that during unidirectional stratified oil outflow the vertical movement of tanker can occur, due to a weight decrease, and therefore the difference between the oil and water surfaces can reveal changes. However, herein the hydraulic modelling is limited to the vertically fixed tank.

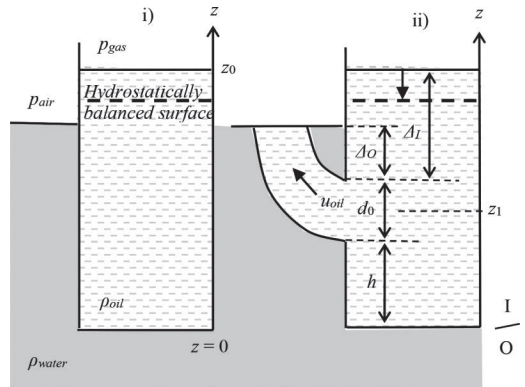


Figure 1. Oil tank sketch with the single-hull side: i) no damage and ii) damaged with unidirectional stratified oil spill through orifice under excess hydrostatic pressure.

2.2 Bidirectional stratified flow

The bidirectional stratified flow through the hole is depicted in Figure 2(i). The equations governing a two-layer flow, with a small density difference and at equal pressures at the water and oil surfaces are following:

$$E_{oil} = \frac{1}{2} \rho_{oil} u_{oil}^2 + p_1 + \rho_{oil} g (d_{oil} + d_{water} + h), \quad (3)$$

$$E_{water} = \frac{1}{2} \rho_{water} u_{water}^2 + p_2 + \rho_{oil} g d_{oil} + \rho_{water} g (d_{water} + h), \quad (4)$$

where $p_1 = p_I$ and $p_2 = p_O$ are the pressures at the upper lip Inside (I) and Outside (O) of the side hole, respectively; d_0 = vertical size of the hole ($d_0 = d_{oil} + d_{water}$); d_{oil} = centre-line depth of the lighter (ρ_{oil}) liquid layer; d_{water} = centre-line depth of the heavier (ρ_{water}) liquid layer; u_{oil} = flow velocity in the upper layer; u_{water} = flow velocity in the lower layer; and h = hole lower lip height measured from the oil-tank bottom.

In the modelling of two-layer flows it is common to define the internal-flow energy equation:

$$E_{int} \equiv \frac{E_{water} - E_{oil}}{\rho_{water} g'}, \quad (5)$$

where E_{water} and E_{oil} correspond to the water and oil layer Bernoulli heads in the stratified flow, respectively; and g' = the reduced gravity which is fixed by the density ratio $r = \rho_{oil}/\rho_{water}$.

It is demonstrated in Kollo et al. (2016) that the upper-layer flow rate i.e. oil outflow during the bidirectional stratified flow under hydrostatically balanced situation is determined by the formula:

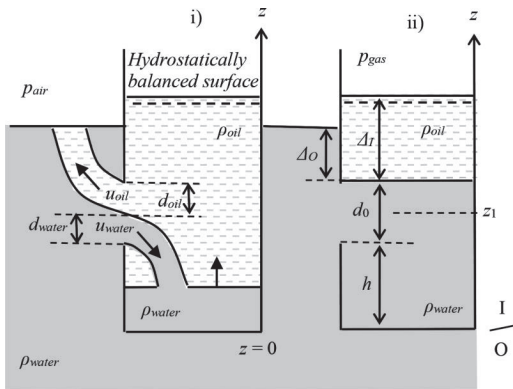


Figure 2. Oil tank sketch with the single-hull side damage: i) bidirectional stratified flow through orifice without excess hydrostatic pressure and ii) no oil spill.

$$Q_{oil} = \left[\frac{g' \pi^2 d_0^3 q^2}{8} \left(\frac{2}{A^{*3}} \frac{\partial A^*}{\partial d^*} + \frac{2q^2}{(1-A^*)^3} \frac{\partial A^*}{\partial d^*} \right)^{-1} \right]^{1/2}, \quad (6)$$

where q = the ratio of upper layer (Q_{oil}) and lower layer (Q_{water}) discharges, and the following functions apply:

$$q^2 = \frac{Q_{oil}^2}{Q_{water}^2} \text{ and}$$

$$\frac{\partial A^*}{\partial d^*} = \frac{2}{\pi} \frac{1}{\sqrt{1-(2d^*-1)^2}} + \frac{4}{\pi} \sqrt{d^*-d^{*2}} + \frac{1}{\pi} \frac{(2d^*-1)}{\sqrt{d^*-d^{*2}}} (1-2d^*),$$

where the dimensionless lower layer area (A^*) and depth (d^*) are defined as:

$$A^* = \frac{A_{water}}{A_0} \text{ and } d^* = \frac{d_{water}}{d_0}.$$

According to Equation 6, the lower-layer flow rate is determined by $Q_{water} = Q_{oil}/q$. Due to the continuity, the flow rates in the lower-and upper-layer are related to the flow velocities and the areas according to $Q_{water} = u_{water} A_{water}$ and $Q_{oil} = u_{oil} A_{oil} = u_{oil} (A_0 - A_{water})$, respectively.

It should be noted that during a bidirectional stratified flow with oil outflow, the vertical movement of tanker can occur, due to a weight increase, and therefore the difference between the oil and water surfaces is changing. Herein a modelling is limited to the vertically fixed tank.

3 PARAMETRISATION

3.1 Unidirectional stratified flow

A particular goal of the hydraulic modelling presented herein is to investigate the sensitivity of unidirectional stratified flow in winter conditions. The effects of emulsification and heat exchange on the unidirectional stratified flow are indicated in Figure 3. It is assumed, that the oil flow separation occurs at orifice outside edges, and this process can be parametrized by the coefficient of discharge (see Kollo et al., 2016). The flow separation of oil results in the formation of emulsions due to the mixing promoted by turbulence. The outflow oil temperature variation ($\rho_{oil}(T_I) \rightarrow \rho_{oil}(T_O)$) results from heat exchange. To consider the effect of heat exchange, the thermal expansion coefficient α is introduced by the simplified state formula $\rho(T) \approx \rho(T_I) + \alpha(T_I - T)$. The oil spill volume due to the density difference between oil at inner temperature and water at outer temperature, and the spilt oil cooling outside is

5 HEAT EXCHANGE

The lost volume due to the cooling of oil during the outflow can be considered as relative change of the upper layer volume:

$$\frac{\delta Q_{oil}}{Q_{water}} \rightarrow \frac{\rho_{oil}(T_I) - \rho_{oil}(T_O)}{\rho_{water}(T_O)} = \frac{\alpha_{oil}}{\rho_{water}(T_O)}(T_I - T_O), \quad (14)$$

where α_{oil} is the thermal expansion coefficient of oil. Thus the flow-rates-ratio parameter at the outside end of the orifice is defined as:

$$q_o = q + (1 - f) - \frac{\alpha_{oil}}{\rho_{water}(T_O)}(T_I - T_O). \quad (15)$$

The added volume due to the heating of seawater during the inflow can be considered as relative change of the lower layer volume:

$$\frac{\delta Q_{water}}{Q_{water}} \rightarrow \frac{\rho_{water}(T_I) - \rho_{water}(T_O)}{\rho_{water}(T_O)} = \frac{\alpha_{water}}{\rho_{water}(T_O)}(T_I - T_O), \quad (16)$$

where α_{water} is the thermal expansion coefficient of seawater. Thus the flow-rates-ratio parameter at the inside end of the orifice is defined as:

$$q_I = \frac{q}{f + \frac{\alpha_{water}}{\rho_{water}(T_O)}(T_I - T_O)}. \quad (17)$$

The coefficient of thermal expansion is defined as $\alpha = -(1/\rho)(d\rho/dT)$, where α is a function of temperature. In the approximate calculations the value around 0.0007 1/K can be used for an unspecified crude oil (cf Manual of Petroleum Measurement Standards 2016).

6 APPLICATION: PHYSICAL PROPERTIES OF FLUIDS

In the Baltic Sea the temperature in the surface layer varies seasonally, and due to strong fresh-water inputs the water salinity is lower (6–7 psu) as compared to the underlying deep waters. The sea water at surface is densest just before it freezes. On the long-term average, the Baltic Sea is ice-covered at the annual maximum for about 45% of its surface area, and the density maximum is about 1006 kg/m³ (Krauss 1973). In oceans the density maximum of water at surface is about 1025 kg/m³, depending on the temperature and salinity (Shokr & Sinha 2015). The winds generated mixed layer is characterized by being nearly uniform in properties such as

temperature and salinity throughout the layer. The mixed layer is usually formed on top of the stably stratified deep water during storms. The Baltic Sea water freezing temperature is $-1...-0.1^\circ\text{C}$. In summer the surface layer temperature is $16...18^\circ\text{C}$ in the southern part and $13...14^\circ\text{C}$ in the northern part of the Baltic Sea (Krauss 1973).

There are many types of oil transported on the Baltic Sea such as crude oil and products refined for use as fuel. Complex processes of oil transformation in the marine environment start developing from the oil's contact with seawater. During oil spill incident, the behaviour of an oil released into the environment is shaped not only by its chemical composition but also by its physical properties, such as density, viscosity, cloud and pour point, and adhesion (Kenneth et al., 2015). Oil outflow dynamics is strongly dependent on temperature and will slow to insignificant rates as temperatures approach freezing (National Academies of Sciences, Engineering, and Medicine 2016). The density of crude oils commonly ranges from 700 to 990 kg/m³ and even the heaviest oils will usually float on top of sea surface. The density decreases more-or-less linearly with the increase of temperature and these values fit in to the equation: $\rho(T) = \rho_0 + T(\partial\rho/\partial T)$, where $\rho(T)$ = density at any temperature T , ρ_0 = standard density (George & Singh 2015).

Like oil density, also oil viscosity is affected by temperature. As temperature decreases, viscosity increases and the variations with temperature are commonly large. Oil that flows readily at 40°C can become a slow-moving, viscous mass at 10°C (George & Singh 2015).

Whenever the oil temperature decreases the dispersed paraffins begin to align together and begin to form a crystalline wax structure. In clear crudes the wax deposition gives the oil a cloudy appearance, thus this temperature is called the cloud point. At some point the precipitates accumulate to the point where the fluid can no longer flow. This phenomenon can occur with light oils as well as heavy oils and is a major problem in the extraction and transportation of oils in offshore (Coutinho & Daridon 2005). The pour point is the lowest temperature at which oil will pour when it cools during spill. The standard range of pour point for lubricating oils is between -45°C and 30°C . The amount of wax contained in a crude oil varies, depending on the geographic source of the crude. High values of pour point $+12...+36$ (16.33°C) indicate waxy nature of the South region (Sindh) crudes; whereas, North region (Punjab) crude oils show extremely low pour point $+18...+30$ (27.43°C) and indicating intermediate or naphthenic nature (Yasin et al., 2013). It is generally observed that the cloud point temperature is $10...20^\circ\text{C}$ higher than the pour point of

crude oils. Unfortunately, most oils have very low precipitation rates close to the cloud point making difficult a reliable measurement of the cloud point. Also all the currently available techniques present shortcomings that prevent the detection of the true cloud point and that the incertitude of the measurements is as much oil as technique dependent since the error is not only associated to the technique but also to the oil composition (Coutinho & Daridon 2005).

Handling and transporting crude represents a major challenge for crude oil producers. Several methods are used to ensure a liquid product and an uninterrupted flow of crude. One of these include additizing crude with pour point depressants to improve low-temperature fluidity of oils used in cold conditions.

7 RESULTS

7.1 Unidirectional stratified flow

The unidirectional stratified oil outflow is exposed to ambient temperatures at opening, the decrease in temperature affects only the spilled oil properties. The difference in spilt oil and sea water temperature changes the density and viscosity values. However, higher flowrates near the opening cause the emulsion formation and water content increase in larger scale.

As shown in Figure 5 the heavy fuel oil (see Table 1) at inner temperature 60°C is reduced by volume 3% and outflowing duration 1% between summer (18°C) and winter (−1°C) conditions. According to Equation 7 the volume of outflowing oil is dependent on density difference between oil at inner temperature and water at outer temperature, and the spilt oil cooling outside. According to Equation 8 it can be easily shown that with small temperature gradients the oil outflow duration is longer as compared to the situation with large temperature gradients.

It can be noted here that in the presence of ice, the oil may be frozen and captured in growing ice or spread below an ice sheet. Therefore, the effects due to cooling of oil may be associated with the blockage of outflow in the winter. This situation is considered to be beyond this study.

7.2 Bidirectional stratified flow

The oil outflow rate and flow-rates-ratio parameter variation of heavy crude oil at different emulsification rates for summer and winter conditions are shown in Figure 6. In the present study the ambient sea water temperature that mimics the summer conditions is 18°C, and the winter conditions is −1°C. The oil at inner temperature 60°C was maintained constant for both seasons.

According to the bidirectional stratified flow hydraulic analysis in Figure 6, the oil outflow volumes and the oil spill time are increasing for larger temperature gradients i.e. in winter conditions. However, the oil spills in winter conditions can reveal different outflow characteristics as compared to spill situations with smaller temperature gradients,

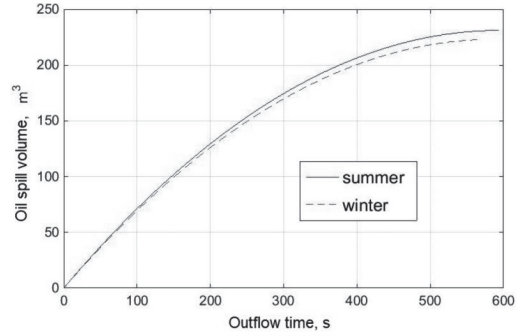


Figure 5. The oil spill volume and duration of heavy crude oil (924 kg/m³ at 60°C) for summer (18°C) and winter (−1°C) conditions for side damaged tanker with $d_0 = 0.5$ m, $S = 281.6$ m², $\Delta_0 = 5.8$ m and $\Delta_l = 7.16$ m.

Table 1. Heavy and light oil physical properties (Neste 2016a, b).

Oil type	Heavy fuel oil	Light fuel oil
Name	PORL80	PÖ-29
Density at 15°C	950 kg/m³	820 kg/m³
Viscosity	24 mm²/s at 80°C	2 mm²/s at 40°C
Pour point	5°C	*
Cloud point	*	−29°C

*Data not available.

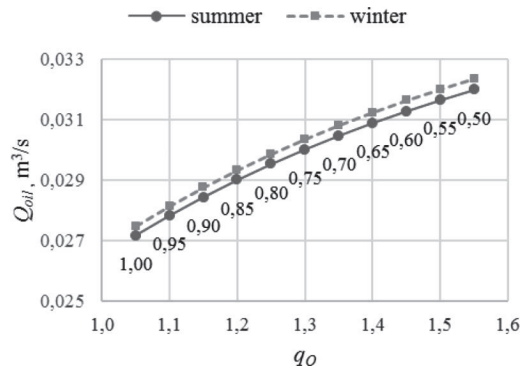


Figure 6. The oil outflow rate and flow-rates-ratio parameter variation of heavy crude oil (924 kg/m³ at 60°C) at different emulsification rates $f = 1 \dots 0.50$ for summer (18°C) and winter (−1°C) conditions.

corresponding to the summer conditions. Similar to the unidirectional flow, in the presence of ice, the oil may be frozen and captured in growing ice or spread below an ice sheet. This situation may be also associated with the blockage of oil outflow. This is considered to be beyond present study. The sea ice results in lowest possible water temperatures near the sea surface. It is shown that the temperature variations due to the warm inside and cold outside fluids can affect the oil outflow volume and duration in tanker accidents. Therefore, the winter conditions more or less dominate the spill situation.

8 CONCLUDING REMARKS

In present study the hydraulic model is extended to consider the effects of emulsification and heat exchange in the winter conditions. For this purpose, the two key parameters were introduced i) the seawater inflow-rate reduction parameter in the bidirectional stratified flow and ii) the thermal expansion coefficient of oil in the uni- and bidirectional stratified flows. The oil flow separation in the uni- and bidirectional stratified flows at orifice outside edges was not considered, because this process can be parametrized by the coefficient of discharge (see Kollo et al., 2016). The parameterization of emulsification was related only to an interfacial mixing and transfer of mass and momentum between the counter-flowing layers.

It was found that the oil spills in winter conditions can reveal different outflow characteristics as compared to spill situations with smaller temperature gradients, corresponding to the summer conditions. According to a parametric study of hydraulic analysis of oil spill from a damaged tanker it can be concluded that:

- without large temperature gradients (summer conditions) the oil outflow volume is larger and the outflow duration is longer for unidirectional stratified flow;
- with large temperature gradients (winter conditions) the oil outflow rate is larger for bidirectional stratified flow;

It can be concluded that winter conditions more or less dominate the spill situation in the unidirectional and bidirectional stratified flows.

ACKNOWLEDGEMENTS

This research work has been financially supported by the BONUS STORMWINDS (Strategic and Operational Risk Management for Wintertime Maritime Transportation System) project, by the research grant IUT1917 from Estonian

Science Foundation and by Tallinn University of Technology project B18 (Tool for direct damage calculations for ship collision and grounding accidents).

REFERENCES

- Alves, T.M., Kokinou, E., Zodiatis, G., Lardner, R., Panagiotakis, C. & Radhakrishnan, H. 2015. Modeling of oil spills in confined maritime basins: The case for early response in the Eastern Mediterranean Sea. *Environmental Pollution* 206: 390–399.
- Coutinho, J. A. P. & Daridon, J. L. 2005. The Limitations of the Cloud Point Measurement Techniques and the Influence of the Oil Composition on Its Detection. *Petroleum Science and Technology* 23(9–10):1113–1128. DOI: 10.1081/lft-200035541
- EMSA. 2010. Maritime Accident Review 2010. Available at: <http://www.emsa.europa.eu/emsa-documents/latest/item/1219-maritime-accident-review-2010.html>. Retrieved 03.03.2015
- EMSA. 2014. Annual overview of marine casualties and incidents 2014. Available at: <http://www.emsa.europa.eu/emsa-documents/latest/item/2303-annual-overview-of-marine-casualties-and-incidents-2014.html>. Retrieved 03.03.2015.
- George, A.K. & Singh, R.N. 2015. Correlation of Refractive Index and Density of Crude Oil and Liquid Hydrocarbon. *International Journal of Chemical, Environmental & Biological Sciences* 3(5): 2320–4087.
- Goerlandt, F. & Montewka, J. 2014. A probabilistic model for accidental cargo oil outflow from product tankers in a ship–ship collision. *Marine Pollution Bulletin* 79 (1–2): 130–44.
- Goerlandt, F., Goite, H., Valdez Banda, O.A., Höglund, A., Ahonen-Rainio, P., Lensu, M. 2017. An analysis of wintertime navigational accidents in the Northern Baltic Sea. *Safety Science*, 92:66–84.
- Kenneth, L., Boufadel, M., Chen, B., Foght, J., Hodson, P., Swanson, S. & Venosa, A. 2015. *Expert Panel Report on the Behaviour and Environmental Impacts of Crude Oil Released into Aqueous Environments*. Ottawa, ON. ISBN: 978-1-928140-02-3: Royal Society of Canada.
- Kollo, M., Laanearu, J. & Tabri, K. 2016. Hydraulic modelling of oil spill through submerged orifices in damaged ship hulls from collisions or grounding. Accepted for publication in journal *Ocean Engineering*.
- Krauss, W. 1973. *Methods and Results of Theoretical Oceanography I: Dynamics of the Homogenous and the Quasihomogenous Ocean*. Berlin: Gebrüder Borntraeger.
- Manual of Petroleum Measurement Standards. 2016. Chapter 11—Physical Properties Data Section 2, Part 4—Temperature Correction for the Volume of NGL and LPG Tables 23E, 24E, 53E, 54E, 59E, and 60E, ASTM Technical Publication [Stock No. PETROLT-BL-TP27], GPA Technical Publication TP-27.
- National Academies of Sciences, Engineering, and Medicine. 2016. *Spills of Diluted Bitumen from Pipelines: A Comparative Study of Environmental Fate, Effects, and Response*. Washington, DC: The National Academies Press.

- Neste Technical Data Sheet. 2016a. Diesel for non-road use –29/–34. For heating—and diesel engine use. Available at: https://www.neste.fi/static/datasheet_pdf/160205_fi.pdf
- Neste Technical Data Sheet. 2016b. Heavy fuel oil 80. Low sulphur. Available at: https://www.neste.fi/static/datasheet_pdf/170246_fi.pdf
- Sergejeva, M., Laanearu, J. & Tabri, K. 2013. Hydraulic modelling of submerged oil spill including tanker hydrostatic overpressure. In: *Proceedings of 4th International Conference on Marine Structures, MARSTRUCT 2013: 4th International Conference on Marine Structures*, Espoo, Finland.
- Shokr, M. & Sinha, N. 2015. *Sea Ice: Physics and Remote Sensing*. New Jersey: John Wiley & Sons.
- Tabri, K., Aps, R., Mazaheri, A., Heinvee, M., Jönsson, A. & Fetisov, M. 2015. Modelling of structural damage and environmental consequences of tanker grounding. *Analysis and Design of Marine Structures V: 5th International Conference on Marine Structures, 25–27.03.2015*, Southampton UK. Ed. C. Guedes Soares and R. Ajit Sheno. Taylor & Francis, 703–710.
- Tavakoli, M.T., Amdahl, J. & Leira, B.J. 2012. Analytical and numerical modelling of oil spill from a side tank with collision damage. *Ships and Offshore Structures* 7 (1): 73–86.
- Valdez Banda, O.A., Goerlandt, F., Kuzmin, V., Kujala, P., Montewka, J. 2016. Risk Management Model of Winter Navigation Operations. *Marine Pollution Bulletin*, 108:242–262.
- Valdez Banda, O.A., Goerlandt, F., Montewka, J., Kujala, P. 2015. A risk analysis for winter navigation in Finnish sea areas. *Accident Analysis & Prevention* 79: 100–116.
- Xie, H., Yapa, P. D. & Nakata, K. 2007. Modeling emulsification after an oil spill in the sea. *Journal of Marine Systems* 68(3–4): 489–506.

Appendix 4

PUBLICATION IV

Sergejeva, M., Laanearu, J. (2013). Optimal utilization of rain-water heat in domestic water system of public building. – *Proceedings of 11th REHVA World Congress and the 8th International Conference on Indoor Air Quality, Ventilation and Energy Conservation in Buildings, CLIMA 2013, 16 – 19 June 2013, Prague, Czech Republic. Elsevier, 1-10.*

Optimal Utilization of Rain-Water Heat in Domestic Water System of Public Building

Monika Sergejeva^{#1} and Janek Laanearu^{#2}

[#]*Faculty of Civil Engineering, Tallinn University of Technology
Ehitajate tee 5, Tallinn 19086, Estonia*

¹monika.sergejeva@ttu.ee

²janek.laanearu @ttu.ee

Abstract

Solutions of the stormwater and public building water-heating integrated system are presented to analyse a possibility of the domestic hot-water production from the gathered rainwater. Maximizing the efficiency of integrated system requires guidelines for engineering design. In Northern countries the public buildings' heating period may last only five months while the hot water demand exists around the whole year. This paper examines six months rain period from May to October. Genetic Algorithm (GA) is employed to optimize the rainwater storage amount and the sub-catchment area size of this integrated system. A simplified approach is used for the system performance - 1) the volume of rainwater gathered in the storage tank is due to the sub-catchment area and the rain intensity and 2) the heat-exchange process between the rainwater and the building water system is due to the daily air temperature and the mixing between stagnant water and stormwater. The stormwater and heat pump integrated system permits to 1) collect the stormwater in storage tanks, 2) absorb the temporal heat from the stormwater volume and 3) transfer the available heat for the hot water production. The efficiency of the integrated solution is found to be dependent on the seasonal temperature and intensity variations in the measured local area rains, available stormwater amount due to the sub-catchment area and de-cooled stormwater infiltration in the pervious area. It is found that GA provides an optimal solution for the stormwater system parameters (storage tank and sub-catchment area), which can be useful in estimating the daily heating time with the stormwater and the public building integrated system during one month of the rain period.

Keywords – stormwater; heat pump; Genetic Algorithm

1. Introduction

Stormwater is an available natural resource which has not been implemented much today in Estonia. The rain falling over a watershed in the urban environment nearly totally becomes runoff. This occurs because urban areas are characterized by widespread impervious areas and man-made water causes. Rainfall precipitates atmospheric pollutants, which together with urban-born pollutants on roads, roofs etc. are transported through the

stormwater network. Therefore the adequate consideration of spatial and temporal variability of rainfall data is important for the modelling of flow in stormwater infrastructure (Laanearu et al., 2009). In Northern countries the public buildings' heating period may be five months while the hot water demand exists around the whole year (Kõiv & Toode, 2010). Usually seven rain months per year are available in Estonia (EMHI, 2011). Precipitations are normally drained into the environment or into the city drainage system, which sometimes can cause widespread flooding during intensive rain events in the city area of Tallinn (Gunter, 2004). An objective of the case study is performance modelling of the stormwater system in the area of the Tallinn University of Technology (TUT). The building stormwater and heat pump integrated system may be of interest in many economic reasons and a public demand to use renewable energy. The rain falling over a watershed in TUT area nearly totally becomes runoff. The rainwater heat may be used for the domestic hot-water production with reasonable expenses only during the summer months (Sergejeva, 2011). The stormwater network under investigation is divided into suitable water sources, connected to sub-catchments, by considering water contamination. It is important to note that the rainwater pollution in the area of question originating from parking areas, roofs etc and may differ considerably by quality. In present study the less polluted rain water, which contains absorbed thermal energy, is used to estimate the rainwater energy (heating hours) available for the hot-water production in a public building. It is shown that the usage of more contaminated rain water for hot water heating is necessary. However, for this purpose the stormwater and public building water-heating integrated system should be modified by the water treatment process. The integrated system optimal solution and the cost effectiveness are also discussed.

Plan of present paper is following. First the stormwater and public building water-heating integrated system functioning is briefly described. Then the measured rainwater characteristics are presented. The optimization procedure and usage of Genetic Algorithm (GA) are then explained. Finally the results are concluded and discussed.

2. System Description

The integrated system consists of three parts: 1) stormwater system, 2) heat-pump system and 3) hot water usage part.

The stormwater system that is located in the area of TUT, is used to analyse the rainwater runoff in the urban environment. The system contains of 42 drainage wells at different levels, pipes with total length of 947 meters, 1 pumping stations, 2 underground vessels with the total volume of 110 m³ and the impervious catchment area of 1/2 hectares (Fig. 1).

The rain water is collected from the roof of the TUT VI Building and parking area nearby. However, the pureness of stormwater is considered in the system without direct water treatment process. The main contaminants

that are washed off are dust, fine fractions of sediments and other pollutants that are accumulated in the sub-catchment area during the dry period. The purity of the collected stormwater is also important for the heat exchange process itself in the designed system. Suspended solids are mainly present in the urban stormwater and the level of the concentration can be very high in several reasons (see Vassiljev, 2005).

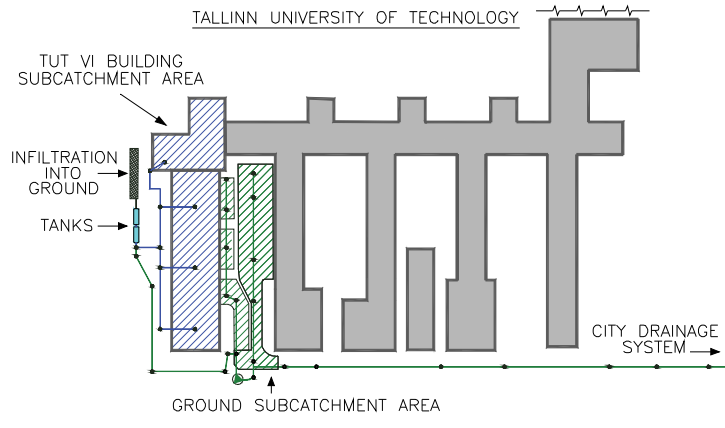


Fig. 1 Sketch of the stormwater system

The designed system has four drains in the roof's sub-catchment and six wells in the parking area sub-catchment. The roof convenience system, which consists of the 150 mm diameter vertical pipes and several wells, is used to drain the collected rainwater. The rainwater from the parking area is collected by 400 mm diameter wells, which can be also used for the integrated heating system or directed to the city stormwater system. The rainwater used for a building heating can be stored in the underground tank. The hydraulic system used for the distribution of water consists of series tanks connected from the bottom and top with two 200 mm diameter pipes. One vessel of fixed volume 55 m³ can be filled from the top by the 250 mm diameter pipe. The second vessel is designed for overflow through the 250 mm pipe, which is submerged to the vessel bottom to siphon the colder water out for natural infiltration in the pervious area of catchment. The formation of cold water in the bottom of vessel is due to the heat exchange process and buoyancy. However, the mixing between the stagnant water and the collected stormwater is important to consider in calculations of water temperature changes controlling the public building hot-water production. The optimal size of the stomwater storage tank will be determined for the six months rain period from May to October henceforth.

The heat pump integrated system consists of four main parts: 1) the heat source circuit, 2) the heat pump circuit, 3) the heat accumulating circuit and 4) an additional hot water heating circuit (Fig. 2).

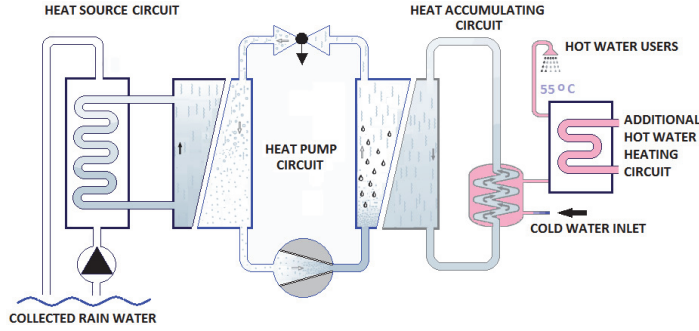


Fig. 2 Heat pump integrated system

The heat source circuit is partially submerged into the stormwater storage vessel. The system is planned for heat pump stop when the water temperature in the stormwater storage vessels drops under 2 degree in order to avoid the freezing conditions or the water level is low.

The heat-pump system located in the building is a closed circuit where the heat transfer medium is used. The heat is carried from the low temperature circuit to the high temperature circuit by the refrigerant liquid.

The main component of the heat accumulating circuit is a boiler. The hot water boiler is connected to the heat pump circuit by spiral tubes (Fig. 2), which warm up the domestic hot water for the building.

An additional hot water circuit is implemented for the situation when the heat-pump system is switched off, is unable to heat up water up to 55 °C or in the situation without rain water during the winter period.

A public building has the hot water consumption all year around. Usually the domestic hot water is used in toilets, shower rooms, for room's maintenance, *etc.* In standard (EVS 835:2003) is suggested two or more times larger values for the designed flow as compared with the actual hot water usage (Kõiv, 2010). New approach is based on several studies carried out in the chair of heat and ventilation at TUT during recent years (e.g. (Kõiv & Toode, 2010). An empirical formula proposed for the designed flow calculus in the public building is:

$$q = 0.008 \cdot N_1 + 0.0016 \cdot N_2 + 0.0032 \cdot N_3, \quad (1)$$

where N_1 , N_2 and N_3 are the numbers of sinks, showers and people attending in the building, respectively. For instance, there are 41 sinks, 16 showers and 160 working places in the TUT's VI building. Therefore the designed hot-water flow in the building is 0.5 lps.

3. Rain Water Characteristics

The urban catchments respond to runoff considerably faster than rural areas. Rainfall varies considerably in the space and time, and reveals the

specific random process character that is dependent on the geographical location (Chow *et al.*, 1988). Some local rainfall characteristics in Tallinn area (northern Estonia) are determined from the standard statistical analysis by Laanearu *et al.* (2009). Long term cumulative precipitation in the Tallinn area is 559 mm during a year, 386 mm of which is rainfall occurring from April to October (EMHI, 2011). In Estonia, the 7 rain month's period per year in average is available. The period 2007 - 2011 mean measured values of the cumulative precipitation for every month are used in the present study. The monthly average air temperature is considered in the calculation of the heat absorbed in the rain water (Table 1).

Table 1. Monthly (Roman numerals) precipitations and rain temperatures

Month	IV	V	VI	VII	VIII	IX	X
[mm]	36	37	61	77	83	75	76
[°C]	3.8	9.8	14.3	16.6	15.6	10.7	6.1

The rain can be several degrees colder than the ambient air at the beginning of the rain event, but after the maximum rainfall rate has been reached, the rain-air temperature differences are usually less than 1 °C (Byers, 1949). The months with comparatively large rain intensity and high air temperatures are July, August and September in Estonia.

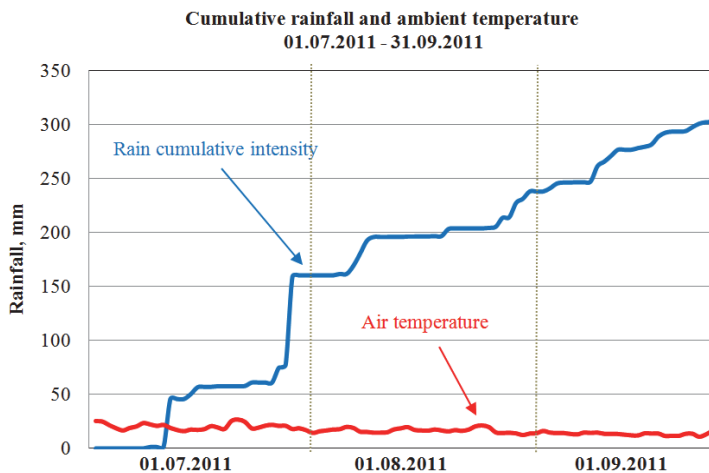


Fig. 3 Cumulative rainfall and rain temperature of measured local rain in Tallinn-Harku Meteorology Station

The designed TUT system should make possible to collect the rain water from the sub-catchments without causing any damages and flooding in the area. The reliability of the stormwater system is tested by the model USEPA SWMM (Sergejeva, 2011). For stormwater system planning the local designed rain q_{20} is 70 lps per 1 hectare during 20 minutes in the area

of Tallinn (EVS 846:2003) is normally used. An example of rain cumulative intensity and air temperature of 2011 three months period is presented in Fig. 3.

The 2008 field study experiment in Tallinn provides suitable rainfall data for the designed system analyses (Koppel *et al.*, 2008). The Tallinn-Harku Meteorology Station point-measured rain is used in present calculations. For instance the measured maximum cumulative intensity was 81.4 mm per day during 2004-2011. The maximum 24 hour average temperature was 26.4 °C during same period. The rain with highest intensive occurred in August 2011.

4. Stormwater Energy

The stormwater tanks may be filled from the roof sub-catchment to the maximum volume of 110 m³ with several rain events. The heat available in the tank water depends on the rain water temperature and on the collected volume of water. For instance, the stormwater volume maximum can be calculated according to the monthly rainfall data (see Table 2).

Table 2. Roof collected rainwater monthly (Roman numerals) volume and rain temperatures

Month	IV	V	VI	VII	VIII	IX	X
[m ³]	106	107	178	225	242	218	222
[°C]	3.8	9.8	14.3	16.6	15.6	10.7	6.1

The USEPA SWMM modelling of the TUT stormwater system shows that the roof sub-catchment area used to fill the tanks is relatively small. It is apparent from the results presented in Table 2, that the tanks can be filled with storm water only once per month in April, May and June. It should be noted that during early spring some rainwater heat is lost also due to difference of water and ground temperatures. During summer and autumn months (July – October) the maximum volume of the tanks is exceeded twice. The heat-transfer process is most favourable from June to September, when the rain water has comparatively large temperature and the water exchange is not limited by the rain occurrence and intensity. The heat exchange due to evaporation from the system's stormwater tanks is isolated by the absence of ventilation.

An average consumption of hot water is 1.05 m³ per day in the TUT VI building. The necessary heat (kW) to warm water from 5 °C up to 55 °C can be calculated by

$$\Phi_{\text{HEAT}} = \frac{q_{\text{HW}} \cdot \rho_{\text{W}} \cdot c_{\text{W}} \cdot \Delta t_{\text{HW}}}{1000}, \quad (2)$$

where q_{HW} is the hot water consumption (l/s), ρ_{W} is the density of water, c_{W} is the specific heat of water and Δt_{HW} is the temperature difference (< 50

°C). According to “(2)” the heat needed for 1 m³ water is 2.51 kW. The daily flow-rate is $q_{\text{HW}} = 0.0012$ lps in the TUT VI building. The energy needed for 1 m³ water in the boiler is 58 kWh, in the case of the cold and hot water temperature difference 50 °C

The warming-up time of the water in boiler may vary from 8.5 to 13.8 hours that also depends on the rain month. The average rain temperature is the highest in July and August (16.6 °C and 15.6 °C, respectively, in Table 2) and the heating time is less than 9 hours. In April and October, when the rain temperature is the lowest (3.8 °C and 6.1 °C, respectively, in Table 2), the water heating time exceeds 12 hours. The boiler water volume forms 95% of the domestic water consumption, and the boiler water can be warmed up during the night time when there is less hot water usage and the electricity tariff is lower. The stormwater energy (MWh) captured is calculated by

$$Q_{\text{RAIN}} = 0.28 \cdot V_{\text{RAIN}} \cdot \rho_{\text{W}} \cdot c_{\text{W}} \cdot \Delta t \cdot 10^{-6}, \quad (3)$$

where V_{RAIN} is the stormwater volume (m³), and the other parameters are same as in “(2)”. By applying “(3)”, we can take the water density $\rho_{\text{W}} = 1000$ kg/m³, the specific heat $c_{\text{W}} = 4.19$ kJ/(kg °C) and the temperature difference Δt as the monthly water temperature subtracted from the minimum allowed water temperature in the stormwater tank (2 °C). It must be taken into account that the stormwater tanks can be filled to the maximum volume 110 m³. It is interesting to know the number of days per month when the storm water and heat pump integrated system can be implemented. The system is designed for 20 days per month for the public building. It was mentioned previously that the heat needed to warm up the daily amount of water in the TUT VI building is 2.51 kW according to “(2)”. The number of hours per month, during which the rainwater heat can be transferred to the domestic water heat is

$$h = \frac{Q_{\text{RAIN}} \cdot 1000}{\Phi_{\text{HV}}}, \quad (4)$$

where Q_{RAIN} is the energy (MWh) captured from the stormwater tanks and Φ_{HEAT} is the heat (kW) needed for warming the daily amount of water. The used stormwater energy calculations are shown in Table 3.

The results presented in Table 3 confirm that monthly used rainwater energy for the domestic water heating depends both on the rainwater temperature and amount. In June, July and August the integrated system is 100% efficient. But in April, May, September and October an additional heat source is needed for the domestic water heating. Tallinn city heating system is representing actually an additional heat source what is used for TUT building heating during December, January, February and March.

Table 3 Rainwater energy and available heating time (and corresponding percent) in a month
(Roman numerals)

Month	IV	V	VI	VII	VIII	IX	X
Q_{RAIN} MWh	0.21	0.92	1.44	1.71	1.60	1.02	0.48
Hours	83	366	480	480	480	405	190
%	17	76	100	100	100	84	40

5. Description of an Optimization Methodology

There are many decision making possibilities that can satisfy required stormwater and public building water-heating integrated system design conditions but they provide different solutions and cost. The price in the local electricity market compels the cost of hot water produced by the integrated system. Here GA is used to provide an optimal solution for the the domestic water heating. Method input parameters are: rain intensity, air temperature, size of sub-catchment area, tank volume for rainwater storage and infiltration area. Available heat captured from collected rainwater is calculated by Equation (3).

GA has been usually applied as a search technique for various engineering problems such as optimization for design and operation of water distribution systems (Simpson et al., 1994; Wu & Simpson, 2001). GA can be described as an artificial evolution search method based on the theories of natural selection and mechanism of population genetics (Holland, 1975). GA in search, optimization and machine learning is by Goldberg (1989). The optimal solutions should be determined due to sampling of all the possible solutions of the particular system. The best of these solutions are then combined, using the genetic operators of crossover and mutation to form new population. The identification of these solutions is done on basis of a set objective function and this process continues until some determination condition is fulfilled. GA optimization herein is based on the following procedure: 1) the model evaluation function takes a single solution as an output parameter and returns a value determined by the hot water usage duration, which indicates how good the solution is, and then the best solution is selected by comparing the fitness value as the hot water usage duration of 24 hours and is returned by all possible solutions; 2) crossover is applied to randomly paired individuals with the constant probability (e.g. 90%) saying how often the crossover is performed. After the match and single crossover of the parental individuals, the two individuals are produced; 3) after selection and crossover, a new population of individuals is created. Some of them are directly copied. In order to ensure that the individuals of new population are not all exactly the same, a small probability of mutation (e.g. 10%) is allowed.

6. Results

The hot-water consumption for a public building is designed for 24 hours with the boiler heating during the night. The optimized stormwater and heat pump integrated system solutions are concluded in Table 3 for six months. GA is used to provide an optimal solution for the stormwater system parameters, such as storage tank volume and sub-catchment area, which are used in estimation of the daily heating time during one month from May to October. It is apparent from the calculated results that the stormwater storage tank volume should be selected in the range of 60-110 m³ and the subcatchment area used for the rainwater gathering should be in the range of 0,133-0,929 ha. The TUT's roof subcatchment area is only 1/2 ha and therefore an additional sub-catchment area of the system should be used. It became also apparent that the integrated system is limited by the hot-water usage time.

Table 3. Optimized stormwater and heat pump integrated system (tank volume and sub-catchment area) and available heating time per day in a month (Roman numerals)

	V	VI	VII	VIII	IX	X
Temperature (°C)	9.8	14.3	16.6	15.6	10.7	6.1
Rain cumulative intensity (mm)	12.31	19.84	28.14	21.50	13.43	18.68
Tank volume (m ³)	110	66	60	101	60	95
Sub-catchment area (ha)	0.133	0.431	0.1264	0.570	0.929	0.133
Time (h)	8.88	6.37	8.65	9.45	10.54	12.4

Conclusion and discussion

The proposed model is shown to perform reliable solutions for design of the stormwater and public building water-heating integrated system for the domestic hot-water production from the gathered rainwater. The results presented in this study support utilization of rain water as an environmental energy source. The energy input into the system was dependent on local rain characteristics, such as the rain intensity and the air temperature.

The main limitation of the integrated system presented in this study was due to the water input from the public building roof's sub-catchment only. However, the rainwater originating from parking areas, roofs etc is differently polluted and the water quality control requires an extra water treatment process, which in turn will reduce also the cost effectiveness of proposed system. The filling of stormwater tank with rainwater was sufficient only during three months (July, August and September) in the TUT's area, when the heat exchange process was most effective.

In future several technical aspects i.e. consumption curves, storm water stratification in tank, etc. in the stormwater and public building integrated model should be considered for more realistic performance of the system.

Acknowledgment

Financial support by Estonian Ministry of Education and Research (SF140072S08) is appreciated. The first author thanks Prof. Teet-Andrus Kõiv from TUT Department of Environmental Engineering. Rain data was provided by Estonian Meteorology and Hydrology Institute.

References

- [1] H. R. Byers, H. Moses & P. J. Hareny. Measurement of Rain Temperature - U. S. Weather Bureau Thunderstorm Project, pp 6, 1949.
- [2] Ven Te Chow, D. R. Maidment & L. W. Mays. Applied Hydrology. New York, McGraw-Hill, 1988.
- [3] A. Gunter. Rainfall causes scattered floods, record water-levels in Tallinn, The Baltic Times, pp 1, 2004.
- [4] D.E. Goldberg. Genetic Algorithms in Search, Optimization & Machine Learning. Massachusetts, USA, 1989. Addition-Wesley Publishing Company, Inc.
- [5] EMHI (Estonian Meteorology and Hydrology Institute). Monthly and annual report (in Estonian), 2011.
- [6] EVS 846:2003. Estonian standard. Site Sewer System. Estonian Centre for Standardisation, 2003.
- [7] EVS 835:2003. Estonian standard. Design of Site Water Supply. Estonian Centre for Standardisation, 2003.
- [8] J. H. Holland. Adaptation in Natural and Artificial Systems (2nd edn). University of Michigan Press, Michigan, USA, 1992.
- [9] T. Koppel, V. Suurkask, A. Vassiljev, J. Laanearu & R. Puust. Storm water investigations in Tallinn (in Estonian). Sweco Project AS, 2008.
- [10] T. A. Kõiv & A. Toode. Hot water usage in buildings. Tallinn, TUT Press, 2010.
- [11] J. Laanearu, I. Annus, A. Vassiljev & T. Koppel. (2009). On determination of flow routes in a stormwater network using the least squares method. In: CCWI2009 Proceedings "Integrating Water Systems: Computing and Control in the Water Industry", pp 731-734, Sheffield, UK, 1-3 September 2009. (Eds.) Joby Boxall, Cedo Maksimovic. Leiden: Taylor & Francis.
- [12] M. Sergejeva. Modelling of stormwater and heat pump integrated system for optimal utilization of rain water in TUT VI building. Master's Degree thesis of Tallinn University of Technology, supervised by Janek Laanearu, 2011.
- [13] A. R. Simpson, G. C. Dandy and L. J. Murphy. Genetic algorithms compared to other techniques for pipe optimization. Journal of Water Resources, Planning and Management, 120(4), pp 423-443, 1994.
- [14] Z. Y. WU and A. R. Simpson. Competent genetic-evolutionary optimization of water distribution systems. Journal of Computing in Civil Engineering, 15(2), pp 89-101, 2001

Appendix 5

PUBLICATION V

Kollo, M., Laanearu, J. (2017). An optimal solution of thermal energy usage in the integrated system of stormwater collection and domestic-water heating. – *Urban Water Journal*, 14 (2), 212–222. doi: 10.1080/1573062X.2015.108600



An optimal solution of thermal energy usage in the integrated system of stormwater collection and domestic-water heating

Monika Kollo & Janek Laanearu


To cite this article: Monika Kollo & Janek Laanearu (2015): An optimal solution of thermal energy usage in the integrated system of stormwater collection and domestic-water heating, Urban Water Journal, DOI: [10.1080/1573062X.2015.1086006](https://doi.org/10.1080/1573062X.2015.1086006)

To link to this article: <http://dx.doi.org/10.1080/1573062X.2015.1086006>



Published online: 16 Oct 2015.



Submit your article to this journal 



Article views: 12



View related articles 



View Crossmark data 

An optimal solution of thermal energy usage in the integrated system of stormwater collection and domestic-water heating

Monika Kollo^a and Janek Laanearu^b

^aFaculty of Civil Engineering, Tallinn University of Technology, Tallinn, Estonia; ^bDepartment of Mechanics, Tallinn University of Technology, Tallinn, Estonia

ABSTRACT

A solution is proposed to make use of the rainwater thermal energy in highly urbanised areas. It is demonstrated that the stormwater heat represents an additional on-site renewable energy available for hot water production. The proposed solution increases multi-functionality in the urban infrastructure that is essentially used to mitigate impacts from extreme climate events. The integrated system model applications correspond to local area conditions in the north-eastern Baltic region. This study considers the optimal collection of stormwater through maximizing the water absorbed heat usage in relation to hot water consumption in different building types (residential, public and commercial). Two key parameters, 'stormwater volume in storage tank' and 'rainwater catchment area', are determined. A genetic algorithm finds a number of storage tank fillings corresponding to rainfall statistics and the hot water consumption of buildings. System cumulative expenses are related to the stormwater storage and the rainwater harvesting expenses.

ARTICLE HISTORY

Received 30 September 2014
Accepted 17 August 2015

KEYWORDS

Optimisation; stormwater runoff; rainwater harvesting; water-energy systems; climate change

1. Introduction

Rainwater harvesting in urban catchments and stormwater storage in tanks have become essential components of water management systems within cities and other densely populated urban areas. Impervious surfaces such as roads, bridges, parking areas and roofs can alter runoff dynamics (Brabec, 2009) and increase flood risks (Zgheib et al., 2012). The direct connectivity of city development with drainage systems is an important attribute of urban imperviousness (Lee & Heaney, 2003). An increased quantity of stormwater runoff from impermeable urban surfaces results in higher peak discharges and shorter travel times (Laanearu et al., 2010). As a consequence, stormwater systems require designs which drain surface waters rapidly away from sensitive urban areas. Finding alternatives in urban flood risk management has become an important issue in dealing with urban runoff (Evers et al., 2012). Storage tanks offer several possibilities to exploit natural water more diversely.

Domestic water heating in the Nordic countries is one of the largest energy usages during the rainy season with a constant demand for hot water required to provide comfortable conditions in a majority of buildings in the urban environment. Additionally, the dense population in urban areas and many of its activities, such as manufacturing and transportation, generate more heat, which, when combined with the wide use of heat-absorbing materials (e.g. concrete, steel and asphalt), results in 'global' thermal differences between urban and rural areas, causing the heat island phenomena. Rainfall events occurring in urban areas not

only have an air cooling effect but also have the possibility to cool urban impermeable surfaces by absorbing excessive heat within catchments (Janke et al., 2013). Stormwater, therefore, represents a thermal energy transporter, affected both by prevalent weather conditions and urban surfaces.

Heat recovery availability from urban wastewater is extensively studied by Liu et al. (2010) and Cipolla (2014). Wastewater as a heat source for buildings has been used widely for hot water heating to increase resilience in terms of remote energy supply (Baek et al., 2004). Examples of how harvested rainwater from the urban environment can be used to combine sustainable energy solutions with stormwater management techniques are studied by Scholz (2009) and Amaya (2013). Nevertheless, it is currently unknown how large an urban catchment area is required to harvest the necessary rainwater to satisfy individual building demands for domestic hot water production. In this sense, the required storage tank size and urban catchment planning will depend on (1) prevalent climate conditions, (2) hot water consumption of the building and (3) the availability of free space. The aim is to find a solution for constant domestic hot water production using local meteorological characteristics, such as rainfall intensity and temperature. While hot water consumption depends on a building usage profile, rainwater input into the stormwater system has a more random character. For this purpose the genetic algorithm (GA), as an optimization method, which is applied as a search technique for solutions to various engineering problems (Simpson et al., 1994; Wu & Simpson, 2001), can be used to find the

Table 1. Tallinn districts, building types, district areas, vegetated areas and pervious areas.

District	Representative building type	District area, % from total area (ha)	Vegetation cover, % from total vegetation cover (ha)	Vegetation cover, % from district area
Kesklinn	Office	19.2 (3059)	13.7 (1234)	40.3
Nõmme	Apartment	18.3 (2919)	23.5 (2121)	72.7
Lasnamäe	Apartment	17.2 (2738)	13.1 (1185)	43.3
Haabersti	Apartment	14.0 (2224)	16.9 (1520)	68.4
Pirita	Apartment	11.8 (1879)	16.3 (1473)	78.4
Põhja-Tallinn	Apartment	9.5 (1519)	7.8 (698)	45.9
Mustamäe	Apartment	5.1 (808)	4.6 (412)	51.0
Kristiine	Shopping centre	4.9 (786)	4.1 (373)	47.4

Table 2. Meteorological data: rainy season rainfall depth and average air temperature.

Year	Rainfall depth (mm)	Air temperature (°C)
2004	713.9	10.3
2005	467.7	11
2006	326.3	11.8
2007	538	10.8
2008	528.9	10.7
2009	572.9	10.5
2010	543.3	10.7
2011	559.3	11.9
Mean	530.4	11

optimal solution for the integrated model parameters as well. Stormwater temperature has a crucial role in determining the thermal energy available for a building's hot water production. The harvested rainwater energy potential varies mainly due to seasonal meteorological conditions, e.g. the frequency of rain events may be a limiting factor. The efficiency of an integrated system for domestic hot water production is dependent on (1) the heat extraction technology; (2) the meteorological conditions, such as the frequency of rain events at a catchment, and (3) the need for heat at a location, e.g. due to seasonally restricted remote heating. In complex systems, it is important that there is no need to seek a large number of combinations to obtain the optimal solutions. An advantage of GA is that only a few combinations are needed to obtain satisfactory results.

The structure of the paper is the following. First the study site and available data are presented. Second, the adopted research methodology is described and used to develop a performance model for the integrated system, which consists of (1) the rainwater harvesting system, (2) the stormwater storage tank and (3) the domestic hot water production system. Next, the optimization method for the integrated system is briefly described with GA used to determine the two key parameters of the integrated system during the rainy season (May–October). The system's *cumulative expenses* are then estimated according to the GA calculated storage tank size and catchment area. Finally, the overall results are discussed and concluded.

2. Study site and data

2.1. Study site

Weather conditions in the north-eastern Baltic Sea region correspond to the boreal and maritime climate conditions. Several cities on the coast of the Baltic Sea with a high population and large impervious areas, such as Tallinn, Helsinki, Riga, Stockholm, St. Petersburg, etc., have large catchments and a

more-or-less similar administrative distribution. Cities are subdivided into several administrative districts according to the use of land and buildings in terms of the purposes of local authorities. For instance, Tallinn is divided into eight districts (Table 1) and Helsinki into seven major districts. Each district includes vegetation coverage, which essentially represents the main portion of the pervious area. The vegetation coverage area in Tallinn city decreased by 274 ha, which is 1.72% of the total area of the city, during the eight years from 2005 to 2012 (Riigi Teataja, 2013). The reduction of green areas in Tallinn affects stormwater quality and quantity, which is straightforwardly related to the stormwater management (cf Maharjan et al., 2013). This results mainly from new developments and renovations of residential areas, altering the former use of pervious areas. The buildings in the different city districts follow a certain pattern. For instance, apartment buildings are located mainly in the residential area, which is the district of Mustamäe in Tallinn (see Table 1). The representative buildings of the commercial and public areas are selected to be located in the business districts, such as Kristiine and Kesklinn in Tallinn.

Information about the Tallinn vegetated areas is also presented in Table 1. The largest of Tallinn's districts is Kesklinn and the smallest is Kristiine. The vegetated coverage in the districts has a varying distribution. The 'greenest' district is Nõmme, where around 72.7% of the area is vegetated. This area predominantly includes detached houses with large green yards. The Kesklinn district area is the office area and has one of the largest impervious areas in Tallinn.

2.2. Meteorological data

The Baltic region is located in Northern Europe where the climate has variable seasons, which vary between humid continental and maritime conditions. The rainy season in the region usually lasts from mid-spring (April, May) to mid-autumn (September, October), when the temperature is above 0 °C. The cities receive 500–700 mm of precipitation annually (cf Tibar, 1989). February, March and April are the driest months with precipitation of about 30 mm per month while July and August are the wettest months with rainfall of about 70 mm per month. The months with comparatively large rain intensity and high air temperatures are June, July and August, with temperatures around 16–22 °C, and the temperature can exceed 30 °C.

The Tallinn region belongs to the southern boreal climate zone and has a mean annual precipitation of 559 mm (Tibar, 1989) and a mean annual air temperature of 4 °C (Karing, 1992). The rainfall data measured by the Tallinn-Harku Meteorology Station is used



Figure 1. Map of Tallinn districts. (1) Apartment, (2) office, (3) shopping, (4) Lake Ülemiste, (5) Tallinn-Harku Meteorology Station and (6) Tallinn Bay.

to estimate the integrated model input parameters (see Table 2). The meteorological station is located 10 km from the city centre of Tallinn, and data is made available by the Estonian Meteorological and Hydrological Institute (EMHI) (see Figure 1). The data consists of rainfall depth and mean temperature during the years 2004–2011 (EMHI, 2011). The daily average values are calculated on the basis of eight observations made with three-hour intervals per day. The measured eight-year mean rainfall depth was 530.4 mm, and the average air temperature was 11.0 °C between May and October. The maximum rainfall depth was 81.4 mm per day, the maximum 24 hour average temperature was 26.4 °C and the minimum was −0.5 °C during the rainy season for the eight years. Daily mean air temperature is used for the rainwater temperature determination. The rain can be several degrees colder than the ambient air at the beginning of a rain event, but, after the maximum rainfall rate has been reached, the rain-air temperature differences are usually less than 1 °C (Byers, 1949).

3. Research methodology

3.1. Rainwater energy

Rainwater energy can be characterised by the heat and volume of atmospheric water that is precipitated on the ground. Rainwater thermal energy can be estimated by enthalpy h_{rain} (kJ/kg) and the rainfall depth INT (mm). Rainfall depth is related to the precipitated water volume at a catchment area (S_{catch}) i.e. $V_{\text{rain}} = INT \cdot S_{\text{catch}}$. The combined energy parameter Π is introduced to explain the complex problem of the heat transfer process between the atmosphere and the domestic hot water system. The rainwater energy parameter has the series representation:

$$\Pi = \sum_{i=1}^m \Delta h_{\text{rain},i} V_{\text{rain},i} \quad (1)$$

where $\Delta h_{\text{rain},i}$ is the enthalpy change, $V_{\text{rain},i}$ (m^3) is the volume of a single rain event i that is available for the heat-exchange process and m is the number of rainfalls during a rainwater harvesting period, corresponding to a building's *duty cycle*. A building's *duty*

cycle is dependent on the usage profile of the building, which will be explained henceforth, and is considerably shorter as compared to the rainfall period.

Storage tanks are useful facilities allowing a reduction of the runoff's peak flow and thus equalising flow rates in a city sewer system (Campisano & Modica, 2014). The stormwater volume in a storage tank V_{tank} (m^3) is also important in regulating the suspension time of the flow through a system. A water tank itself is also useful for the subtraction of thermal energy, represented by $c_{\text{SW}} \Delta T_{\text{tank}} \cdot V_{\text{tank}}$, where c_{SW} (kJ/kg · K) is the specific heat and ΔT_{tank} (K) represents the stormwater excess temperature in a storage tank. In the design of a tank, it is important to determine tank fillings (n). This depends on the heat exchange process and a tank's usage, e.g. for hot water production. The rate of heat exchanged between a domestic water-heating system and a stormwater system is related to the heat influxes and outfluxes of the storage tank control volume (CV). The energy change in the CV is essentially considered according to enthalpy change. A system's heat influx is due to the stormwater inflow into a tank (I process), and the heat outflux is due to the not-fully-cooled down stormwater outflow from the CV (II) and the extraction of stormwater heat for domestic water heating (III) (characterised usually by the coefficient of performance (COP) of a heat pump), see Figure 2. The increase of water temperature in the CV is due to random rain events ($\Delta h_{\text{rain}} \cdot V_{\text{rain}}$), and the decrease of stormwater temperature in a storage tank is predominantly due to the more-or-less constant heat extraction ($n V_{\text{tank}} c_{\text{SW}} \Delta T_{\text{extract}}$) and losses ($\Delta h_{\text{loss}} \cdot V_{\text{tank}}$), e.g. not fully cooled outflows, where $\Delta T_{\text{extract}}$ is the extracted temperature and Δh_{loss} is the enthalpy change due to heat losses. The integration of these three processes (I, II, III) is a complicated task since (1) rains have a random character, (2) the heat extraction process is dependent on the available heat transfer technology and (3) the usage of stormwater heat varies by location. The efficiency of thermal energy transfer between the atmosphere and a domestic system can be represented by the parameter:

$$\eta = \frac{n V_{\text{tank}} c_{\text{SW}} \Delta T_{\text{extract}}}{\Pi} 100 \quad (2)$$

The efficiency parameter η in Equation (2) depends essentially on the ratio of rain and stormwater heat fluxes. It is apparent that, in a lossless system, the efficiency parameter is $\eta = 1$, i.e. rainwater thermal energy is fully utilized for hot water production ($\Delta T_{\text{extract}} = \Delta T_{\text{tank}}$, $\Delta h_{\text{loss}} = 0$). However, in a real situation, this

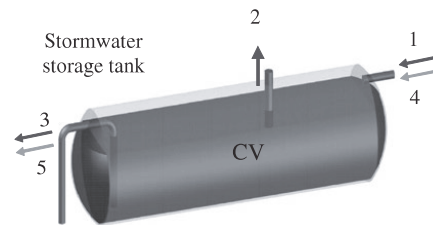


Figure 2. Stormwater storage tank control volume (CV). (1) Heat influx due to the stormwater inflow (4) into the tank, (2) extraction of stormwater heat for the domestic-water heating and (3) heat outflux due to the stormwater outflow (5) from the tank.

assumption cannot be accomplished due to several reasons: rainwater loss in an urban catchment, i.e. the runoff coefficient is less than one, the stormwater system is not thermally isolated and the rain return period varies, i.e. some heat can be taken out from the tank CV by outflow. The heat transfer for the hot water production is also dependent on the heat pump efficiency.

The collected stormwater thermal energy in a storage tank is also not fully available for hot water production since the water can be cooled down to 4 °C, which is the lowest acceptable water temperature in a storage tank. In most cases, the time of concentration, representing the time required for water to travel from the most hydraulically-remote portion of a catchment to a place of interest, is required to be less than 1 hour. The runoff coefficients of paved surfaces can be determined for each urban catchment (see Koppel et al., 2014) and considered in stormwater system modelling.

3.2. Stormwater heat extraction

The energy (MWh) available from a storage tank can be calculated by the stormwater heat extraction equation:

$$Q_{sw} = 0.28 \cdot n \cdot V_{\text{tank}} \cdot \rho_{sw} \cdot c_{sw} \cdot \Delta T_{\text{tank}} \cdot 10^{-6}, \quad (3)$$

where V_{tank} (m³) is the stormwater volume in a storage tank, ρ_{sw} (kg/m³) is the density, c_{sw} (kJ/kg · K) is the specific heat and ΔT_{tank} (°C) is the excess temperature available for the heat-exchange process. Parameter n in Equation (3) also represents the frequency of tank emptying in terms of the collected stormwater heat ($\Delta T_{\text{tank}} \cdot V_{\text{tank}}$). In a lossless situation, it is anticipated that all heat due to excess rain temperature ΔT_{rain} is used for the heat exchange process, i.e. $\Pi = n V_{\text{tank}} c_{sw} \Delta T_{\text{extract}}$. This is apparently not possible due to several reasons, such as heat loss through non isolated sections, water mixing in a tank, evaporation, system leaks, water pollution, etc.

3.3. Domestic hot water heat load

Average daily domestic hot water consumption is strongly related to the functionality of a building. It is reflected in the flow rate, occupancy rate, house composition, installed appliances, consumption trends and usage period. Hot water systems are usually designed to operate at a temperature of 55 °C in order to avoid intensive descaling of the heat-pump system (Kõiv et al., 2010). The cold water in the Tallinn city water network used for hot water production is above 5 °C. However, the fresh water supply to the Tallinn city water network is essentially the surface water of Lake Ülemiste (see Figure 1), the temperature of which varies seasonally, being in the range of 4–20 °C (cf Pedusaar,

2010). It can be mentioned that the fresh water in the Helsinki water system originates from Lake Päijänne, in Stockholm from Lake Mälaren and in St. Petersburg from Lake Laadoga. A heat flux (kW) is required to warm up the water from the initial temperature of 5 °C to 55 °C. This can be calculated by the heat load formula:

$$\Phi_{\text{HEAT}} = \frac{q_{\text{HW}} \cdot \rho_{\text{DW}} \cdot c_{\text{DW}} \cdot \Delta t_{\text{HW}}}{1000}, \quad (4)$$

where q_{HW} (l/s) is the hot water consumption, ρ_{DW} (kg/m³) is the density of domestic water, c_{DW} (kJ/kg · K) is the specific heat and Δt_{HW} is the temperature range required (<50 °C). According to Equation (4) the power needed to warm up 1.05 m³ domestic water per day is 2.51 kW. For instance, in the study by Sergejeva and Laanearu (2013), this situation corresponded to the flow rate in a public building in Tallinn. The flow rate $q_{\text{HW}} = 0.012$ l/s accounted for 160 working places, 41 sinks and 16 showers. (In comparison, the energy needed for warming up 1 m³ of boiler water is 58 kWh in the case of the cold and hot water temperature range of 50 °C.)

4. Functionality of buildings

The functionality of a building is usually determined by the number of people using the building according to the same daily behaviour and purpose. In this study, the three most commonly used building types are considered: (1) an apartment building, (2) an office and (3) a shopping centre. These buildings are most appropriate for on-site stormwater collection for the purpose of domestic water heating in terms of technological solutions and infrastructure availability. Daily consumptions of the volumetric flow rate in the cases of the representative buildings are calculated from the hot water demand according to Kõiv and Toode (2010), where data is based on extensive measurements of real hot water consumption in Tallinn city.

It is important to fix a building's *duty cycle* for calculations of hot water production using rainwater thermal energy. In the present study, an approximate method is considered to define a building's *duty cycle*, including main water usage trends in the building. For instance, in the case of a residential building, the domestic hot water usage-profile global peak is expected to occur during one week. According to the available data by Kõiv and Toode (2010), domestic hot water usage in public and commercial buildings is more smoothly distributed as compared to that in residential buildings. Also, buildings with large catchment areas allow harvesting of more rainwater for longer usage. In the present paper, the buildings' *duty cycles* are determined with a one-week precision. Three different *duty cycles* are used for calculations according

Table 3. Representative buildings' case studies parameters.

	Apartment building	Office building	Shopping centre
Sinks	180	42	46
Showers	90	5	6
Average daily hot water consumption, l/s	0.1	0.026	0.054
Duty cycle	1 week	2 weeks	3 weeks
Roof area, ha	0.10	0.36	0.48
Minimum parking lot area, ha ¹	0.12	0.078	0.78

Note: 1. Parking lot areas for representative buildings are calculated according to parking normative (EVS 843:2003), taking into account minimum parking place area 5 x 2.5 m².

to the importance of hot water production and the functionality of the building: (1) one week for the residential building, (2) two weeks for the public building and (3) three weeks for the commercial building.

4.1. Residential

The representative residential building is an apartment building with around 90 flats, each of which is equipped with a shower and sinks (see Table 3). The usage of hot water includes cooking, cleaning, showering, bathing and hand washing. Results of a recent study carried out by Kõiv and Toode (2010) show that consumption curves of apartment buildings vary for several reasons. There is a distinct difference in consumption during business days, where main consumption peaks occur in the morning and evening times. During the weekend, the consumption is 1.2 times higher than during business days.

4.2. Public

The representative public building is an office building with around 200 workers, including a number of showers and sinks (see Table 3). Hot water usage is mainly due to hand washing and showering, and, in this case, the building is not designed with leisure rooms. The overall trend of hot water usage on business days is from 8 am to 5 pm, and peak consumption occurs mostly at noon. Usually, no hot water is used during weekends. The *duty cycle* of the office building is two apartment building *duty cycles*, representing a reference period.

4.3. Commercial

The representative commercial building is a shopping centre with weekly visitors of around 50,000, including a number of showers and sinks (see Table 3). Hot water consumption includes cooking, cleaning maintenance, showering and hand washing. An essential difference in consumption compared to the other type buildings is the usage period, which mainly occurs at noon and after 5 pm when the business day ends. During weekends, the water consumption is even greater than on business days. The *duty cycle* of the shopping centre is three reference periods.

5. GA problem formulations

The complex system requires guidelines for engineering design and everyday usage. The integrated system under investigation consists of (1) the rainwater harvesting area, (2) the stormwater storage tank and (3) the hot water production system. The aim is to determine the rainwater and stormwater system parameters

that guarantee the building's hot water consumption. The solution to the proper functioning of the stormwater and domestic water integrated system depends on a number of parameters (see Table 4).

The GA is considered herein as a tool to determine two key parameters of this integrated system during the local rainy season and in accordance with the building's functionality: the stormwater volume in the storage tank (V_{tank}) and the rainwater catchment area (S_{catch}).

The integrated system model input parameters are rainfall depth INT , rain temperature T_{rain} , hot water consumption q_{HW} and hot and cold water temperature range Δt_{HW} . The available heat Q_{SW} captured from the stored stormwater is calculated by Equation (3). The necessary heat Φ_{HEAT} required for hot water production is calculated according to Equation (4).

The following simplified approach is used for the performance of the integrated system:

- (1) the stormwater volume in the storage tank is due to the catchment area and the rainfall depth during the building's *duty cycle*;
- (2) the rain temperature is due to the air temperature conditions averaged over the building's *duty cycle*;
- (3) the stormwater storage tank is filled with non-stratified water during the building's *duty cycle*;
- (4) heat pump efficiency is fixed to a constant value of COP during stormwater temperature depletion in the storage tank;
- (5) the building's daily consumption curve volumetric flux is approximated by its mean value;
- (6) the heat exchange due to evaporation from the stormwater storage tank is isolated by the absence of vents;
- (7) the heat losses in drainage pipelines and connecting systems are not considered in the calculations.

Thus, the efficiency of such a conservative integrated system is predominantly dependent on rainwater loss in the catchment area. For instance, the runoff coefficient for the Tallinn sub-catchments varied between 0.19 and 1.00 during the year 2008 rainfall period (Koppel et al., 2014). In optimizing the integrated system, the loss in water volume and changes in thermal energy are uncertainties essentially determining the efficiency parameter (η) for hot water production.

The integrated system model is based on two variables: (1) the stormwater volume in the storage tank and (2) the number of storage tank fillings, $X = [V_{\text{tank}}, n]$ (see Table 5). The corresponding catchment area is $S_{\text{catc.}} = V_{\text{tank}} \cdot n \cdot 1000 / INT$ (mm).

System energetic optimization is performed as an attempt to reach the target value (days) of the representative building's *duty cycle*. The problem is solved as the following:

Table 4. Integrated system parameters.

(1) Rainwater harvesting	(2) Stormwater storage	(3) Hot water production
INT – rainfall depth, mm	V_{tank} – stormwater storage tank volume, m ³	Φ_{HEAT} – necessary heat required for hot water production, kW
T_{rain} – rain temperature, °C	ΔT_{tank} – stormwater excess temperature, °C	q_{HW} – hot water consumption, l/s
S_{catch} – catchment area, ha	n – number of storage tank fillings	ρ_{DW} – domestic water density, kg/m ³
V_{rain} – precipitated (rain) water volume, m ³	Q_{SW} – available stormwater energy in storage tank, MWh	c_{DW} – specific heat of domestic water, kJ/kg·K
Π – combined energy parameter, kJ/kg·m ³	ρ_{SW} – stormwater density, kg/m ³	Δt_{HW} – hot and cold water temperature range required, °C
ρ_{RW} – rainwater density, kg/m ³	c_{SW} – specific heat of stormwater, kJ/kg·K	COP – heat-pump coefficient of performance

Table 5. Integrated model input parameters.

Parameters	Apartment building	Office building	Shopping centre
Duty cycle	1 week	2 weeks	3 weeks
Target value	7 days	14 days	21 days
Rainfall depth variation (mm)	2.89–46.41	9.12–64.13	14.44–84.39
Mean temperature variation (°C)	5.87–18.56	6.11–18.36	5.19–18.21
Heat needed per day (kWh)	502.8	130.72	271.51
Nr of fillings	0.1–10	0.1–10	0.1–10
Tank volume (m ³)	10–100	10–125	10–200

$$C(X) = [0.28 \times n \times V_{\text{tank}} \times \rho_w \times c_w \times \Delta T_{\text{tank}} \times 10^{-6} / (24 \times \Phi_{\text{HEAT}})],$$

where quantity $24 \cdot \Phi_{\text{HEAT}}$ corresponds to the energy needed by the representative building during a day, with unit kWh per day. Thus, $C(X)$ represents the number of days required to satisfy the building's consumption of thermal energy for hot water production. For instance, the storage tank size and the number of fillings for the representative residential building provide hot water production during the building's *duty cycle* of 7 days. The minimum catchment area of the proposed optimal solution is determined by the parameters V_{tank} and INT . The rainfall depth is represented by an ensemble of averages of rainfalls between May and October during years 2004–2011 according to the following intervals: one week in the case of the residential building, two weeks in the case of the public building and three weeks in the case of the commercial building (see Table 5). The rainwater temperature is represented by the mean diurnal air temperature during the building's *duty cycle* averaged over a rainfall period of eight years.

6. Data analyses

Harku meteorological data is used to estimate the short-term mean values of the temperature and rainfall depth according to the building's functionality. Data processing involved averaging over the eight years for each day during the rainy season. The buildings' *duty cycles* are then used for determining the one, two and three week duration running averages for the temperature and rainfall depth for each day of the rainy season. For instance, the apartment building's *duty cycle* is one week, and thus the rainfall depth is calculated over the period of seven days (shown by a dotted curve in Figure 3) using data of the mean rainfall depth for eight years (shown by a full curve in Figure 3). The eight-year rainfall depth for the office and shopping centre (shown by dashed and dash-dotted curves in Figure 3, respectively) is determined accordingly. The stormwater temperatures for the case of the apartment, office and shopping centre *duty cycles* are shown by dotted, dashed and dashed-dotted curves in Figure 4, respectively. The mean temperature over the eight years for each day during the rainy season is shown by a full curve in Figure 4.

7. Results

The availability of stormwater thermal energy for domestic hot-water consumers depends essentially on (1) the stormwater heat extraction possibility from a storage tank, (2) the harvested rainwater convergence in a catchment area and (3) the cost effectiveness of an integrated system. In the GA algorithm, the

stormwater heat extraction for the number of storage tank fillings per specific building's *duty cycle* represents the hot water production days.

7.1. Stormwater storage tank

The stormwater volume in the storage tank in the GA constraints is allowed to vary within certain limits, which correspond to the representative building's location. In Figure 5 the estimated stormwater volumes needed for the residential, public and commercial representative buildings' hot water production, respectively, are related to the average temperature and the rainfall depth during the rainy season, i.e. from May to October, with an interval of 5 days.

7.1.1. Residential

The GA results in Figure 5a confirm that the stormwater volume in the storage tank varies between 21 m³ (in mid-August when the rainwater mean temperature is over 18 °C and one-week's rainfall depth is 19 mm) and 100 m³ (in late October when the temperature is under 7 °C and the rainfall depth is 16 mm), which represents the upper limit of parameter V_{tank} for the apartment building. Note that the *cumulative expenses* in Figure 5a almost correspond to the *storage expenses* during the summer months. Peaks of the stormwater volume during several summer months in Figure 5a correspond to the storage tank, which is seldom filled during the building's *duty cycle* and, thus, represents a comparatively expensive solution.

7.1.2. Public

The model results in Figure 5b show that the stormwater volume in the storage tank varies between 19 m³ (in mid-September when the rainwater mean temperature is 15 °C and the two-week's rainfall depth is 46 mm) and 125 m³ (in early May when

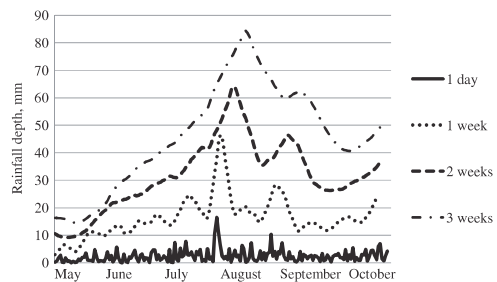


Figure 3. Daily mean rainfall-depth for years 2004 to 2011. Mean rainfall-depth averaged over eight years. Calculated mean rainfall-depth over the period: one week, two weeks and three weeks.

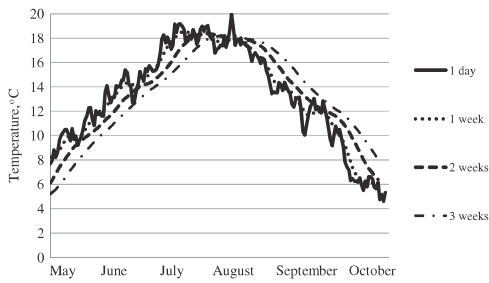


Figure 4. Daily mean rainwater temperature for years 2004 to 2011. Mean rainwater temperature averaged over eight years. Mean rainwater temperature averaged over the period: one week, two weeks and three weeks.

the temperature is under 7 °C and the rainfall depth is under 10 mm), representing the upper limit for the office building.

7.1.3. Commercial

The model results in Figure 5c show that the stormwater volume in the storage tank varies between 43 m³ (in late July when the rainwater mean temperature is over 16 °C and the three-week's rainfall depth is 51 mm) and 200 m³ (mostly in early May when the temperature is under 7 °C and the rainfall depth is 16 mm), representing the upper limit for the shopping centre. It is interesting to note that value limit of the stormwater volume in the storage tank is not approached in October when rain is frequently present.

It can be concluded that the maximum stormwater volume in the storage tank is generally obtained for colder and less intense rain periods. Smaller storage tank sizes are obtained for the months when the rain temperature is high and the rain intensity is comparatively large, such as June, July and August.

7.2. Rainwater catchment area

The stormwater temperature essentially defines the stormwater volume that has to be collected from a catchment. The catchment area results from May to October with an interval of 5 days are presented in Figures 6 for residential, public and commercial representative buildings respectively.

7.2.1. Residential

The GA results in Figure 6a confirm that the catchment area varies between 0.47 ha (in early August when the rainwater mean temperature is over 17 °C and one-week's rainfall depth is 46 mm) and 24.56 ha (in early May when the temperature is 8 °C and the rainfall depth is 5 mm). It is found that the catchment area mainly stays in the range of 0.48 ha and 3.50 ha. It was found that the building's roof and parking area catchments (see Section 4.1) are not sufficient to supply the needed rainwater volume for the integrated system. Also, the integrated system is *cost effective* during the period between the end of May and the beginning of October.

7.2.2. Public

The GA results in Figure 6b show that the catchment area varies between 0.18 ha (in mid-August when the rainwater mean temperature is over 18 °C and the two-week's rainfall depth is the

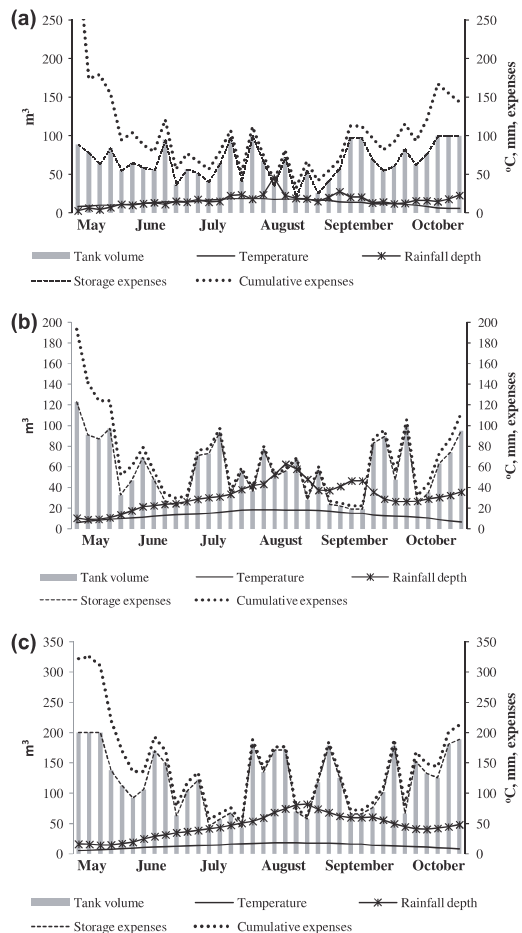


Figure 5. Optimal tank volume, temperature, mean rainfall-depth and expenses on dates: 5th, 10th, 15th, 20th, 25th and 30th of the rainy months for (a) apartment building, (b) office building and (c) shopping centre.

largest, 63 mm) and 7.02 ha (in early May when the temperature is 7 °C and the rainfall depth is 10 mm). The catchment area stays under 1.00 ha during the period from June to September (representing the *cost effective* months). The office building's roof catchment (see Section 4.2) is sufficient to provide the needed amount of stormwater for the integrated system during the period between mid-July and mid-September.

7.2.3. Commercial

The GA results in Figure 6c confirm that the catchment area varies between 0.42 ha (in mid-August when the rainwater mean temperature is the highest, 18 °C, and the three-week's rainfall depth is the highest, 82 mm) and 12.49 ha (in early May when the temperature is 5 °C and the rainfall depth is 16 mm). It can be also noted that the average catchment area stays under 1.00 ha from early June to late September. The shopping centre's roof catchment area (see Section 4.3) is sufficient to provide the needed amount of stormwater for the integrated system only in

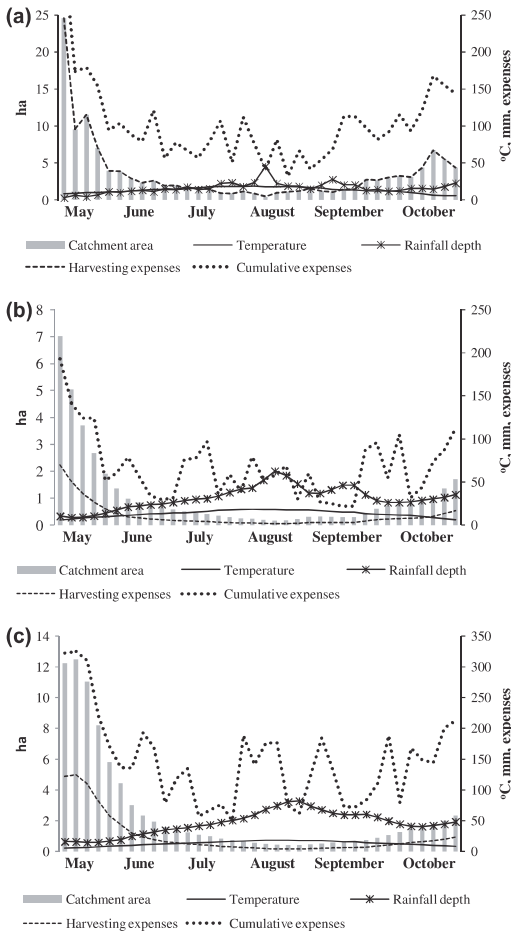


Figure 6. Optimal catchment area, temperature, mean rainfall-depth and expenses on dates: 5th, 10th, 15th, 20th, 25th and 30th of rainy months for a) apartment building, b) office building and c) shopping centre.

August. The parking area allows the supply of needed stormwater thermal energy to the integrated system from late June until the end of September.

It can be concluded that the public and commercial buildings' roofs are sufficient to provide the needed amount of rainwater for the integrated system during the hot rainfall period. In the case of the apartment building, the roof size is a limiting factor. An additional catchment is needed during the cold rainfall period or an additional heat source should be used to provide the sufficient amount of thermal energy for the building. However, the energy could be sufficient for one to four family one-floor houses because such buildings have more or less the same roof area of a ten-floor building but reduced energy requirements.

7.3. Cumulative expenses

The GA findings confirmed that June, July and August are the most efficient months for using the stormwater integrated

system with respect to hot water heating. Both rainwater temperature and intensity are high during this period, allowing the use of smaller storage tanks and catchments. According to the integrated system model, the number of storage tank fillings determines the volume of stormwater needed for hot water production. The more frequently a storage tank is filled during the building's *duty cycle*, the smaller the storage tank size needed. Expenses for rainwater harvesting and stormwater storage depend on the scale and complexity of the system. In the present work, a simple parameter, the *cumulative expenses* parameter, is introduced. It corresponds to the sum of two control factors: (1) stormwater *storage expenses* and (2) stormwater *harvesting expenses*. Stormwater *storage expenses* are estimated according to the stormwater-volume unit (1.0 m³) in the storage tank. Rainwater *harvesting expenses* are estimated according to the catchment-area unit (0.1 ha). The *cumulative expenses* parameter is determined by the formula:

$$f = V_{\text{tank}}/a + S_{\text{catch}}/b, \quad (6)$$

where a is the stormwater-volume unit and b is the catchment-area unit. Parameter f is essentially introduced to determine the system expenses according to the different GA-calculated solutions for storage tank size (V_{tank}) and catchment area (S_{catch}). The *cost effective* solution corresponds to the GA solutions in the vicinity of the Pareto curves in Figure 7.

7.3.1. Residential

The apartment building requires more-or-less stable hot water production for its inhabitants' comfort during business days and a higher flowrate during the weekend. It was found that the average number of storage tank fillings is in the range of two and six per the building's *duty cycle* (one week). Frequent filling of the storage tanks enables rapid replacement of stormwater, guaranteeing continuous hot water production. However, it is not possible to continuously charge the storage tanks during the rainfall period from May to October. The results in Figure 7a indicate that the optimal solutions are most expensive in May and October when the rainwater temperature is low and a large number of tank fillings is required. This confirms that, during the cold rainfall period months, a large amount of stormwater is needed to provide the building with the necessary thermal energy. The *cost effective* optimal solutions are apparent for June, July and August, when there is a small number of storage tank fillings.

7.3.2. Public

Hot water is used in the office building during the working time of business days. The average number of storage tank fillings is in the range one and seven per the building's *duty cycle* (two weeks). Results in Figure 7b indicate that the optimal solutions are most expensive in early May and in late October. The *cost effective* optimal solutions are possible from late May until early September when the number of tank fillings is over four times per two-week period.

7.3.3. Commercial

The shopping centre requires more-or-less stable hot water production during the day to provide service for customers during the whole week. Results in Figure 7c indicate that the optimal

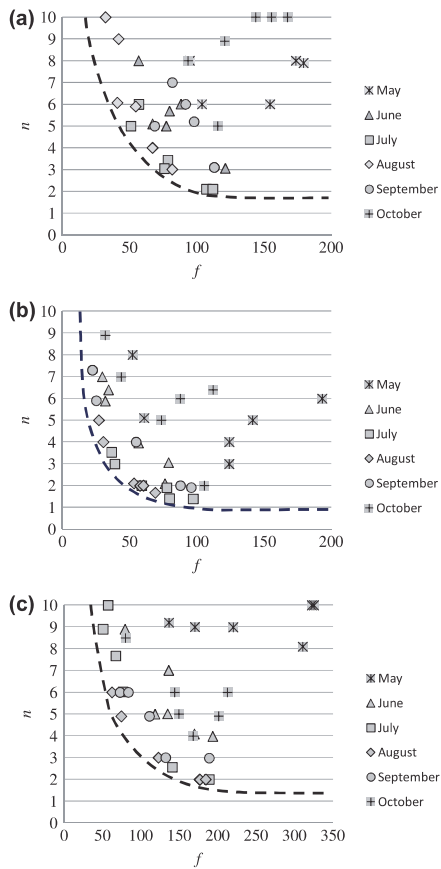


Figure 7. Estimated cumulative expenses parameter (f) for a number of tank fillings (n) for the, a) apartment building, b) office building and c) shopping centre during a rainfall period.

solutions are more sparsely distributed on the graph. The storage tank fillings are in the range of two and 10 per the building's duty cycle (three weeks). The cost effective optimal solutions are possible from early July until mid-September when the number of tank fillings is over five times per three-week period.

Although the rain characteristics do not match with the building's thermal energy usage profile, the cumulative expenses essentially follow the seasonal weather pattern. However, the cost effective solutions appear in July, August and September, when the average number of tank fillings is five times per building's duty cycle. It can be concluded that the less cost effective solutions are represented with a large number of tank fillings.

8. Discussion

It is generally accepted that climate changes exert a strong influence on precipitation with global warming known to result in an increase in air temperature and water vapour in the atmosphere and the overall effect of more frequent, intense rainfall events (Trenberth, 2011). During the years 2004–2011, annual

precipitation varied between 326–713 mm in northern Estonia while annual maximum air temperature varied between 19–26 °C during the same period. It should be underlined that stormwater has a large heat capacity, and, therefore, city-sized catchment volumes of collected stormwater represent a considerable potential source of thermal energy. For instance, the total available heat due to stormwater cooling from a seasonal air temperature down to 4 °C is about 50–137 MW in the case of Tallinn's impervious area. In the near future, the growing demand for energy in urban areas makes extraction of thermal energy from renewable energy sources inevitable. The usage of stormwater energy's potential is favourable for several reasons:

- (1) rainfall events have become more frequent over the last decade;
- (2) there is a requirement to collect and store stormwater locally within an urban area to reduce flood risk;
- (3) stormwater heat represents on-site thermal energy for local users;
- (4) stormwater heat is a renewable energy;
- (5) the implementation of heat pumping technology for stormwater heat extraction is feasible;
- (6) stormwater storage tanks could be integrated with SUDS (Sustainable Urban Drainage Systems);
- (7) thermal energy reduction reduces biological activity in the sewage system;
- (8) local removal of pollutants allows impregnation of the stormwater.

The GA results of the cold rainfall period require large storage tanks, which may result out of the hydraulic sizing range of detention tanks in consideration of reduced space in urban contexts. However, it should be noted that hydraulically sized tanks and corresponding catchments areas (Li et al., 2015) are within the limits of the GA sized tanks and catchment areas during the hot rainfall period. A large underground space for stormwater collection in modern cities is feasible if a number of hydraulically connected smaller tanks are used instead of one storage tank. It should be underlined here that the number of stormwater tanks in a city area should correspond to the number of catchment areas, not particularly to the number of buildings in a catchment area.

The cost of on-site stormwater facilities is commonly evaluated on the basis of approximating the total cost based on a single variable power function of the detention tank volume and the land area of each tank (see Li et al., 2015). In the case of a rainwater harvesting system for domestic hot water production, stormwater treatment expenses according to catchment area should also be included. The GA calculated stormwater volume (corresponding to storage expenses according to a stormwater-volume unit) determines the cost of storage tank(s), installation, land use, etc. The catchment area (corresponding to harvesting expenses according to a catchment-area unit) is related to the cost for stormwater drainage into a city's sewage system. However, the removal of chemicals is required when stormwater is impregnated on-site. Sediment removal is considered in the stormwater system by using facilities such as sediment traps, etc. Also, the elimination of bacteriological contamination in large water volumes needs chemical or physical disinfection. The inclusion of cumulative expenses in the management cost is not considered herein since

the selection of the final design for the integrated stormwater system for domestic hot water production will largely depend on the local economic conditions and the decision-maker's preference.

9. Conclusions

This study proposes solutions for the optimal collection of stormwater for maximizing the usage of stormwater absorbed heat in different building types. Stormwater collection and the domestic water heating system is optimized for two key parameters and targeted according to a building's hot-water consumption days. The GA targets correspond to the integrated model system *duty cycles* according to the importance of hot water production and the functionality of buildings.

The stormwater heat extraction equation is combined with the domestic hot water heat-load formula to determine the days representing target periods for the different buildings. It is considered that the hot water consumption of a building determines the required heat load while the rainfall intensity over an urban catchment and air temperature define the thermal energy of stormwater available for usage. The ratio between rainwater volume in a catchment and stormwater volume in a storage tank determine the number of tank fillings required during a building's *duty cycle*. The overall established relationships between fixed parameters and variables of the integrated system are solved using GA to satisfy the hot water demand of a building under specific limits for the stormwater volume in a storage tank and catchment. The ratio of time scales of stormwater heat extraction from a tank and the rainfall return period are expressed virtually by the number of stormwater tank fillings required during a building's *duty cycle*.

The GA findings for stormwater volume and catchment area for different building types vary on a large scale during the rainfall period. The minimum tank volume can be 21% of the limiting volume in the case of the apartment building, 15% in the case of the office building and 20% in the case of the shopping centre in Tallinn. Similarly, the smallest catchment area can be 11% of the limiting area for the residential building, 1.4% for the public building and 3.2% for the commercial building. The large values of storage tank size and catchment area characterize the driest months with low rainfalls and moderate air temperatures (e.g. April, May and the early June), as well as months with moderate precipitations and lower air temperatures (e.g. October). Usually, months with higher rainfall totals and higher air temperatures (e.g. July, August and early September) result in a small tank size and catchment area. We note here that this may be in contrast with the ordinary use of a rainwater harvesting system that is to save potable water from the mains. During the period from late May to early September when the daily mean temperature is above 10 °C, mean tank size and catchment area remain below 65% and 14% of the limiting values for residential buildings, 48% and 14% for public buildings, and 62% and 12% for commercial buildings.

The Pareto solutions, with maximal stormwater heat usage, are calculated for the buildings separately. The heat extraction for the hot water production of the different buildings represents the number of stormwater storage tank fillings well. The *cumulative expenses* analyses of the integrated system solutions consider the seasonal pattern. There is less cost for needed infrastructure for small tanks and catchments if high intensity and temperature rainfalls exist. However, additional expenses for domestic water heating are expected in the case of a lack of

stormwater thermal heat. Stormwater heat extraction for buildings depends on the decision making process that considers the available catchment area and the possibility to use a nearby storage tank. Hot water production from stormwater is feasible in the case of a building that has a large catchment area, where flood risk is an important issue and more-or-less stable hot water consumption exists. There is great potential for the application of the integrated stormwater system for thermal energy extraction in urban areas.

Funding

Financial support by Estonian Ministry of Education and Research (IUT 19–7) is appreciated.

References

- Amaya, N., Bayon, J., and Castro-Fresno, D., 2013. Temperature performance of different pervious pavements: Rainwater harvesting for energy recovery purposes. *Water Resources Management*, 27 (15), 5003–5016.
- Baek, N.C., Shin, U.C., and Yoon, J.H., 2004. A study on the design and analysis of a heat pump heating system using wastewater as a heat source. *Solar Energy*, 78, 427–440.
- Brabec, E., 2009. Imperviousness and land-use policy: Toward an effective approach to watershed planning. *Journal of Hydrologic Engineering*, 14 (4), 425–433.
- Byers, H.R., Moses, H., and Harney, P.J., 1949. Measurement of rain temperature. *Journal of Meteorology*, 6, 51–55.
- Campisano, A. and Modica, C., 2014. Selecting time scale resolution to evaluate water saving and retention potential of rainwater harvesting tanks. *Procedia Engineering*, 70, 218–227.
- Cipolla, S.S. and Maglionico, M., 2014. Heat recovery from urban wastewater: analysis of the variability of flow rate and temperature. *Energy and Buildings*, 69, 122–130.
- Estonian Meteorology and Hydrology Institute (EMHI), 2011. *Monthly and annual report* (in Estonian).
- Estonian Centre for Standardization 2003. *Town streets*. EVS 843: 2003. Estonian: Estonian Centre for Standardization.
- Evers, M., Jonoski, M., Maksimović, Č., Lange1, L., Ochoa Rodriguez, S., Teklesadiq, A., Cortes Arevalo, J., Almoradie, A., Eduardo Simões N., Wang, L., and Makropoulos, C., 2012. Collaborative modelling for active involvement of stakeholders in urban flood risk management. *Natural Hazards and Earth System Sciences*, 12, 2821–2842.
- Janke, B.D., Herb, W.R., Mohseni, O., and Stefan, H.G., 2013. Case study of simulation of heat export by rainfall runoff from a small urban watershed using MINUHET. *Journal of Hydrologic Engineering*, 18 (8), 995–1006.
- Karing, P., 1992. Air temperature in Estonia. *Estonian Academy of Sciences*, 78. (In Estonian)
- Koppel, T., Vassiljev, A., Puust, R., and Laanearu, J., 2014. Modelling of stormwater discharge and quality in urban area. *International Journal of Ecological Science and Environmental Engineering*, 1 (3), 80–90.
- Köiv, T.A. and Toode, A., 2010. *Hot water usage in buildings*. Tallinn: TUT Press.
- Laanearu, J., Annus, I., Vassiljev, A., and Koppel, T., 2010. On determination of flow routes in a stormwater network using the least squares method. In: J. Boxall and C. Maksimović, eds. *CCWI2009 Integrating Water Systems: Computing and Control in the Water Industry*. Sheffield, UK: Taylor & Francis, 731–734.
- Lee, J., and Heaney, J.P., 2003. Urban imperviousness and its impacts on stormwater systems. *Journal of Water Resources Planning and Management*, 129 (5), 419–426.
- Li, F., Duan, H.-F., Yan, H., and Tao, T., 2015. Multi-objective optimal design of detention tanks in the urban stormwater drainage system: Framework development and case study. *Water Resource Management*, 29, 2125–2137. doi:10.1007/s11269-015-0931-0
- Liu, L., Fu, L., and Jiang, Y., 2010. Application of an exhaust heat recovery system for domestic hot water. *Energy*, 35 (3), 1476–1481.
- Maharjan, B., Pachel, K., and Loigu, E., 2013. Urban stormwater quality and quantity in the city of Tallinn. *European Scientific Journal*, 3, 305–314.

- Pedusaar, T., Sammalkorpi, I., Hautala, A., Salujõe, J., Järvalt, A., and Pihlak, M., 2010. Shifts in water quality in a drinking water reservoir during and after the removal of cyprinids. *Hydrobiologia*, 649 (1), 95–106.
- Riigi Teataja, 2013. *Tallinn green areas agenda for the years 2013–2025*. Regulation 40. Tallinn, Estonia: Kirjastus "Perioodika"
- Scholz, M. and Grabowiecki, P., 2009. Combined permeable pavement and ground heat source heat pump systems to treat urban runoff. *Journal of Chemical Technology and Biotechnology*, 84 (3), 405–423.
- Sergejeva, M. and Laanearu, J., 2013. Optimal utilization of rain-water heat in domestic water system of public building. In *CLIMA 2013. 11th REHVA World Congress and the 8th International Conference on Indoor Air Quality, Ventilation and Energy Conservation in Buildings*, 16–19 June 2013 Prague, Czech Republic. Society of Environmental Engineering (STP).
- Simpson, A.R., Dandy, G.C., and Murphy, L.J., 1994. Genetic algorithms compared to other techniques for pipe optimization. *Journal of Water Resources, Planning and Management*, 120 (4), 423–443.
- Tibar, H., 1989. *Stormwater combined sewers and separate storm sewers*. Tallinn: Tallinn University of Technology (In Estonian).
- Trenberth, K.E., 2011. Changes in precipitation with climate change. *Climate Research*, 47, 123–138. doi: [10.3354/cr00953](https://doi.org/10.3354/cr00953)
- Wu, Z.Y. and Simpson, A.R., 2001. Competent genetic-evolutionary optimization of water distribution systems. *Journal of Computing in Civil Engineering*, 15 (2), 89–101.
- Zgheib, S., Moilleron, R., and Chebbo, G., 2012. Priority pollutants in urban stormwater: Part 1-Case of separate storm sewers. *Water Research*, 46 (20), 6683–6692.

Curriculum vitae

Personal data

Name: Monika Kollo
Date of birth: 23.12.1987
Place of birth: Viljandi, Estonia
Citizenship: Estonian

Contact data

E-mail: monika.kollo@ttu.ee

Education

2011–2018 Tallinn University of Technology—PhD
2006–2011 Tallinn University of Technology, Heating and ventilation—
MSC (cum laude)
1994–2006 C.R. Jakobson Gymnasium—High school

Language competence

Estonian Native language
English Fluent
Russian Fluent

Professional employment

2017– ... TUT Department of Civil Engineering and Architecture,
technician
2012– ... Filter AS, project manager
2012– 2013 TUT Department of Mechanics, engineer
2008– 2012 Filter AS, designer

Main areas of scientific work

Hydraulic modelling of stratified flows in built environment, hydraulic-systems process parameters optimisation, integrated-systems design parameters optimisation.

Honours & certifications

2014 FEANI EUR ING License 32844
2013 Jaan Poska Scholarship
2011 Alexela Master's Scholarship
2010 Alexela Master's Scholarship
2009 Jaan Poska Scholarship
2009 Alexela Master's Scholarship
2008 Alexela Scholarship

Scientific Work

Sergejeva, M., Laanearu, J., Tabri, K. (2017). On parameterization of emulsification and heat exchange in the hydraulic modelling of oil spill from a damaged tanker in winter conditions. – *Proceedings of 6th International Conference on Marine Structures, MARSTRUCT 2017, 8 – 10 May 2017, Lisbon Portugal.*

Kollo, M., Laanearu, J., Tabri, K. (2017). Hydraulic modelling of oil spill through submerged orifices in damaged ship hulls. – *Ocean Engineering*, 130, 385–397. doi: 10.1016/j.oceaneng.2016.11.032

Kollo, M., Laanearu, J. (2017). An optimal solution of thermal energy usage in the integrated system of stormwater collection and domestic-water heating. – *Urban Water Journal*, 14 (2), 212–222. doi: 10.1080/1573062X.2015.1086006

- Carr, M., Cuthbertson, A., Laanearu, J., Sommeria, J., Kean, J., Lilover, M.-J., **Kollo, M.**, Berntsen, J., Thiem, Ø., Viboud, S. (2015). Experimental studies of internal and near-bed dynamics of restricted exchange flows. – *E-proceedings of the 36th IAHR World Congress, 28 June – 3 July, 2015, The Hague, the Netherlands. International Association for Hydro-Environment Engineering and Research, 1–4.*
- Laanearu, J., Annus, I., **Sergejeva, M.**, Koppel, T. (2014). Semi-empirical method for estimation of energy losses in a largescale pipeline. – *Procedia Engineering, 70, 969–977. doi: 10.1016/j.proeng.2014.02.108.*
- Carr, M., Cuthbertson, A., Laanearu, J., Sommeria, J., Berntsen, J., Lilover, M.-J., **Kollo, M.**, Thiem, Ø., Viboud, S. (2014). Experimental study of internal mixing and near-bed dynamics induced by restricted stratified exchange flows. – *Proceedings of the HYDRALAB IV Joint User Meeting, Lisbon, July 2014: HYDRALAB IV Joint User Meeting, Lisbon, July 2014. Lisbon, Portugal: Hydralab, 1–5.*
- Sergejeva, M.**, Laanearu, J., Tabri, K. (2013). Hydraulic modelling of submerged oil spill including tanker hydrostatic overpressure. – *Proceedings of 4th International Conference on Marine Structures, MARSTRUCT 2013, 25–27 March 2013, Espoo, Finland. Taylor & Francis, 209–217.*
- Sergejeva, M.**, Laanearu, J. (2013). Optimal utilization of rain-water heat in domestic water system of public building. – *Proceedings of 11th REHVA World Congress and the 8th International Conference on Indoor Air Quality, Ventilation and Energy Conservation in Buildings, CLIMA 2013, 16 – 19 June 2013, Prague, Czech Republic. Elsevier, 1–10.*
- Laanearu, J., Annus, I., **Sergejeva, M.**, Koppel, T., Puust, R. (2012). Parametric modelling study for filling of horizontal pipe containing water. – *Proceedings of WDSA 2012: 14th Water Distribution Systems Analysis Conference, Adelaide (Australia), September 24–27, 2012. Ed. Engineers Australia. Engineers Australia.*
- Sergejeva, M.** (2011). Modelling of stormwater and heat pump integrated system for optimal utilization of rain water in TUT VI building : Masters's Thesis (sup) Janek Laanearu. Tallinn : Tallinna Tehnikaülikool.
- Voll, H., Kõiv, T.A., Tark, T., **Sergejeva, M.** (2010). Cooling Demand in Commercial Buildings - The Influence of Daylight Window Design. – *WSEAS Transactions on Applied and Theoretical Mechanics, 1 (5), 101–111.*
- Voll, H., Kõiv, T.A., **Sergejeva, M.** (2010). Direct Solar and Diffuse Daylight Analysis for Apartment Buildings in Urban Planning. – *Latest Trends on Urban Planning and Transportation: 3 rd WSEAS International Conference on Urban Planning and Transportation (UPT 10), 22–24 July 2010, Corfu Island, Greece,. Ed. M. Jha. WSEAS, 48–52.2013*

Signature:

Date:

Elulookirjeldus

Isikuandmed

Nimi: Monika Kollo
Sünniaeg: 23.12.1987
Sünnikoht: Viljandi, Eesti
Kodakondsus: Eesti

Kontaktandmed

E-post: monika.kollo@ttu.ee

Hariduskäik

2011–2018 Tallinna Tehnikaülikool – PhD
2006–2011 Tallinna Tehnikaülikool, Küte ja ventilatsioon – MSC (cum laude)
1994–2006 Carl Robert Jakobsoni nimeline Gümnaasium – Keskkharidus

Keelteoskus

Eesti keel Emakeel
Inglise keel Kõrgtase
Vene keel Kõrgtase

Teenistuskäik

2017– ... TTÜ Ehituse ja arhitektuuri instituut, tehnik
2012– ... Filter AS, projektijuht
2012– 2013 TTÜ Mehaanikainstituut, insener
2008– 2012 Filter AS, disainer

Teadustöö põhisuunad

Stratifitseeritud voolamise hüdrauliline modelleerimine tehiskeskkonnas, hürauliliste süsteemide protsessiparameetrite optimeerimine, integreeritud insenersüsteemide disainiparameetrite optimeerimine.

Tunnustused

2014 FEANI EUR ING Litsents 32844
2013 Jaan Poska nimeline stipendium - Tunnistus väljaandud Tallinna Tehnikaülikooli poolt koostöös Tallinna Linnavalitsusega
2011 SA Tallinna Tehnikaülikooli Arengufondi Alexela magistriõppe stipendium
2010 SA Tallinna Tehnikaülikooli Arengufondi Alexela magistriõppe stipendium
2009 Jaan Poska nimeline stipendium - Tunnistus väljaandud Tallinna Tehnikaülikooli poolt koostöös Tallinna Linnavalitsusega
2009 SA Tallinna Tehnikaülikooli Arengufondi Alexela magistriõppe stipendium
2008 SA Tallinna Tehnikaülikooli Arengufondi Alexela inseneriõppe stipendium

Teadustöö

- Sergejeva, M.,** Laanearu, J., Tabri, K. (2017). On parameterization of emulsification and heat exchange in the hydraulic modelling of oil spill from a damaged tanker in winter conditions. – *Proceedings of 6th International Conference on Marine Structures, MARSTRUCT 2017, 8 – 10 May 2017, Lisbon Portugal.*
- Kollo, M.,** Laanearu, J., Tabri, K. (2017). Hydraulic modelling of oil spill through submerged orifices in damaged ship hulls. – *Ocean Engineering*, 130, 385–397. doi: 10.1016/j.oceaneng.2016.11.032
- Kollo, M.,** Laanearu, J. (2017). An optimal solution of thermal energy usage in the integrated system of stormwater collection and domestic-water heating. – *Urban Water Journal*, 14 (2), 212–222. doi: 10.1080/1573062X.2015.1086006

- Carr, M., Cuthbertson, A., Laanearu, J., Sommeria, J., Kean, J., Lilover, M.-J., **Kollo, M.**, Berntsen, J., Thiem, Ø., Viboud, S. (2015). Experimental studies of internal and near-bed dynamics of restricted exchange flows. – *E-proceedings of the 36th IAHR World Congress, 28 June – 3 July, 2015, The Hague, the Netherlands. International Association for Hydro-Environment Engineering and Research, 1–4.*
- Laanearu, J., Annus, I., **Sergejeva, M.**, Koppel, T. (2014). Semi-empirical method for estimation of energy losses in a largescale pipeline. – *Procedia Engineering, 70, 969–977. doi: 10.1016/j.proeng.2014.02.108.*
- Carr, M., Cuthbertson, A., Laanearu, J., Sommeria, J., Berntsen, J., Lilover, M.-J., **Kollo, M.**, Thiem, Ø., Viboud, S. (2014). Experimental study of internal mixing and near-bed dynamics induced by restricted stratified exchange flows. – *Proceedings of the HYDRALAB IV Joint User Meeting, Lisbon, July 2014: HYDRALAB IV Joint User Meeting, Lisbon, July 2014. Lisbon, Portugal: Hydralab, 1–5.*
- Sergejeva, M.**, Laanearu, J., Tabri, K. (2013). Hydraulic modelling of submerged oil spill including tanker hydrostatic overpressure. – *Proceedings of 4th International Conference on Marine Structures, MARSTRUCT 2013, 25–27 March 2013, Espoo, Finland. Taylor & Francis, 209–217.*
- Sergejeva, M.**, Laanearu, J. (2013). Optimal utilization of rain-water heat in domestic water system of public building. – *Proceedings of 11th REHVA World Congress and the 8th International Conference on Indoor Air Quality, Ventilation and Energy Conservation in Buildings, CLIMA 2013, 16 – 19 June 2013, Prague, Czech Republic. Elsevier, 1–10.*
- Laanearu, J., Annus, I., **Sergejeva, M.**, Koppel, T., Puust, R. (2012). Parametric modelling study for filling of horizontal pipe containing water. – *Proceedings of WDSA 2012: 14th Water Distribution Systems Analysis Conference, Adelaide (Australia), September 24–27, 2012. Ed. Engineers Australia. Engineers Australia.*
- Sergejeva, M.** (2011). Modelling of stormwater and heat pump integrated system for optimal utilization of rain water in TUT VI building : Masters's Thesis (sup) Janek Laanearu. Tallinn : Tallinna Tehnikaülikool.
- Voll, H., Kõiv, T.A., Tark, T., **Sergejeva, M.** (2010). Cooling Demand in Commercial Buildings - The Influence of Daylight Window Design. – *WSEAS Transactions on Applied and Theoretical Mechanics, 1 (5), 101–111.*
- Voll, H., Kõiv, T.A., **Sergejeva, M.** (2010). Direct Solar and Diffuse Daylight Analysis for Apartment Buildings in Urban Planning. – *Latest Trends on Urban Planning and Transportation: 3 rd WSEAS International Conference on Urban Planning and Transportation (UPT 10), 22–24 July 2010, Corfu Island, Greece,. Ed. M. Jha. WSEAS, 48–52.2013*

Signature:

Date:

